

UNCLASSIFIED

AD NUMBER

AD261976

LIMITATION CHANGES

TO:

Approved for public release; distribution is unlimited.

FROM:

Distribution authorized to U.S. Gov't. agencies and their contractors;
Administrative/Operational Use; 15 APR 1960.
Other requests shall be referred to Wright Air Development Division, Wright-Patterson AFB, OH 45433.

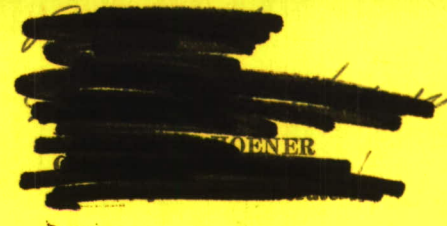
AUTHORITY

WL/AFSC ltr, 28 Mar 1961

THIS PAGE IS UNCLASSIFIED

ADO261976

WADD TECHNICAL REPORT 60-411 - PART I



PREDICTION OF CREEP EFFECTS IN AIRCRAFT STRUCTURES

C. W. Alesch, C. Riparbelli, W. H. Steurer and W. Robe

*Convair, A Division of General Dynamics Corporation
Engineering Department
San Diego, California*

ASTIA Release To OTS
Not Authorized

20080818 025

WRIGHT AIR DEVELOPMENT DIVISION

NOTICES

When Government drawings, specifications, or other data are used for any purpose other than in connection with a definitely related Government procurement operation, the United States Government thereby incurs no responsibility nor any obligation whatsoever; and the fact that the Government may have formulated, furnished, or in any way supplied the said drawings, specifications, or other data, is not to be regarded by implication or otherwise as in any manner licensing the holder or any other person or corporation, or conveying any rights or permission to manufacture, use, or sell any patented invention that may in any way be related thereto.



Qualified requesters may obtain copies of this report from the Armed Services Technical Information Agency, (ASTIA), Arlington Hall Station, Arlington 12, Virginia.



Copies of WADD Technical Reports and Technical Notes should not be returned to the Wright Air Development Division unless return is required by security considerations, contractual obligations, or notice on a specific document.

**PREDICTION OF CREEP EFFECTS IN
AIRCRAFT STRUCTURES**

C. W. Alesch, C. Riparbelli, W. H. Steurer and W. Robe

*Convair, A Division of General Dynamics Corporation
Engineering Department
San Diego, California*

Flight Dynamics Laboratory
Contract No. AF 33(616)-6567
Project No. 1367
Task No. 13584

WRIGHT AIR DEVELOPMENT DIVISION
AIR RESEARCH AND DEVELOPMENT COMMAND
UNITED STATES AIR FORCE
WRIGHT-PATTERSON AIR FORCE BASE, OHIO

AD261976

FOREWORD

This report was prepared by the Engineering Technical Materials Group, Engineering Department, Convair, A Division of General Dynamics Corporation, San Diego, California under Contract AF 33(616)-6567, "A Study of Structural Design Criteria, Covering Creep Prediction Methods for Structural Configuration." This contract was initiated under Project 1367, "Structural Design Criteria", Task No. 13584, "Design Criteria For Heated Airframes." This contract was administered under the direction of the Flight Dynamics Laboratory, Wright Air Development Division, with Lt. J. M. O'Connor and later Mr. R. M. Bader acting as project engineer.

This report covers the period of work from April 15, 1959 to April 15, 1960.

The Convair personnel who contributed to the project were: Dr. W. H. Steurer, Chief of Engineering Materials, Dr. Carlo Riparbelli, Structural Research Design Specialist, C. W. Alesch, Engineering Metallurgy Design Specialist, W. Robe, Structural Engineer, G. de Vries, Design Engineer, H. H. Stier, J. M. Harvey and W. M. Parker, Metallurgists, and A. T. Green and L. F. Minkler, Structural Test Engineers.

ABSTRACT

A step-by-step numerical process for introducing thermal and creep effects into a redundant structural analysis was developed. This process involves seven consecutive steps: (1) elastic thermal stress determination; (2) unit displacement determination in terms of stiffness patterns; (3) relaxation increment determination; (4) real thermal stress determination resulting from summation of thermal and relaxation stresses; (5) incremental stress determination; (6) determination of stress redistribution attendant to creep and (7) summation of elastic, thermal and creep stresses. Calibrations with model materials and structural elements, seeking verification of structural criteria introduced into numerical processes are demonstrated. An example problem for a delta wing illustrates method of calculation.

A critical re-examination of interpretative approaches for reducing creep data derived from materials tests into simplified form suitable for numerical analysis of redundant structures is introduced.

The creep test independent variables, time, temperature and stress, were examined with reference to their influence upon the dependent variable, strain. These examinations explored three fields of creep activity operative under conditions of (1) constant stress and constant temperature, (2) varying stress and constant temperature, and (3) constant stress and varying temperature. Comparisons of effects arising from constant stress and constant temperature creep exposure with those arising from cyclic stress and constant temperature exposures also are presented.

PUBLICATION REVIEW

This report has been reviewed and is approved.

FOR THE COMMANDER

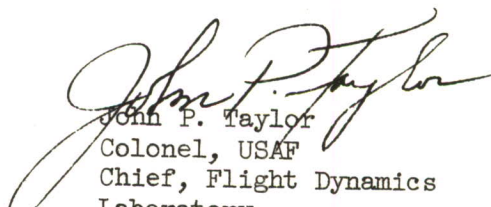

John P. Taylor
Colonel, USAF
Chief, Flight Dynamics
Laboratory

TABLE OF CONTENTS

		<u>Page</u>
I	Part I NUMERICAL METHOD FOR INTRODUCTION OF CREEP EFFECTS INTO STRUCTURAL ANALYSIS	1
	1. Introduction	1
	2. Basic Assumptions	2
	3. The Creep Threshold	3
	4. Overstress	3
	5. Viscosity Representation of Creep	3
	6. Limits of Useful Ranges of Plastic Strains	3
	7. Biaxial and Triaxial States of Stress	4
	8. Relaxation of Biaxially Stressed Panels	5
	9. Relaxation of Panels Rigidly Held at Their Edges	6
	10. Substructures	7
	11. Numerical Analysis: Synthesis Approach: Method Outline	7
	12. Numerical Analysis: Substructures Approach: Discussion	9
	13. List of References	10
II	Part II CALIBRATION METHODS IN SUPPORT OF NUMERICAL METHOD	16
	1. Introduction	16
	2. Calibration Method: Restrained Panels	16
	3. Calibration Method: Beams Under Pure Bending	16
	4. Calibration Method: Shear Panels	17
	5. Calibration Results: Restrained Panels	18
	6. Calibration Results: Beams Under Pure Bending	18
	7. Calibration Results: Shear Panels	19
III	Part III DEMONSTRATION OF NUMERICAL METHOD	43
	1. Plan For Problem Solution	43
	2. Example Problem Statement	44
	3. Assumptions Incorporated in Example Problem	45
	4. Example Problem Materials	45
	5. Example Problem Solution	45
	a. Stresses in The Locked Structure	45
	b. Stiffness Coefficients for Single Elements	46
	c. Stiffness Coefficients for Wing Structure	48
	d. Creep Effect	48
IV	Part IV MATERIALS CHARACTERISTICS IN RELATION TO CREEP AND ITS PREDICTION	129
	1. Introduction	129
	2. Significant Variables Influencing Materials Performance in Heated Environments	129
	3. The Deformation Variable	130
	4. "Standard" Creep Tests	131

TABLE OF CONTENTS
(Continued)

	<u>Page</u>
IV Part IV MATERIALS CHARACTERISTICS IN RELATION TO CREEP AND ITS PREDICTION (Continued)	
5. Limiting Deformation: Stress Strain Diagram Approach	131
6. Limiting Deformation: Creep (Time-Deformation) Diagram Approach	132
7. Strain Modes Appearing in Creep Tests	132
8. Incremental Loading Tests	133
a. Initial Incremental Loading Cycles	133
b. Secondary Incremental Loading Cycles	134
9. Repeated Loading Tests	136
10. Transient Heating Tests	137
11. Pulsed Cycle Heating Tests	138
12. Comparison of Effects of "Conventional" Creep With Those of "Pulsed Step Load" Creep	139
13. Summary of Test Findings	141
APPENDIX I - Bibliography	236
APPENDIX II - Material Data	245

LIST OF TABLES

<u>TABLE</u>	<u>TITLE</u>	<u>PAGE</u>
1	Position of Neutral Axis and Radius of Curvature of a Beam Under Simple Bending	20
2	Relationship of Uniaxial to Biaxial Loading-Criteria Verification Data	21
3	Effective Plastic Strains	23
4	Strain Rate Comparison	25
5	Thermal Stresses in Example Problem Wing	50
6	Computed Spar Element Stresses and Forces in Example Problem Wing	51
7	Stiffness Coefficient Matrix Multiplication For Front Spar in Example Problem Wing	52
8	Computed Rectangular Plate Stresses and Forces in Example Problem Wing	53
9	Stiffness Coefficients for Rectangular Plates In Example Problem Wing	54
10	Stiffness Coefficient Matrix for Triangular Plates in Example Problem Wing	56
11	Stiffness Coefficients for Triangular Plates In Example Problem Wing	58
12	Summary of Stiffness Coefficients and Displacements at Each Node of Example Problem Wing	60
13	Stiffness Coefficient Matrix for Example Problem Solution Input	73
14	Node Displacements in Example Problem Wing	77
15	Stiffness Coefficients, Forces and Displacements for Rectangular Panels in Example Problem Wing	78
16	Stiffness Coefficients, Forces and Displacements for Triangular Panels in Example Problem Wing	80
17	Stresses In Rectangular and Triangular Panels In Example Problem Wing	82
18	Strain Derivation and Stress Increments in Example Problem Wing Spars Exclusive of Front Spar	84
19	Stresses in Example Problem Wing Spars	86

LIST OF TABLES
(Continued)

<u>TABLE</u>	<u>TITLE</u>	<u>PAGE</u>
20	Stresses in Example Problem Wing Spar Webs	87
21	Principal Stress Computations for Example Problem Wing Panels at Time Zero	88
22	Angle of Principal Axes Computations for Example Problem Wing at Time Zero	89
23	Equivalent Uniaxial Stresses in Example Problem Wing Panels according to von Mises-Prager Criteria	90
24	Computations Involving Deviator Components in Example Problem Wing Panels	91
25	Creep Rates in Principal Directions and in the Elastic Strain Increment in "Locked" Example Problem Wing Panels	92
26	Rate of Change of Stress With Respect to Time in Principal Directions of Example Problem Wing	94
27	Principal Stress Increments Arising From Relaxation in Locked Example Problem Wing Panels After a Creep Interval of 4 Minutes	95
28	Stress Increments Due to Relaxation in Locked Panels of Example Problem Wing	96
29	Shear Stress Increments Due to Relaxation in Locked Panels of Example Problem Wing	97
30	Force Input at Locked Nodes of Rectangular Plates in Example Problem Wing	98
31	Force Input at Locked Nodes of Triangular Plates in Example Problem Wing	100
32	Resultant Forces in "x" Direction at Locked Nodes of Example Problem Wing	102
33	Resultant Forces in "y" Direction at Locked Nodes of Example Problem Wing	103
34	Spar Cap Stress Arising From Node Unloading in Example Problem Wing	104
35	Stress Increments Arising In Spar Caps From Node Unlocking in Example Problem Wing	106
36	Strain Increments Arising From Node Unlocking in Example Problem Wing Panels	107

LIST OF TABLES
(Continued)

<u>TABLE</u>	<u>TITLE</u>	<u>PAGE</u>
37	Distortion Increments Arising From Node Unlocking in Example Problem Wing Panels	109
38	Stress Increments Arising From Node Unlocking in Example Problem Wing Panels	110
39	Resultant Stresses in Example Problem Wing After 4 Minute Creep Interval	111
40	Conditions of Test and Pertinent Data Point Values Found in "Standard" Creep Tests	143
41	Effect of Various Temperatures on the Modulus of Elasticity of Aluminum Alloys	245
42	Average Coefficient of Thermal Expansion for Some Aluminum Alloys	246
43	Average Coefficient of Thermal Expansion for Various Metals	246

LIST OF FIGURES

<u>FIGURE</u>	<u>TITLE</u>	<u>PAGE</u>
1	Creep Rates at Constant Stress Levels (Schematic. See Figures 23 through 26 numerical data)	11
2	Creep Rate as a Function of Stress and Plastic Strain at Constant Temperature (Schematic)	12
3	"Threshold" and Lines of Equal Initial Creep in the Stress - Temperature Plane (Schematic)	13
4	"Threshold" Surface in the Stress - Strain Temperature Space. (Schematic)	14
5	Condition of Plasticity for Biaxial Stress	15
6	Test Specimen Assembly	26
7	Residual Strain in Aluminum Plates	27
8	Creep Bending of a Beam - Lines of Equal Time Rate of Curvature (Schematic)	28
9	Beam Test Apparatus (Schematic)	29
10	Test Beam Assembly and Supports	30
11	Test Beam Instrumentation and Supports	31
12	Uniaxial Loading State Test Apparatus	32
13	Biaxial Loading State Test Apparatus	33
14	Test Panel Instrumentation and Restraining Plates Used in Biaxial Tests	34
15	Incremental Strain - Bending Moment Relationships in Test Beams	35
16	Incremental Strain - Bending Moment Relationships in Test Beams	36
17	Stress - Strain - Time Relationships for Various Thicknesses of Copper in Tension	37
18	Stress - Strain - Time Relationships for Various Thicknesses of Copper in Shear	38
19	Stress - Strain - Time Relationships for Various Thicknesses of Lead in Tension	39
20	Stress - Strain - Time Relationships for Various Thicknesses of Lead in Shear	40

LIST OF FIGURES
(Continued)

<u>FIGURE</u>	<u>TITLE</u>	<u>PAGE</u>
21	Stress - Strain - Time Relationships for Various Thicknesses of Aluminum in Tension	41
22	Stress - Strain - Time Relationships for Various Thicknesses of Aluminum in Shear	42
23	A Possible Subdivision of a Delta Wing into Sub-structures (Schematic)	112
24	Node Point Location and Attachment Scheme for Example Problem Wing	113
25	Force Input at Nodes of Locked Example Problem Wing	114
26	Node Forces on Triangular Panels in Example Problem Wing	115
27	Stiffness Coefficients for Beam Elements in Example Problem Wing	116
28	Stiffness Coefficients for Beam Elements in Example Problem Wing	117
29	Oblique Frame Elements in Example Problem Wing	118
30	Stiffness Coefficients for Front Spar (Oblique Bar) in Example Problem Wing	119
31	Mode of Displacement of Nodes of Example Problem Wing After Unlocking	120
32	Thermal Stresses In Spar Caps of Example Problem Wing	121
33	Thermal Stresses In Spar Webs of Example Problem Wing	122
34	Thermal Stresses In Panels of Example Problem Wing	123
35	Creep Rates for 75 S-T Aluminum Alloy at 300°F	124
36	Creep Rates for 75 S-T Aluminum Alloy at 400°F	125
37	Creep Rates for 75 S-T Aluminum Alloy at 600°F	126
38	Creep Rates for 75 S-T Aluminum Alloy at 450°F	127
39	Creep Rate for 75 S-T Aluminum Alloy at 450°F at One Minute	128
40	Time-Deformation Data, Armco PH 15-7 Mo 700°F, 180 KSI, "Standard" Creep Test	144

LIST OF FIGURES
(Continued)

<u>FIGURE</u>	<u>TITLE</u>	<u>PAGE</u>
41	Time-Deformation Data, Armco PH 15-7 Mo 700°F., 180 KSI, "Standard" Creep Test	145
42	Time-Deformation Data, Armco PH 15-7 Mo 700°F., 182 KSI, "Standard" Creep Test	146
43	Time-Deformation Data, Armco PH 15-7 Mo 700°F., 182 KSI, "Standard" Creep Test	147
44	Time-Deformation Data, Armco PH 15-7 Mo 800°F., 170 KSI, "Standard" Creep Test	148
45	Time-Deformation Data, Armco PH 15-7 Mo 800°F., 170 KSI, "Standard" Creep Test	149
46	Time-Deformation Data, Armco PH 15-7 Mo 800°F., 175 KSI, "Standard" Creep Test	150
47	Time-Deformation Data, Armco PH 15-7 Mo 800°F., 175 KSI, "Standard" Creep Test	151
48	Time-Deformation Data, Armco PH 15-7 Mo 900°F., 130 KSI, "Standard" Creep Test	152
49	Time-Deformation Data, Armco PH 15-7 Mo 900°F., 130 KSI, "Standard" Creep Test	153
50	Time-Deformation Data, Armco PH 15-7 Mo 900°F., 135 KSI, "Standard" Creep Test	154
51	Time-Deformation Data, Armco PH 15-7 Mo 900°F., 135 KSI, "Standard" Creep Test	155
52	Time-Deformation Data, Armco PH 15-7 Mo 1000°F., 55 KSI, "Standard" Creep Test	156
53	Time-Deformation Data, Armco PH 15-7 Mo 1000°F., 55 KSI, "Standard" Creep Test	157
54	Time-Deformation Data, Armco PH 15-7 Mo 1000°F., 77 KSI, "Standard" Creep Test	158
55	Time-Deformation Data, Armco PH 15-7 Mo 1000°F., 77 KSI, "Standard" Creep Test	159
56	"Make-up" of Loading Strains in "Standard" Creep Tests with Armco PH 15-7 Mo	160

LIST OF FIGURES
(Continued)

<u>FIGURE</u>	<u>TITLE</u>	<u>PAGE</u>
57	"Make-up" of Unloading Strains in "Standard" Creep Tests with Armco PH 15-7 Mo.	161
58	Comparison of Time Independent Strains Observed upon Loading and Unloading "Standard" Creep Tests with Armco PH 15-7 Mo at 700°F and 800°F.	162
59	Comparison of Time Independent Strains Observed upon Loading and Unloading "Standard" Creep Tests with Armco PH 15-7 Mo at 900°F and 1000°F.	163
60	Comparison of Total Elastic Recovery Observed upon Unloading "Standard" Creep Tests with Armco PH 15-7 Mo at 700°F and 800°F with the Input Strain Converted into Permanent Set upon Loading	164
61	Comparison of Total Elastic Recovery Observed upon Unloading "Standard" Creep Tests with Armco PH 15-7 Mo at 900°F and 1000°F with the Input Strain Converted into Permanent Set upon Loading	165
62	Typical Field of Deformation Activity Observed upon Incremental Step Loading Armco PH 15-7 Mo at Elevated Temperature	166
63	Typical Field of Deformation Activity Observed upon Unloading Incremental Step Loaded Armco PH 15-7 Mo at Elevated Temperatures	167
64	Program for Incremental Step Loaded Test (Schematic)	168
65	Time-Deformation Data Armco PH 15-7 Mo 700°F, 185 KSI, Incremental Step Loading (Loading Condition)	169
66	Time-Deformation Data Armco PH 15-7 Mo 700°F., 185 KSI, Incremental Step Loading (Loading Condition)	170
67	Time-Deformation Data Armco PH 15-7 Mo 700°F., 185 KSI, Incremental Step Loading (Unloading Condition)	171
68	Time-Deformation Data Armco PH 15-7 Mo 800°F., 175 KSI, Incremental Step Loading (Loading Condition)	172
69	Time-Deformation Data Armco PH 15-7 Mo 800°F., 175 KSI, Incremental Step Loading (Unloading Condition)	173
70	Time Deformation Data Armco PH 15-7 Mo 900°F., 135 KSI, Incremental Step Loading (Loading Condition)	174

LIST OF FIGURES
(Continued)

<u>FIGURE</u>	<u>TITLE</u>	<u>PAGE</u>
71	Time-Deformation Data Armco PH 15-7 Mo 900°F., 135 KSI, Incremental Step Loading (Loading Condition)	175
72	Time-Deformation Data Armco PH 15-7 Mo 900°F., 135 KSI, Incremental Step Loading (Unloading Condition)	176
73	Time-Deformation Data Armco PH 15-7 Mo 1000°F., 77 KSI, Incremental Step Loading (Loading Condition)	177
74	Time-Deformation Data Armco PH 15-7 Mo 1000°F., 77 KSI, Incremental Step Loading (Loading Condition)	178
75	Time-Deformation Data Armco PH 15-7 Mo 1000°F., 77 KSI, Incremental Step Loading (Unloading Condition)	179
76	"Make-up" of Loading Strains in Increment Loaded Creep Tests with Armco PH 15-7 Mo.	180
77	"Make-up" of Unloading Strains in Increment Loaded Creep Tests with Armco PH 15-7 Mo.	181
78	Comparison of Strains Incidental to Loading with Elastic Strain Recovery Occurring Upon Load Release (700° F & 800°F).	182
79	Comparison of Strain Incidental to Loading with Elastic Strain Recovery Occurring Upon Load Release (900°F & 1000°F)	183
80	Program for Repeated Load Tests	184
81	Strains Resulting from Successive Applications of 182 KSI Load to Armco PH 15-7 Mo at 700°F.	185
82	Strains Resulting from Successive Applications of 175 KSI Load to Armco PH 15-7 Mo at 800°F.	186
83	Strains Resulting from Successive Applications of 135 KSI Load to Armco PH 15-7 Mo at 900°F.	187
84	Strains Resulting from Successive Applications of 77 KSI Load to Armco PH 15-7 Mo at 1000°F.	188
85	"Make-up" of Strain Patterns Occurring Upon Load Release in Repeated Loading Tests (700°F 182 KSI Stress)	189
86	"Make-up" of Strain Patterns Occurring Upon Load Release in Repeated Loading Tests (800°F 175 KSI Stress)	190
87	"Make-up" of Strain Patterns Occurring Upon Load Release in Repeated Loading Tests (900°F 135 KSI)	191

LIST OF FIGURES
(Continued)

<u>FIGURE</u>	<u>TITLE</u>	<u>PAGE</u>
88	"Make-up" of Strain Patterns Occurring Upon Load Release in Repeated Loading Tests (1000°F, 77 KSI)	192
89	Strain Changes Incidental to Repeated Load Tests (700°F, 182 KSI)	193
90	Strain Changes Incidental to Repeated Load Tests (800°F, 175 KSI)	194
91	Strain Changes Incidental to Repeated Load Tests (900°F, 135 KSI)	195
92	Strain Changes Incidental to Repeated Load Tests (1000°F, 77 KSI)	196
93	Permanent Set Accumulation Observed in Repeated Load Tests Run at Various Temperatures	197
94	Elastic Recovery Accumulation Observed in Repeated Load Tests Run at Various Temperatures	198
95	Program for Transient Heating Tests	199
96	Initial Cycle, Transient Heating Creep Curves	200
97	Initial Cycle, Transient Heating Creep Curves (Logarithmic 700° & 800°F)	201
98	Initial Cycle Transient Heating Creep Curves (Logarithmic 900° & 1000°F)	202
99	Strain Transition - Temperature Relations in Initial Transient Heating Cycles	203
100	Initial Cycle Transient Heating Creep Curves for Constant Temperature Varying Stress Conditions	204
101	Initial Cycle Transient Heating Creep Curves for Constant Stress, Varying Temperature Conditions (700°F, 182 & 185 KSI)	205
102	Initial Cycle Transient Heating Creep Curves for Constant Stress, Varying Temperature Conditions (700°F, 188 & 191 KSI)	206
103	Strain Transition - Temperature Relations in Initial Transient Heating Cycles	207

LIST OF FIGURES
(Continued)

<u>FIGURE</u>	<u>TITLE</u>	<u>PAGE</u>
104	Transient Heating Creep Curves (700°F, 182 KSI)	208
105	Transient Heating Creep Curves (700°F, 185 KSI)	209
106	Transient Heating Creep Curves (700°F, 188 KSI)	210
107	Transient Heating Creep Curves (700°F, 191 KSI)	211
108	Transient Heating Creep Curves (800°F, 175 KSI)	212
109	Transient Heating Creep Curves (900°F, 135 KSI)	213
110	Transient Heating Creep Curves (1000°F, 77 KSI)	214
111	Program for Pulsed Heating Tests	215
112	Pulsed Heating Creep Curves (700°F)	216
113	Pulsed Heating Creep Curves (800°F)	217
114	Pulsed Heating Creep Curves (900°F)	218
115	Pulsed Heating Creep Curves (1000°F)	219
116	Effect of Stress Variation at 700°F Upon 5 Minute Pulsed Heating Creep	220
117	Effect of Stress Variation at 900°F Upon 5 Minute Pulsed Heating Creep	221
118	Effect of Stress Variation at 1000°F Upon 5 Minute Pulsed Heating Creep	222
119	Effect of Stress Variation at 1000°F Upon 25 Minute Pulsed Heating Creep	223
120	Effect of Stress Variation at 700 °F Upon 125 Minute Pulsed Heating Creep	224
121	Effect of Stress Variation at 900°F Upon 125 Minute Pulsed Heating Creep	225
122	Effect of Stress Variation at 1000°F Upon Pulsed Heating Creep at Various Stress Levels	226
123	Effect of Pulse Time Variation at Constant Stress at 700°F on Pulsed Creep (180 KSI)	227

LIST OF FIGURES
(Continued)

<u>FIGURE</u>	<u>TITLE</u>	<u>PAGE</u>
124	Effect of Pulse Time Variation at Constant Stress at 700°F on Pulsed Creep (185 KSI)	228
125	Effect of Pulse Time Variation at Constant Stress at 1000°F on Pulsed Heating Creep (77 KSI)	229
126	Effect of Pulse Time Variation at Constant Stress at 1000°F on Pulsed Heating Creep (60 KSI)	230
127	Effect of Stress and Temperature Variation at 5 Minute Pulse Intervals Upon Creep	231
128	Effect of Stress and Temperature Variation at 125 Minute Pulse Intervals Upon Creep	232
129	Program for Pulsed Step Load Tests	233
130	Comparisons of Creep Resulting From Constant Stress - Constant Temperature and Pulsed Step Loading - Constant Temperature Applications	234
131	Comparison of Creep Trends in Constant Stress and Pulsed Step Load Tests	235

LIST OF SYMBOLS

<u>SYMBOL</u>	<u>REPRESENTATION</u>
t	time (min)
E	modulus of elasticity (lbs/in ²)
ν	Poisson's ratio
α	thermal expansion coefficient (°F) ⁻¹
T	Temperature (°F)
σ	normal stress (with subscripts) (lbs/in ²)
τ	shear stress (with subscripts) (lbs/in ²)
$\sigma_1, \sigma_2, \sigma_3$	principal stresses (lbs/in ²)
p	hydrostatic term of the normal stress distribution (lbs/in ²)
s_1, s_2, s_3	components of the deviator (lbs/in ²)
ϵ_e	elastic unit elongation component
ϵ_p	plastic unit elongation component
$\dot{\epsilon}_p$	creep rate (min ⁻¹)
γ	distortion
$\dot{\gamma}_p$	time rate of plastic distortion (min ⁻¹)
S	power dissipated per unit volume (lb in ² sec ⁻¹)
ξ	ratio of the principal stresses in the panel
U, u	displacement in horizontal (x) direction
V, v	displacement in vertical (y) direction
K	stiffness coefficient

PREDICTION OF CREEP EFFECTS

IN

AIRCRAFT STRUCTURES

PART I

NUMERICAL METHOD FOR INTRODUCTION OF CREEP EFFECTS INTO STRUCTURAL ANALYSIS

INTRODUCTION

A method for introducing creep factors into numerical structural analysis is presented. The creep effect is assumed to be both small and local so that creep deformation may be tolerated, to an extent, in structures exposed to the combined action of loads and high temperatures. The introduction of creep factors into numerical structural analysis aims primarily to extend the limits of velocity and acceleration to which a material and a structure built from it can be submitted for a limited time.

The word "creep" as used herein connotes a time dependent plastic deformation activated by heat. The dependence of creep upon time, a characteristic implied in all plastic deformations, is essential in the definition of creep. Rigorously speaking, time is always a factor in plastic flow. Practically speaking, creep becomes significant when the rate at which it takes place is appreciable to our senses and measurements. By "creep rate" the partial derivative of the plastic deformation with respect to time "for constant stress" is meant, but this does not mean that in a practical structure the stress must actually remain constant in conformance with mathematical visualization. Also, since creep (time rate of plastic deformation at constant stress) and relaxation (time rate of stress decrease at constant strain) are practically the same thing, distinction in this regard is not made herein. In fact plastic deformation is introduced into the numerical process in the form of a relaxation term.

The nature of plastic deformation, including creep and relaxation is presently explained in the dislocation theory of crystals (1)(2)*, and its discussion is beyond the scope of this report. Its essential features need, however, to be borne in mind for a rational, even if crude representation needed for a numerical analysis.

The constitution of the equilibrium of a dissipative system, such as a structure undergoing deformation, depends at any time upon the sequence of the deformations involved in the history of the structure. Accordingly a numerical solution for equilibrium must necessarily be found for successive time intervals. The effects of various loads cannot be superimposed irrespective of their sequence as, by way of contrast, can be done in a linear elastic system.

* Numbers in parentheses indicate literature references listed on Page 10.

Manuscript released by the authors 30 June 1960 for publication as a WADD Technical Report.

If the plastic strain component is appreciable, it cannot be introduced in one lump because the stresses depend on the plastic deformation and further plastic deformation depends on the stresses. This physical fact finds its counterpart in the time dependence of the plastic flow. Even if plastic strain of appreciable magnitude appears within a negligible time compared to the total assumed duration time, it is still necessary to divide it into fractions and to introduce these in the structural analysis, taking into account the change caused in the stresses at each step.

BASIC ASSUMPTIONS

When a material segment of finite length is inscribed on a structural element, this length undergoes a change, ΔL , after a time lapse, Δt , at a temperature, T . In the elongation, ΔL , three terms can be distinguished: a thermal expansion, $\alpha \Delta T$; an elastic strain component, ϵ_e ; and a plastic strain component, ϵ_p . In terms of unit elongation

$$\frac{\Delta L}{L} = \epsilon_e + \epsilon_p + \alpha \cdot \Delta T \quad (1)$$

of which:

- ϵ_e represents reversible, time independent, temperature dependent elongation,
- ϵ_p represents irreversible, time dependent, temperature dependent elongation, and
- $\alpha \Delta T$ represents reversible, time independent, temperature dependent elongation.

A unit-elastic elongation is related to stress by means of Hooke's law and the strain is simultaneous with the stress. Plastic strain is the result of "slip" at certain surfaces within crystals and depends on the history of shear stress at these slip surfaces. Upon application of load, plastic strain, if any, follows in time:

$$\epsilon_p = \int_0^t \dot{\epsilon}_p dt \quad (2)$$

and it is a deformation at constant volume.

In a region of a structure under a given time dependent load and, in which the temperature and the state of stress are also known, only elastic strain, perfectly reversible, will be observed up to a certain limiting stress. The limiting stress is dependent on the state of stress, on the temperature and on the past history of the stresses. When the stress is increased above the limiting stress, or what amounts to the same thing, the state of stress is maintained and the temperature is increased, plastic flow, delayed in time with respect to the stress increment (3) is observed to take place at a rate usually decreasing, and, provided the stress is constant, this decrease proceeds until it becomes negligible. In the method at hand those conditions which define the occurrence of negligible creep are said to define the points of creep threshold in the stress plane: $\sigma(\epsilon_p)$.

If stress is diminished, under conditions of creep, the elastic strain incorporated in the overall deformation diminishes according to Hooke's law. The plastic deformation, however, does not reverse appreciably until the direction of the shear at the slip surfaces is deliberately reversed. This view omits consideration of self induced plastic deformation reversal under conditions of stress diminution (strain recovery). This omission is made in view of a need for a simplified representation.

THE CREEP THRESHOLD

In order to introduce the creep effect into numerical analysis, the usual diagrams showing creep deformation with respect to time under constant stress and temperature conditions are used. In using this information, data in the region of primary creep are required, but under current conditions are seldom available. When data plots are available which show creep rates in stress-strain planes for given temperatures, as shown in Figure 1 which is extrapolated from data given in (4), they also may be used. In this approach lines are traced through points which represent stresses at which the creep rate has a small value which is arbitrarily called negligible and is known as "threshold". The arbitrary, negligible creep rate utilized in Figure 1 is $\dot{\epsilon} = 3 \times 10^{-5} \text{ min}^{-1}$. The "threshold" is defined as $\bar{\sigma} = \bar{\sigma}(\epsilon_p)$.

OVERSTRESS

Below the threshold, creep is considered negligible and is set equal to zero. Above the threshold creep occurs at a rate increasing as the distance of points of observation recede from the threshold. In plots of the kind shown in Figure 1 lines of equal creep rate can be interpolated to produce a diagram of the kind shown in Figure 2 in which the "overstress" ($\sigma - \bar{\sigma}$) is indicated for a certain stress and strain related by point A of Figure 2, for example. In charts of the kind shown by Figure 2 the lines of equal creep rates corresponding to equal increments in the creep rates are not equally spaced because the creep rate is not a linear function of the overstress. For instance the representation

$$\dot{\epsilon}_p = A \sinh(\sigma - \bar{\sigma}) \quad (3)$$

was proposed in the past (5), (6).

VISCOSITY REPRESENTATION OF CREEP

It is convenient to use a representation of creep by means of an equation of the viscosity type (7) (8) such as:

$$\begin{aligned} \dot{\epsilon}_p &= 0 & \text{for } |\sigma| \leq |\bar{\sigma}| \\ \epsilon_p &= K(\sigma - \bar{\sigma}) & \text{for } |\sigma| > |\bar{\sigma}| \end{aligned} \quad (4)$$

In general, K , is not a constant. It can, however, be considered a constant in well behaved materials wherein phase changes in the temperature ranges considered are absent and the overstress and strain increments are small. A representation according to a viscosity law of the type of equation (4), obtained by linearizing the true creep law in the neighborhood of the threshold of creep, is useful for computation because it offers a rational basis for the use of the condition of plasticity in dealing with creep.

LIMITS OF USEFUL RANGES OF PLASTIC STRAINS

The plastic strain components in the stress and deformation analysis described here is limited to "small" plastic strains, that is to plastic strain components of the same order as the maximum elastic strain that can be imposed at the same region of the structural element considered. For instance if a uniaxial stress of 180,000 lbs/in² in a steel member is allowed, an elastic strain of 6×10^{-3} follows and it may be decided to limit analysis to plastic deformations in the order of 1% or at

most 2%. The allowable maximum creep rates corresponding to the 1% to 2% plastic strain mentioned will be determined by the total time of the high speed and high load factor phases of flight during which creep may be allowed. For instance, if a plastic strain of 1% during a combat phase of a flight of 30 minutes duration is allowed, it will be necessary to consider those combinations of stresses and temperatures which will produce creep rates averaging $3 \times 10^{-4} \text{ min}^{-1}$ throughout aircraft life.

The reasons for such limitations are the following:

1. In applications involving aircraft structures, plastic strain components of the same order as the elastic ones are sufficient to cause basic changes in stress distributions and in deflections. This range of strain relations is therefore important in structural analysis.
2. Aerodynamic and dynamic considerations limit permissible deformations in ordinary flight conditions.
3. Because of the complexity of creep, a feasible representation of its action needs to be limited to a narrow range, essentially to a fraction of the primary creep range, with exceptions.
4. No plastic component of strain was ever allowed previously in aircraft structures within limit load, except a residual 2×10^{-3} considered negligible. This convention will be maintained herein. In other words no appreciable plastic deformation is assumed under conditions wherein plastic deformation occurs in negligible time, especially when this time is negligible in comparison with that assumed for creep action. On the same ground creep rates apt to produce plastic deformations of 2×10^{-3} strain within assumed times are neglected. Consequently, combinations of temperatures and states of stress are defined wherein creep rates are assumed to be negligible. Such combinations are limited by a "threshold" as depicted in Figures 1, 2, 3 and 4.

BIAXIAL AND TRIAXIAL STATES OF STRESS

While most available test data pertaining to creep are obtained under uniaxial and constant stress, biaxial and triaxial strain rates need be introduced into numerical stress analysis. For this purpose the von Mises condition of plasticity is applied to creep according to Prager's suggestion to furnish a working assumption (8), (9) and (10). In essence the von Mises condition of plasticity defines a relation among the stress components for which plastic deformation will appear. All that is required in addition to this is the amount of plastic strain which can be considered non-negligible and how long stresses may act before creep strains evidence themselves.

Specifically, when the principal stresses σ_1 , σ_2 and σ_3 are given, the value of the invariant of the stress tensor, T , is computed as follows:

$$T = (\sigma_1 - \sigma_2)^2 + (\sigma_2 - \sigma_3)^2 + (\sigma_3 - \sigma_1)^2 \quad (5)$$

and this is equated to its value, $2\sigma_0^2$, in the corresponding uniaxial stress condition. Then σ_0 is entered in a diagram as shown in Figure 1 or Figure 2, and the creep rate, $\dot{\epsilon}_{po}$, in the corresponding uniaxial condition is found. In addition the hydrostatic term of the given state of stress is computed as follows:

$$p = 1/3 (\sigma_1 + \sigma_2 + \sigma_3) \quad (6)$$

along with the components of the stress deviator

$$\begin{aligned}s_1 &= \sigma_1 - p \\ s_2 &= \sigma_2 - p \\ s_3 &= \sigma_3 - p\end{aligned}\tag{7}$$

Then since the power dissipated per unit volume in the uniaxial specimen is

$$S = \sigma_o \cdot \dot{\epsilon}_o\tag{8}$$

it is possible to proceed under the following working assumptions:

1. The power dissipated per unit volume under the von Mises-Prager rule is the same value as the invariant in equation (5).
2. For a given state of stress the strain rate components are such that the power dissipated is a maximum (11), (12) and (13). If the deviator components are visualized as the components of a vector and the strain rate components as the components of another vector, the power dissipated is a maximum if the scalar product of these two vectors is a maximum. Therefore the creep rates will be proportional to the components of the deviator.

These two conditions are written:

$$S = s_1 \dot{\epsilon}_1 + s_2 \dot{\epsilon}_2 + s_3 \dot{\epsilon}_3 = \sigma_o \dot{\epsilon}_o\tag{9}$$

$$\frac{s_1}{\dot{\epsilon}_1} = \frac{s_2}{\dot{\epsilon}_2} = \frac{s_3}{\dot{\epsilon}_3} = \gamma = \text{const.}\tag{10}$$

Consequently

$$\gamma = \frac{s_1^2 + s_2^2 + s_3^2}{\sigma_o \dot{\epsilon}_o}\tag{11}$$

from which the creep rates are determined.

RELAXATION OF BIAXIALLY STRESSED PANELS

In the case of biaxially stressed panels, the stress normal to the surface is zero. Assuming the principal stresses, σ_1 and σ_2 , in the plane of the panel are known at a certain time, while $\sigma_3 = 0$, equation (5) is written

$$\sigma_1^2 + \sigma_2^2 - \sigma_1 \sigma_2 = \sigma_o^2\tag{12}$$

Then for a given value of one of the two principal stresses, for instance the larger in absolute value, any plane stress distribution may be represented by

$$\sigma_2 = \xi \sigma_1 \quad -1 < \xi < 1\tag{13}$$

Giving recognition to particular cases:

$$\xi = 1 \quad \sigma_2 = \sigma_1 \quad \text{Hydrostatic plane stress} \quad (14)$$

$$\xi = 0 \quad \sigma_2 = 0 \quad \text{Uniaxial stress} \quad (15)$$

$$\xi = -1 \quad \sigma_2 = -\sigma_1 \quad \text{Pure shear} \quad (16)$$

equation (12) may be written:

$$\sigma_1^2 (1 + \xi^2 - \xi) = \sigma_0^2 \quad (17)$$

from which

$$\frac{\sigma_0}{\sigma_1} = \pm \sqrt{1 + \xi^2 - \xi} \quad (18)$$

Equation (18) relates the maximum absolute stress in the biaxial stress distribution to the uniaxial stress, σ_0 , to be introduced in the diagram giving the creep rate.

Equation (18) is plotted in Figure 5. If $\sigma_2 = \sigma_1$, hydrostatic plane stress, the condition of plasticity is the same as if $\sigma_2 = 0$, uniaxial stress. In the case of pure shear $\sigma_2 = -\sigma_1 = C$ the condition is reached for a value of the shear stress smaller than for the uniaxial stress by a factor of 1.73.

The deviator components for the case of biaxial stress are (equation 7)

$$s_1 = \frac{2}{3} \sigma_1 - \frac{1}{3} \sigma_2 \quad (19)$$

$$s_2 = \frac{2}{3} \sigma_2 - \frac{1}{3} \sigma_1 \quad (20)$$

$$s_3 = \frac{1}{3} (\sigma_1 + \sigma_2) \quad (21)$$

and in general all three differ from zero.

RELAXATION OF PANELS RIGIDLY HELD AT THEIR EDGES

In this case the assumption is made that the plane state of stress is uniform in a panel and that its components are known and expressed in terms of the principal stresses and the orientation of their axes. There by means of equation (18) the equivalent uniaxial stress, σ_0 , is computed. This stress is next introduced into the experimental diagram shown in Figure 1 where $\dot{\epsilon}_{p0}$ is obtained. Following this the deviator components are computed from equations 19, 20, 21 and the known components of the plane state of stress. Finally from equations (10) and (11) the creep rates in the directions of the principal axes in the plane of the panel are computed. These creep rates are assumed to remain constant during a time interval, Δt , which is chosen to be sufficiently short for the assumed condition to be fulfilled. In addition the temperature is also assumed to be constant during the time interval, Δt .

The conditions of zero elongation in both directions, denoted subscript 1 and 2, give rise to

$$\dot{\epsilon}_{p_1} \Delta t + \frac{1}{E} (\Delta \sigma_1 - \nu \Delta \sigma_2) = 0 \quad (22)$$

$$\dot{\epsilon}_{p_2} \Delta t + \frac{1}{E} (\Delta \sigma_2 - \nu \Delta \sigma_1) = 0 \quad (23)$$

which when solved for the stress increments in the direction of the principal axes, result in

$$\Delta \sigma_1 = - \frac{E}{1-\nu^2} \left(\dot{\epsilon}_{p_1} + \nu \dot{\epsilon}_{p_2} \right) \Delta t \quad (24)$$

$$\Delta \sigma_2 = - \frac{E}{1-\nu^2} \left(\dot{\epsilon}_{p_2} + \nu \dot{\epsilon}_{p_1} \right) \Delta t \quad (25)$$

The stress increments are determined by the increments of elastic strain, according to Hooke's law. Poisson's ratio has the value of $\nu \approx .3$ as in most materials for the application of Hooke's law. The increments of plastic strain appear in equations (24) and (25) inasmuch as they are equal and opposite to the increments of elastic strain in the relaxation process considered. From $\Delta \sigma_1$ and $\Delta \sigma_2$ the increments of the stress components in the direction of the sides of the panel or in any other chosen direction may be computed.

The relaxation process due to creep is an essential part of the numerical analysis. In the form described here it is only a rational guide to the systematic interpretation of test data.

SUBSTRUCTURES

As used herein, the word "substructure" denotes a region of a structure limited by an arbitrarily chosen boundary which is so selected that the stiffness measured on the substructure, taken separately, is the stiffness of the real structure at the region considered. A substructure is composed of several structural elements and its stiffness depends on the stiffness of the elements which compose it and includes their interaction, local instability, connections, etc. For example, a grid of conveniently spaced planes may be traced by means of lines drawn on the planform of a wing, thus defining boxes which are considered substructures. Each box, in turn is comprised of panels, stringers webs, etc. In the assessment of this, a number of boxes can be built and tested to observe the displacement versus time of a node or of a section with respect to a reference plane during the time known external loads and a known heat input are imposed.

NUMERICAL ANALYSIS: SYNTHESIS APPROACH: METHOD OUTLINE

The case of a structure whose mechanical model is composed of single elements such as stringers, plates, etc. is considered first. These elements are joined at nodes at which internal forces equivalent to the stresses and external forces equivalent to the given loads are applied. Consequently the structure may be viewed as being

synthesized from elementary components. The deformation of a resultant structure is accordingly represented by means of displacements of the nodes. The states of stress and the temperature in each element are represented by nominal values as if they were uniform throughout the element.

In analysis, the stiffness coefficients for each element are computed first and they depend on the modulus of elasticity of the material used. The modulus of elasticity in turn depends on the temperature. The stiffness coefficients relate to forces acting on elements with the elastic deformation component only. Continuity of structure is preserved at all times because the nodes are common to the joined elements. The equations used in analysis fulfill the condition of equilibrium and define the positions of the nodes.

The stress analysis is performed by a step by step process. Each step of the analytical process covers a time interval, Δt , and consists essentially of five phases. Analysis is started at time, t , at which the structure is in equilibrium and its configuration and state of stress are known at all elements. The analytical steps are as follows:

PHASE I. All the nodes of the structure are locked to a jig of infinite rigidity. The temperature increment, ΔT , corresponding to the time interval, Δt , is applied at each structural element. The corresponding "hydrostatic" stress terms are computed. These have the form

$$\Delta \sigma_n = -E \alpha \Delta T \quad (26)$$

for bars and stringers and the form

$$\Delta \sigma_x = \Delta \sigma_y = \frac{E \alpha}{1-\nu} \Delta T \quad (27)$$

for panels.

Using these stress terms, the stresses acting within the structural elements are computed and at the node points these stresses are replaced with equivalent forces acting at the nodes. Then increments of external loads are applied during the same time interval used in arriving at the stress terms and then these are replaced with equivalent concentrated forces at the nodes. Finally the resultant forces at the nodes and their components in the direction of chosen coordinate axes are computed.

PHASE II. Starting with the conditions established in Phase I, which reflect conditions of non-equilibrium, the node displacements necessary to reestablish equilibrium on the "unlocked" structure are determined. Following this the stresses corresponding with the displaced node conditions are computed. At this point the stress analysis, considering thermal effects but neglecting creep in the time interval considered, has been performed.

PHASE III. The average stresses in the time interval considered are estimated according to creep rates which are recorded on calibration diagrams derived from experiment. The creep rates are interdependent with stresses. A stress increment corresponding to a convenient fraction of the overstress and the time interval consistent with this overstress may be alternatively chosen for stabilization.

In this step it is necessary to take into account the "weight" of the section areas under creep versus the remaining section areas in order to predict the change of stress caused by creep.

PHASE IV. The structure is again "locked" at the nodes and then the force increments corresponding to the stress relaxation terms over the whole time interval are introduced.

PHASE V. The deformation analysis of the structure is repeated as in Phase II on the basis of the force increments determined in Phase IV. The corresponding stress increments due to relaxation are added to those found in Phase II.

The process deals with stress relieving increments and therefore it is inherently convergent.

NUMERICAL ANALYSIS: SUBSTRUCTURES APPROACH: DISCUSSION

The numerical analysis is simpler and more reliable if calibration tests directly obtained in substructures are available. Then, for a given heat input per time unit, or, for a given boundary layer temperature, direct data on thermic deformation and on creep rates which depend on thermic effect and on the applied load are provided. In this situation the numerical analysis is done by the same essential steps already outlined.

The numerical process described above takes advantage of the digital computer and is preferred because of the labor saving advantage gained thereby. Otherwise a solution could be obtained by more laborious relaxation methods which introduce the groups of internal "forces" with zero resultant in those regions where creep occurs.

LIST OF REFERENCES

1. Cottrell, A. H., "Dislocations and Plastic Flow in Crystals", Oxford University, Press, 1953.
2. Freudentahl, A. H., "The Inelastic Behavior of Engineering Materials and Structures", J. Wiley & Sons, New York.
3. Shanley, F. R., "Weight-Strength Analysis of Aircraft Structures" RAND Series, Chapter 19, McGraw-Hill, New York, 1952.
4. Simmons, W. F., Van Echo, J. A., and Cross, H. A., "Short Time High Temperature Properties of Heat Resisting Alloy Sheet", RAND Report R-147 (U.S.A.F. Project RR-1), Battelle Memorial Institute, Columbus, Ohio, June 1949.
5. Ilyushin, A. A., "The Deformation of a Visco-Plastic Solid", Free Translation prepared for D. W. Taylor Model Basin, US Navy Contract NObs 34166, Graduate Division of Applied Mathematics Brown University, 1947.
6. Sokolovskii, V. V., "The Propagation of Elastic Viscous Plastic Waves in Bars", Translation O.N.R. 358, Graduate Division of Applied Mathematics, Brown University.
7. Riparbelli, C., "On the Relation Among Stress, Strain and Strain Rate In Copper Wires Submitted To Longitudinal Impact", Proceedings of the Society for Experimental Stress Analysis, Vol XIV, No. 1, pp. 55-70.
8. Riparbelli, C., "Residual Stress Distribution Due To Creep In A Framed Plate", III European Aeronautical Conference, Brussels, 1958. Unpublished.
9. Prager, W., "Total Creep Under Varying Loads", Journal of Aeronautical Sciences, Vol. 24, No. 2, pp. 154, 1947.
10. Hoff, N. J., "Stress Distribution In The Presence Of Creep", Ardograph 28: "High Temperature Effects in Aircraft Structures", p. 28, Pergamon Press, New York, 1958.
11. Riparbelli, C., "A Principle Of Maximum Power For Real Fluids In Steady Motion", Journal of Aeronautical Sciences, Vol. 23, No. 10, October 1956.
12. Riparbelli, C., "An Analytic Form Of The Principal Of Maximum Power", Journal Of Aeronautical Sciences, Vol. 24, No. 4, April 1957.
13. Prager, W., "On Slow Visco-Plastic Flow", Studies in Mathematics and Mechanics Presented to R. von Mises, Academic Press, New York, 1954.

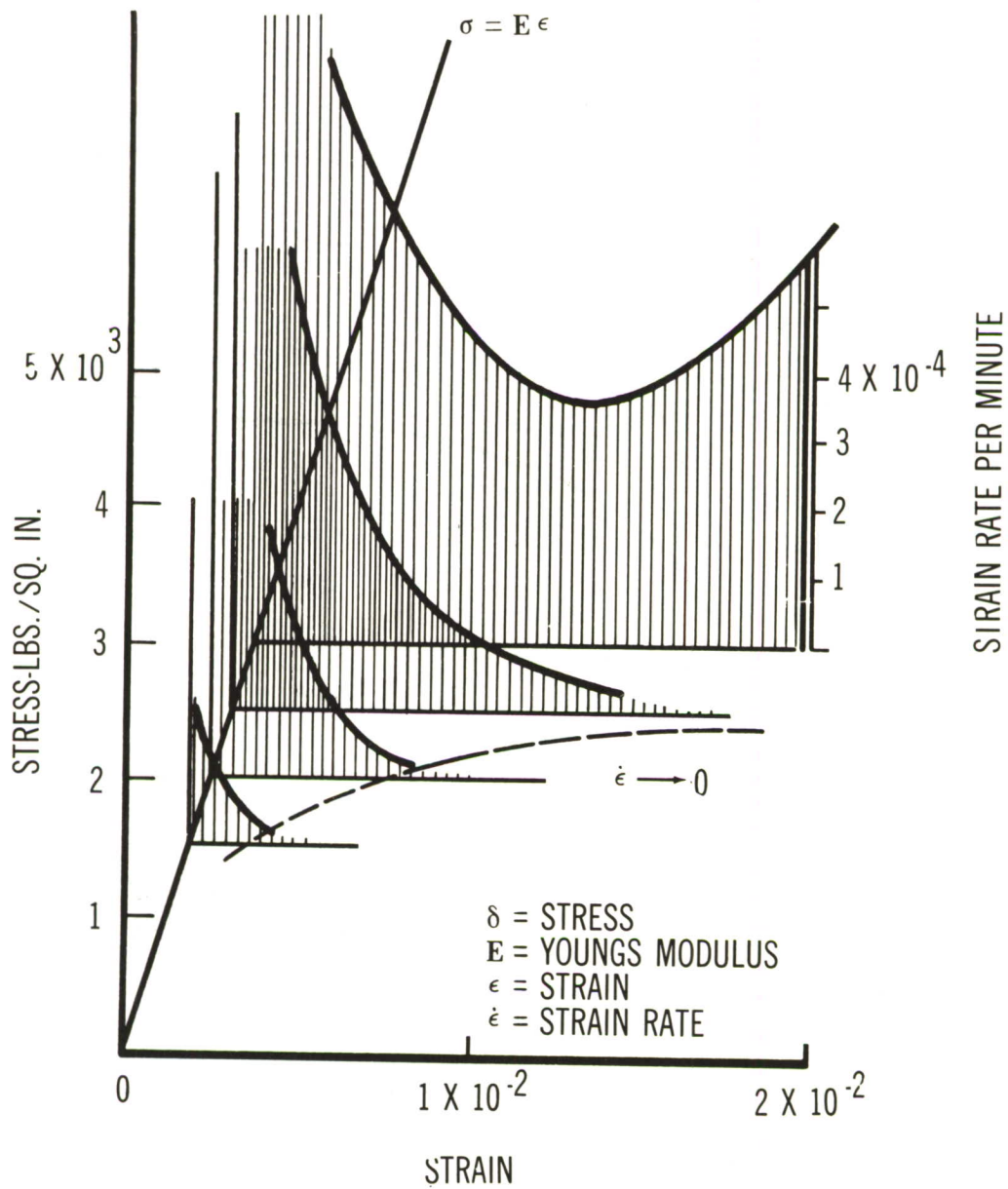


Figure 1. Creep Rates at Constant Stress Levels (Schematic-See Figures 23 through 26 Numerical Data)

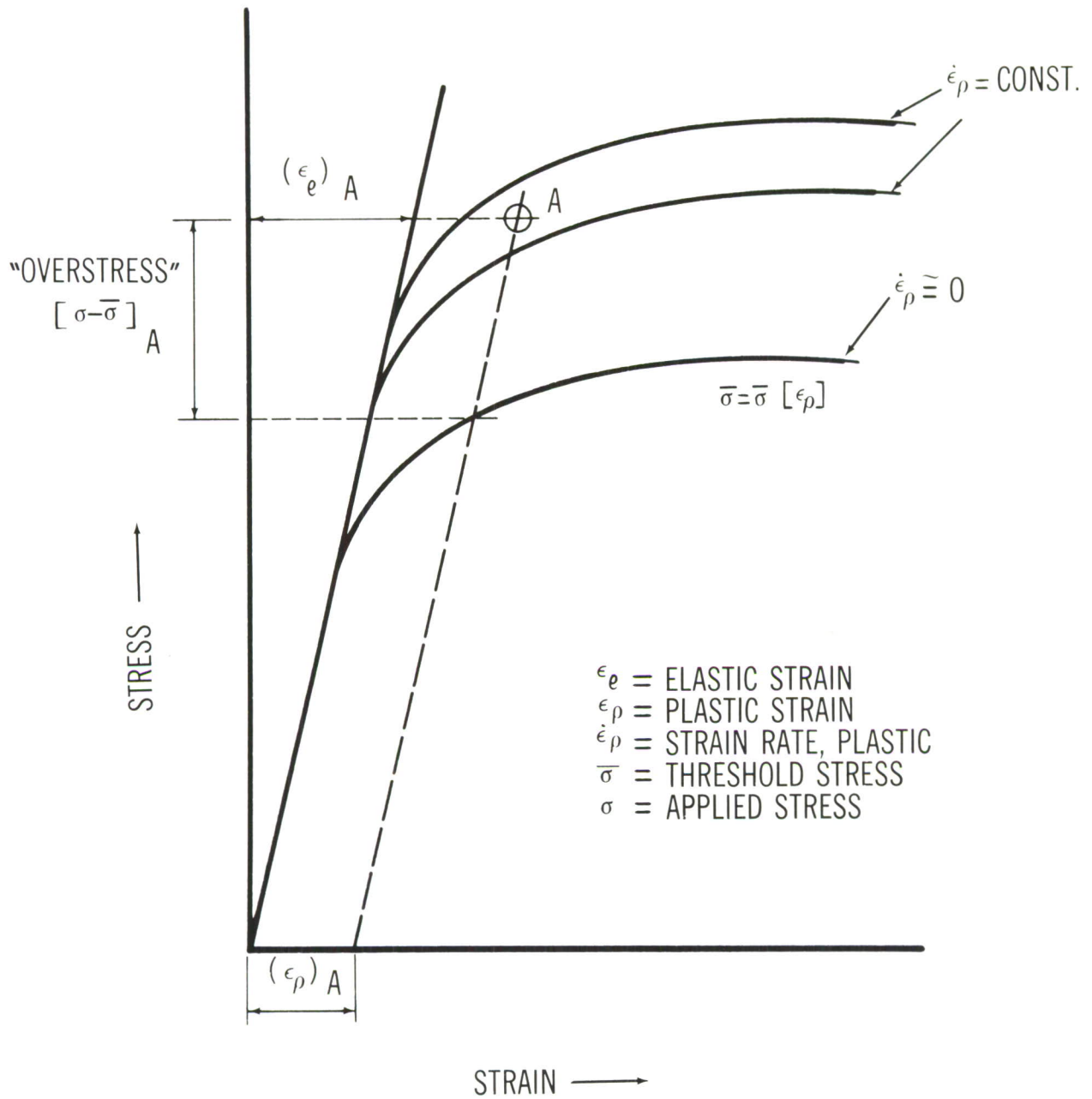


Figure 2. Creep Rate as a Function of Stress and Plastic Strain at Constant Temperature (Schematic)

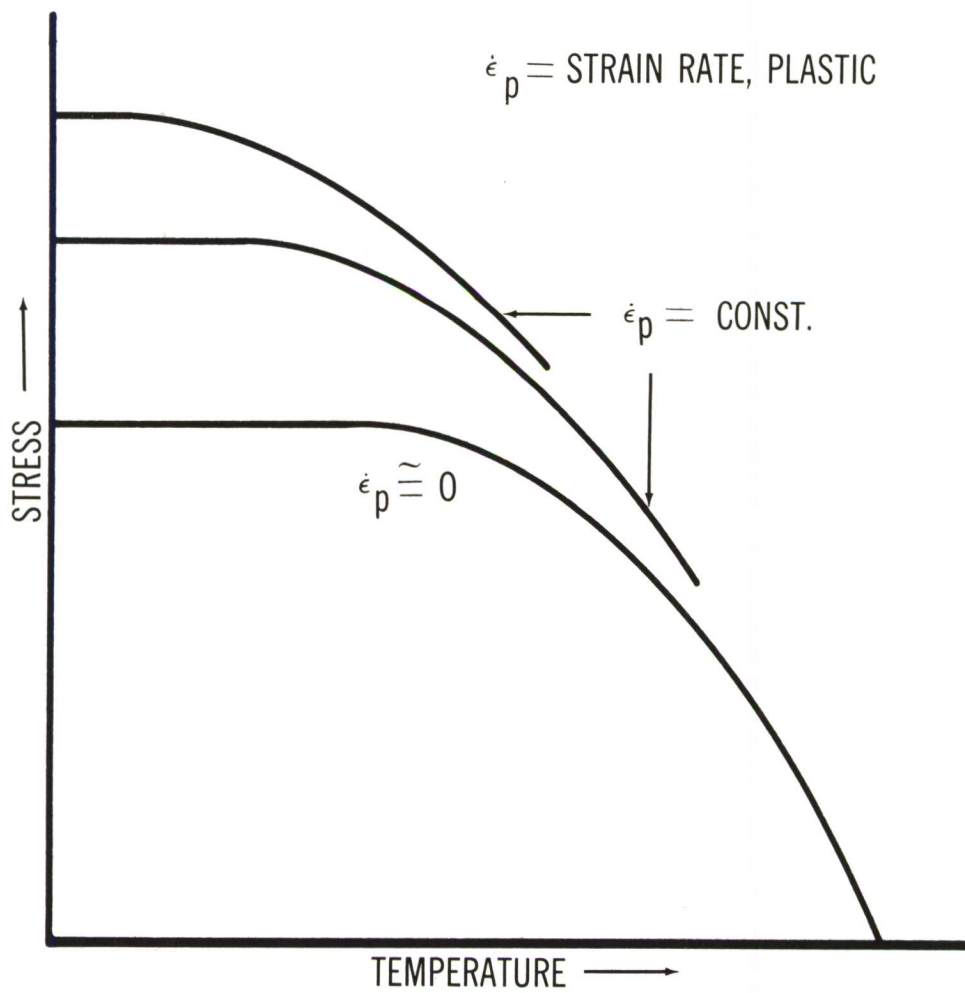


Figure 3. "Threshold" and Lines of Equal Initial Creep in the Stress-Temperature Plane (Schematic)

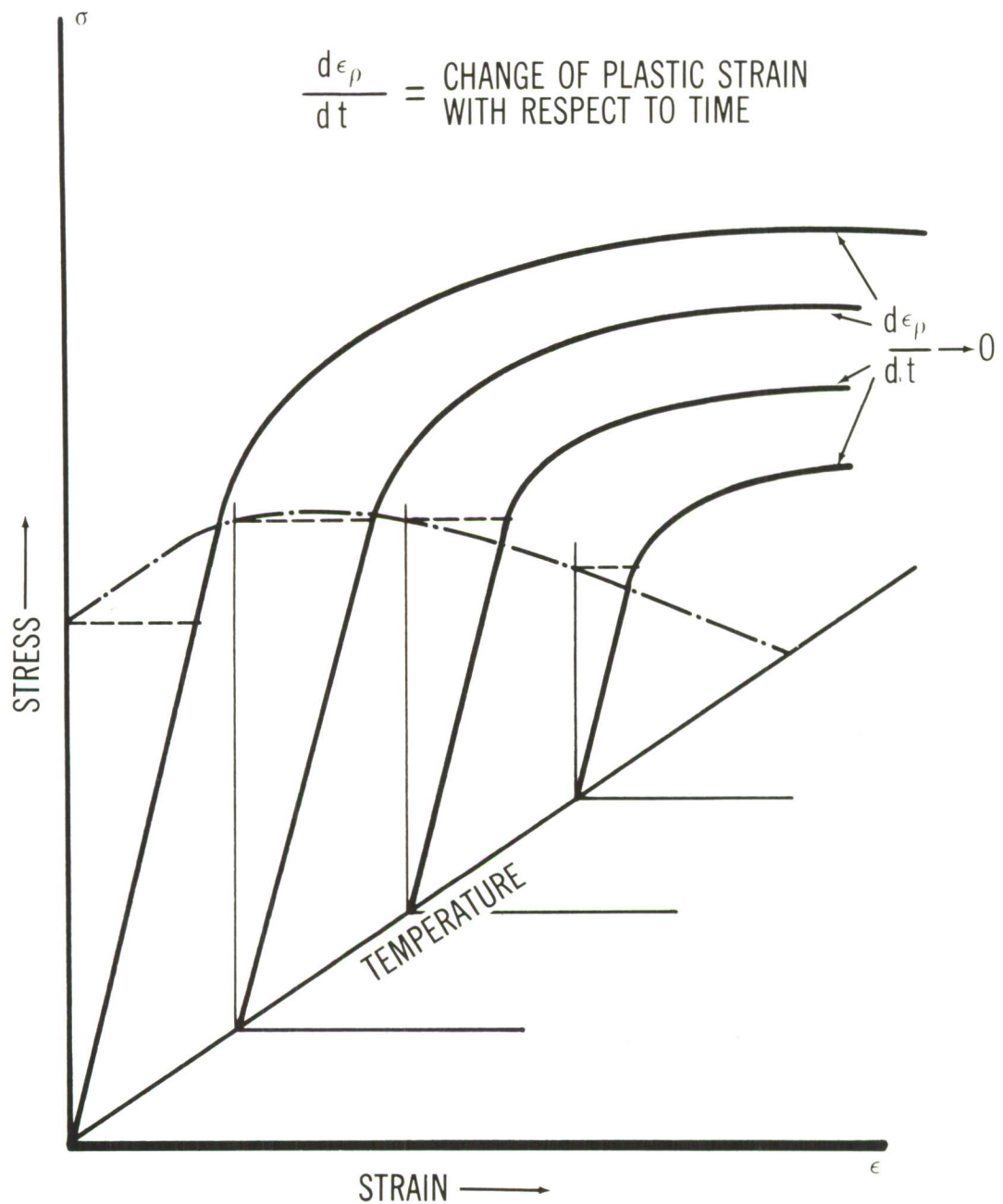


Figure 4. "Threshold" Surface in the Stress-Strain Temperature Space (Schematic)

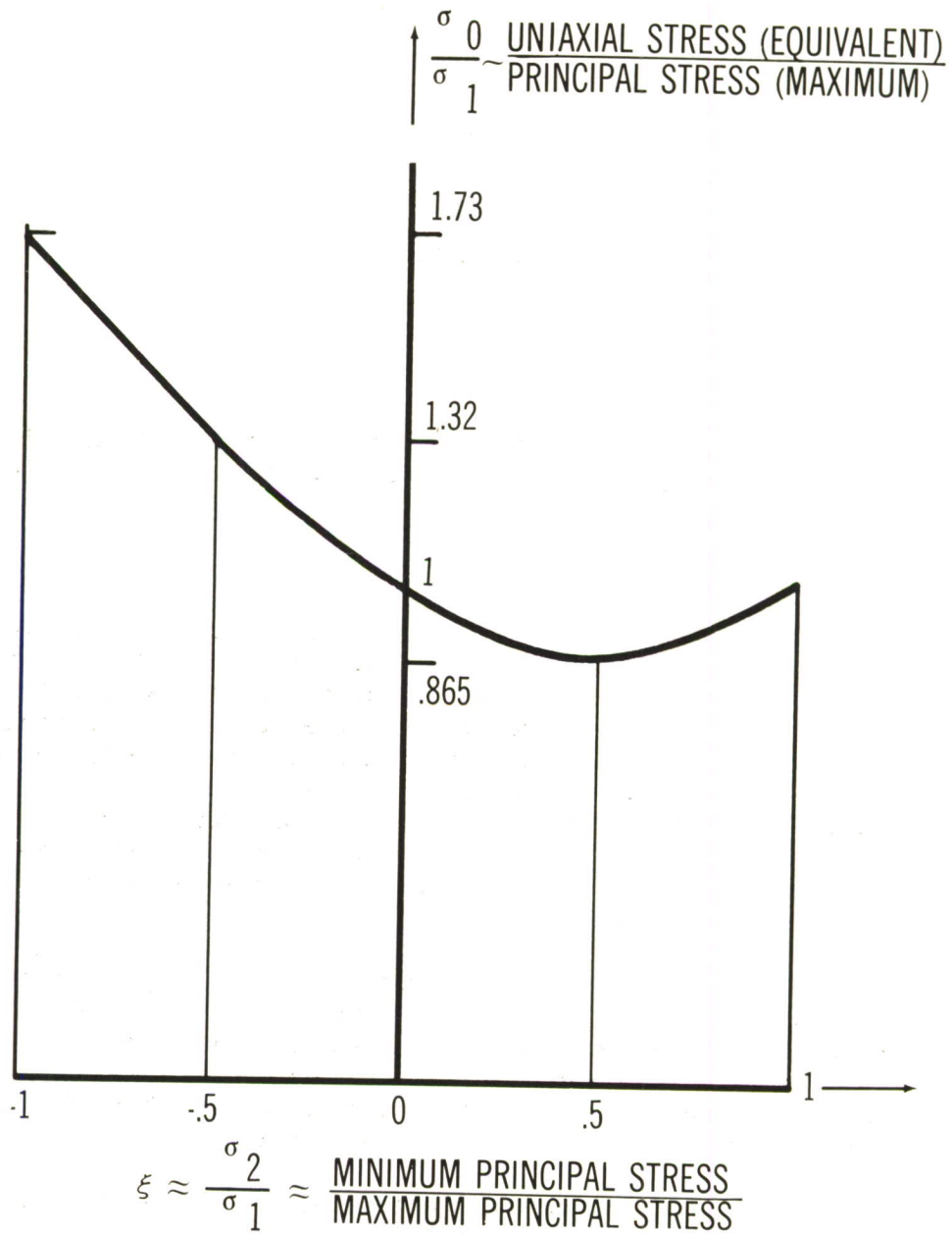


Figure 5. Condition of Plasticity for Biaxial Stress

PREDICTION OF CREEP EFFECTS

IN

AIRCRAFT STRUCTURES

PART II

CALIBRATION METHODS IN

SUPPORT OF NUMERICAL METHOD

INTRODUCTION

The special technique specifically aimed to determine threshold and initial creep rates to be applied to panels and shell elements is fully described in reference (9).

CALIBRATION METHOD: RESTRAINED PANELS

In effecting a calibration, a panel of the material under study is clamped into a frame in the manner shown in Figure 6. The material used in the clamping frame is different from that under study and is so selected that it has a different expansion coefficient, usually smaller, than the material under examination. The first calibration step involves heating the clamped assembly in an oven or furnace at a predetermined temperature for a stated time. Since the panel expands at a greater rate during heating than the clamping frame, it is put under compression stress when heated. Providing the stresses generated are sufficient, creep takes place in the specimen upon heating. Upon completion of heating the assembly is allowed to slow cool to room temperature in still air.

After the clamped assembly is at room temperature, strain gages are applied, as illustrated in Figure 6, and the bolts which attach the test panel to the clamping frame are released. The difference in strain gage readings caused by release of the bolts measures the stress relaxation which occurs from removal of restraint on the panel. The stress generated in a panel can be assigned, within limits, by choosing the ratio of the section areas of the panel and of the frame.

The residual stress for a given constant temperature, and therefore constant stress, has the form of a coexponential as a function of the exposure time. This is shown in terms of strain-time variables in Figure 7. The coexponential relationship confirms the assumption of viscosity at least for well behaved materials.

In these tests the information sought consists of a threshold line limiting the combinations of force or moment and temperature for which creep is negligible as illustrated in Figure 8, and those combinations of forces and heat input for which creep rates within acceptable ranges are observed. Thus calibration diagrams of the same type as those shown in Figures 2 and 3 are obtained.

CALIBRATION METHOD: BEAMS UNDER PURE BENDING

In these tests the required information sought consists of a threshold line limiting totally reversible strain in a beam, the onset of plastic flow and lines of equal strain rates or curvature rates for combinations of temperature and bending moments. The growth of the region of a beam which undergoes plastic deformation, the amount of plastic deformation in those regions undergoing plastic flow and the instability of the material, if any, determine the curvature, and therefore, the strain at the

upper and lower surfaces of the beam under test. In the results from beam tests the difference in materials properties in tension and compression, and, resultant changes in the neutral axis are implied. The neutral axis of a rectangular section should remain at the centroid of the section providing geometric changes do not occur. In the event that the geometry remains constant and the neutral axis shifts during test, the indication is that material properties changes took place. To determine the rate of rotation of the beam with respect to time, incremental strains are noted as they result from incremental increases in moment. Figure 9 schematically diagrams the bend test apparatus used for tests described. Figure 10 displays a side view of a test beam assembly and its supports. Figure 11 indicates the instrumentation and support provided a beam test specimen.

CALIBRATION METHOD: SHEAR PANELS

Shear panel calibration tests are made in conjunction with uniaxial calibration tests in order to provide correlation data representative of both uniaxial and biaxial states of loading. Uniaxial loading state tests are made with flat strips with the apparatus pictured in Figure 12. The uniaxial test performance consists of determining by trial the loading required to produce 0.0001 inch per inch strain in ten minutes.

The biaxial or "pure shear" tests are made with square specimens mounted in a steel shear frame as shown in Figure 13. Strains are measured during test in the direction of load application by means of a strain gage located at the center of the square plate. In order to avoid buckling of the test plates, restraining plates as shown in Figure 14 are lightly pressed upon the test plates and serve to distribute loads from the loading connections to the plate in addition to offering the desired buckling restraint.

In the analysis of data from the biaxial tests described, two general yield criteria which are widely accepted are those of Tresca and von Mises. The mathematical statement of the two theories are:

Tresca

$$\sigma_o = \sigma_1 - \sigma_2 \quad (28)$$

where σ_3 is numerically between σ_1 and σ_2 and

von Mises

$$\sigma_o = \left(\frac{1}{2} (\sigma_1 - \sigma_2)^2 + (\sigma_2 - \sigma_3)^2 + (\sigma_3 - \sigma_1)^2 \right)^{\frac{1}{2}} \quad (29)$$

In the case of pure shear where $\sigma_1 = -\sigma_2$ and $\sigma_3 = 0$, the two conditions become

$$\text{Tresca} \quad \sigma_o = 2\sigma_1 \quad (30)$$

$$\text{von Mises} \quad \sigma_o = \sqrt{3} \cdot \sigma_1 = 1.73\sigma_1 \quad (31)$$

It is not possible, however, to evaluate frictional effects of the plates which restrain the shear test plates from buckling.

An effective strain in the test material is expressed by

$$d\epsilon_p = \left(\frac{2}{9} \left[(d\epsilon_1 - d\epsilon_2)^2 + (d\epsilon_2 - d\epsilon_3)^2 + (d\epsilon_3 - d\epsilon_1)^2 \right] \right)^{1/2} \quad (32)$$

by using the fact that plastic (creep) action takes place at constant volume where $d\epsilon_1 = -d\epsilon_2$ and $d\epsilon_3 = 0$. Accordingly, in the shear test, the effective strain in terms of strain measured in the direction of the load is

$$d\epsilon_o = \frac{2}{\sqrt{3}} d\epsilon_1 = 1.15\epsilon_1 \quad (33)$$

In order to check the concept of overstress, where

$$\dot{\epsilon} = K (\sigma - \sigma_o) \quad (34)$$

the tensile and shear specimens are subjected to a load ten percent greater than that required to cause a plastic strain of 0.0001 inch per inch for five minutes. Under this condition strain increments are read at five minute intervals and average creep rates are computed from these as functions of time and the shapes of the strain curves for the uniaxial and biaxial conditions are compared to note the differences in outcome from both conditions of test.

CALIBRATION RESULTS: RESTRAINED PANELS

Calibrations employing circular restrained plates, although planned, were not accomplished because of material procurement difficulties which arose out of the 1959 steel strike.

CALIBRATION RESULTS: BEAMS UNDER PURE BENDING

The results deriving from incremental applications of moment to a cantilever beam of the kind shown in Figure 9 are given in Table 1. The beam material was Armco PH 15-7 Mo Condition RH 950 stainless steel. The beam dimensions were 0.125 inch wide by 1.0 inch deep by 10 inches long. The incremental moment loads and the strains at the top and bottom of the beams were measured during the test and are shown in Table 1 along with the calculated neutral axis locations and radii of curvature. These tabulations show the tendency for the neutral axis to shift as loading increases and offers some evidence of non-uniformity in the material's reaction to tensile and compressive forces. Figures 15 and 16 plot the results from a second series of bend tests run to expand upon the findings of the initial series. These curves plot bending moment against incremental strain and show a distinct cyclic pattern in the stress-strain relationships obtaining in a beam. The out of phase relationship of the tension and compression portions of the beams also is noteworthy. These circumstances suggest action taking place within the metal itself which is intimately associated with slip, rotational and gliding mechanisms operative within the metallic lattice structures. Beam tests thus present themselves as a useful tool for correlating simultaneous interactions of materials and possibly structural elements to tensile stresses, which ordinarily are measured in simplified testing practice, and compressive stresses, which usually are measured under conditions of experimental difficulty and complexity.

CALIBRATION RESULTS: SHEAR PANELS

Initial calibrations were made with copper, lead and aluminum shear panels and intended to verify the usefulness of the von Mises and Tresca criteria for study of biaxiality. Table 2 shows data obtained from tests made with restrained shear panels in the manner described above. In performing these tests, the strain and time were held constant, so that a 0.001 strain was attained in 10 minutes, while the stresses were allowed to increase. The Table 2 data sums the stresses parallel and transverse to the loading direction for differing thicknesses of each of the three materials tested and also shows the ratio of the sums of the directional stresses. In considering the outcome from the individual test cases, a wide variation in the stress ratio was apparent. This immediately suggested the existence of varying states of strain arising from the reaction of the metal itself to applied force and from those effects arising from thickness variations. On this basis verifications of the two theoretical criteria were not apparent. However, when all stresses for all materials were summed and ratioed, the "average" result fell within the range of value encompassed by the two theoretical criteria.

The foregoing experiment emphasizes a need for judicious selection of "model materials" for demonstration of the validity of theoretical criteria for use in practical studies. This apparently arises from strain reactions peculiar to a base metal subjected to stress. However, in the long run, the need for a suitable model is expressed in the desirability for test conditions under which thermal expansion and buckling effects can be minimized and thus bring focus of attention upon the object of verification rather than the "side effect".

Tables 3 and 4 show results obtained from test runs of 30 minutes duration made to examine stress and strain relations in tension and shear panels. The test data themselves are given in Figures 17 through 22. In both Tables 3 and 4 a wide range of variation in effective plastic strain and in strain rate is reflected in a summary of the 30 minute condition. An outstanding characteristic shown in Figures 17 through 22 is the reaction of the materials to load application as is indicated by the variations in ordinate values shown in the several charts.

TABLE 1 POSITION OF NEUTRAL AXIS AND RADIUS OF CURVATURE
OF A BEAM UNDER SIMPLE BENDING

Temperature	Moment lbs.	Strains			Neutral Axis Position Y "	Radius of Curvature R "
		ϵ_T "1"	ϵ_B "1"	$\epsilon_T + \epsilon_B$ "1"		
75	3000	4042×10^{-6}	3435×10^{-6}	7477×10^{-6}	.460	133.74
75	3150	4140	3545	7685	.461	130.12
75	3300	4250	3645	7895	.462	126.66
75	3450	4380	3770	8150	.463	122.70
75	3600	4600	3980	8580	.464	116.55
75	3750	5070	4365	9435	.463	105.99

Material - Armco PH 15-7 Mo, Cond. RH 950

Symbols - ϵ_T , strain at top of beam

ϵ_B , strain at bottom of beam

Y_2 , neutral axis distance
(see sketch)

R, radius of curvature of beam

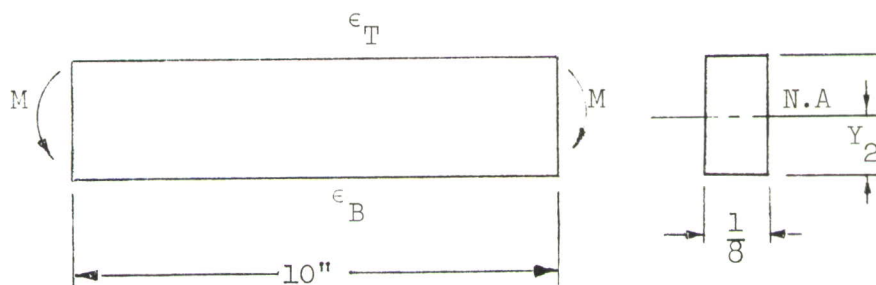


TABLE 2 RELATIONSHIP OF UNIAXIAL TO BIAXIAL LOADING

- CRITERIA VERIFICATION DATA

Material	Thickness in.	Stress (1) lb/sq. in.			
		σ_o	σ_1	σ_o/σ_1	
Copper	.0216	5,850	--	--	
"	"	5,850	--	--	
"	"	---	4,550	--	
"	"	---	4,550	--	
"	"	11,700	8,830	1.325	Total
"	.037	10,500	--	--	
"	"	11,450	--	--	
"	"	---	5,000	--	
"	"	---	5,230	--	
"	"	21,950	10,230	2.140	Total
"	.0647	5,150	--	--	
"	"	5,200	--	--	
"	"	---	2,650	--	
"	"	---	--	--	
"	"	10,350	--	1.950	Total
Sum of Totals		44,000	24,360	1.806 (Ave.)	
Lead	.0312	1,125	--	--	
"	"	1,070	--	--	
"	"	---	835	--	
"	"	---	835	--	
"	"	2,195	1,640	1.338	Total
"	.039	1,000	--	--	
"	"	1,000	--	--	
"	"	---	1,250	--	
"	"	---	1,000	--	
"	"	2,000	2,250	0.888	Total
"	.0652	880	--	--	
"	"	835	--	--	
"	"	---	730	--	
"	"	---	675	--	
"	"	1,715	1,405	1.221	Total
Sum of Totals		5,910	5,295	1.118 (Ave.)	

TABLE 2 RELATIONSHIP OF UNIAXIAL TO BIAxIAL LOADING
(Cont'd) - CRITERIA VERIFICATION DATA

Material	Thickness in.	Stress (1)			
		σ_o	$\frac{\text{lb/sq. in.}}{\sigma_1}$	σ_o/σ_1	
Aluminum (3)	.020	22,200	---	---	
"	"	19,500	---	---	
"	"	---	9,650	---	
"	"		10,150	---	
"	"	31,700	19,800	1.601	Total
"	.040	18,000	---	---	
"	"	16,800	---	---	
"	"	---	7,700	---	
"	"	---	---	---	
"	"	34,800	15,400 (2)	2.260	Total
Sum of Totals		66,500	35,200	1.889 (Ave.)	

Sum of Totals of Stress for All Materials

$$\sigma_o = 116,410$$

$$\sigma_1 = 64,855$$

$$\sigma_o/\sigma_1 = 1.795$$

$$\text{Value of } \sigma_o/\sigma_1 \text{ from von Mises criterion} = 1.795$$

$$\text{Value of } \sigma_o/\sigma_1 \text{ from Tresca's criterion} = 2.000$$

Notes: (1) Stresses given are those in the direction of the load required to produce 0.001 strain in 10 minutes where

$$\sigma_o = \text{load} / 2 \times \text{thickness}$$

$$\sigma_1 = \text{load} / \sqrt{2} \times \text{length of side} \times \text{thickness}$$

(2) Twice the value of σ_1 is taken as the total since only one shear test was made for the material and thickness.

(3) 7178-0 aluminum alloy

TABLE 3 EFFECTIVE PLASTIC STRAINS

Material	Thickness in.	Strain in/in 10^6 (1)	Stress PSI	Modulus Of Elasticity	Elastic Strain $\times 10^6$ (2)	Plastic Strain $\times 10^6$	Effective Plastic Strain $\times 10^6$ (3)
Copper	.0216	3625T	5850	16.3×10^6 $\mu = .3$	359	3266	3266
Copper	.0216	1015S	7638		609	406	467
Copper	.0216	1545S	7638		609	936	1076
Copper	.037	2370T	10975		673	1697	1697
Copper	.037	2870T	10975	3×10^6 $\mu = .3$	673	2197	2197
Copper	.037	1885S	8849		706	1149	1321
Copper	.037	3200S	8849		706	2494	2867
Copper	.0647	4455T	5175		317	4138	4138
Copper	.0647	4780T	5175	10.5×10^6 $\mu = .3$	317	4463	4463
Copper	.0647	1010S	4585		366	644	741
Lead	.0312	1485T	1097		366	1119	1119
Lead	.0312	940T	1097		366	574	574
Lead	.0312	728S	1419	10.5×10^6 $\mu = .3$	675	113	130
Lead	.0312	505S	1419		675	110	126
Lead	.039	940T	1060		333	607	607
Lead	.039	1700T	1000		333	1367	1367
Lead	.039	930S	1946	10.5×10^6 $\mu = .3$	844	86	99
Lead	.039	885S	1946		844	41	47
Lead	.0652	1350T	857		286	1064	1064
Lead	.0652	1505T	857		286	1219	1219
Lead	.0652	815S	1214	10.5×10^6 $\mu = .3$	427	388	446
Lead	.0652	425S	1214		427	- 2	- 2
Aluminum	.020	17135T	10850		1033	16102	16102
Aluminum	.020	13010T	10850		1033	11977	11977
Aluminum	.020	2810S	17130	10.5×10^6 $\mu = .3$	2121	689	792
Aluminum	.020	8000S	17130		2121	5879	6761
Aluminum	.040	8380T	17400		1657	6723	6723
Aluminum	.040	5450T	17400		1657	3793	3793
Aluminum	.040	2040S	13321		1649	391	450

TABLE 3 EFFECTIVE PLASTIC STRAINS
(Cont'd)

<u>Notes:</u>	(1) Suffix "T" denotes tension test: suffix "S" indicates shear test.
(2)	The elastic strain for tension tests is
$\epsilon_E = \sigma/E, \text{ and}$	
for shear tests is	
$\epsilon_E = (1 + \mu) \sigma/E$	
where	
ϵ_E	represents elastic strain
σ	represents stress
E	represents modulus of elasticity
μ	represents Poisson's ratio
(3)	The effective plastic strain for shear tests is $1.15 \epsilon_p$

TABLE 4 STRAIN RATE COMPARISON

Material	Thickness in.	Total Strain in 30 min. in. x 10 ⁶ (1)	Average Strain in 30 min. $\frac{1}{n} \sum_{(2)} \epsilon_i$	Deviation Of Strain From Average	Deviation of Strain ÷ Average Strain
Copper	.0216	225T	198	27	.136
Copper	.0216	180T	198	- 18	-.091
Copper	.0216	190S	198	- 8	-.043
Copper	.037	2540T	1468	1072	.731
Copper	.037	2395T	1468	927	.632
Copper	.037	585S	1468	-883	-.602
Copper	.037	425S	1468	-1043	-.711
Copper	.0647	435T	348	87	.250
Copper	.0647	250S	348	- 88	-.250
Lead	.0312	905T	812	- 93	.114
Lead	.0312	1380T	812	568	.699
Lead	.0312	150S	812	-662	-.816
Lead	.039	675T	728	- 53	-.073
Lead	.039	790T	728	62	.085
Lead	.039	720S	728	- 8	-.011
Lead	.0652	440T	1014	-574	-.566
Lead	.0652	1588S	1014	574	.566
Aluminum	.020	65T	72.5	-7.5	-.135
Aluminum	.020	80S	72.5	7.5	.135
Aluminum	.040	215T	222.5	-7.5	-.034
Aluminum	.040	230S	222.5	7.5	.034

- Notes:
- (1) Suffix "T" denotes tension test: suffix "S" indicates shear test.
 - (2) Where n represents material thickness, and ϵ_i represents incremental strain.

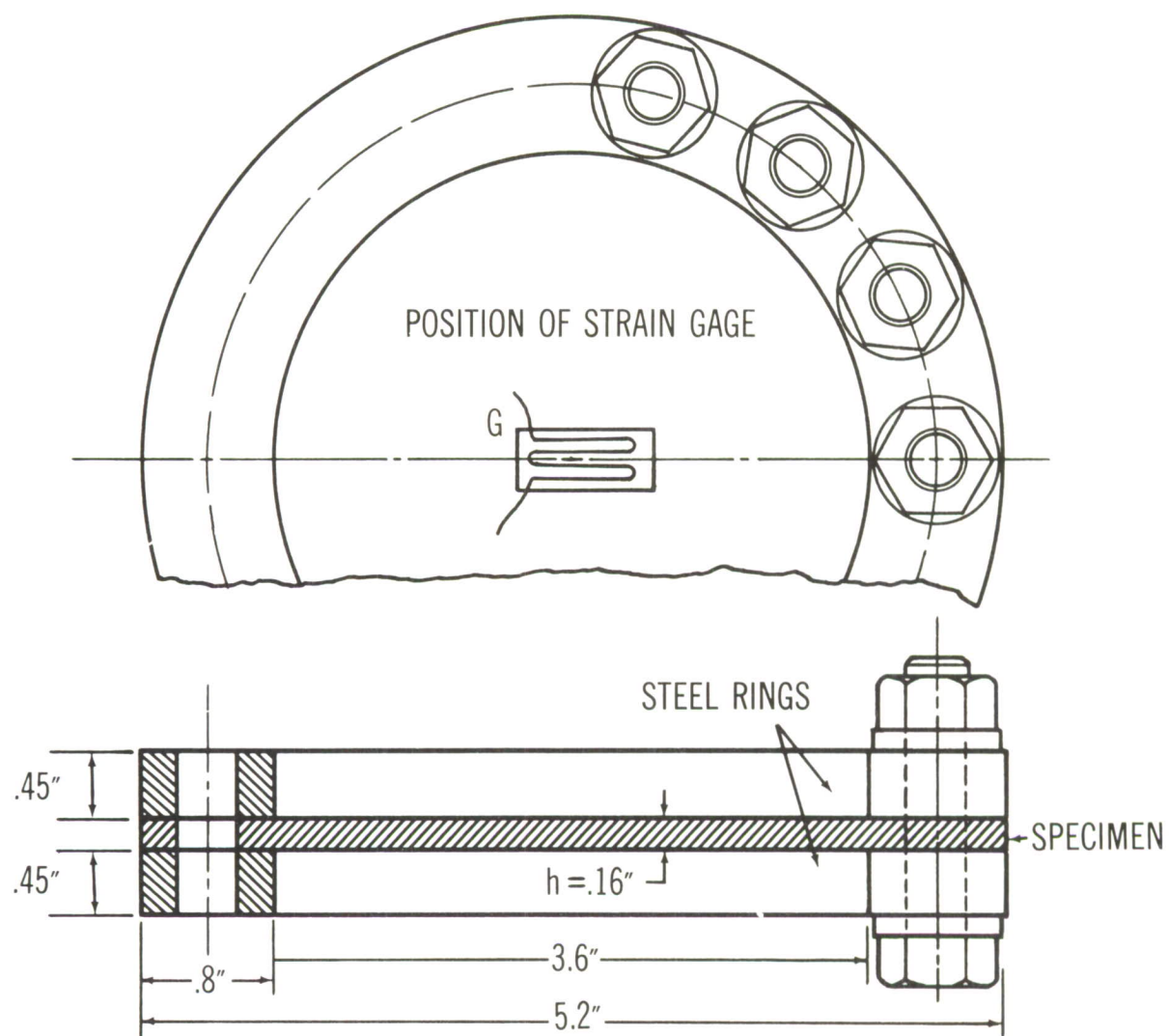


Figure 6. Test Specimen Assembly

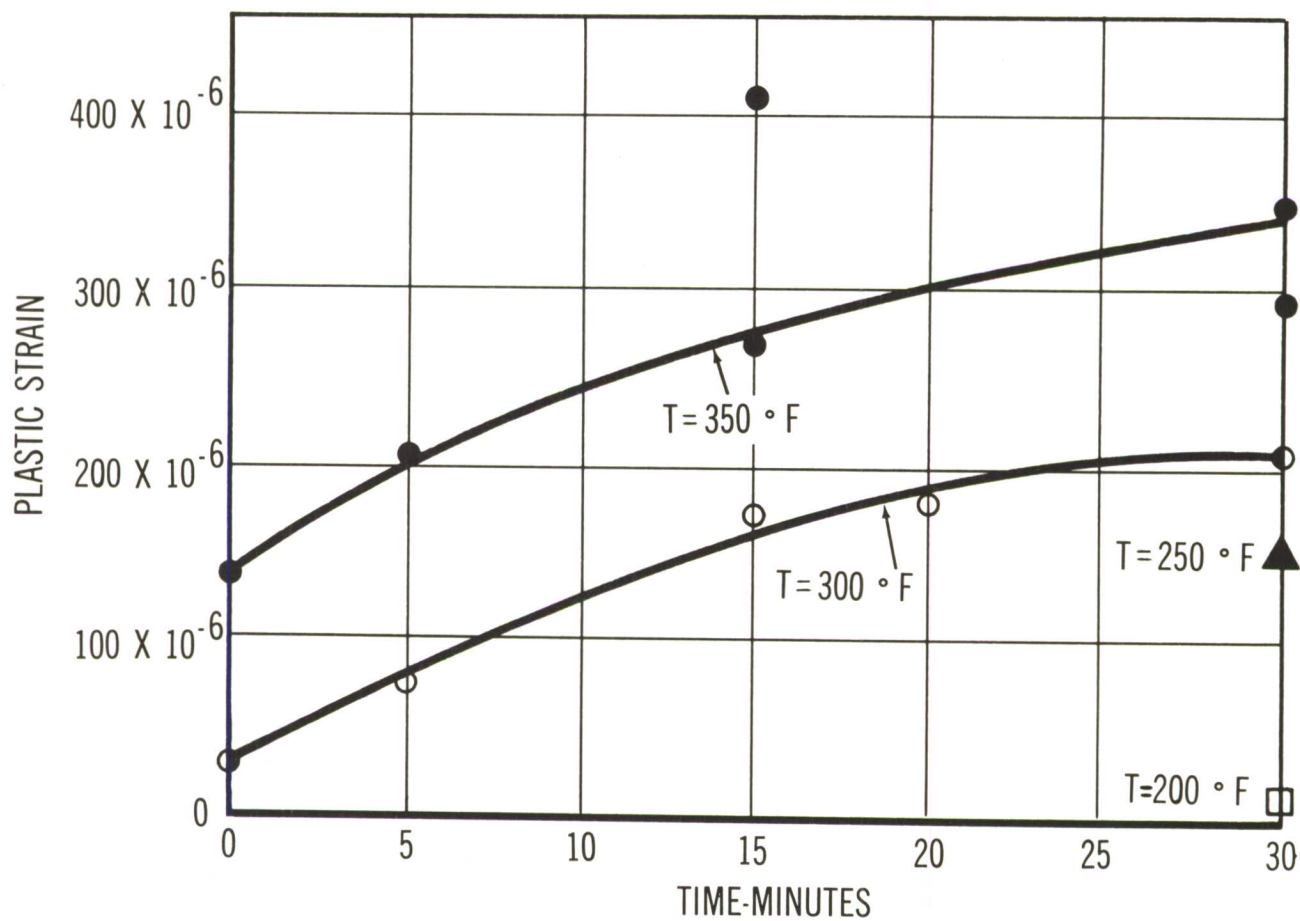


Figure 7. Residual Strain in Aluminum Plates

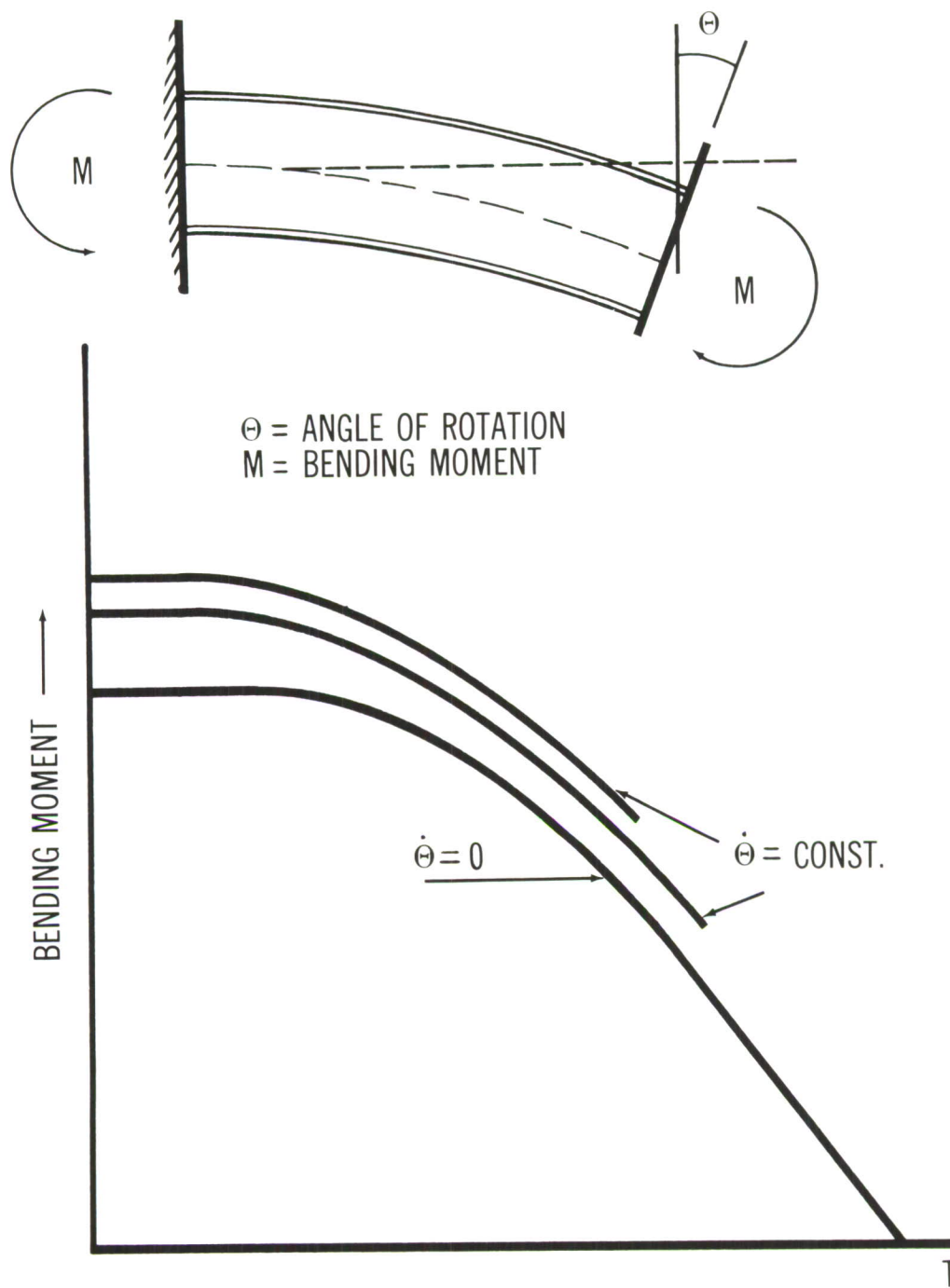


Figure 8. Creep Bending of a Beam - Lines of Equal Time Rate of Curvature (Schematic)

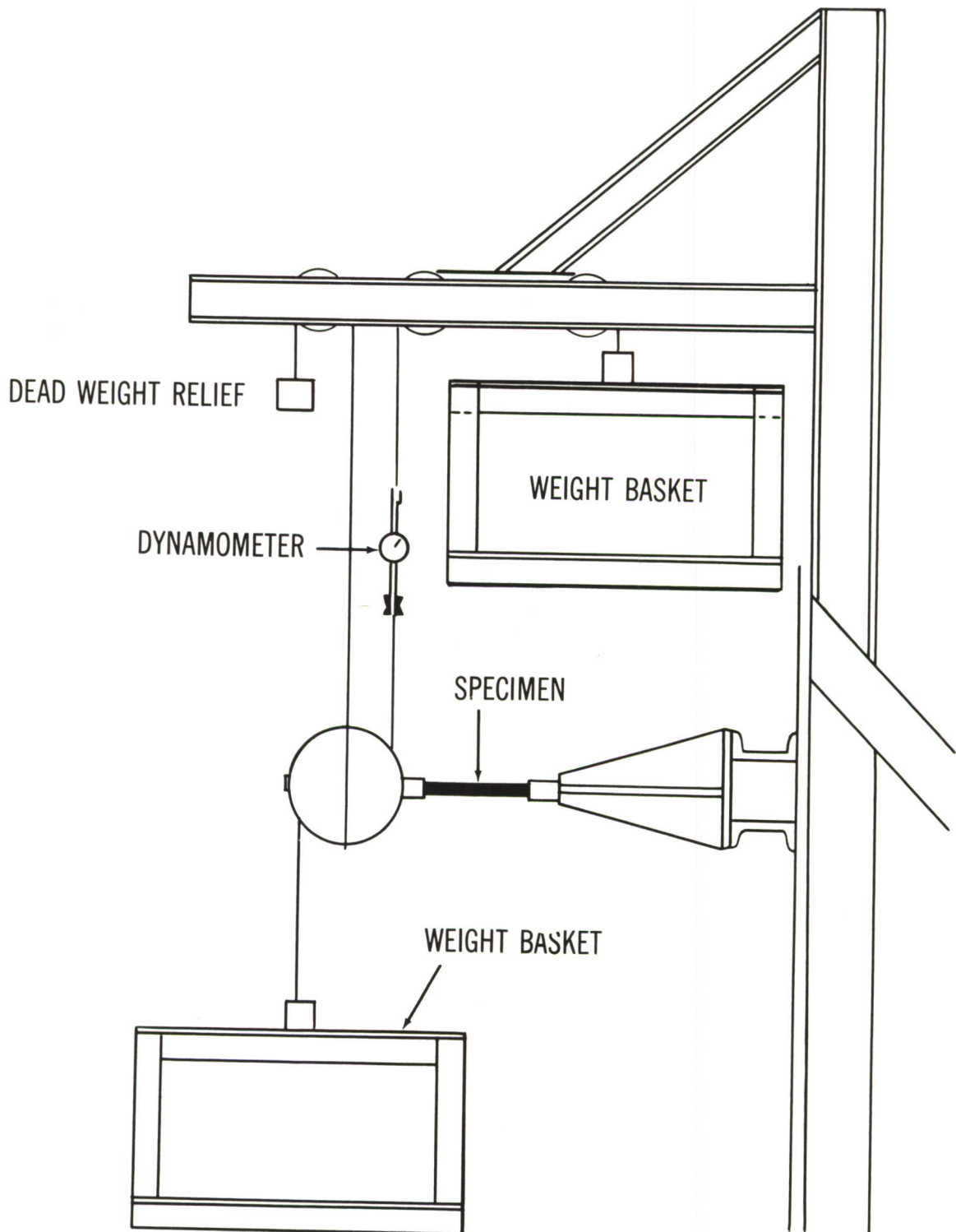


Figure 9. Beam Test Apparatus (Schematic)

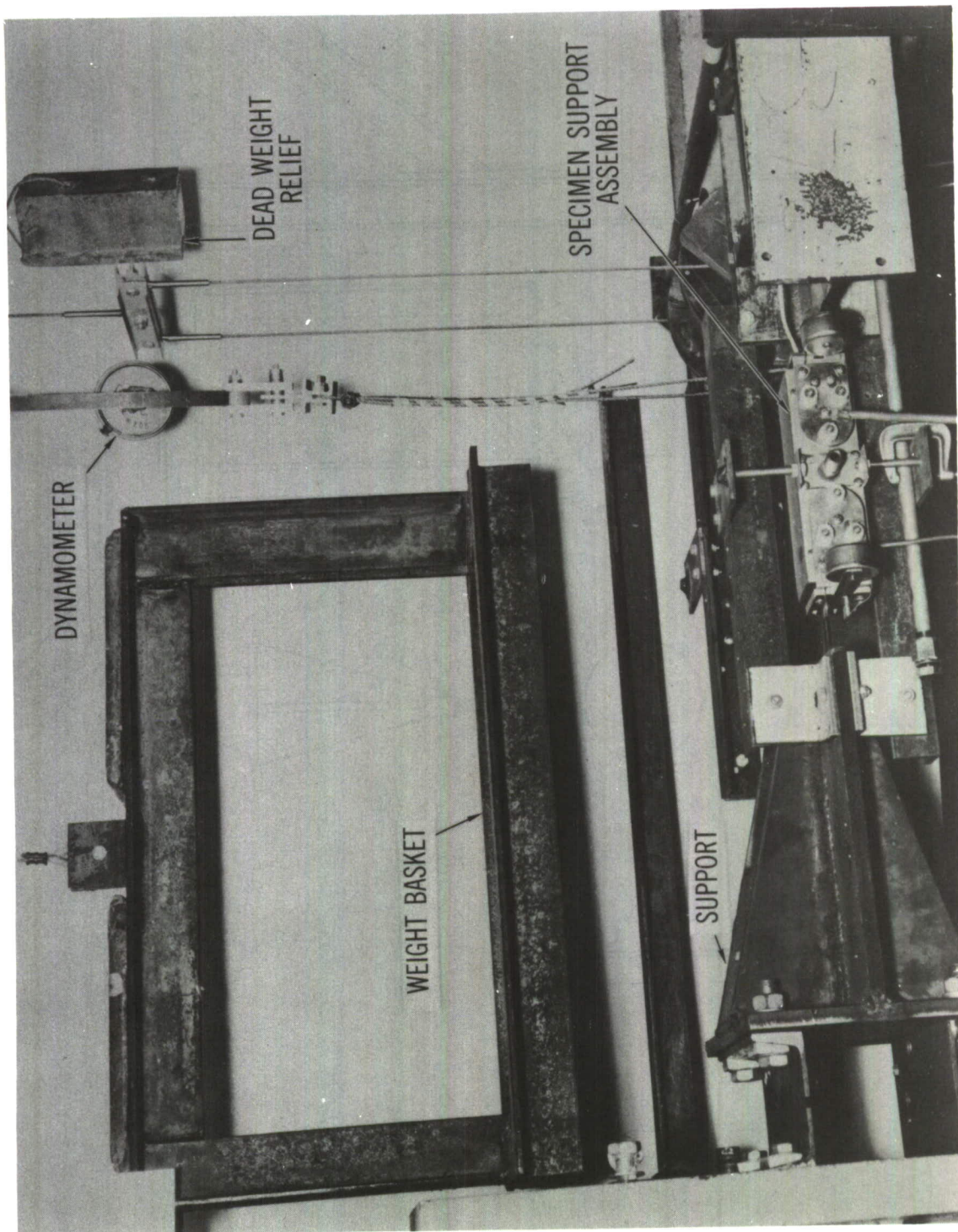


Figure 10. Test Beam Assembly and Supports

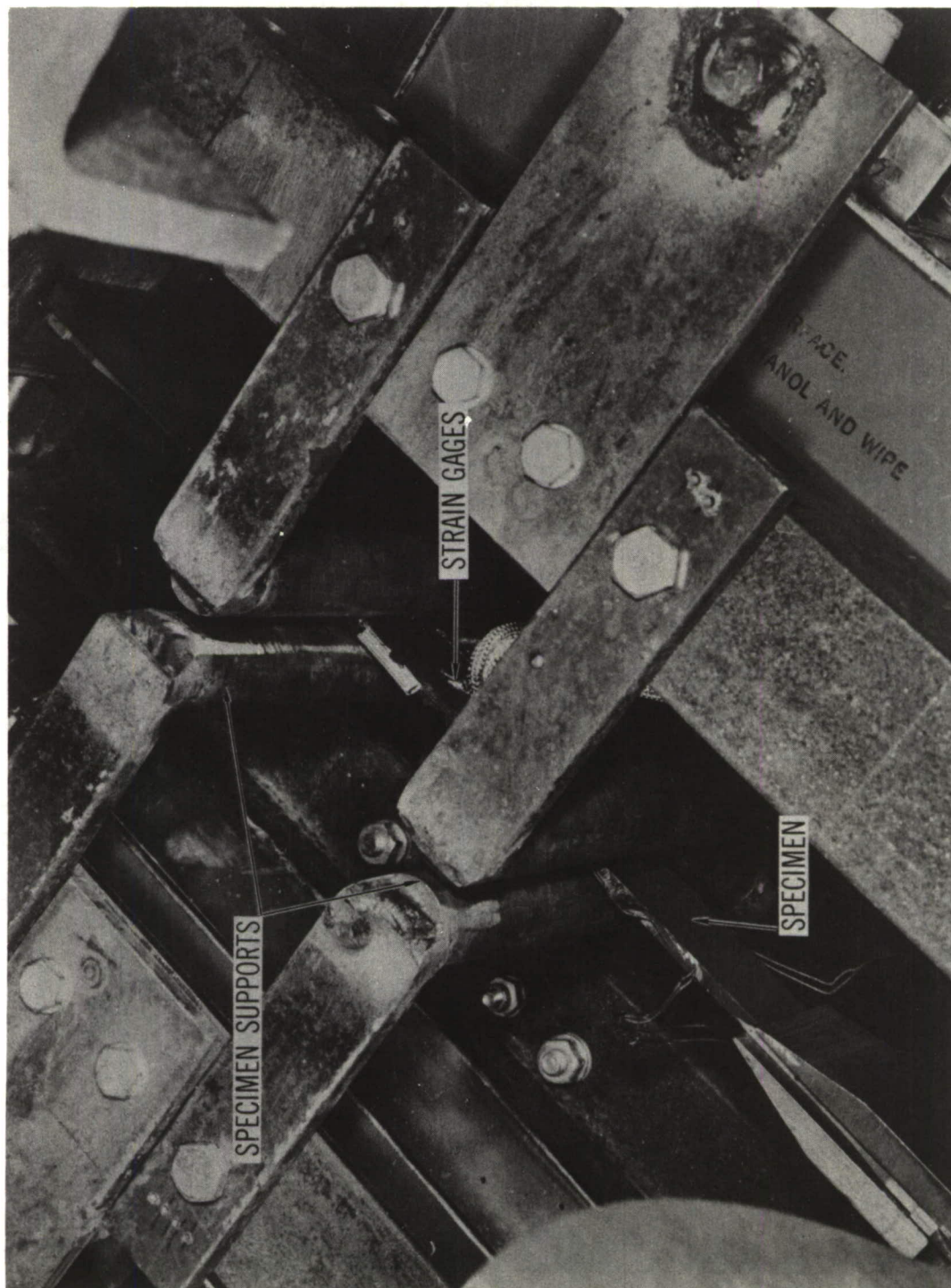


Figure 11. Test Beam Instrumentation and Supports

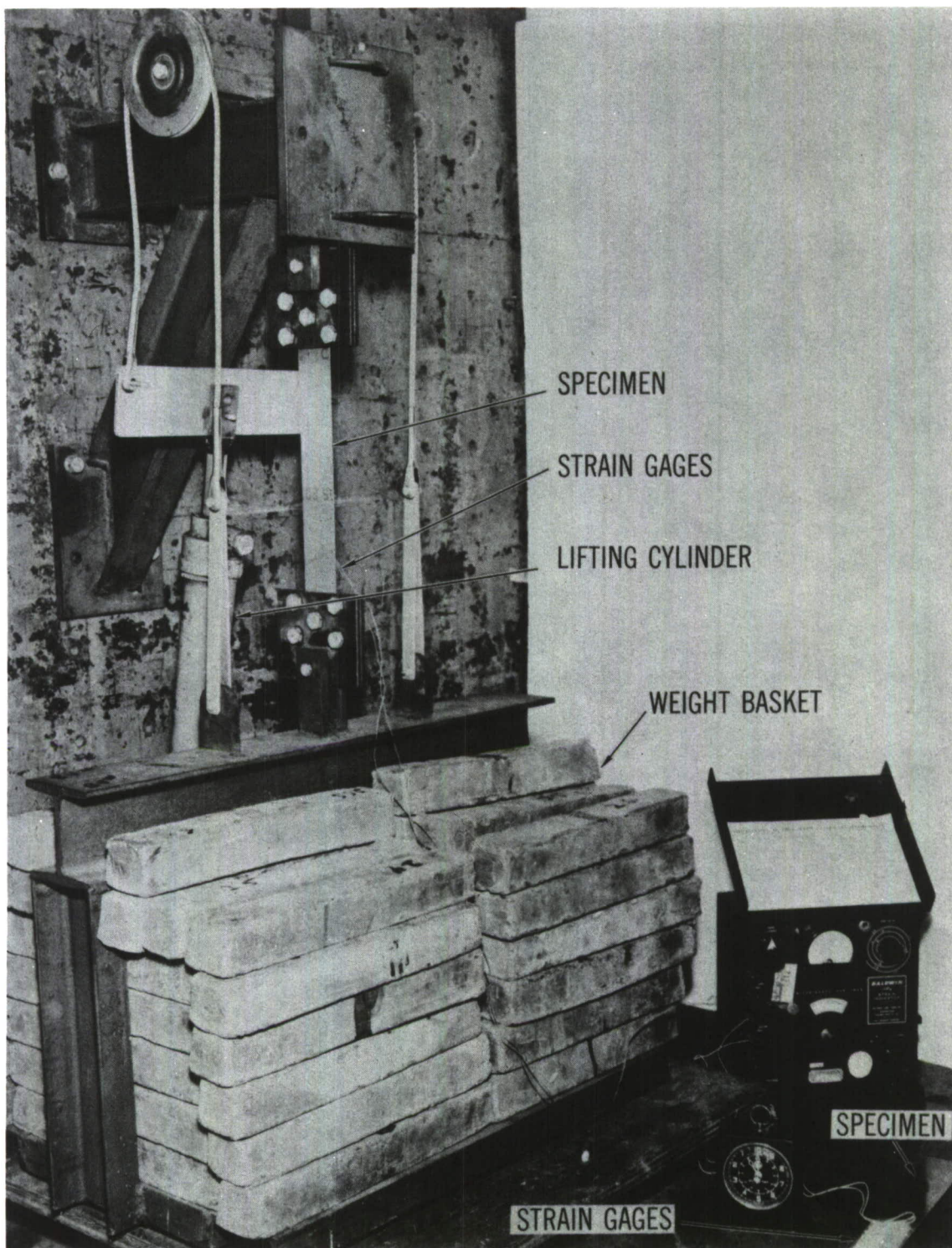


Figure 12. Uniaxial Loading State Test Apparatus

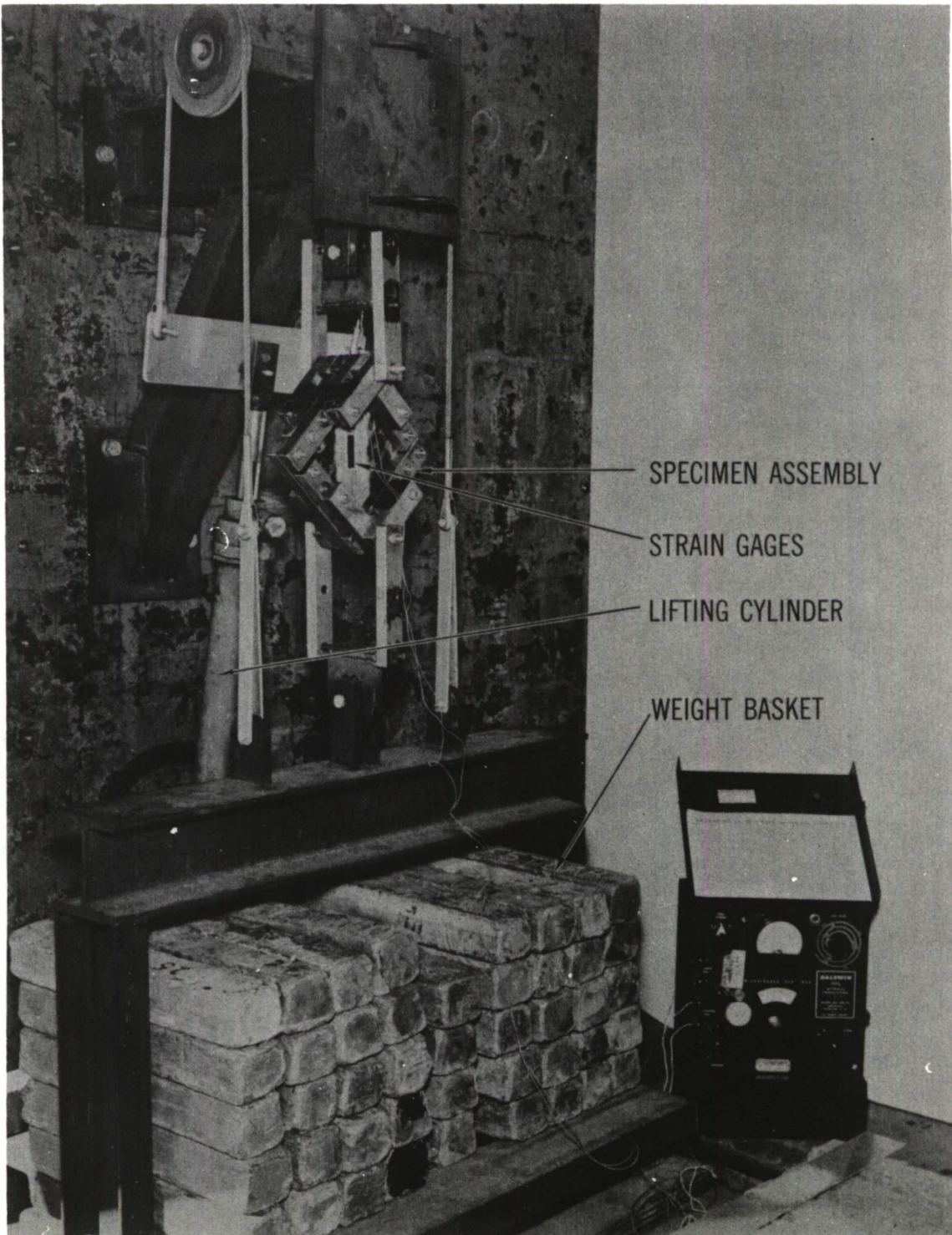


Figure 13. Biaxial Loading State Test Apparatus

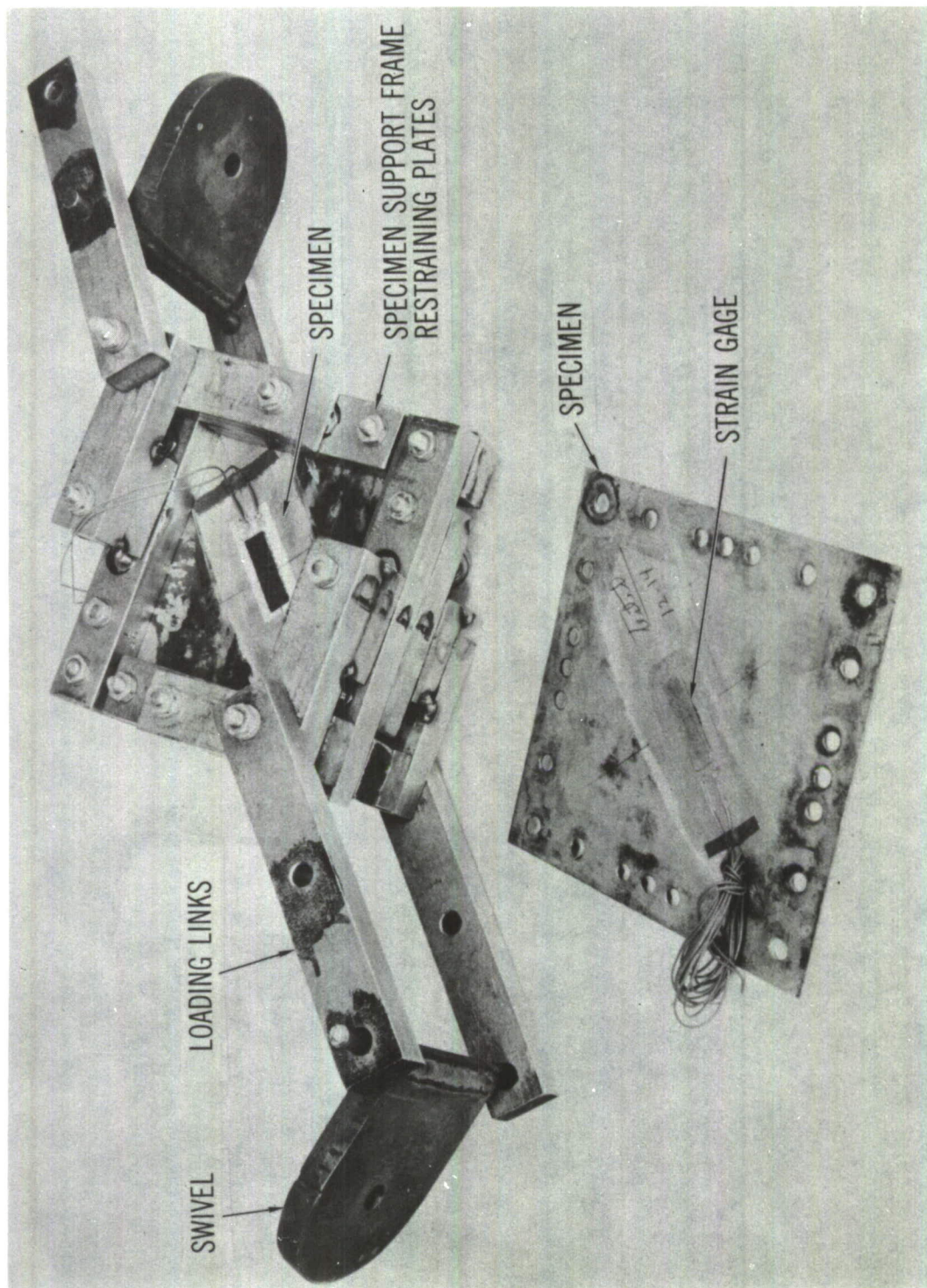


Figure 14. Test Panel Instrumentation and Restraining Plates Used in Biaxial Tests

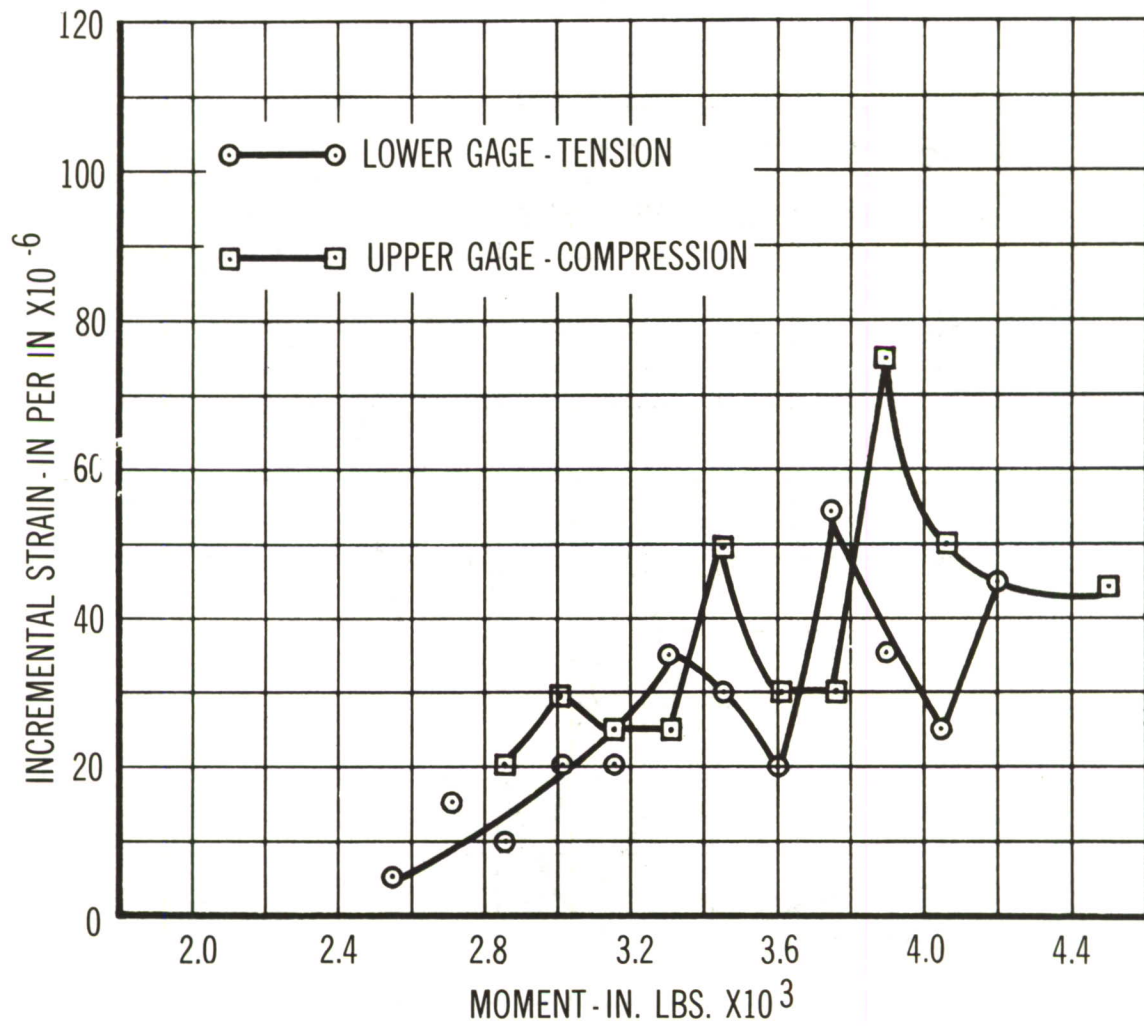


Figure 15. Incremental Strain-Bending Moment Relationships in Test Beams

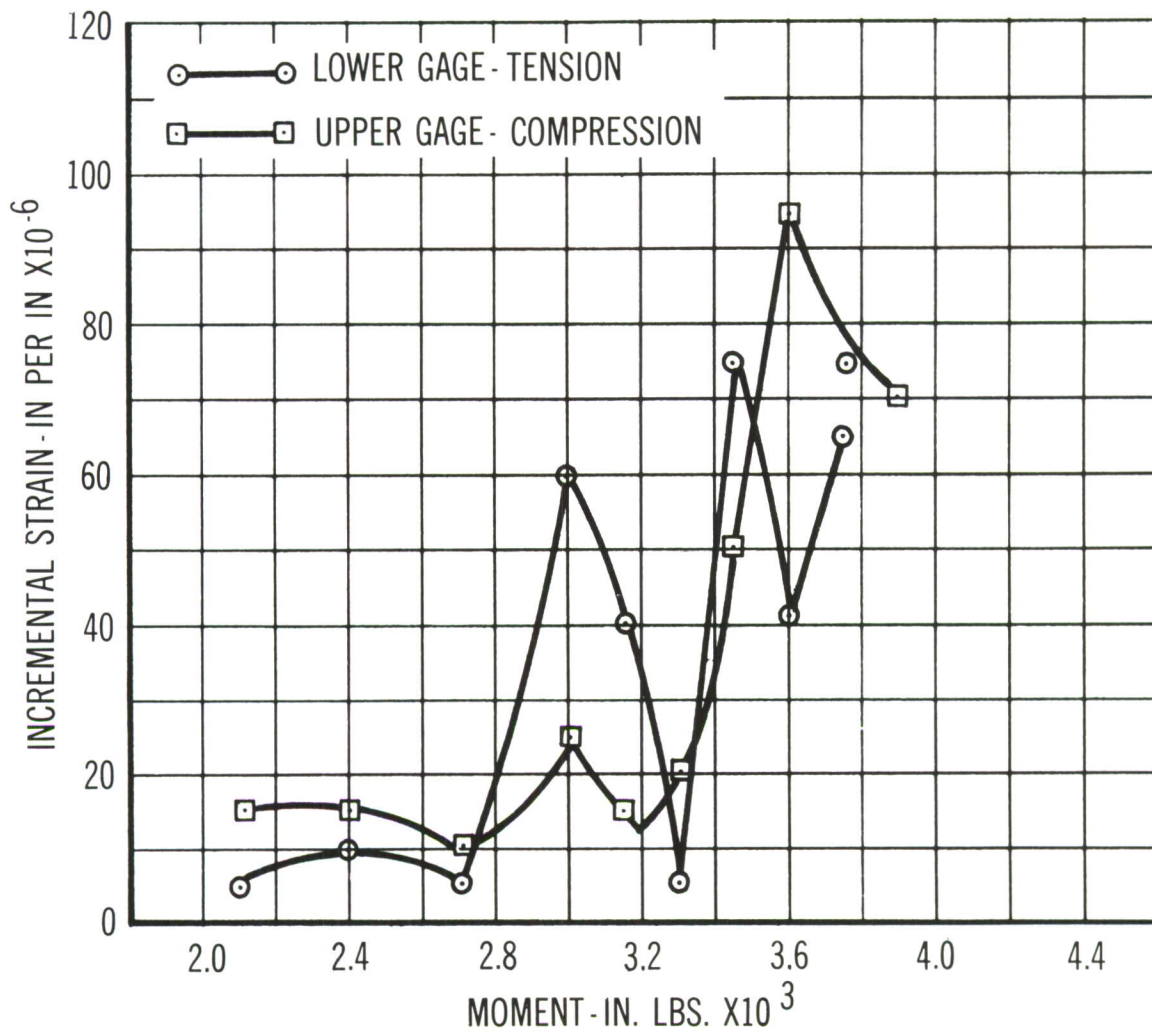


Figure 16. Incremental Strain-Bending Moment Relationships in Test Beams

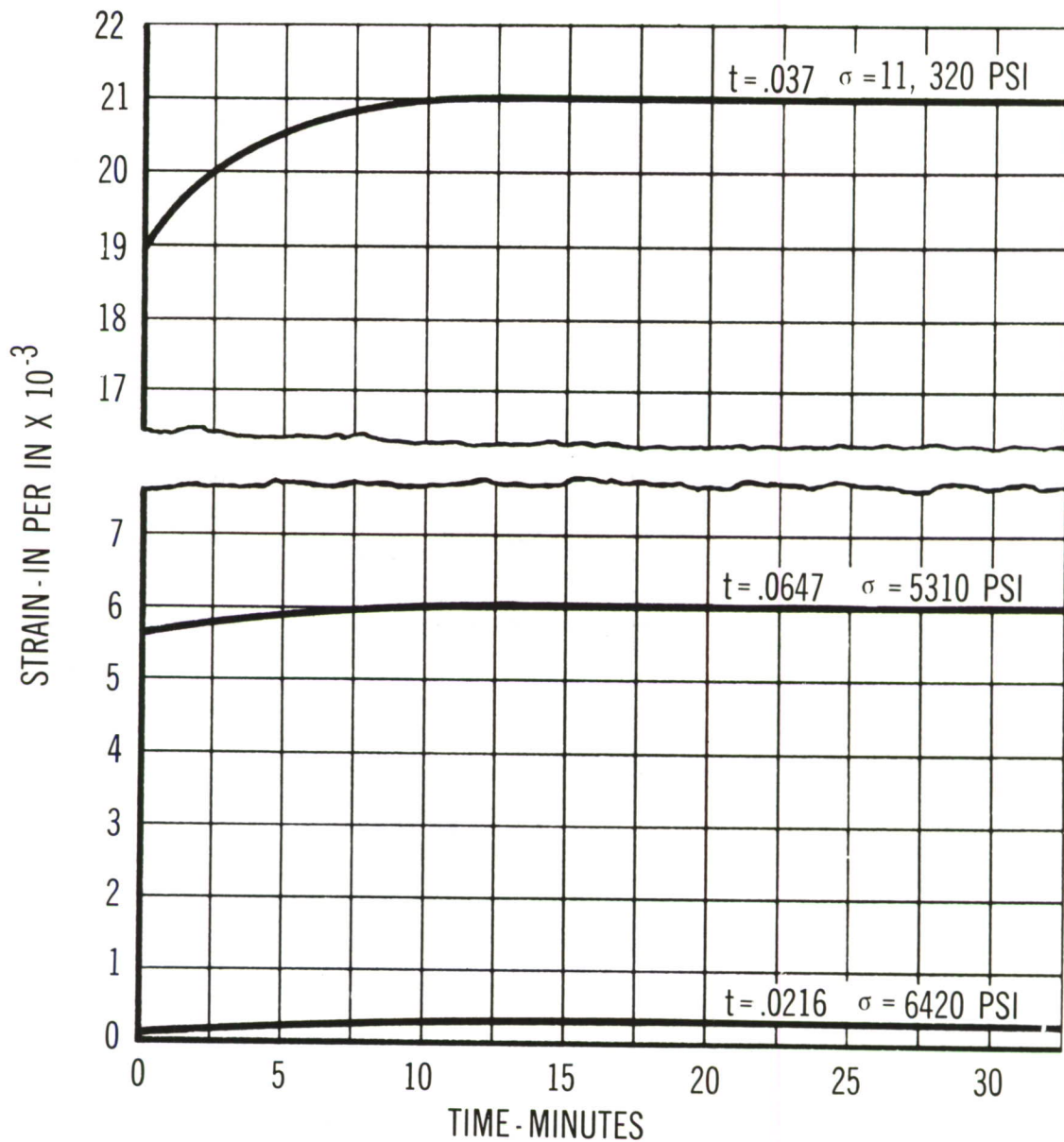


Figure 17. Stress-Strain-Time Relationships for Various Thicknesses of Copper in Tension

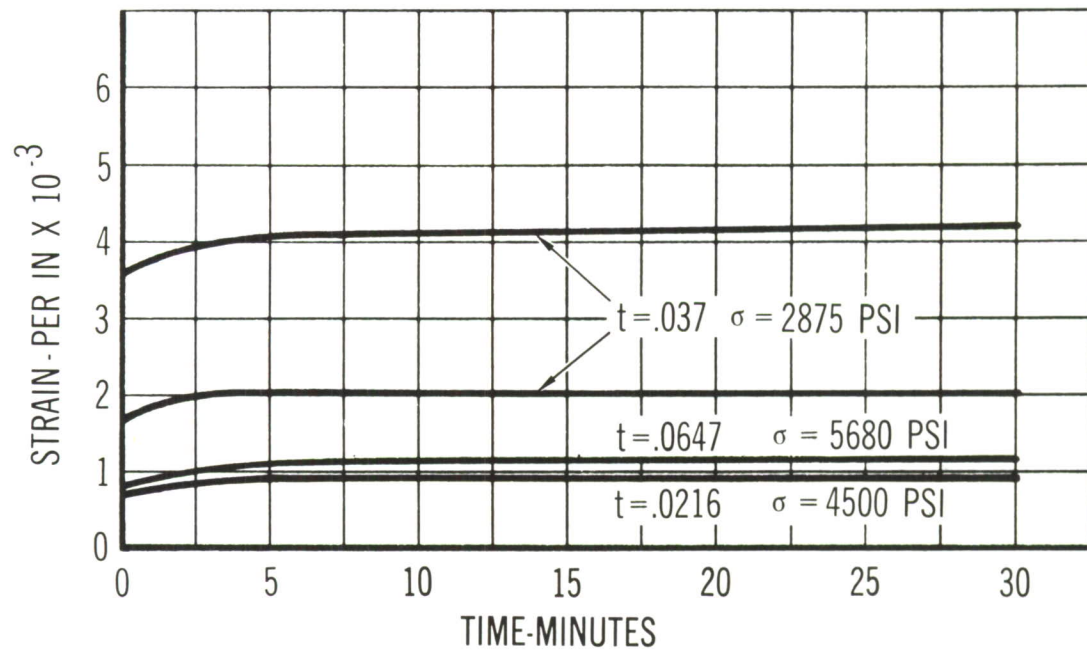


Figure 18. Stress-Strain-Time Relationships for Various Thicknesses of Copper in Shear

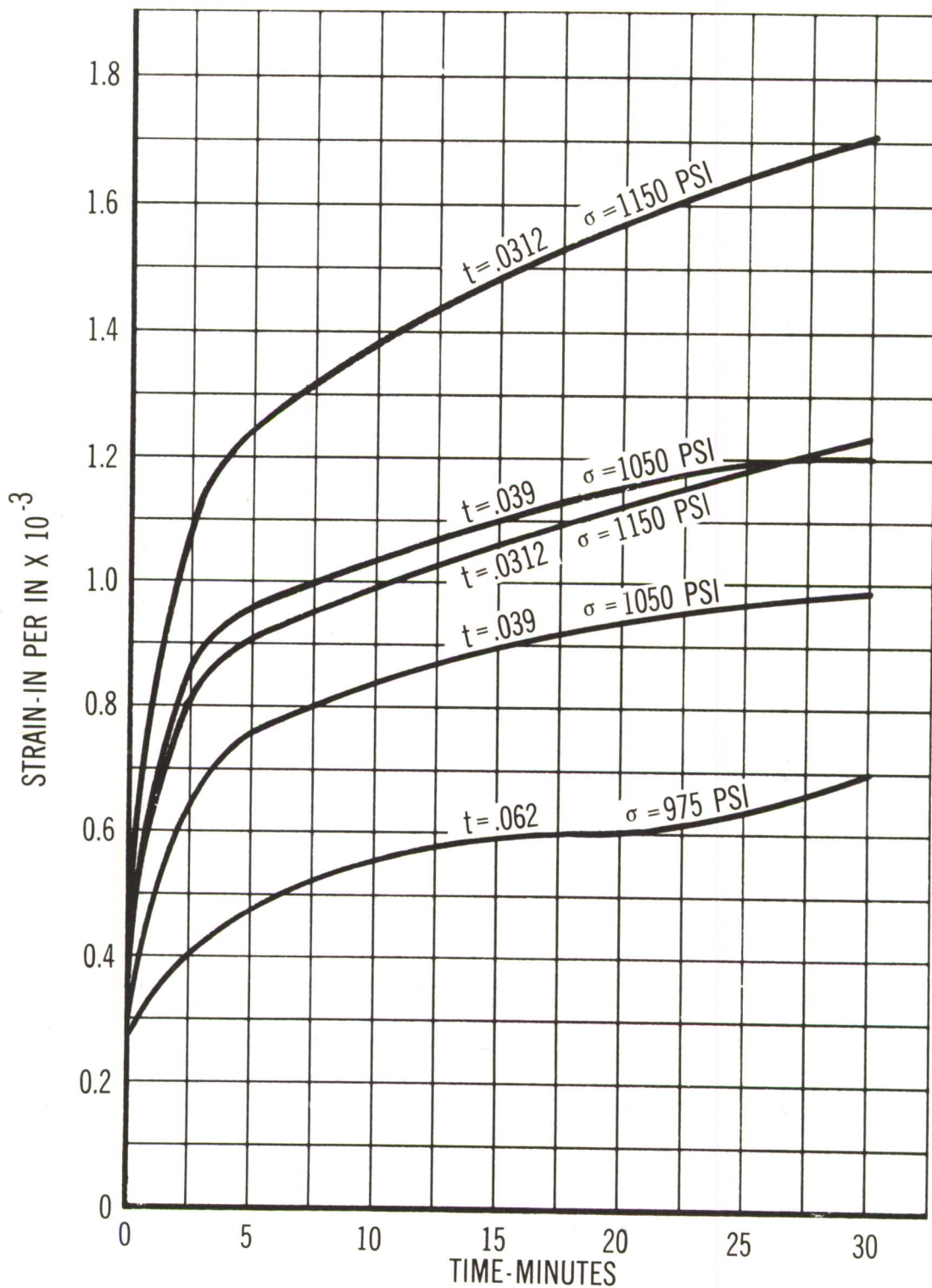


Figure 19. Stress-Strain-Time Relationships for Various Thicknesses of Lead in Tension

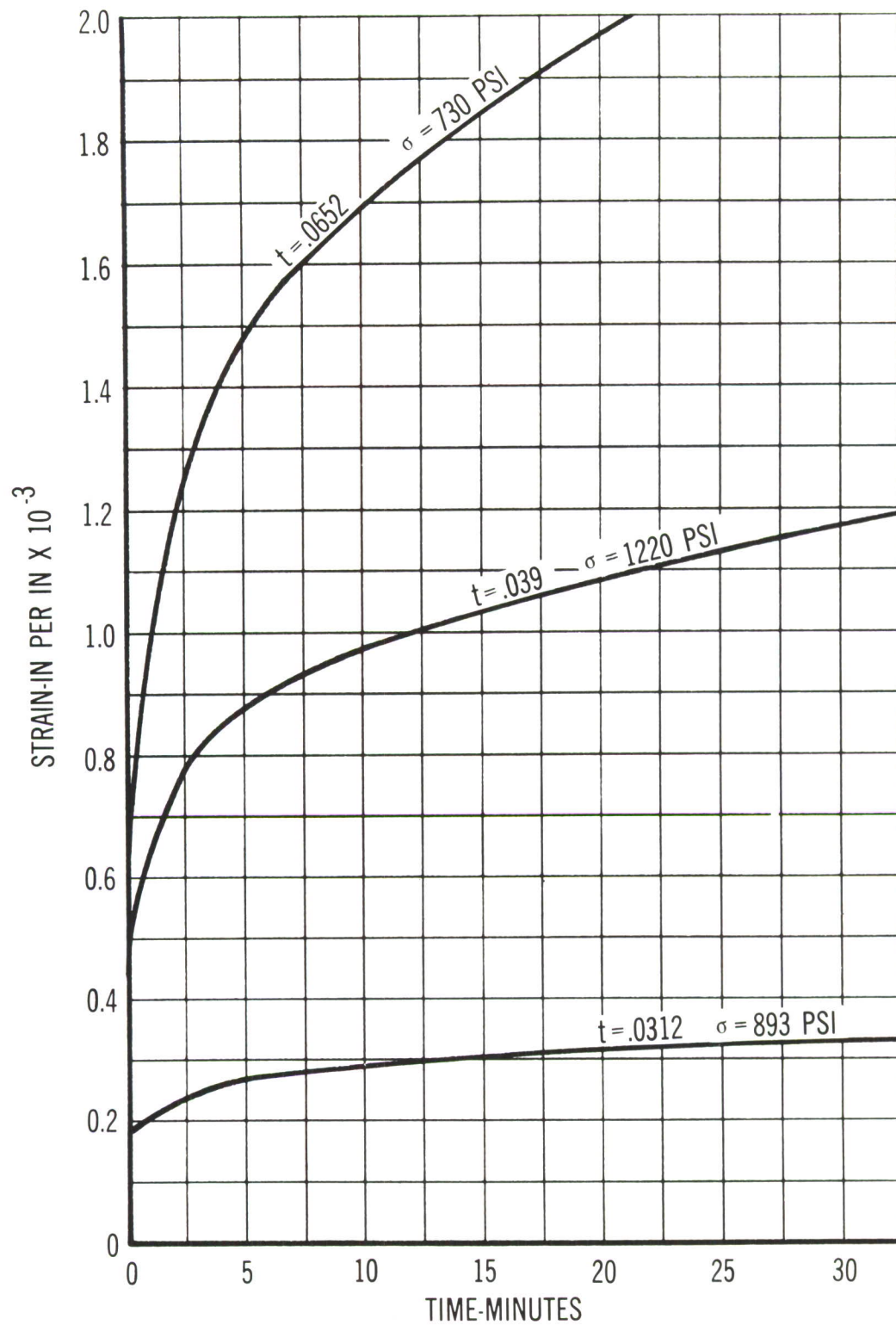


Figure 20. Stress-Strain-Time Relationships for Various Thicknesses of Lead in Shear

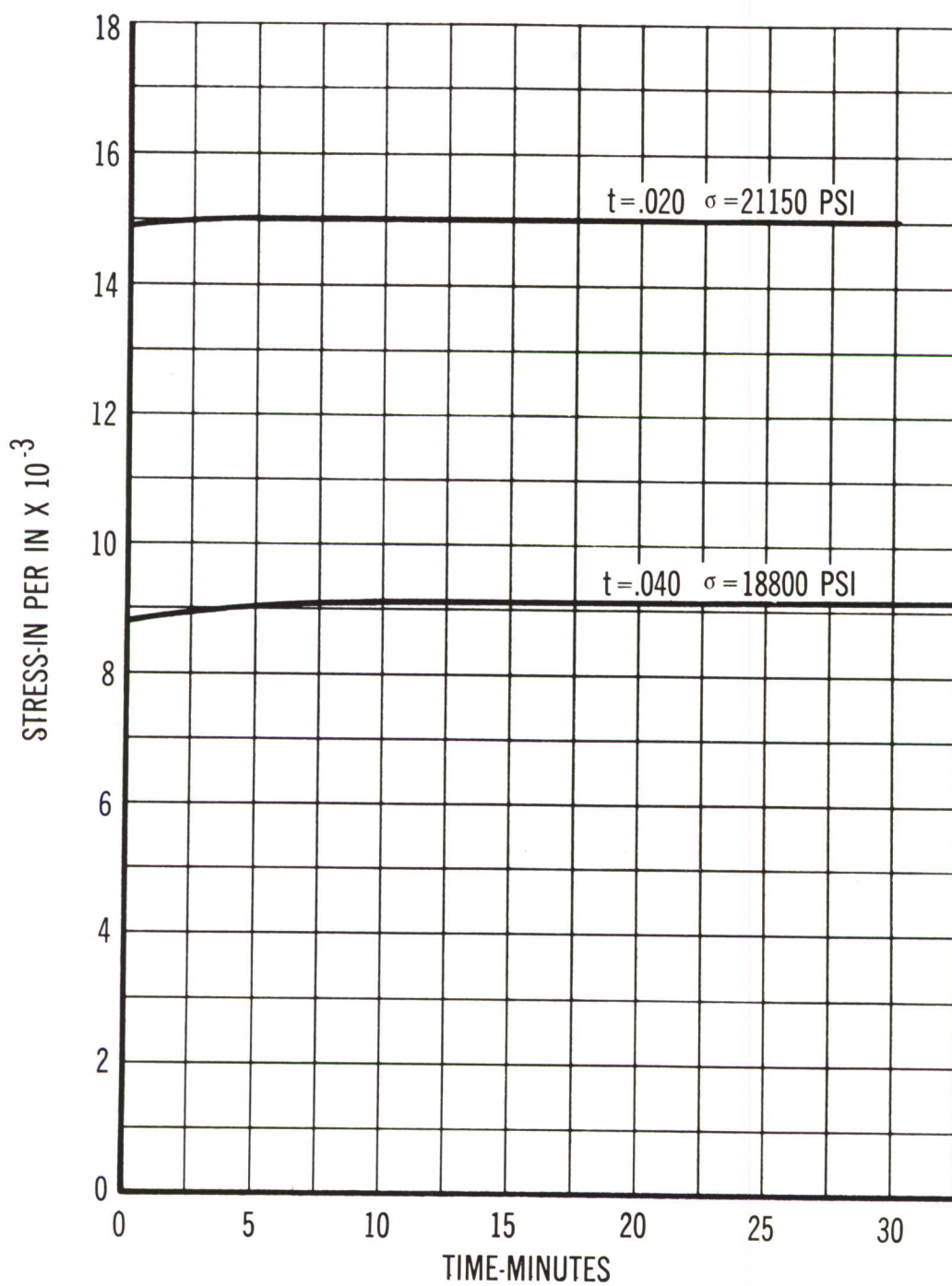


Figure 21. Stress-Strain-Time Relationships for Various Thicknesses of Aluminum in Tension

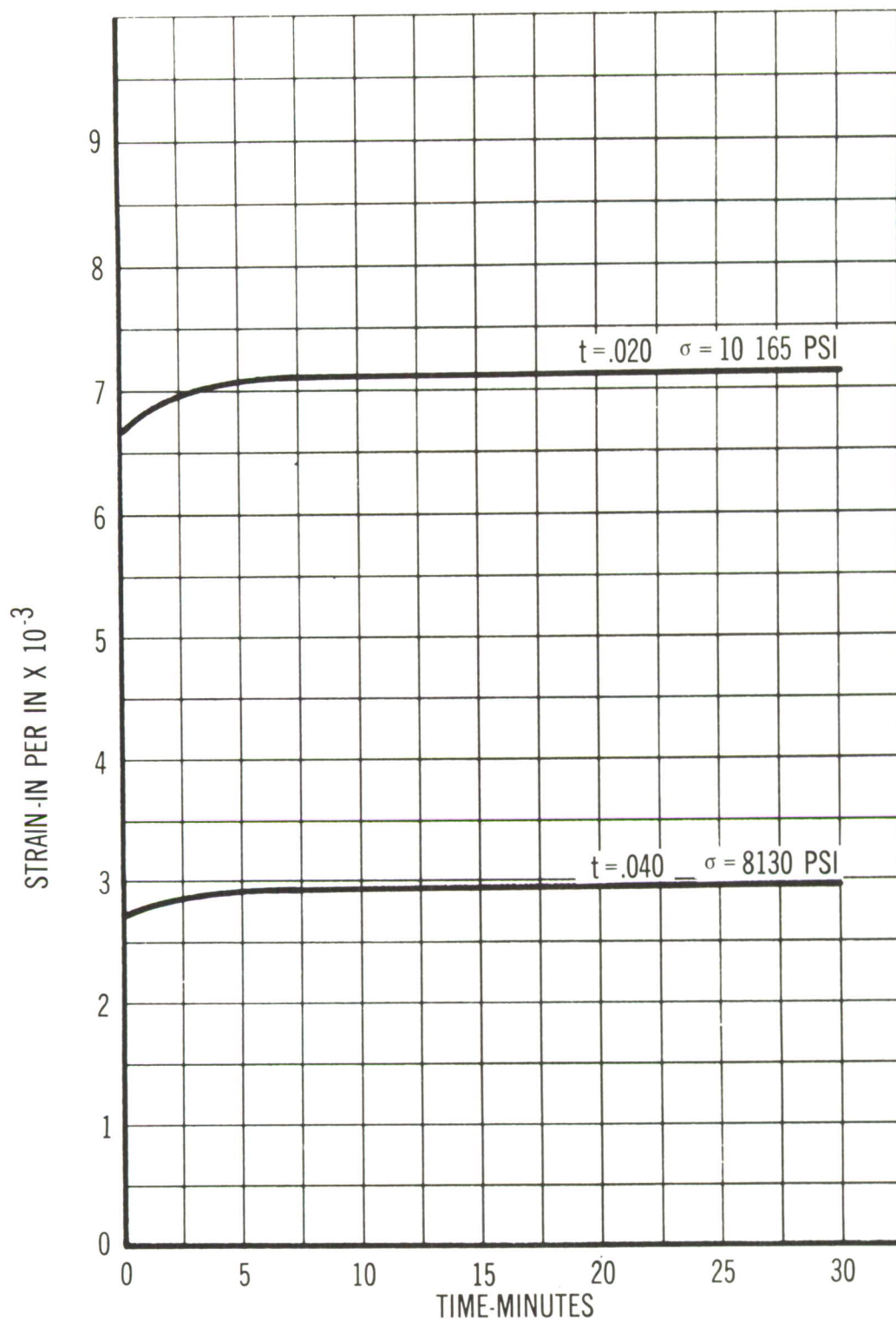


Figure 22. Stress-Strain-Time Relationships for Various Thicknesses of Aluminum in Shear

PREDICTION OF CREEP EFFECTS

IN

AIRCRAFT STRUCTURES

PART III

DEMONSTRATION OF NUMERICAL

METHOD

PLAN FOR PROBLEM SOLUTION

The plan of attack for problem solution must necessarily follow a time sequence because of the dissipative nature of plastic flow. A relaxation pattern was used for convenience and possibly some of the intermediate outlined phases can be lumped together in a new numerical scheme.

In a visualization of the sequence of physical processes identified at each phase of problem attack, the following events are pictured. First, a structure is locked into a rigid restraining frame at some uniform reference temperature, say room temperature. The structure is locked at node points and is in a state of equilibrium. Then the structure is considered heated in such a manner that temperature distributions within it replicate a given condition of structural operation. During heating the following events are visualized as taking place in two successive steps: an accumulation of thermal expansion stress followed by an accumulation of dilation effects. In the analysis, stress build-up is visualized as taking place in a "locked" structure, and, the expansion or dilation as taking place upon "unlocking" of the structure. In the analysis of stresses and deformations taking place under these hypothetical conditions, the structure is considered an elastic unit moving from a condition of equilibrium at low temperature to a new condition of equilibrium dependent upon conditions of a specified elevated temperature distribution. Finally in completion of problem solution, readjustments in stresses and deformations taking place at elevated temperatures as a consequence of creep are superimposed upon those stresses and deformations which result from elastic action taking place because of thermal expansion.

In detail, the attack for problem solution follows the sequence of steps given below:

1. The stresses in the heated and locked structure are computed.
2. The resultant forces and moments at nodes are computed from stress distributions determined in the preceeding step.
3. The forces and moments, so far as they are carried by the locks, are applied on the structure as external loads. At this stage of procedure forces and moments are treated separately. Moments are treated according to existing routine for the stress analysis of wings. Accordingly, the treatment at hand is only concerned with forces acting in the plane of a wing.
4. The stiffness coefficients, applicable to various structural elements, such as panels, spar caps and spar webs, are computed to represent temperature conditions under which individual elements operate.
5. The stiffness coefficients for each node of the structure are computed.

6. Using the loads acting upon the nodes, which were determined in step 3, and, the stiffness coefficients, determined in step 5, the displacements taking place at the nodes are computed.
7. The stress-increments arising from load displacements determined in step 6 are computed.
8. Stress increments found in step 7 are superposed upon stresses determined for the locked structure in step 1. These are thermal stresses present in a perfectly elastic structure before creep is introduced to it.
9. Using thermal stresses determined in step 8, equivalent uniaxial stresses are determined in accordance with equation (12) given under Numerical Method. These equivalent uniaxial stresses are introduced into creep charts of the kind shown in Figures 35 to 38 inclusive to determine the possibility of creep action being present in various structural elements. Where creep is activated, components of the deviator are computed and corresponding creep rates are ascertained from data of the kind shown in Figures 35 to 38 inclusive.
10. By applying simple uniaxial relaxation to one section and by proportioning relaxation in this section and proportioning then relaxation the stress increments in terms of overstress, a suitable time interval is determined. Using this time value, relaxation stress increments are computed in terms of principal and resolved stress increments.
11. Using resolved stress increments, corresponding forces at the locked nodes are determined and these are used to compute corresponding node displacements. Finally, stress increments due to these displacements are computed.
12. The incremental stresses computed in step 11 are superimposed upon the stresses determined in step 8. These totalized stresses are the thermal stresses in the structure and reflect elastic and creep actions.

EXAMPLE PROBLEM STATEMENT

A conventional delta wing structure is assumed for this example and is shown in Figure 23. The surfaces are equal and have the same temperature distributions. The temperatures assumed are:

Panels	450°F
Spar Caps	300°F
Spar Webs	150°F
Front Spar (caps and webs)	450°F

For purposes of this example, the structure shown in Figure 24 has its node [1] hinged to a rigid reference frame. The nodes [5], [8] and [10] are hinged to carriages, so that displacements in the "x" direction are prevented and those in the "y" direction are unrestricted. In proceeding, the method of stiffness coefficients is used and forces acting on nodes in the locked structure are assumed as input for solution as shown in Figure 25. The final force and stress distribution arrived at in problem solution results from superposition of force and stress increments, developed in the course of redundant analysis, upon those initial forces and stresses introduced at the onset as shown in Figure 25.

ASSUMPTIONS INCORPORATED IN EXAMPLE PROBLEM

Assumptions immediately applicable in analysis are:

1. Linear relations between forces and displacements exist. Buckling and plastic deformations are excluded from the general assumption.
2. Actions of forces in the plane of the wing and of moments bending the spars are separately computed. Their effects are additive.
3. The deformation of the entire structure in its middle plane is described in terms of displacement of its nodes. The spar elements are considered as bars hinged at nodes. These bars remain straight between nodes.
4. Buckling of panels, bending of spar elements between nodes, shear lag, and, effects of local thermal gradients are assumed negligible in initial analysis. These assumptions aim to obtain average stresses in the structural elements. In the event consideration need be given these conditions, their effects may be introduced into the solution, at an appropriate point, in the form of corrections.

EXAMPLE PROBLEM MATERIALS

The material assumed for the problem is 7075-T6 aluminum alloy. The value of Young's modulus, E , as a function of temperature is taken from NACA-TN-3584, Figure 15, page 23. The coefficient of expansion, also a function of temperature, is assumed constant but is used only in the presence of vertical stress and strain. The value, $\alpha = 12.8 \times 10^{-6} \text{ } ^\circ\text{F}^{-1}$, is used in the absence of more precise information. Poisson's modulus is taken at $\nu = .3$ throughout the example. Detailed modulus of elasticity and thermal expansion coefficient data are shown in Appendix II.

EXAMPLE PROBLEM SOLUTION

Initially all nodes of the structure are "locked" against all displacement and rotation as shown in Figures 24 and 25. In this initial condition all elements of the structure are at a uniform temperature, T_0 , assumed as reference temperature. The temperature, T_i , for each element, i , is given in Table 5. Temperature increments are computed according to the equation, $\Delta T = T_i - T_0$. The Young's modulus, E , and the expansion coefficient, α , are determined as functions of the temperature, T_i , according to the respective equations, $\alpha = \alpha(T_i)$ and $E = E(T_i)$.

STRESSES IN THE LOCKED STRUCTURE

The axial stress, σ , and the Force N , due to the temperature increment, ΔT_i , in each bar (spar cap) having cross section area, A , is computed while the bar ends are restrained against displacement according to the formulas, $\sigma = -E\alpha\Delta T$ and $N_0 = AE\alpha\Delta T$. The hydrostatic stress, σ , and the uniform edge thrust, p , in each plate of thickness, t , are computed according to the formulas.

$$\sigma = \sigma_1 = \sigma_2 = - \frac{E}{1 - \nu} \alpha \Delta T \quad \text{and}$$

$$p_1 = p_2 = - \frac{Et}{1 - \nu} \alpha \Delta T.$$

These thrust components are the force inputs for the stress analysis. They are reduced to nodes (panel points) in the usual way by integrating and distributing them to adjacent nodes in proportion to distances to the nodes.

The loads to the locked nodes from adjacent panels are at least partially balanced. The resultant forces at the locked nodes are the force inputs for the stress analysis which will give the second term for the stresses.

The computed stresses and forces in the spar elements of the locked structure are given in Table 6 and those for the plate elements or panels are given in Table 7. The resultant forces acting on the nodes of the locked structure are shown in Figure 25 which presents the force input for solution of the redundant structure. Figure 26 augments Figure 25 and Table 7 in that it diagrams the node forces balancing hydrostatic pressure in triangular panels incorporated in the delta wing plan shown in Figure 25.

STIFFNESS COEFFICIENTS FOR SINGLE ELEMENTS

In a spar element of length, L , and cross section area, A , which is fixed at its left end and free to move at its right end, as shown in Figure 27, the stiffness coefficients, measured by forces acting on the bar, are given in terms of horizontal displacement, U , and vertical displacement, V . In most cases vertical displacements are small and are neglected in the example problem. In the example problem stiffness coefficients for spar and rib elements in the "x" and "y" directions are evaluated in Figure 28.

In consideration of oblique frame elements, Figure 29 illustrates a spar element of length, L , whose projection on the x-axis is, a , and on the y-axis is, b , so that

$L = \sqrt{a^2 + b^2}$. When a unit displacement is imposed upon node B in the x-direction, the relation,

$$\frac{DE}{DB} = \frac{\delta L}{1} = \frac{a}{L},$$

arises from similarity of the triangles ABC and EDB. Therefore the strain follows the relation,

$$\epsilon = \frac{\delta L}{L} = \frac{a}{L^2}$$

and the axial force, N , follows

$$N = EA\epsilon = EA \frac{a}{L^2}.$$

The force component in the x-direction, N_x , follows the relation

$$N_x = N \frac{a}{L} = EA \frac{a^2}{L^3}$$

and the force component in the y-direction, N_y follows the relation

$$N_y = -N \frac{b}{L} = -EA \frac{ab}{L^3}.$$

In the same way, when unit displacement is imposed on the node B in the y-direction, the axial force and its components follow the relations,

$$N = -EA \frac{b}{L^2}$$

$$N_x = -EA \frac{ab}{L^3}$$

and

$$N_y = EA \frac{b^2}{L^3}.$$

The stiffness coefficients for the oblique bar, shown in Figure 30, which arise from the relations given above are tabulated in Table 8 where the subscripts, "B" and "C", denote applicable node points. In addition, the stiffness coefficients for the

oblique bar can be written analytically as it follows with $L = \sqrt{(a^2 + b^2)}$ that

$$\frac{\partial L}{\partial a} = \frac{2a}{2L} = \frac{a}{L}$$

and for a displacement, u , of the node B, that is an increment, u , of length a , the relation

$$\delta L = \frac{\partial L}{\partial a} u = \frac{au}{L}$$

obtains, and therefore,

$$\epsilon = \frac{\delta L}{L} = \frac{au}{L^2},$$

and, for an incremental displacement of $u = 1$, the results shown in Table 8 can be derived. The numerical results obtained for the example problem conditions through use of the stiffness coefficients given in Table 8 are shown in Figure 31.

The stiffness coefficients for the rectangular plates are computed from the equations given in Table 9 which are taken from J. H. Argyris, "Energy Theorems and Structural Analysis", Aircraft Engineering, April 1955, page 125.

The stiffness coefficients for the triangular plates are computed from the equations given in Table 10 and which are taken from Turner, M. J., Clough, R. W., Martin, H. C. and Topp, L. S., "Stiffness and Deflection Analysis of Complex Structures", Journal of Aeronautical Sciences, September 1956. The numerical stiffness coefficients applicable to the triangular plates of the example problem are given in Table 11.

The computation of stiffness coefficients for each node of the structure, and each displacement, y , taking place at respective nodes is summarized in Table 12. The assembled matrix is given in Table 13. The degrees of freedom u_1 , v_1 , u_5 , u_8 and u_{10} at the node points [1] [5] [8] and [10] are set equal to zero according to the boundary conditions established and shown in Figure 24. The loads applied are those acting on the nodes of the locked structure as diagrammed in Figure 25. The

displacements of the nodes resulting from digital computer calculations for the load input given in Figure 25 are summarized in Table 14 and are indicated in Figure 31 in an exaggerated scale with respect to that used to diagram the structure.

STIFFNESS COEFFICIENTS FOR WING STRUCTURE

The stiffness coefficients defined for unit displacements of each node of the wing structure in the directions, u, and v, are computed as sums of the stiffness coefficients common to a given node. The assembled matrix of stiffness coefficients is given in Table 13. The force inputs are those shown in Figure 25. The result of combining these coefficients with the force inputs appears in terms of displacement of nodes as shown in Table 14 and Figure 31.

In proceeding to wing structure, stress increments due to the load displacements are computed. The internal forces are next determined as products of the displacements and the element stiffness coefficient matrix. This matrix multiplication is performed on a digital computer and the resulting product is shown in Table 15 which lists the forces on rectangular panels or plates and in Table 16 which lists the forces on triangular panels.

Following this, stress increments for panels are computed from the forces given in Tables 15 and 16. Final stresses are found by superposition of stress increments upon stresses in the locked structure shown in Table 5. The computations for arriving at incremental stresses in panels of the wing are given in Table 17. Computations of stress increments in spar caps and webs are shown in Table 18. Final stresses resulting from thermal expansion effects and effects arising from displacements attendant to thermal expansion are given, for the spar caps in Table 19, and, for the spar webs in Table 20. The final thermal stresses in the spar caps, spar webs and wing panels are shown in Figures 32, 33 and 34 respectively. Those stresses shown in Figures 32, 33 and 34 represent thermal stresses in perfectly elastic structure prior to introducing effects arising from creep action.

CREEP EFFECT

The computation of the creep effect proceeds in accordance with the method developed in the Numerical Method section of this report. The creep calculations are entered by transforming the component thermal stresses shown in Figures 32, 33 and 34 into equivalent uniaxial stresses by means of the von Mises-Prager method discussed in the Numerical Method section. The results of such calculations with respect to the panels in the example problem wing are given in Tables 21, 22 and 23 and apply at the beginning of a creep period where time is considered at zero value. In particular, the uniaxial stresses sought are tabulated in column 4 of Table 23. When these stresses are entered into creep charts of the type shown in Figures 35 through 39 inclusive, the creep rates shown in column 6 of Table 23 are developed for the temperatures shown in column 5 of the table. Then returning to the stress components shown in Table 21 the components of the deviator are computed in accordance with equations (19), (20) and (21) of the Numerical Method section. The outcome of these computations is given in Table 24. Employing the stress deviator values given in Table 24, the creep rates in the principal directions are calculated in accordance with equations (10) and (11) of the Numerical Method section to develop creep rates corresponding to components of the stress deviator as shown in Table 25.

A numerical value for the time interval, Δt , was determined as shown in Table 26 by applying a simple uniaxial relaxation to one section and by imposing the condition that the relaxation stress increments would be of the order of 10% of the overstress. The time interval resulting is $\Delta t = 4$ minutes. The relaxation stress increments in the locked panels of the wing are computed as shown in Table 27 in terms of the

principal stresses $\Delta\sigma_1$ and $\Delta\sigma_2$. The corresponding stress increments $\Delta\sigma_x$, $\Delta\sigma_y$ and $\Delta\tau_{xy}$ are calculated as shown in Tables 28 and 29.

Continuing with the calculations, the force inputs at the locked nodes are computed for the rectangular and triangular plates as shown in Tables 30 and 31 according to formulas given in respective tables. These force inputs are subsequently resolved into resultant forces (See Tables 32 and 33) acting at the locked nodes. These resultant forces are introduced as known terms in the system of equations represented in Table 13. The corresponding displacements obtained by combining Table 31 and 32 data with that given in Table 13 through matrix multiplication by means of a digital computer are found in Table 34. The increments of stresses due to these displacements which represent relaxation of the nodes are computed as shown in Tables 35 to 38.

The total stresses, the sum of the initial thermal expansion stress given in Table 5, the relaxation increment applied to the thermal expansion stress condition given in Table 16, and the stress increments arising subsequent to creep as given in Table 38, are given in Table 39.

TABLE 5 THERMAL STRESSES IN EXAMPLE PROBLEM WING

Element	Temperature °F	Modulus Of Elasticity PSI x 10 ⁶ (1)	Thermal Stresses	
			"Bar" Elements PSI (2)	"Plate" Elements PSI (3)
Panel	450	8.4	--	- 68,400
Cap - Spar	300	9.6	- 36,900	--
Web - Spar	150	9.8	- 18,750	- 26,700
Caps & Webs (Front Spar)	450	8.8	- 50,700	--

Notes:

- (1) The moduli were found slightly in error. Since a method is demonstrated corrections are not made to correct the moduli given.
- (2) Where the thermal stresses in "bar" elements are computed from the formula

$$- E\alpha T.$$

- (3) Where the thermal stresses in "plate" elements is computed from the formula

$$- \frac{E\alpha T}{1-\nu}, \text{ and}$$

E represents modulus of elasticity

α represents coefficient of thermal expansion

T represents temperature differential

ν represents Poisson's ratio

TABLE 6 COMPUTED SPAR ELEMENT STRESSES AND FORCES⁽¹⁾
 IN EXAMPLE PROBLEM WING

Spar Caps

Area, A , = 1 sq. in where each cap area is 0.5 sq. in.
 Temperature Differential, T , = 300°F
 Axial Stress, $\sigma_o = -E\alpha T = -36,900$ lbs/sq in (See Table 5)
 Axial Force, $N_o = -36,900$ lbs. for both caps.

Spar Web

Area, A , = 1 sq. in. where depth = 5 in. and thickness = .2 in
 Temperature differential, T , = 150°F
 Axial stress, $\sigma_o = -E\alpha T = -18,750$ lbs/sq in. (See Table 5)
 Axial Force, $N_o = -18,750$ lbs.

Axial Force in Locked Spar

Axial Force, $N_o = -36,900$ lbs. (spar caps) -18,750 lbs. (spar web)
 = -55,650 lbs

Front Spar

Area, $A = 2$ sq. in.
 Temperature differential, T , = 450°F
 Axial stress, $\sigma_o = -E\alpha T = -50,700$ lbs/sq. in. (See Table 5)
 Axial Force, $N_o = 2 \sigma_o = 101,400$ lbs.

Note:

(1) Horizontal and vertical directions.

TABLE 7 STIFFNESS COEFFICIENT MATRIX MULTIPLICATION FOR FRONT SPAR

IN EXAMPLE PROBLEM WING.

	<u>U_B</u>	<u>V_B</u>	<u>U_C</u>	<u>V_C</u>
<u>U_B</u>	$+\frac{a^2}{L^3}$	$-\frac{ab}{L^3}$	$-\frac{a^2}{L^3}$	$+\frac{ab}{L^3}$
<u>V_B</u>	$-\frac{ab}{L^3}$	$+\frac{b^2}{L^3}$	$+\frac{ab}{L^3}$	$-\frac{b^2}{L^3}$
<u>U_C</u>	$-\frac{a^2}{L^3}$	$+\frac{ab}{L^3}$	$+\frac{a^2}{L^3}$	$-\frac{ab}{L^3}$
<u>V_C</u>	$+\frac{ab}{L^3}$	$-\frac{b^2}{L^3}$	$-\frac{ab}{L^3}$	$+\frac{b^2}{L^3}$

. EA

TABLE 8 COMPUTED RECTANGULAR PLATE STRESSES AND FORCES

IN EXAMPLE PROBLEM WING

DATA

Temperature Differential, T , = 450°F
Modulus of Elasticity, E , = 8.4×10^6 lbs/sq. in.
Coefficient of Thermal Expansion, α , = 12.8×10^{-6} in/in/ $^{\circ}\text{F}$
Thickness, t , = 0.1 in.

SOLUTION

Then where the horizontal stress, σ_1 , equals the vertical stress, σ_2 ,

$$\sigma_1 = \sigma_2 = -\frac{E T}{1-\nu} = -68,400 \text{ lbs/sq. in.}$$

and the edge thrust, p , equals -68,400 lbs/sq. in.

Hence the thrust on the upper edge, P_u , and on the lower edge, P_ℓ , sums as

$$P_u + P_\ell = 136,800 \text{ lbs/sq. in.}$$

Considering a 10 in (x-direction) by 20 in. (y-direction) panel

the reaction in the x-direction, R_x , = 237,600 lbs, and

the reaction in the y-direction, R_y , = 138,600 pounds.

TABLE 9 STIFFNESS COEFFICIENTS FOR RECTANGULAR PLATES

IN EXAMPLE PROBLEM WING

List of Coefficients

$$K_{13} = - \frac{E}{1 - \nu^2} \frac{d \cdot t}{3l} + \frac{G \cdot t \cdot l}{6d}$$

$$K_{23} = - \frac{E}{1 - \nu^2} \frac{d \cdot t}{6l} - \frac{G \cdot t \cdot l}{6d}$$

$$K_{33} = \frac{E}{1 - \nu^2} \frac{d \cdot t}{3l} + \frac{G \cdot t \cdot l}{3d}$$

$$K_{43} = \frac{E}{1 - \nu^2} \frac{d \cdot t}{6l} - \frac{G \cdot t \cdot l}{3d}$$

$$K_{53} = - \frac{\nu E t}{4(1 - \nu^2)} + \frac{G t}{4}$$

$$K_{63} = \frac{\nu E t}{4(1 - \nu^2)} + \frac{G t}{4}$$

$$K_{73} = - \frac{\nu E t}{4(1 - \nu^2)} - \frac{G t}{4}$$

$$K_{83} = \frac{\nu E t}{4(1 - \nu^2)} - \frac{G t}{4}$$

TABLE 9 STIFFNESS COEFFICIENTS FOR RECTANGULAR PLATES
(Cont'd) IN EXAMPLE PROBLEM WING

List of Symbols

- K represents the stiffness coefficient where the first digit of the subscript denotes the node point at which load application is considered and the second digit of the subscript denotes the node at which displacements are under consideration.
- E represents Young's modulus.
- ν represents Poisson's ratio
- d represents dimension (see sketch)
- ℓ represents dimension (see sketch)
- t represents thickness
- G represents shear modulus

Reference

Argyres, J. H., "Energy Theorems and Structural Analysis", Aircraft Engineering, Vol 2, No. 4, April 1955, page 125.

Sketch

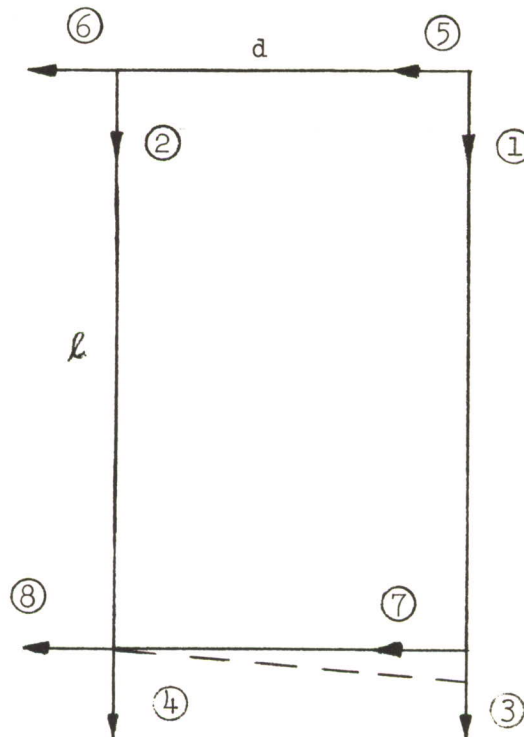


TABLE 10 STIFFNESS COEFFICIENT MATRIX FOR TRIANGULAR PLATES IN EXAMPLE PROBLEM WING

Matrix

	U_1	U_2	U_3	V_1	V_2	V_3
U_1	$\frac{h}{d} + \lambda_1 \frac{d}{h}$					
U_2	$-\frac{h}{d}$	$\frac{h}{d}$				
U_3	$-\lambda_1 \frac{d}{h}$	0	$\lambda_1 \frac{d}{h}$			
V_1	λ_2	$-\nu$	$-\lambda_1$	$\frac{d}{h} + \lambda_1 \frac{h}{d}$		
V_2	$-\lambda_1$	0	λ_1	$-\lambda_1 \frac{h}{d}$	$\lambda_1 \frac{h}{d}$	
V_3	$-\nu$	ν	0	$-\frac{d}{h}$	0	$\frac{d}{h}$

$$\cdot \frac{E t}{2(1 - \nu^2)}$$

TABLE 10 STIFFNESS COEFFICIENT MATRIX FOR TRIANGULAR PLATES IN EXAMPLE PROBLEM WING
(Cont'd)Basic Formulae

$$\lambda_1 = \frac{1 - \nu}{2} \quad (\text{horizontal})$$

$$\lambda_2 = \frac{1 + \nu}{\nu} \quad (\text{vertical})$$

List of Symbols

- U represents horizontal stiffness coefficient
 V represents vertical (shear) stiffness coefficient
 h represents dimension
 d represents dimension
 λ represents matrix factor (horizontal projection of incremental length)
 ν represents Poisson's ratio
 E represents Young's modulus
 t represents thickness

Reference: Turner, M. J., Clough, R. W., Martin, H. C. and Topp, L. S. "Stiffness and Deflection Analysis of Complex Structures", Journal of Aeronautical Sciences, Vol. 23, No. 9, September 1956, page 805.

TABLE 11 STIFFNESS COEFFICIENTS FOR TRIANGULAR PLATES IN EXAMPLE PROBLEM WING

Matrix

	U_1	U_2	U_3	V_1	V_2	V_3
U_1	2.0075	-1.846	-0.1615	0.6	-0.323	-0.277
U_2	-1.846	1.846	0	-0.277	0	0.277
U_3	-0.1615	0	0.1615	-0.323	0.323	0
V_1	0.6	-0.277	-0.323	1.108	-0.646	-0.462
V_2	-3.23	0	0.323	-0.646	0.646	0
V_3	-0.277	0.277	0	-0.462	0	0.462

 $\times 10^6$

TABLE 11 STIFFNESS COEFFICIENTS FOR TRIANGULAR PLATES IN EXAMPLE PROBLEM WING
(Cont'd)

List of Symbols

U	represents horizontal stiffness coefficient
V	represents vertical (shear) stiffness coefficient
h	represents dimension
d	represents dimension
λ	represents matrix factor (horizontal projection of incremental length)
ν	represents Poisson's ratio
E	represents Young's modulus
t	represents thickness

TABLE 12 SUMMARY OF STIFFNESS COEFFICIENTS AND DISPLACEMENTS

AT EACH NODE OF EXAMPLE PROBLEM WING

NODE 1

NODE	STIFFNESS COEFFICIENTS $\times 10^6$					
	U ₁ DISPLACEMENT			V ₁ DISPLACEMENT		
	STRINGER	PANEL 1256	TOTAL	STRINGER	PANEL 1256	TOTAL
U ₁	1.94	1.3374	3.2744	----	0.3	0.3
V ₁	----	0.3	0.3	0.97	0.7382	1.7082
U ₂	-1.94	-1.1758	-3.1158	----	0.0231	0.0231
V ₂	----	0.0231	-0.0231	----	-0.277	-0.277
U ₅	----	0.5072	0.5072	----	-0.0231	-0.0231
V ₅	----	0.0231	0.0231	-0.97	-0.0921	-1.0621
U ₆	----	-0.6688	-0.6688	----	-0.3	-0.3
V ₆	----	-0.3	-0.3	----	-0.3691	-0.3691

TABLE 12
(Cont'd)SUMMARY OF STIFFNESS COEFFICIENTS AND DISPLACEMENTS
AT EACH NODE OF EXAMPLE PROBLEM WING

NODE 2

NODE	STIFFNESS COEFFICIENTS $\times 10^6$							
	U ₂ DISPLACEMENT				V ₂ DISPLACEMENT			
	STRINGER	PANEL	PANEL	TOTAL	STRINGER	PANEL	PANEL	TOTAL
		1256	2367			1256	2367	
U ₁	-1.94	-1.1758	----	-3.1158	----	-0.0231	----	-0.0231
V ₁	----	0.0231	----	0.0231	----	-0.277	----	-0.0277
U ₂	3.88	1.3374	1.3374	6.5548	----	-0.3	0.3	0
V ₂	----	-0.3	0.3	0	0.97	0.7382	0.7382	2.4464
U ₃	-1.94	----	-1.1758	-3.1158	----	----	0.0231	0.0231
V ₃	----	----	-0.0231	-0.0231	----	----	-0.277	-0.277
U ₅	----	-0.6688	----	-0.6688	----	0.3	----	0.3
V ₅	----	-0.3	----	0.3	----	-0.3691	----	-0.3691
U ₆	----	0.5072	0.5072	1.0144	----	0.0231	-0.0231	0
V ₆	----	-0.0231	0.0231	0	-0.97	-0.0921	-0.0921	-1.1542
U ₇	----	----	-0.6688	-0.6688	----	----	-0.3	-0.3
V ₇	----	----	-0.3	-0.3	----	----	-0.3691	-0.3691

TABLE 12
(Cont'd)SUMMARY OF STIFFNESS COEFFICIENTS AND DISPLACEMENTS
AT EACH NODE OF EXAMPLE PROBLEM WINGNODE 3

NODE	STIFFNESS COEFFICIENTS $\times 10^6$							
	U ₃ DISPLACEMENT				V ₃ DISPLACEMENT			
	STRINGER	PANEL	PANEL	TOTAL	STRINGER	PANEL	PANEL	TOTAL
		2367	347			2367	347	
U ₂	-1.94	-1.1758	----	-3.1158	----	-0.0231	----	-0.0231
V ₂	----	0.0231	----	0.0231	----	-0.277	----	-0.277
U ₃	3.88	1.3374	2.0075	7.2249	----	-0.3	0.6	0.3
V ₃	----	-0.3	0.6	0.3	.97	0.7382	1.108	2.8162
U ₄	-1.94	----	-1.846	-3.786	----	----	-0.277	-0.277
V ₄	----	----	-0.323	-0.323	----	----	-0.646	-0.646
U ₆	----	-0.6688	----	-0.6688	----	0.3	----	0.3
V ₆	----	0.3	----	-0.3	----	-0.3691	----	-0.3691
U ₇	----	0.5072	-0.1615	-0.3457	----	0.0231	-0.323	-0.2999
V ₇	----	-0.0231	-0.277	-0.3001	-0.97	-.0921	-0.462	-1.5241

TABLE 12
(Cont'd)

SUMMARY OF STIFFNESS COEFFICIENTS AND DISPLACEMENTS
AT EACH NODE OF EXAMPLE PROBLEM WING

NODE 4						
NODE	STIFFNESS COEFFICIENTS $\times 10^6$					
	U_4 DISPLACEMENT			V_4 DISPLACEMENT		
	STRINGER	PANEL 347	TOTAL	STRINGER	PANEL 347	TOTAL
U_3	-1.94	-1.846	-3.786	----	-0.323	-0.323
V_3	----	-0.277	-0.277	----	-0.646	-0.646
U_4	2.114	1.846	3.960	-0.348	0	-0.348
V_4	-0.348	0	-0.348	0.696	0.646	1.342
U_7	-0.174	0	-0.174	0.348	0.323	0.671
V_7	0.348	0.277	0.625	-0.696	0	-0.696

TABLE 12 SUMMARY OF STIFFNESS COEFFICIENTS AND DISPLACEMENTS
(Cont'd) AT EACH NODE OF EXAMPLE PROBLEM WING

NODE 5

NODE	STIFFNESS COEFFICIENT $\times 10^6$							
	U ₅ DISPLACEMENT				V ₅ DISPLACEMENT			
	STRINGER	PANEL 1256	PANEL 5689	TOTAL	STRINGER	PANEL 1256	PANEL 5689	TOTAL
U ₁	----	0.5072	---	0.5072	----	0.0231	---	0.0231
V ₁	----	-0.0231	---	-0.0231	-0.97	-0.0921	---	-1.0621
U ₂	----	-0.6688	---	-0.6688	----	0.3	---	0.3
V ₂	----	0.3	---	0.3	----	-0.3691	---	-0.3691
U ₅	1.94	1.3374	1.3374	4.6148	----	-0.3	0.3	0
V ₅	----	-0.3	0.3	0	1.94	0.7382	0.7382	3.4164
U ₆	-1.94	-1.1758	-1.1758	-4.2916	----	-0.0231	0.0231	0
V ₆	----	0.0231	-0.0231	0	----	-0.277	-0.277	-0.554
U ₈	----	---	0.5072	0.5072	----	---	-0.0231	-0.0231
V ₈	----	---	0.0231	0.0231	- .97	---	-0.0921	-1.0621
U ₉	----	---	-0.6688	-0.6688	----	---	-0.3	-0.3
V ₉	----	---	-0.3	-0.3	----	---	-0.3691	-0.3691

TABLE 12 SUMMARY OF STIFFNESS COEFFICIENTS AND DISPLACEMENTS
(Cont'd) AT EACH NODE OF EXAMPLE PROBLEM WING

NODE 6

NODE	STIFFNESS COEFFICIENT $\times 10^6$ HORIZONTAL (U_6) DISPLACEMENT					TOTAL
	STRINGER	PANEL 1256	PANEL 2367	PANEL 5689	PANEL 679	
U_1	----	-0.6688	----	----	----	-0.6688
V_1	----	-0.3	----	----	----	-0.3
U_2	----	0.5072	0.5072	----	----	1.0144
V_2	----	0.0231	-0.0231	----	----	0
U_3	----	----	-0.6688	----	----	-0.6688
V_3	----	----	0.3	----	----	-0.3
U_5	-1.94	-1.1758	----	-1.1758	----	-4.2916
V_5	----	-0.0231	----	0.0231	----	0
U_6	3.88	1.3374	1.3374	1.3374	2.0075	9.8997
V_6	----	0.3	-0.3	-0.3	0.6	0.3
U_7	-1.94	----	-1.1758	----	-1.846	-4.9618
V_7	----	----	0.0231	----	-0.323	-0.2999
U_8	----	----	----	-0.6688	----	-0.6688
V_8	----	----	----	0.3	----	0.3
U_9	----	----	----	0.5072	-0.1615	0.3457
V_9	----	----	----	-0.0231	-0.277	-0.3001

TABLE 12 SUMMARY OF STIFFNESS COEFFICIENTS AND DISPLACEMENTS
(Cont'd) AT EACH NODE OF EXAMPLE PROBLEM WING

NODE 6

NODE	STIFFNESS COEFFICIENT $\times 10^6$					
	VERTICAL (V_6) DISPLACEMENT					
	STRINGER	PANEL 1256	PANEL 2367	PANEL 5689	PANEL 679	TOTAL
U_1	----	-0.3	----	----	----	-0.3
V_1	----	-0.3691	----	----	----	-0.3691
U_2	----	-0.0231	0.0231	----	----	0
V_2	-0.97	-0.0921	-0.0921	----	----	-1.1542
U_3	----	----	0.3	----	----	-0.3
V_3	----	----	-0.3691	----	----	-0.3691
U_5	----	0.0231	----	0.0231	----	0
V_5	----	-0.277	----	-0.277	----	-0.554
U_6	----	0.3	-0.3	-0.3	0.6	0.3
V_6	1.94	0.7382	0.7382	0.7382	1.108	5.2626
U_7	----	----	-0.0231	----	-0.277	-0.3001
V_7	----	----	-0.277	----	-0.646	-0.923
U_8	----	----	----	0.3	----	0.3
V_8	----	----	----	-0.3691	----	-0.3691
U_9	----	----	----	0.0231	-0.323	-0.2999
V_9	-0.97	----	----	-0.0921	-0.462	-1.5241

TABLE 12
(Cont'd)SUMMARY OF STIFFNESS COEFFICIENTS AND DISPLACEMENTS
AT EACH NODE OF EXAMPLE PROBLEM WINGNODE 7

NODE	STIFFNESS COEFFICIENT $\times 10^6$				
	HORIZONTAL (U ₇) DISPLACEMENT				
	STRINGER	PANEL 2367	PANEL 347	PANEL 679	TOTAL
U ₂	----	-0.6688	----	----	-0.6688
V ₂	----	-0.3	----	----	-0.3
U ₃	----	0.05072	-0.1615	----	0.3457
V ₃	----	0.0231	-0.323	----	-0.2999
U ₄	-0.174	----	0	----	-0.174
V ₄	0.348	----	0.323	----	0.671
U ₆	-1.94	-1.1758	----	-1.846	-4.9618
V ₆	----	-0.0231	----	-0.277	-0.3001
U ₇	2.288	1.3374	0.1615	1.846	5.6329
V ₇	-0.696	0.3	0	0	-0.396
U ₉	-0.174	----	----	0	-0.174
V ₉	0.348	----	----	0.277	0.625

TABLE 12
(Cont'd)SUMMARY OF STIFFNESS COEFFICIENTS AND DISPLACEMENTS
AT EACH NODE OF EXAMPLE PROBLEM WING

NODE 7					
NODE	STIFFNESS COEFFICIENT $\times 10^6$				
	VERTICAL (V_7) DISPLACEMENT				
	STRINGER	PANEL 2367	PANEL 347	PANEL 679	TOTAL
U_2	----	-0.3	----	----	-0.3
V_2	----	-0.3691	----	----	-0.3691
U_3	----	-0.0231	-0.277	----	-0.3001
V_3	-0.97	-0.0921	-0.462	----	-1.5241
U_4	0.348	----	0.277	----	0.625
V_4	-0.696	----	0	----	-0.696
U_6	----	0.0231	----	-0.323	-0.2999
V_6	----	-0.277	----	-0.646	-0.923
U_7	-0.696	0.3	0	0	-0.396
V_7	2.362	0.7382	0.462	0.646	4.2082
U_9	0.348	----	----	0.323	0.671
V_9	-0.696	----	----	0	-0.696

TABLE 12 SUMMARY OF STIFFNESS COEFFICIENTS AND DISPLACEMENTS
(Cont'd) AT EACH NODE OF EXAMPLE PROBLEM WING

NODE 8

NODE	STIFFNESS COEFFICIENT $\times 10^6$							
	U_8 DISPLACEMENT				V_8 DISPLACEMENT			
	STRINGER	PANEL 5689	PANEL 8-9-10	TOTAL	STRINGER	PANEL 5689	PANEL 8-9-10	TOTAL
U_5	----	0.5072	----	0.5072	----	0.0231	----	0.0231
V_5	----	-0.0231	----	-0.0231	-0.97	-0.0921	----	-1.0621
U_6	----	-0.6688	----	-0.6688	----	0.3	----	0.3
V_6	----	0.3	----	0.3	----	-0.3691	----	-0.3691
U_8	1.94	1.3374	2.0075	5.2849	----	-0.3	0.6	0.3
V_8	----	-0.3	0.6	0.3	1.94	0.7382	1.108	3.7862
U_9	-1.94	-1.1758	-1.846	-4.9618	----	-0.0231	-0.277	-3.001
V_9	----	0.0231	-0.323	-0.2999	----	-0.277	-0.646	-0.923
U_{10}	----	----	-0.1615	-0.1615	----	----	-0.323	-0.323
V_{10}	----	----	-0.277	-0.277	-0.97	----	-0.462	-1.432

TABLE 12
(Cont'd)SUMMARY OF STIFFNESS COEFFICIENTS AND DISPLACEMENTS
AT EACH NODE OF EXAMPLE PROBLEM WINGNODE 9

NODE	STIFFNESS COEFFICIENT $\times 10^6$ HORIZONTAL (U_9) DISPLACEMENT				TOTAL
	STRINGER	PANEL 5689	PANEL 679	PANEL 8-9-10	
U_5	----	-0.6688	----	----	-0.6688
V_5	----	-0.3	----	----	-0.3
U_6	----	0.5072	-0.1615	----	0.3457
V_6	----	0.0231	-0.323	----	-0.2999
U_7	-0.174	----	0	----	-0.174
V_7	0.348	----	0.323	----	0.671
U_8	-0.194	-1.1758	----	-1.846	-4.9618
V_8	0.0231	----	----	-0.277	-0.3001
U_9	2.288	1.3374	0.1615	1.846	5.6329
V_9	-0.696	0.3	0	0	-0.396
U_{10}	-0.174	----	----	0	-0.174
V_{10}	0.348	----	----	0.277	0.625

TABLE 12
(Cont'd)SUMMARY OF STIFFNESS COEFFICIENTS AND DISPLACEMENTS
AT EACH NODE OF EXAMPLE PROBLEM WINGNODE 9

NODE	STIFFNESS COEFFICIENTS $\times 10^6$ VERTICAL (V_9) DISPLACEMENT				
	STRINGER	PANEL 5689	PANEL 679	PANEL 8-9-10	TOTAL
U_5	----	-0.3	----	----	-0.3
V_5	----	-0.3691	----	----	-0.3691
U_6	----	-0.0231	-0.277	----	-0.3001
V_6	-0.97	-0.0921	-0.462	----	-1.5241
U_7	0.348	----	0.277	----	0.625
V_7	-0.696	----	0	----	-0.696
U_8	----	0.0231	----	-0.323	-0.2999
V_8	----	-0.277	----	-0.646	-0.923
U_9	-0.696	0.3	----	0	-0.396
V_9	2.362	0.7382	0.462	0.646	4.2082
U_{10}	0.348	----	----	----	0.671
V_{10}	-0.696	----	----	----	-0.696

TABLE 12
(Cont'd)

SUMMARY OF STIFFNESS COEFFICIENTS AND DISPLACEMENTS
AT EACH NODE OF EXAMPLE PROBLEM WING

NODE 10

NODE	STIFFNESS COEFFICIENTS $\times 10^6$					
	U ₁₀ DISPLACEMENT			V ₁₀ DISPLACEMENT		
	STRINGER	PANEL	TOTAL	STRINGER	PANEL	TOTAL
		8-9-10			8-9-10	
U ₈	----	-0.1615	-0.1615	----	-0.277	-0.277
V ₈	----	-0.323	-0.323	0.97	-0.462	-1.432
U ₉	-0.174	0	-0.174	0.348	0.277	0.625
V ₉	0.348	0.323	0.671	-0.696	0	-0.696
U ₁₀	0.174	0.1615	0.3355	-0.348	0	-0.348
V ₁₀	-0.348	----	-0.348	1.666	0.462	2.128

TABLE 13 STIFFNESS COEFFICIENT MATRIX FOR EXAMPLE PROBLEM
SOLUTION INPUT

NODES 1, 2 & 3

DISPLACE- MENT	STIFFNESS COEFFICIENTS $\times 10^6$					
	U_1	V_1	U_2	V_2	U_3	V_3
U_1	3.2744	0.3	-3.1158	-0.0231	----	----
V_1	0.3	1.7082	0.0231	0.277	----	----
U_2	-3.1158	0.0231	6.5548	0	-3.1158	-0.0231
V_2	0.0231	-0.277	0	2.4464	0.0231	-0.277
U_3	----	----	-3.1158	0.0231	7.2249	0.3
V_3	----	----	-0.231	-0.277	0.3	2.8162
U_4	----	----	----	----	-3.786	-0.277
V_4	----	----	----	----	-0.323	-0.646
U_5	0.5072	-0.231	-0.6688	0.3	----	----
V_5	0.0231	-1.0621	-0.3	-0.3691	----	----
U_6	0.6688	-0.3	1.0144	0	-0.6688	0.3
V_6	-0.3	-0.3691	0	-1.1542	0.3	-0.3691
U_7	----	----	-0.6688	-0.3	0.3457	-0.2999
V_7	----	----	-0.3	-0.3691	-0.3001	-1.5241
U_8	----	----	----	----	----	----
V_8	----	----	----	----	----	----
U_9	----	----	----	----	----	----
V_9	----	----	----	----	----	----
U_{10}	----	----	----	----	----	----
V_{10}	----	----	----	----	----	----

TABLE 13 STIFFNESS COEFFICIENT MATRIX FOR EXAMPLE PROBLEM
(Cont'd) SOLUTION INPUT

NODES 4, 5 & 6

STIFFNESS COEFFICIENTS $\times 10^6$						
DISPLACE- MENT	U_4	V_4	U_5	V_5	U_6	V_6
U_1	----	----	0.5072	0.0231	0.6688	0.3
V_1	----	----	0.0231	1.0621	0.3	0
U_2	----	----	0.6688	0.3	1.0144	-1.1542
V_2	----	----	0.3	-0.3691	0	0.3
U_3	-3.786	-0.323	----	----	-0.6688	-0.3691
V_3	-0.277	-0.646	----	----	0.3	----
U_4	3.960	-0.348	----	----	----	----
V_4	-0.348	1.342	----	----	----	----
U_5	----	----	4.610	0	4.2916	0
V_5	----	----	0	3.4164	0	-0.544
U_6	----	----	-4.2916	0	9.8997	0.3
V_6	----	----	0	-0.554	0.3	5.2626
U_7	-0.174	0.671	----	----	-4.9618	-0.3001
V_7	-0.625	-0.696	----	----	-0.2999	-9.23
U_8	----	----	-0.5072	-0.0231	-0.6688	-0.3
V_8	----	----	0.0231	-1.0621	0.3	-0.3691
U_9	----	----	0.6688	-0.3	0.3457	-0.2999
V_9	----	----	-0.3	-0.3691	-0.3001	-1.5241
U_{10}	----	----	----	----	----	----
V_{10}	----	----	----	----	----	----

TABLE 13 STIFFNESS COEFFICIENT MATRIX FOR EXAMPLE PROBLEM
(Cont'd) SOLUTION INPUT

NODES 7, 8 & 9

STIFFNESS COEFFICIENTS $\times 10^6$						
DISPLACE- MENT	U_7	V_7	U_8	V_8	U_9	V_9
U_1	----	----	----	----	----	----
V_1	----	----	----	----	----	----
U_2	-0.6688	-0.3	----	----	----	----
V_2	-0.3	-0.3691	----	----	----	----
U_3	0.3457	-0.3001	----	----	----	----
V_3	-0.2999	-1.5241	----	----	----	----
U_4	-0.174	0.625	----	----	----	----
V_4	0.671	-0.696	----	----	----	----
U_5	----	----	0.5072	0.231	-0.6688	-0.3
V_5	----	----	0.0231	-1.0621	-0.3	-0.3691
U_6	-4.9618	-0.2999	-0.6688	0.3	0.3457	-0.3001
V_6	-0.3001	-0.923	-0.3	-0.3691	-0.2999	-1.5241
U_7	5.6329	-0.396	----	----	-0.174	0.625
V_7	-0.396	4.2082	----	----	0.671	-0.696
U_8	----	----	5.2849	0.3	4.9618	-0.2999
V_8	----	----	0.3	3.7862	-0.3001	-0.923
U_9	-0.174	0.671	-4.9618	-0.3001	5.6329	-0.396
V_9	0.625	-0.696	-0.2999	-0.923	-0.396	4.2082
U_{10}	----	----	-0.1615	-0.323	-0.174	0.671
V_{10}	----	----	-0.277	-1.432	0.625	-0.696

TABLE 13 STIFFNESS COEFFICIENT MATRIX FOR EXAMPLE PROBLEM
SOLUTION INPUT

NODE 10

STIFFNESS COEFFICIENTS $\times 10^6$			
DISPLACE- MENT	U_{10}	V_{10}	LOADS $\times 10^6$
U_1	----	----	-0.19245
V_1	----	----	-0.12405
U_2	----	----	0
V_2	----	----	-0.19245
U_3	----	----	0
V_3	----	----	-0.19245
U_4	----	----	0.2379
V_4	----	----	-0.0909
U_5	----	----	-0.32925
V_5	----	----	0
U_6	----	----	0
V_6	----	----	0
U_7	----	----	0.32925
V_7	----	----	0.19245
U_8	-0.1615	0.277	-0.32925
V_8	-0.323	-1.432	0
U_9	-0.174	0.625	0.32925
V_9	0.671	-0.696	0.19245
U_{10}	0.3555	-0.348	0.04545
V_{10}	-0.348	2.128	0.21495

TABLE 14 NODE DISPLACEMENTS IN EXAMPLE PROBLEM WING

Assumption

$$U_1 = V_1 = U_5 = U_8 = U_{10} = 0$$

Displacement

Displacement Mode	Magnitude in. x 10
U_2	0.042428
V_2	-0.011423
U_3	0.085230
V_3	-0.022482
U_4	0.130206
V_4	-0.040740
V_5	0.079823
U_6	0.051957
V_6	0.075393
U_7	0.103587
V_7	0.068127
V_8	0.162927
U_9	0.051068
V_9	0.161250
V_{10}	0.24839

Symbols

U represents horizontal displacement

V represents vertical displacement

Subscript denotes node point location

TABLE 15 STIFFNESS COEFFICIENTS, FORCES AND DISPLACEMENTS FOR RECTANGULAR PANELS IN EXAMPLE PROBLEM WING

<u>Stiffness Coefficient Matrix</u>							
	<u>U_A</u>	<u>V_A</u>	<u>U_B</u>	<u>V_B</u>	<u>U_C</u>	<u>V_C</u>	
<u>U_A</u>	1.3374	.3	-1.1758	-.0231	.5072	.0231	- .6688
<u>V_A</u>	.3	.7382	.0231	-.277	-.0231	-.0921	- .3691
<u>U_B</u>	-1.1758	.0231	1.3374	-.3	-.6688	.3	-.0231
<u>V_B</u>	-.0231	-.277	-.3	.7382	.3	-.3691	-.0921
<u>U_C</u>	.5072	-.0231	-.6688	.3	1.3374	-.3	.0231
<u>V_C</u>	.0231	-.0921	.3	-.3691	-.3	.7382	-.277
<u>U_D</u>	-.6688	-.3	.5072	.0231	-1.1758	-.0231	.3
<u>V_D</u>	-.3	-.3691	-.0231	-.0921	.0231	-.277	.7382

TABLE 15
(Cont'd)STIFFNESS COEFFICIENTS, FORCES AND DISPLACEMENTS
FOR RECTANGULAR PANELS IN EXAMPLE PROBLEM WING

<u>Forces</u>				
<u>PANEL</u>	<u>UA</u>	<u>VA</u>	<u>UB</u>	<u>VB</u>
1256	-0.10515	-0.04662	+0.10873	-0.05837
2367	-0.10800	-0.05187	0.10941	-0.05610
5689	-0.11765	-0.05060	0.11977	-0.05585
<u>PANEL</u>	<u>UC</u>	<u>VC</u>	<u>UD</u>	<u>VD</u>
1256	-0.11510	0.05379	0.11152	0.04920
2367	-0.11532	0.05483	0.11706	0.05162
<u>Displacements</u>				
	<u>PANEL 1256</u>	<u>PANEL 2367</u>	<u>PANEL 5689</u>	
<u>U_A</u>	0	0.042428	0	
<u>V_A</u>	0	-0.011423	0.079823	
<u>U_B</u>	0.042428	0.08523	0.51957	
<u>V_B</u>	-0.011423	-0.022482	0.075393	
<u>U_C</u>	0	0.051957	0	
<u>V_C</u>	0.079823	0.075393	0.162927	
<u>U_D</u>	0.051957	0.103587	0.051068	
<u>V_D</u>	0.075393	0.068127	0.16125	

TABLE 16 STIFFNESS COEFFICIENTS, FORCES AND DISPLACEMENTS
FOR TRIANGULAR PANELS IN EXAMPLE PROBLEM WING

Stiffness Coefficient Matrix

	<u>U_A</u>	<u>V_A</u>	<u>U_B</u>	<u>V_B</u>	<u>U_C</u>	<u>V_C</u>
<u>U_A</u>	2.0075	.6	-1.846	- .323	- .1615	- .277
<u>V_A</u>	.6	1.108	- .277	- .646	- .323	- .462
<u>U_B</u>	-1.846	- .277	1.846	0	0	.277
<u>V_B</u>	- .323	- .646	0	.646	.323	0
<u>U_C</u>	- .1615	- .323	0	.323	.1615	0
<u>V_C</u>	- .277	- .462	.277	0	0	.462

Forces

<u>PANEL</u>	<u>U_A</u>	<u>V_A</u>	<u>U_B</u>	<u>V_B</u>	<u>U_C</u>	<u>V_C</u>
347	-0.10520	-0.04846	0.10813	-0.00587	-0.00293	0.05432
679	-0.11660	-0.04899	0.11909	-0.00498	-0.00249	0.05397
8-9-10	-0.11740	-0.05255	0.11794	-0.00108	-0.00054	0.05363

TABLE 16 STIFFNESS COEFFICIENTS, FORCES AND DISPLACEMENTS FOR TRIANGULAR
(Cont'd) PANELS IN EXAMPLE WING

	<u>Displacements</u>		
	<u>PANEL 347</u>	<u>PANEL 679</u>	<u>PANEL 8-9-10</u>
U_A	0.085230	0.051927	0
V_A	0.022482	0.75393	0.162927
U_B	0.130206	0.103587	0.51068
V_B	0.040740	0.069127	0.161250
U_C	0.103587	0.051068	0
V_C	0.068127	0.161250	0.24839

TABLE 17 STRESSES IN RECTANGULAR AND TRIANGULAR PANELS IN EXAMPLE PROBLEM WING

Panel 1256

$$\Delta\sigma_x = - \frac{U_1 + U_5}{4} = 55061$$

$$\Delta\sigma_y = - \frac{V_1 + V_2}{2} = 51495$$

$$\tau_{xy} = - \frac{V_1 + V_5 - V_2 - V_6}{4} = - 3582$$

$$\sigma_x = -68400 + \Delta\sigma_x = -13339 \text{ lbs./in.}^2$$

$$\sigma_y = -68400 + \Delta\sigma_y = -16905 \text{ lbs./in.}^2$$

Panel 2367

$$\Delta\sigma_x = \frac{U_3 + U_7}{4} = 55828 \text{ lbs./in.}^2$$

$$\Delta\sigma_y = \frac{V_6 + V_7}{2} = 53988 \text{ lbs./in.}^2$$

$$\tau_{xy} = - \frac{U_6 + U_7 - U_2 - U_3}{2} = -14145 \text{ lbs./in.}^2$$

$$\sigma_x = - 68400 + \Delta\sigma_x = - 12572 \text{ lbs./in.}^2$$

$$\sigma_y = - 68400 + \Delta\sigma_y = - 14412 \text{ lbs./in.}^2$$

Panel 5689

$$\Delta\sigma_x = \frac{U_6 + U_9}{4} = 59206 \text{ lbs./in.}^2$$

$$\Delta\sigma_y = \frac{V_8 + V_9}{2} = 53226 \text{ lbs./in.}^2$$

$$\tau_{xy} = - \frac{U_5 + U_6 - U_8 - U_9}{2} = -2116 \text{ lbs./in.}^2$$

$$\sigma_x = - 68400 + \Delta\sigma_x = -9194 \text{ lbs./in.}^2$$

$$\sigma_y = - 68400 + \Delta\sigma_y = -15174 \text{ lbs./in.}^2$$

TABLE 17 STRESSES IN RECTANGULAR AND TRIANGULAR PANELS IN EXAMPLE PROBLEM WING
(Cont'd)

Panel 347

$$\Delta\sigma_x = \frac{U_4}{2} = 54063 \text{ lbs./in.}^2$$

$$\Delta\sigma_y = \frac{V_7}{1} = 54320 \text{ lbs./in.}^2$$

$$\tau_{xy} = \frac{V_4}{2} = -2933 \text{ lbs./in.}^2$$

$$\sigma_x = -68400 + \Delta\sigma_x = -14337 \text{ lbs./in.}^2$$

$$\sigma_y = -68400 + \Delta\sigma_y = -14080 \text{ lbs./in.}^2$$

Panel 679

$$\Delta\sigma_x = \frac{U_7}{2} = 59546 \text{ lbs./in.}^2$$

$$\Delta\sigma_y = \frac{V_9}{1} = 53970 \text{ lbs./in.}^2$$

$$\tau_{xy} = \frac{V_7}{2} = -2490 \text{ lbs./in.}^2$$

$$\sigma_x = -68400 + \Delta\sigma_x = -8854 \text{ lbs./in.}^2$$

$$\sigma_y = -68400 + \Delta\sigma_y = -14433 \text{ lbs./in.}^2$$

Panel 8-9-10

$$\Delta\sigma_x = \frac{U_9}{2} = 58971 \text{ lbs./in.}^2$$

$$\Delta\sigma_y = \frac{V_{10}}{1} = 53630 \text{ lbs./in.}^2$$

$$\tau_{xy} = \frac{V_9}{2} = -541 \text{ lbs./in.}^2$$

$$\sigma_x = -68400 + \Delta\sigma_x = -9429 \text{ lbs./in.}^2$$

$$\sigma_y = -68400 + \Delta\sigma_y = -14771 \text{ lbs./in.}^2$$

TABLE 18 STRAIN DERIVATION AND STRESS INCREMENTS IN EXAMPLE PROBLEM WING SPARS EXCLUSIVE OF FRONT SPAR

STRAIN DERIVATION	STRESS-CAPS $E = .96 \times 10^7$ $\Delta\sigma$ (lbs./in. ²)	STRESS-WEBS $E = .98 \times 10^7$ $\Delta\sigma$ (lbs./in. ²)
<u>"X"-direction Components</u>		
$\epsilon_{x_{1-2}} = \frac{U_2 - U_1}{10} = 0.0042427$	40730	41579
$\epsilon_{x_{2-3}} = \frac{U_3 - U_2}{10} = 0.0042801$	41089	41945
$\epsilon_{x_{3-4}} = \frac{U_4 - U_3}{10} = 0.0044977$	43178	44078
$\epsilon_{x_{5-6}} = \frac{U_6 - U_5}{10} = 0.0051957$	49879	50918
$\epsilon_{x_{6-7}} = \frac{U_7 - U_6}{10} = 0.0051630$	49565	50597
$\epsilon_{x_{8-9}} = \frac{U_9 - U_8}{10} = 0.0051068$	49025	50046
<u>"Y"-direction Components</u>		
$\epsilon_{y_{1-5}} = \frac{V_5 - V_1}{20} = 0.0039912$	38316	39114
$\epsilon_{y_{2-6}} = \frac{V_6 - V_2}{20} = 0.0043407$	41821	42539
$\epsilon_{y_{3-7}} = \frac{V_7 - V_3}{20} = 0.0045305$	43492	44398
$\epsilon_{y_{5-8}} = \frac{V_8 - V_5}{20} = 0.0041553$	39891	40722
$\epsilon_{y_{6-9}} = \frac{V_9 - V_6}{20} = 0.0042929$	41211	42070
$\epsilon_{y_{8-10}} = \frac{V_{10} - V_8}{20} = 0.00427$	41023	41877

TABLE 18
(Cont'd)

STRAIN DERIVATION AND STRESS INCREMENTS IN EXAMPLE PROBLEM WING
SPARS EXCLUSIVE OF FRONT SPAR

STRAIN DERIVATION	STRESS $\frac{E}{\Delta\sigma} = .88 \times 10^7$ (lbs./in. ²)
$\epsilon_{4-7} = \frac{1}{500} \left[10 (u_4 - u_7) - 20 (v_4 - v_7) \right] = 0.0048870$	43006
$\epsilon_{7-9} = \frac{1}{500} \left[10 (u_7 - u_9) - 20 (v_7 - v_9) \right] = 0.0047753$	42023
$\epsilon_{9-10} = \frac{1}{500} \left[10 (u_9 - u_{10}) - 20 (v_9 - v_{10}) \right] = 0.0045069$	39661

TABLE 19 STRESSES IN EXAMPLE PROBLEM WING SPARS

MEMBER	THERMAL STRESS $\sigma_o = E\alpha T$ (Locked)	STRESS INCREMENT $\Delta\sigma$	TOTAL STRESS $\sigma = \sigma_o + \Delta\sigma$
<u>WING SPARS EXCLUSIVE OF FRONT SPAR (1)</u>			
1-2	-36900	40731	3831
2-3	-36900	41089	4189
3-4	-36900	43179	6279
5-6	-36900	49878	12978
6-7	-36900	49565	12665
8-9	-36900	49025	12125
1-5	-36900	38316	1416
5-8	-36900	41670	4770
8-10	-36900	43492	6592
2-6	-36900	39891	2991
6-9	-36900	41211	4311
3-7	-36900	41022	4122
<u>FRONT SPAR (2)</u>			
4-7	-50700	43006	-7694
7-9	-50700	42022	-8677
9-10	-50700	39662	-11038

NOTES: (1) $T = 200^\circ\text{F}$, $E = .96 \times 10^7 \text{ lbs/in}^2$, $\alpha = 12.8 \times 10^{-6}$
 (2) $T = 450^\circ\text{F}$, $E = .88 \times 10^7 \text{ lbs/in}^2$, $\alpha = 12.8 \times 10^{-6}$

TABLE 20 STRESSES IN EXAMPLE PROBLEM WING SPAR WEBS

MEMBER	THERMAL STRESS $\sigma_o = E\alpha T$ (1) (Locked)	STRESS INCREMENT $\Delta\sigma$	TOTAL STRESS $\sigma = \sigma_o + \Delta\sigma$
1-2	-18750	41578	22828
2-3	-18750	41945	23194
3-4	-18750	44077	25327
5-6	-18750	50917	32167
6-7	-18750	50598	31848
8-9	-18750	50046	31296
1-5	-18750	39114	20364
5-8	-18750	42538	23788
8-10	-18750	44398	25648
2-6	-18750	40722	21972
6-9	-18750	42070	23320
3-7	-18750	41877	23127

NOTE: (1) $T = 100^\circ\text{F.}$, $E = .98 \times 10^7$, $\alpha = 12.8 \times 10^{-6}$

TABLE 21 PRINCIPAL STRESS COMPUTATIONS FOR EXAMPLE PROBLEM
WING PANELS AT TIME ZERO

PANEL	STRESS COMPONENTS			PRINCIPAL STRESSES	
	σ_x	σ_y	τ_{xy}	$\sigma_1^{(1)}$	$\sigma_2^{(2)}$
1-2-5-6	- 13339	- 16905	- 3582	- 11124	- 19122
2-3-6-7	- 12571	- 14412	- 1414	- 11805	- 15180
5-6-8-9	- 9193	- 15174	- 2116	- 8518	- 15847
3-4-7	- 14337	- 14085	- 2932	- 11274	- 17145
6-7-9	- 7639	- 14433	- 2490	- 7962	- 15327
8-9-10	- 9429	- 14770	- 541	9375	- 14823

NOTES:

$$(1) \left(\frac{\sigma_x + \sigma_y}{2} \right) + \left(\frac{\sigma_x - \sigma_y}{2} \right)^2 + \tau_{xy}^2 = \sigma_1$$

$$(2) \left(\frac{\sigma_x + \sigma_y}{2} \right) - \left(\frac{\sigma_x - \sigma_y}{2} \right)^2 + \tau_{xy}^2 = \sigma_2$$

TABLE 22 ANGLE OF PRINCIPAL AXES COMPUTATIONS FOR EXAMPLE
PROBLEM WING AT TIME ZERO

PANEL	STRESS COMPONENTS		
	σ_x	σ_y	τ_{xy}
1-2-5-6	- 13339	- 16905	- 3582
2-3-6-7	- 12571	- 14412	- 1414
5-6-8-9	- 9193	- 15174	- 2116
3-4-7	- 14337	- 14085	- 2932
6-7-9	- 7639	- 14433	- 2490
8-9-10	- 9429	- 14770	- 541

PANEL	Tan 2α (1)	ANGLE OF PRINCIPAL AXES DATA				
		2α	α	Sin 2α	Cos 2α	Sin 2α Cos 2α
1-2-5-6	- 2.008	63°31'	31°45'	0.2769	0.7231	0.6677
2-3-6-7	1.537	56°57'	68° '	0.2271	0.7728	0.4189
5-6-8-9	- 0.7078	35°17'	17°38'	0.0917	0.9082	0.2887
3-4-7	22.866	87°29'	43°45'	0.4782	0.5217	0.4995
6-7-9	- 0.8928	41°45'	20°53'	0.1272	0.8729	0.3331
8-9-10	- 0.2028	11°28'	5°44'	0.00998	0.990	0.0994

NOTE:

$$(1) \quad \tan 2\alpha = \frac{2\tau_{xy}}{\sigma_x - \sigma_y}$$

TABLE 23 EQUIVALENT UNIAXIAL STRESSES IN EXAMPLE PROBLEM WING PANELS
 ACCORDING TO von MISES-PRAGER CRITERIA

PANEL	PRINCIPAL STRESSES		EQUIVALENT STRESS	TEMP.	STRAIN	POWER
	σ_1	σ_2	σ_o (1)	$^{\circ}\text{F}$	RATE, $\dot{\epsilon}_o$ (2)	DISSIPATION $\sigma_o \cdot \dot{\epsilon}_o$ (3)
1-2-5-6	-11124	-19122	16572	450	1.28×10^{-4}	2.12
2-3-6-7	-11805	-15180	13806	450	0.71×10^{-4}	0.980
5-6-8-9	- 8518	-15847	13746	450	0.70×10^{-4}	0.962
3-4-7	-11274	-17145	15103	450	0.95×10^{-4}	1.43
6-7-9	- 7962	-15327	13276	450	0.13×10^{-4}	0.836
8-9-10	- 9375	-14823	12985	450	0.58×10^{-4}	0.753

NOTES:

$$(1) \quad \sigma_o = \sigma_1^2 + \sigma_2^2 - \sigma_1 \sigma_2$$

(2) Taken from calibration chart.

(3) Expressed in pound minutes per square inch.

TABLE 24 COMPUTATIONS INVOLVING DEVIATOR COMPONENTS IN EXAMPLE PROBLEM

WING PANELS

PANEL	PRINCIPAL STRESSES		HYDROSTATIC TERM (1)	DEVIATOR COMPONENTS (2)		
	σ_1	σ_2		s_1	s_2	s_3
1-2-5-6	- 11124	- 19120	- 10081	- 1042	- 9040	10082
2-3-6-7	- 11805	- 15180	- 8995	- 2809	- 6184	8993
5-6-8-9	- 8518	- 15847	- 8122	- 396	- 7725	8121
3-4-7	- 11274	- 17145	- 9472	- 1801	- 7672	9473
6-7-9	- 7962	- 15327	- 7762	- 200	- 7564	7764
8-9-10	- 9375	- 14823	- 8060	- 1310	- 6757	8067

PANEL	ENERGY DISSIPATION COMPONENT	POWER DISSIPATION (3)	PROPORTIONALITY FACTOR (4)
1-2-5-6	184.46×10^6	2.12	1.15×10^{-8}
2-3-6-7	127.06×10^6	0.980	0.771×10^{-8}
5-6-8-9	125.83×10^6	0.9262	0.765×10^{-8}
3-4-7	151.84×10^6	1.43	0.942×10^{-8}
6-7-9	117.52×10^6	0.836	0.712×10^{-8}
8-9-10	111.47×10^6	0.753	0.676×10^{-8}

NOTES:

(1) Hydrostatic term = $(\sigma_1 + \sigma_2)/3$

(2) $s_1 = \sigma_1 - \left(\frac{\sigma_1 + \sigma_2}{3}\right)$; $s_2 = \sigma_2 - \left(\frac{\sigma_1 + \sigma_2}{3}\right)$; $s_3 = -\left(\frac{\sigma_1 + \sigma_2}{3}\right)$

(3) See Table XXIII

(4) $\frac{\text{Energy Dissipation Component}}{\text{Power Dissipation}}$

TABLE 25 CREEP RATES IN PRINCIPAL DIRECTIONS AND IN THE ELASTIC STRAIN INCREMENT IN "LOCKED" EXAMPLE PROBLEM WING PANELS

PANEL	DEVIATOR COMPONENTS			PROPORTIONALITY FACTOR
	s_1	s_2	s_3	$1/r$
1-2-5-6	- 1042	- 9040	10082	1.15×10^{-8}
2-3-6-7	- 2809	- 6184	8993	0.771×10^{-8}
5-6-8-9	- 396	- 7725	8121	0.765×10^{-8}
3-4-7	- 1801	- 7672	9473	0.942×10^{-8}
6-7-9	- 200	- 7564	7764	0.712×10^{-8}
8-9-10	- 1310	- 6757	8067	0.676×10^{-8}

PANEL	CREEP RATES IN PRINCIPAL DIRECTIONS (1)		
	$\dot{\epsilon}_1$	$\dot{\epsilon}_2$	$\dot{\epsilon}_3$
1-2-5-6	- 1.198×10^{-5}	- 10.396×10^{-5}	11.594×10^{-5}
2-3-6-7	- 2.166×10^{-5}	- 4.768×10^{-5}	6.934×10^{-5}
5-6-8-9	- 0.303×10^{-5}	- 5.909×10^{-5}	6.212×10^{-5}
3-4-7	- 1.697×10^{-5}	- 7.227×10^{-5}	8.924×10^{-5}
6-7-9	- 0.142×10^{-5}	5.385×10^{-5}	5.527×10^{-5}
8-9-10	- 0.885×10^{-5}	- 4.568×10^{-5}	5.453×10^{-5}

TABLE 25 CREEP RATES IN PRINCIPAL DIRECTIONS AND IN THE ELASTIC STRAIN
(Cont'd) INCREMENT IN "LOCKED" EXAMPLE PROBLEM WING PANELS

PANEL	ELASTIC STRAIN INCREMENTS (2)		
	$\Delta\epsilon_1$	$\Delta\epsilon_2$	$\Delta\epsilon_3$
1-2-5-6	- 4.792x10 ⁻⁵	41.584x10 ⁻⁵	46.376x10 ⁻⁵
2-3-6-7	- 8.664x10 ⁻⁵	-19.072x10 ⁻⁵	27.736x10 ⁻⁵
5-6-8-9	- 1.212x10 ⁻⁵	-23.636x10 ⁻⁵	24.848x10 ⁻⁵
3-4-7	- 6.788x10 ⁻⁵	-28.908x10 ⁻⁵	35.696x10 ⁻⁵
6-7-9	- 0.568x10 ⁻⁵	-21.540x10 ⁻⁵	22.108x10 ⁻⁵
8-9-10	- 3.540x10 ⁻⁵	-18.272x10 ⁻⁵	21.812x10 ⁻⁵

NOTES:

$$(1) \quad s_1/r = \dot{\epsilon}_1 ; \quad s_2/r = \dot{\epsilon}_2 ; \quad s_3/r = \dot{\epsilon}_3 .$$

$$(2) \quad \dot{\epsilon}_1 \Delta t = \Delta\epsilon_1 ; \quad \dot{\epsilon}_2 \Delta t = \Delta\epsilon_2 ; \quad \dot{\epsilon}_3 \Delta t = \Delta\epsilon_3 .$$

where Δt = time increment = 4 min.

TABLE 26 RATE OF CHANGE OF STRESS WITH RESPECT TO TIME IN PRINCIPAL DIRECTIONS
OF EXAMPLE PROBLEM WING

PANEL	CROSS SECTIONAL AREA SQ. IN.	STRAIN RATES (1)			INCREMENTAL STRESS- INCREMENTAL TIME RATIO (2)		
					$\frac{\Delta\sigma_1}{\Delta t}$	$\frac{\Delta\sigma_2}{\Delta t}$	$\frac{\Delta\sigma_3}{\Delta t}$
		$\dot{\epsilon}_1$	$\dot{\epsilon}_2$	$\dot{\epsilon}_3$			
1-2-5-6	2	1.198	10.39	11.594	44.44	607.3	651.0
2-3-6-7	2	2.166	4.76	6.934	122.7	152.6	274.5
3-4-7	1	1.697	7.22	8.924	84.76	351.2	435.3
1-5	2	0	0	0			
2-6	2	0	0	0			
3-7	2	0	0	0			
4-7	2	0	0	0			

NOTE: (1) Multiply values shown by 10^{-5} to arrive at true value.

$$(2) \frac{\Delta\sigma_i}{\Delta t} = -E \left[\dot{\epsilon}_1 - \frac{\sum A_i \dot{\epsilon}_i}{\sum A_i} \right] \text{ lbs/sq in/min}$$

where $i = 1, 2, 3$.

$$E = 8.08 \times 10^6$$

TABLE 27 PRINCIPAL STRESS INCREMENTS ARISING FROM RELAXATION IN LOCKED EXAMPLE
PROBLEM WING PANELS AFTER A CREEP INTERVAL OF 4 MINUTES

PANEL	ELASTIC STRAIN INCREMENTS		PRINCIPAL STRESS INCREMENT DUE TO RELAXATION (1)	
	$\Delta\epsilon_1$	$\Delta\epsilon_2$	$\Delta\sigma_1$	$\Delta\sigma_2$
1-2-5-6	4.792×10^{-5}	41.584×10^{-5}	+ 1534	+ 3820
2-3-6-7	-8.662×10^{-5}	-19.072×10^{-5}	+ 1277	+ 1924
5-6-8-9	-1.212×10^{-5}	-23.636×10^{-5}	+ 737.2	+ 2131
3-4-7	-6.788×10^{-5}	-28.905×10^{-5}	+ 1373	+ 2748
6-7-9	-0.568×10^{-5}	-21.540×10^{-5}	+ 642.2	+ 1928
8-9-10	-3.540×10^{-5}	-18.272×10^{-5}	+ 901.1	+ 1717

NOTE:

$$(1) \quad \Delta\sigma_1 = - \frac{E}{1-\mu^2} (\Delta\epsilon_1 - V\Delta\epsilon_2), \text{ and}$$

$$\Delta\sigma_2 = - \frac{E}{1-\mu^2} (\Delta\epsilon_2 - V\Delta\epsilon_1) \text{ where}$$

$$\frac{E}{1-\mu^2} = 8.879 \times 10^6 \text{ lb/sq in.}, \text{ and}$$

$$E = 8.08 \times 10^6 \text{ and}$$

$$\mu = 0.3$$

TABLE 28 STRESS INCREMENTS DUE TO RELAXATION IN LOCKED
PANELS OF EXAMPLE PROBLEM WING

PANEL	PRINCIPAL STRESS ANGLE DATA		PRINCIPAL STRESS COMPONENTS (INCREMENTAL)		PRINCIPAL STRESSES (INCREMENTAL)	
	Sin α	Cos α	$\Delta\sigma_1$	$\Delta\sigma_2$	$\Delta\sigma_{x_e}$ (1)	$\Delta\sigma_y$ (2)
1-2-5-6	0.2769	0.7231	1534.	3820	2167	3186.8
2-3-6-7	0.2271	0.7728	1277.	1924	1423.8	1777.
5-6-8-9	0.0917	0.9082	737.2	2131	864.9	2002.6
3-4-7	0.4782	0.5217	1373	2748	2030.3	2090.6
6-7-9	0.1271	0.8729	624.2	1928	789.9	1762.3
8-9-10	0.00998	0.9900	801.1	1717	810.2	1708

NOTE:

$$(1) \quad \Delta\sigma_x = \Delta\sigma_1 \cdot \cos \alpha \cdot \Delta\sigma_2 \sin \alpha$$

$$(2) \quad \Delta\sigma_y = \Delta\sigma_2 \cos \alpha \cdot \Delta\sigma_1 \sin \alpha$$

TABLE 29 SHEAR STRESS INCREMENTS DUE TO RELAXATION IN LOCKED PANELS OF
EXAMPLE PROBLEM WING

PANEL	PRINCIPAL STRESS (INCREMENTAL) $\Delta_{txy}^{(1)}$	PRINCIPAL STRESS ANGLE DATA		PRINCIPAL STRESS COMPONENTS (INCREMENTAL)	
		$\sin \alpha$	$\cos \alpha$	$\Delta\sigma_1$	$\Delta\sigma_2$
1-2-5-6	456.7	0.4477		2167	3187
2-3-6-7	147.9	0.4189		1424	1777
5-6-8-9	328.5	0.2887		865.	2003
3-4-7	30.47	0.4995		2030	2091
6-7-9	323.1	0.3331		790	1762
8-9-10	89.26	0.0994		810	1708

NOTE:

$$(1) \quad \Delta_{txy} = (\Delta\sigma_2 - \Delta\sigma_1) \cdot \sin \alpha \cos \alpha$$

TABLE 30 FORCE INPUT AT LOCKED NODES OF RECTANGULAR PLATES IN EXAMPLE

PROBLEM WING

PANEL	FORCE COMPONENT			
	$\frac{\Delta F_x}{2}(1)$	$\frac{\Delta S_x}{2}(2)$	$\frac{\Delta F_y}{2}(3)$	$\frac{\Delta S_y}{2}(4)$
1-2-5-6	2167	457	6347	913
2-3-6-7	1424	148	3554	296
5-6-8-9	865	329	4005	657

NOTES:

$$(1) \quad \frac{\Delta F_x}{2} = \frac{\Delta \sigma_x}{2} \cdot A_x \text{ since when } A_x = 10 \times 0.2 = 2 \text{ sq. in.}$$

$$\Delta F_x = \frac{\Delta \sigma_x}{2} \cdot 2 = \Delta \sigma_x$$

$$(2) \quad \frac{\Delta S_x}{2} = 2\Delta \sigma_x$$

$$(3) \quad \frac{\Delta F_y}{2} = \frac{\Delta \sigma_y}{2} \cdot A_y \text{ since when } A_y = 20 \times 0.2 = 4 \text{ sq. in.}$$

$$\frac{\Delta F_y}{2} = \Delta \sigma_y$$

$$(4) \quad \frac{S_y}{2} = 2\Delta \sigma_y$$

TABLE 30
(Cont.)FORCE INPUT AT LOCKED NODES OF RECTANGULAR PLATES IN EXAMPLE
PROBLEM WING

PANEL	DEGREE OF FREEDOM(5)							
	U ₁	U ₂	U ₃	U ₄	V ₁	V ₂	V ₃	V ₄
1-2-5-6 -	2624	1710	1710	2624	7287	5466	5466	7287
2-3-6-7 -	1572	1276	1276	1572	3850	3258	3258	3850
5-6-8-9 -	1194	536	536	1194	4662	3676	3676	4662

NOTE

(5) The degrees of freedom are computed from the following relations

$$U_1 = \frac{\Delta F_x}{2} - \frac{\Delta S_x}{2}$$

$$V_1 = \frac{\Delta F_y}{2} - \frac{\Delta S_u}{2}$$

$$U_2 = \frac{\Delta F_x}{2} - \frac{\Delta S_x}{2}$$

$$V_2 = \frac{\Delta F_y}{2} - \frac{\Delta S_y}{2}$$

$$U_3 = \frac{\Delta F_x}{2} - \frac{\Delta S_x}{2}$$

$$V_3 = \frac{\Delta F_y}{2} - \frac{\Delta S_y}{2}$$

$$U_4 = \frac{\Delta F_x}{2} - \frac{\Delta S_y}{2}$$

$$V_4 = \frac{\Delta F_y}{2} + \frac{\Delta S_y}{2}$$

applicable at each node point represented at the corner of a given panel.

TABLE 31

FORCE INPUT AT LOCKED NODES OF TRIANGULAR PLATES IN EXAMPLE
PROBLEM WING

PANEL	FORCE COMPONENT			
	$\frac{\Delta F_x}{2}$	$\frac{\Delta S_x}{2}(1)$	$\frac{\Delta F_y}{2}$	$\frac{\Delta S_y}{2}(2)$
3-4-7	2030	30	4181	61
6-7-9	790	323	3525	646
8-9-10	810	89	3416	179

NOTES:

$$(1) \quad \frac{\Delta S_x}{2} = \frac{\Delta \tau_{xy}}{2} \cdot A_x \quad \text{since when } A_x = 10 \times 0.2 = .2 \text{ sq. in.}$$

$$\frac{\Delta S_{xy}}{2} \cdot 2 = \tau_{xy}$$

$$(2) \quad \frac{\Delta S_y}{2} = \frac{\Delta \tau_{xy}}{2} \cdot A_y \quad \text{since when } A_y = 20 \times 0.2 = .4 \text{ sq. in.}$$

$$\frac{\Delta S_y}{2} = \frac{\Delta \tau_{xy}}{2} \cdot 4 = 2\tau_{xy}$$

TABLE 31
(Cont.)

FORCE INPUT AT LOCKED NODES OF TRIANGULAR PLATES IN EXAMPLE
PROBLEM WING

PANEL	DEGREE OF FREEDOM (3)			
	U_3	U_4	V_3	V_7
3-4-7	-2060	2060	-4242	4242
6-7-9	-1113	1113	-4171	4171
8-9-10	- 899	899	-3595	3595

NOTE:

(3) The degrees of freedom are computed from the following relations

$$\bar{u}_7 = \bar{V}_4 = 0$$

$$u_3 = \frac{\Delta F_x}{2} - \frac{\Delta S_x}{2}$$

$$V_3 = \frac{-\Delta F_y}{2} - \frac{\Delta S_y}{2}$$

$$u_4 = \frac{\Delta F_x}{2} + \frac{\Delta S_x}{2}$$

$$\bar{V}_7 = \frac{\Delta F_y}{2} + \frac{\Delta S_y}{2}$$

applicable at each node point represented at the corner of a given panel.

TABLE 32 RESULTANT FORCES IN "X" DIRECTION AT LOCKED NODES (1) OF EXAMPLE PROBLEM WING

PANEL	NODE									
	[1]	[2]	[3]	[4]	[5]	[6]	[7]	[8]	[9]	[10]
	U ₁	U ₂	U ₃	U ₄	U ₅	U ₆	U ₇	U ₈	U ₉	U ₁₀
DEGREE OF FREEDOM (2)										
1-2-56	- 2624	1710	-----	-----	- 1710	2624	-----	-----	-----	---
2-3-6-7	-----	- 1572	1276	-----	-----	- 1276	1572	-----	-----	---
5-6-8-9	-----	-----	-----	-----	- 1194	536	-----	- 536	1194	---
3-4-7	-----	-----	- 2060	2060	-----	-----	-----	-----	-----	---
6-7-9	-----	-----	-----	-----	-----	- 1113	1113	-----	-----	---
8-9-10	-----	-----	-----	-----	-----	-----	-----	- 899	89.9	---
Total	- 2624	138	- 784	2060	- 2904	771	2685	- 1435	2093	0

NOTE:

- (1) Input for numerical solution
- (2) Degree of freedom in "X" direction

TABLE 33 RESULTANT FORCES IN "Y" DIRECTION AT LOCKED NODES (1) OF EXAMPLE PROBLEM WING

PANEL	NODE									
	[1]	[2]	[3]	[4]	[5]	[6]	[7]	[8]	[9]	[10]
	DEGREE OF FREEDOM (2)									
1-2-5-6	-7287	-5466	-----	---	-5466	7287	-----	----	----	----
2-3-6-7	----	-3850	-3258	---	----	3258	3850	----	----	----
5-6-8-9	----	----	----	---	-4662	-3676	----	3676	4662	----
3-4-7	----	----	-4242	---	----	----	4242	----	----	----
6-7-9	----	----	----	---	----	-4171	----	----	4171	----
8-9-10	----	----	----	---	----	----	-3595	----	----	3595
Total	-7287	-9316	-7500	0	804	2698	8092	81	8833	3595

NOTES:

- (1) Input for numerical solution.
- (2) Degree of freedom in "x" direction.

TABLE 34 SPAR CAP STRESS ARISING FROM NODE UNLOADING IN EXAMPLE PROBLEM WING (1)

NODE	NODE DISPLACEMENTS			
	"X" DIRECTION		"Y" DIRECTION	
	IDENTITY	MAGNITUDE	IDENTITY	MAGNITUDE
[1]	ϵ_{1x}	0	ϵ_{1y}	0
[2]	ϵ_{2x}	3.723	ϵ_{2y}	9.024
[3]	ϵ_{3x}	5.519	ϵ_{3y}	29.075
[4]	ϵ_{4x}	6.630		
[5]	ϵ_{5x}	0	ϵ_{5y}	46.591
[6]	ϵ_{6x}	-0.448	ϵ_{6y}	57.182
[7]	ϵ_{7x}	-1.865	ϵ_{7y}	66.375
[8]	ϵ_{8x}	0	ϵ_{8y}	78.609
[9]	ϵ_{9x}	0.863	ϵ_{9y}	90.742
[10]	ϵ_{10x}	0	ϵ_{10y}	99.217

TABLE 34
(Cont'd)SPAR CAP STRESS ARISING FROM NODE UNLOADING
IN EXAMPLE PROBLEM WING (1)

SPAR CAP	STRAIN				STRESS $\Delta\sigma_y$
	"X" DIRECTION- $\Delta\epsilon_x$ (3)		"Y" DIRECTION- $\Delta\epsilon_y$ (3)		
	FORMULA (2)	MAGNITUDE	FORMULA (2)	MAGNITUDE	
2-1	$\frac{\epsilon_{2x} - \epsilon_{1x}}{10}$	0.3723×10^{-4}	$\frac{\epsilon_{5y} - \epsilon_{1y}}{20}$	2.3295×10^{-4}	2050
3-2	$\frac{\epsilon_{3x} - \epsilon_{2x}}{10}$	0.1796×10^{-4}	$\frac{\epsilon_{8y} - \epsilon_{5y}}{20}$	1.6004×10^{-4}	1408
4-3	$\frac{\epsilon_{4x} - \epsilon_{3x}}{10}$	0.1111×10^{-4}	$\frac{\epsilon_{10y} - \epsilon_{8y}}{20}$	1.0104×10^{-4}	899.2
6-5	$\frac{\epsilon_{6x} - \epsilon_{5x}}{10}$	-0.0448×10^{-4}	$\epsilon_{6y} - \epsilon_{2y}$	2.4029×10^{-4}	2115
7-6	$\frac{\epsilon_{7x} - \epsilon_{6x}}{10}$	-0.1417×10^{-4}	$\frac{\epsilon_{9y} - \epsilon_{6y}}{20}$	1.6780×10^{-4}	1477
9-8	$\frac{\epsilon_{9x} - \epsilon_{8x}}{10}$	0.0863×10^{-4}	$\epsilon_{7y} - \epsilon_{3y}$	1.8335×10^{-4}	1613

NOTE:

- (1) $T = 300^\circ\text{F}$.
 $E = 8.8 \times 10^6 \text{ lbs/sq in.}$
- (2) First digit of subscript denotes node point: the second the direction.
The term ϵ_{ij} is a deformation term.
- (3) $\Delta\epsilon_j$ is a strain term where j denotes direction of strain.

TABLE 35 STRESS INCREMENTS ARISING IN SPAR CAPS FROM NODE UNLOCKING
IN EXAMPLE PROBLEM WING

FOR DEFORMATION PATTERN - Refer to Table 36

SPAR CAP	STRAIN INCREMENT		
	DIFFERENTIAL INCREMENT		EFFECTIVE INCREMENT
	$\Delta\epsilon_x$	$\Delta\epsilon_y$	$\Delta\epsilon (1)$
4-7	$\epsilon_{4x} - \epsilon_{7x} = 8.495$	$\epsilon_{7y} - \epsilon_{4y} = 13.621$	0.7167×10^{-4}
7-9	$\epsilon_{7x} - \epsilon_{9x} = -2.728$	$\epsilon_{9y} - \epsilon_{7y} = 4.367$	0.9201×10^{-4}
9-10	$\epsilon_{9x} - \epsilon_{10x} = 0.863$	$\epsilon_{10y} - \epsilon_{9y} = 8.475$	0.3563×10^{-4}

SPAR CAP STRESS INCREMENT (2)- $\Delta\sigma$	
4-7	579.1
7-9	743.4
9-10	287.9

NOTES:

$$(1) \quad \Delta\epsilon = (a\Delta\epsilon_x + b\Delta\epsilon_y)/e^2$$

where

$$a = 10 \text{ in.}$$

$$b = 20 \text{ in.}$$

$$e = 500 \text{ in.} = a^2 + b^2$$

$$(2) \quad \Delta\sigma = E\Delta\epsilon$$

where

$$E = 8.08 \times 10^6 \text{ lbs/sq in.}$$

TABLE 36

STRAIN INCREMENTS ARISING FROM NODE UNLOCKING
IN EXAMPLE PROBLEM WING PANELS

NODE	DEFORMATION (1)	
	"X" DIRECTION	"Y" DIRECTION
[1]	$\epsilon_{1x} = 0$	$\epsilon_{1y} = 0$
[2]	$\epsilon_{2x} = 3.723$	$\epsilon_{2y} = 9.024$
[3]	$\epsilon_{3x} = 5.519$	$\epsilon_{3y} = 29.705$
[4]	$\epsilon_{4x} = 6.630$	$\epsilon_{4y} = 52.704$
[5]	$\epsilon_{5x} = 0$	$\epsilon_{5y} = 46.591$
[6]	$\epsilon_{6x} = -0.448$	$\epsilon_{6y} = 57.182$
[7]	$\epsilon_{7x} = -1.865$	$\epsilon_{7y} = 66.375$
[8]	$\epsilon_{8x} = 0$	$\epsilon_{8y} = 78.069$
[9]	$\epsilon_{9x} = 0.863$	$\epsilon_{9y} = 90.742$
[10]	$\epsilon_{10x} = 0$	$\epsilon_{10y} = 99.217$

NOTE: (1) Subscript notation: number indicates effective node point;
letter indicates direction.

TABLE 36 STRAIN INCREMENTS ARISING FROM NODE UNLOCKING IN EXAMPLE PROBLEM WING PANELS
(cont'd)

PANEL	STRAIN INCREMENT (2)	
	"X" DIRECTION- $\Delta\epsilon_x$	"Y" DIRECTION- $\Delta\epsilon_y$
1-2-5-6	$\frac{\epsilon_{2x} - \epsilon_{1x} + \epsilon_{6x} - \epsilon_{5x}}{20} = 0.1638 \times 10^{-4}$	$\frac{\epsilon_{5y} - \epsilon_{1y} + \epsilon_{6y} - \epsilon_{2y}}{40} = 2.3662 \times 10^{-4}$
2-3-6-7	$\frac{\epsilon_{3x} - \epsilon_{2x} + \epsilon_{7x} - \epsilon_{6x}}{20} = 0.0189 \times 10^{-4}$	$\frac{\epsilon_{6y} - \epsilon_{2y} + \epsilon_{7y} - \epsilon_{3y}}{40} = 2.1202 \times 10^{-4}$
5-6-8-9	$\frac{\epsilon_{6x} - \epsilon_{5x} + \epsilon_{9x} - \epsilon_{8x}}{20} = 0.0207 \times 10^{-4}$	$\frac{\epsilon_{8y} - \epsilon_{5y} + \epsilon_{9y} - \epsilon_{6y}}{40} = 1.6392 \times 10^{-4}$
3-4-7	$\frac{\epsilon_{4x} - \epsilon_{3x}}{20} = 0.1111 \times 10^{-4}$	$\frac{\epsilon_{7y} - \epsilon_{3y}}{40} = 1.8335 \times 10^{-4}$
6-7-9	$\frac{\epsilon_{7x} - \epsilon_{6x}}{20} = -0.1237 \times 10^{-4}$	$\frac{\epsilon_{9y} - \epsilon_{6y}}{40} = 1.6780 \times 10^{-4}$
8-9-10	$\frac{\epsilon_{9x} - \epsilon_{8x}}{20} = 0.863 \times 10^{-4}$	$\frac{\epsilon_{10y} - \epsilon_{8y}}{40} = 1.0304 \times 10^{-4}$

NOTE: (2) Subscript notation: number indicates effective node point; letter indicates direction.

TABLE 37 DISTORTION INCREMENTS ARISING FROM NODE UNLOCKING
IN EXAMPLE PROBLEM WING PANELS

DEFORMATION INCREMENT PATTERN

PANEL	DEFORMATION INCREMENT- Δy_y
1-2-5-6	$\left(\frac{\epsilon_{2y} - \epsilon_{1y} + \epsilon_{6y} - \epsilon_{5y}}{20} \right) + \left(\frac{\epsilon_{5x} - \epsilon_{1x} + \epsilon_{6x} - \epsilon_{2x}}{40} \right) = 0.8765 \times 10^{-4}$
2-3-6-7	$\left(\frac{\epsilon_{3y} - \epsilon_{2y} + \epsilon_{7y} - \epsilon_{6y}}{20} \right) + \left(\frac{\epsilon_{6x} - \epsilon_{2x} + \epsilon_{7x} - \epsilon_{3x}}{40} \right) = 1.210 \times 10^{-4}$
5-6-8-9	$\left(\frac{\epsilon_{6y} - \epsilon_{5y} + \epsilon_{9y} - \epsilon_{8y}}{20} \right) + \left(\frac{\epsilon_{8x} - \epsilon_{5x} - \epsilon_{9x} - \epsilon_{6x}}{40} \right) = 1.169 \times 10^{-4}$
6-7-9	$\left(\frac{\epsilon_{7y} - \epsilon_{6y}}{10} \right) + \left(\frac{\epsilon_{9x} - \epsilon_{6x}}{20} \right) = 0.9848 \times 10^{-4}$
8-9-10	$\left(\frac{\epsilon_{9y} - \epsilon_{8y}}{10} \right) + \left(\frac{\epsilon_{10x} - \epsilon_{8x}}{20} \right) = 1.2133 \times 10^{-4}$

DEFORMATION PATTERN - Refer to Table 27

TABLE 38 STRESS INCREMENTS ARISING FROM NODE UNLOCKING IN EXAMPLE PROBLEM WING PANELS

PANEL	STRAIN INCREMENTS (1)		STRESS INCREMENTS		
	$\frac{\Delta \epsilon}{\Delta x}$	$\frac{\Delta \epsilon}{\Delta y}$	$\frac{\Delta \sigma_x}{\Delta x}$	$\frac{\Delta \sigma_y}{\Delta y}$	$\frac{\Delta \tau_{xy}}{\Delta xy}$
1-2-5-6	0.1636×10^{-4}	2.3662×10^{-4}	775.6	2144.5×10^{-4}	0.8765×10^{-4}
2-3-6-7	0.0189×10^{-4}	2.1202×10^{-4}	581.5	1887.6	1.210×10^{-4}
5-6-8-9	0.0207×10^{-4}	1.6392×10^{-4}	455.0	1461.0	1.169×10^{-4}
3-4-7	0.1111×10^{-4}	1.8335×10^{-4}	587.1	1657.5	1.9307×10^{-4}
6-7-9	-0.1237×10^{-4}	1.6780×10^{-4}	337.1	1457.0	0.9848×10^{-4}
8-9-10	0.0863×10^{-4}	1.0304×10^{-4}	351.1	937.9	1.2133×10^{-4}

NOTES:

(1) Refer to Table 36.

(3) Refer to Table 37.

(2) Given $\mu = 0.3$ and $E = 8.08 \times 10^6$ lbs/in²

$$\frac{E}{1-\mu^2} = 8.879 \times 10^6 \text{ lbs/sq. in. and } G = \frac{E}{2(1+\mu)} = 3.1077 \times 10^6 \text{ lbs/sq. in.}$$

$$\Delta \sigma_x = \frac{E}{1-\mu^2} (\Delta \epsilon_x + \mu \Delta \epsilon_y); \Delta \sigma_y = \frac{E}{1-\mu^2} (\Delta \epsilon_y + \mu \Delta \epsilon_x); \Delta \tau_{xy} = \frac{E}{2(1+\mu)} \Delta \gamma_{xy}$$

TABLE 39 RESULTANT STRESSES IN EXAMPLE PROBLEM WING
AFTER 4 MINUTE CREEP INTERVAL

PANEL	INCREMENT IDENTITY	INITIAL STRESS PSI	STRESS RELAXATION INCREMENT PSI	UNLOCKED CREEP PSI	TOTAL PSI
		(1)		(2)	
1-2-5-6	$\Delta\sigma_x$	-13,339	2,167	776	-11,948
"	$\Delta\sigma_y$	-16,905	3,187	2,145	-15,863
"	$\Delta\tau_{xy}$	- 3,582	457	272	- 2,853
2-3-6-7	$\Delta\sigma_x$	-12,571	1,424	582	-11,729
"	$\Delta\sigma_y$	-14,412	1,777	1,888	-14,523
"	$\Delta\tau_{xy}$	- 1,414	148	376	- 890
5-6-8-9	$\Delta\sigma_x$	- 9,193	865	455	- 8,783
"	$\Delta\sigma_y$	-15,174	2,003	1,461	-14,632
"	$\Delta\tau_{xy}$	- 2,116	329	363	- 1,424
3-4-7	$\Delta\sigma_x$	-14,337	2,030	587	-12,894
"	$\Delta\sigma_y$	-14,085	2,091	1,658	-13,652
"	$\Delta\tau_{xy}$	- 2,932	30	600	- 2,302
6-7-9	$\Delta\sigma_x$	- 7,639	790	337	- 7,186
"	$\Delta\sigma_y$	-14,433	1,762	1,457	-14,128
"	$\Delta\tau_{xy}$	- 2,490	323	306	- 1,861
8-9-10	$\Delta\sigma_x$	- 9,429	810	351	- 8,970
"	$\Delta\sigma_y$	-14,770	1,708	938	-14,000
"	$\Delta\tau_{xy}$	- 541	89	377	- 75

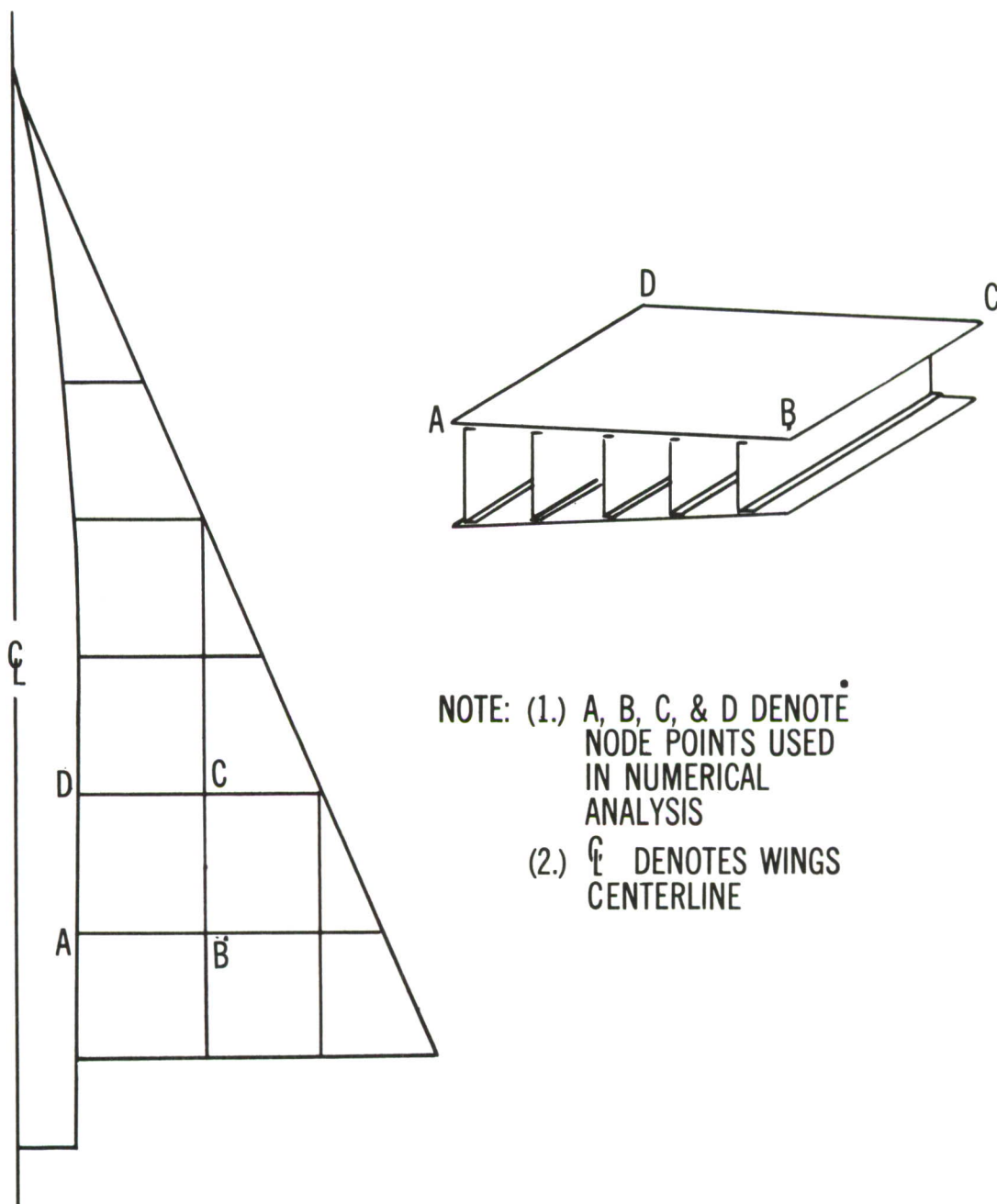


Figure 23. A Possible Subdivision of a Delta Wing into Sub-structures (Schematic)

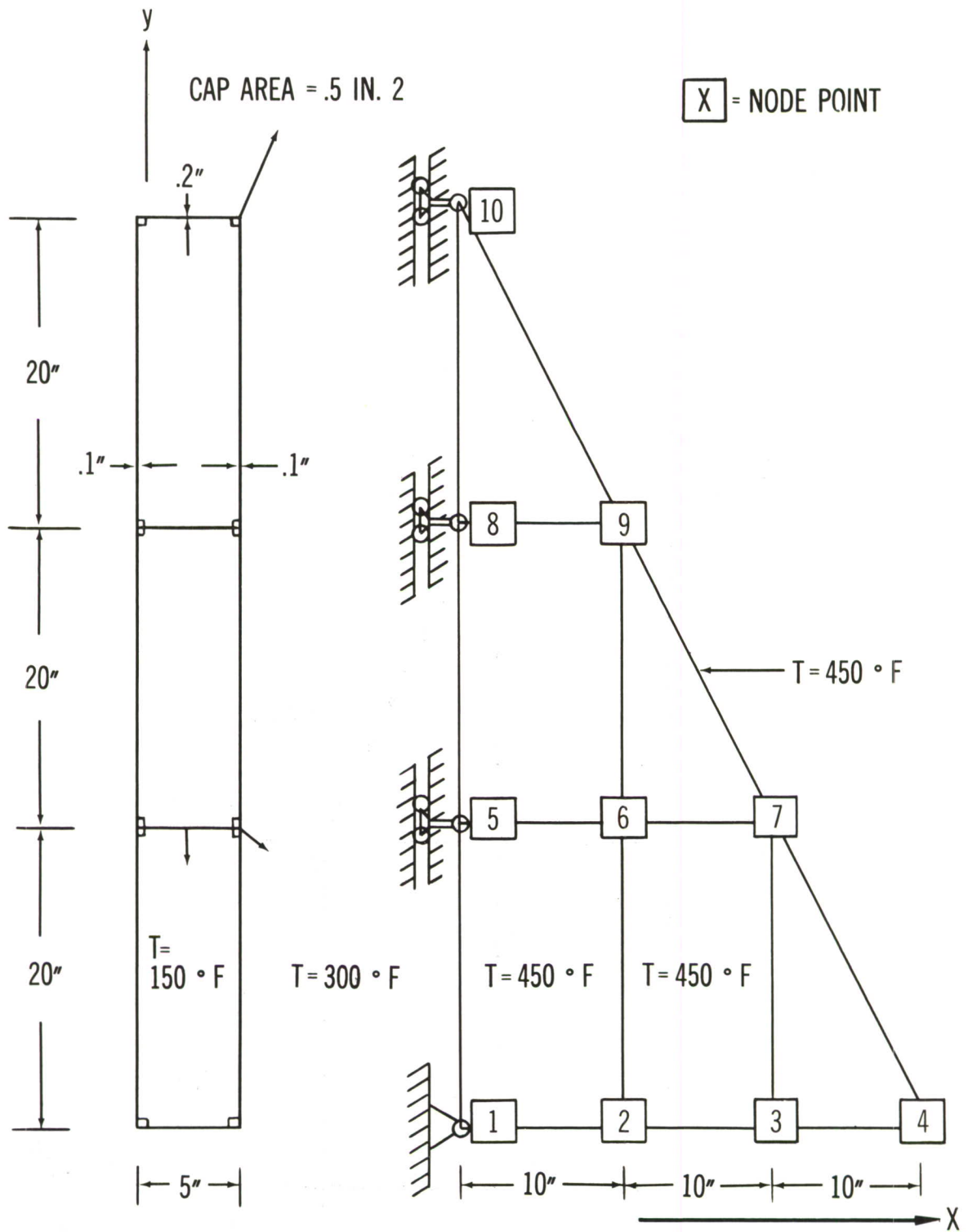


Figure 24. Node Point Location and Attachment Scheme for Example Problem Wing

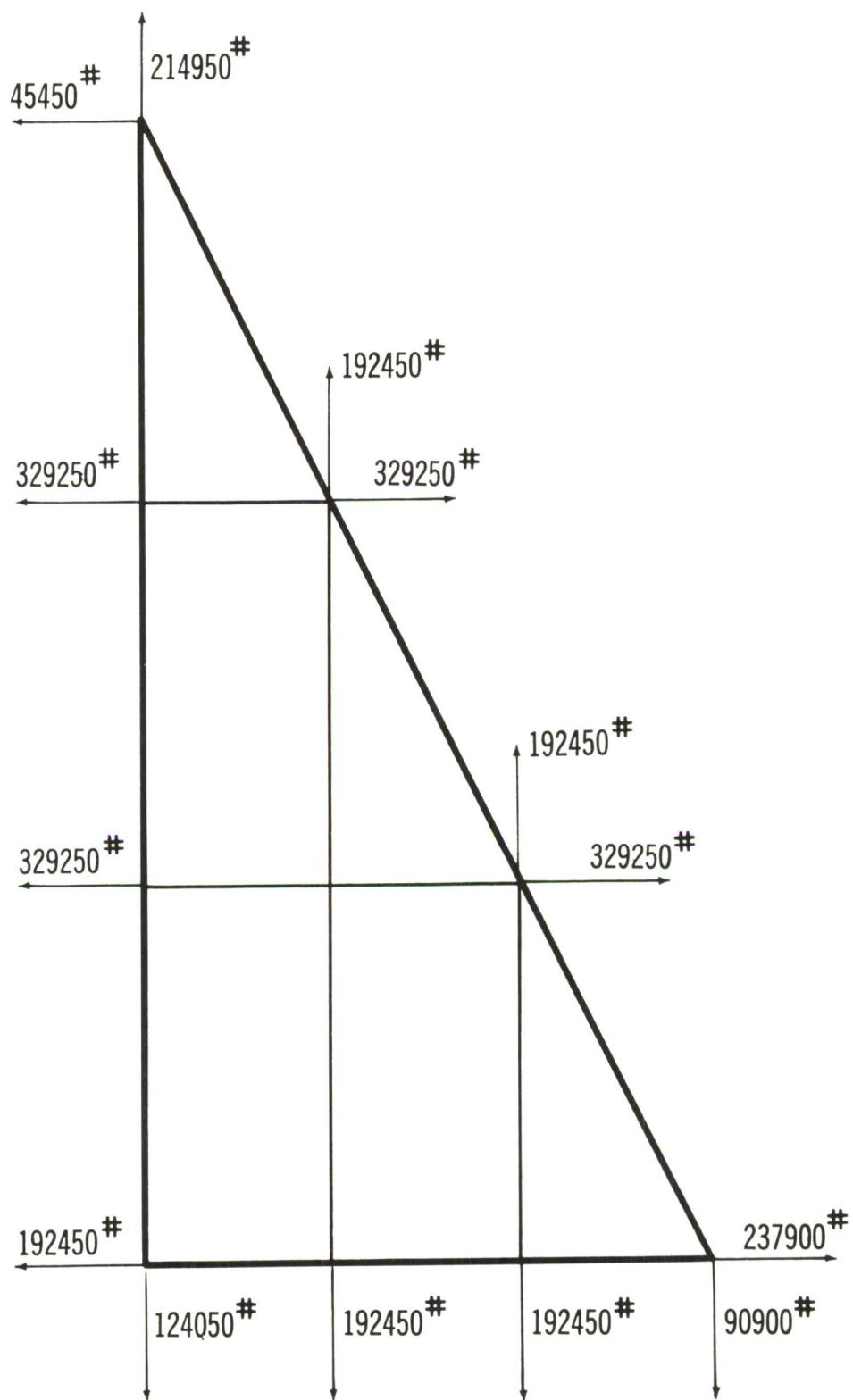
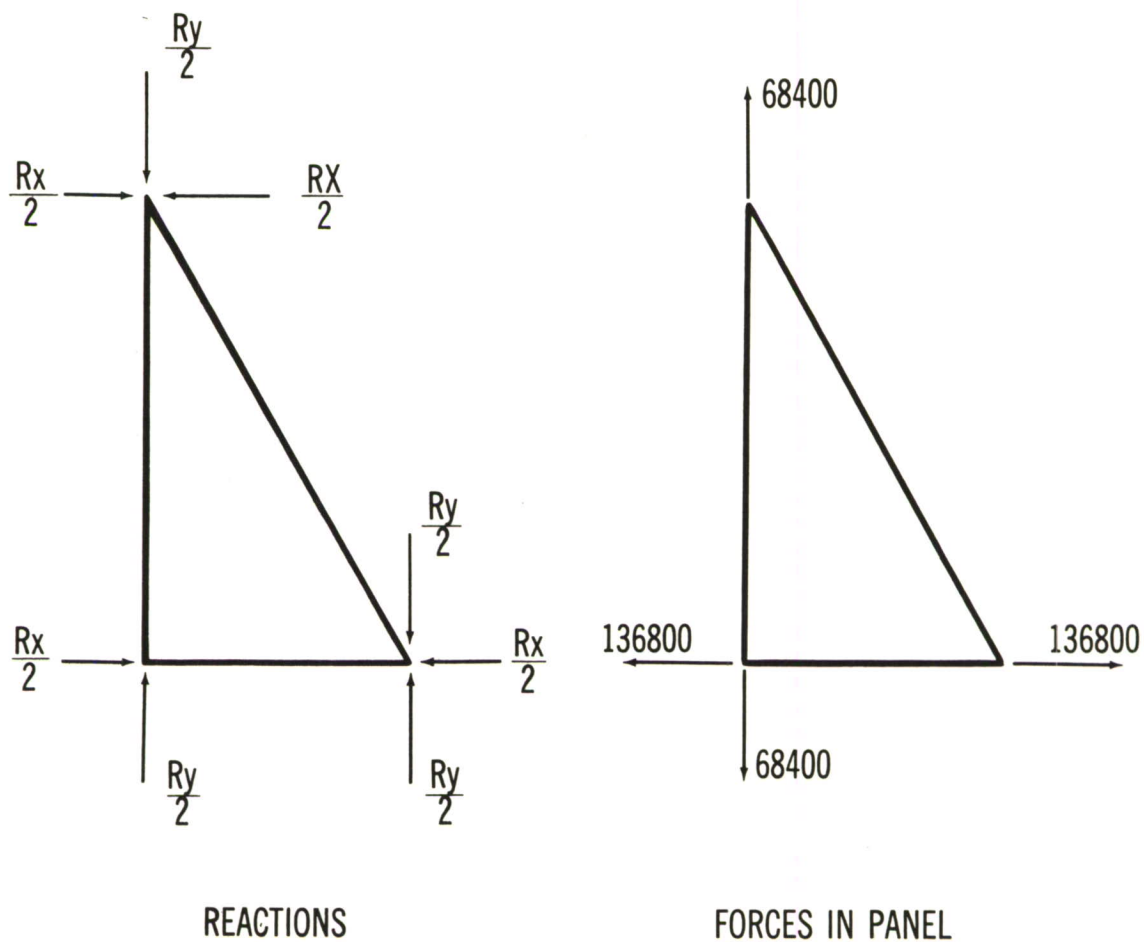


Figure 25. Force Input at Nodes of Locked Example Problem Wing



NOTE: ACTION ON LOCKS DUE TO p - 136800 LBS./IN.

Figure 26. Node Forces on Triangular Panels in Example Problem Wing

HORIZONTAL DISPLACEMENT



VERTICAL DISPLACEMENT

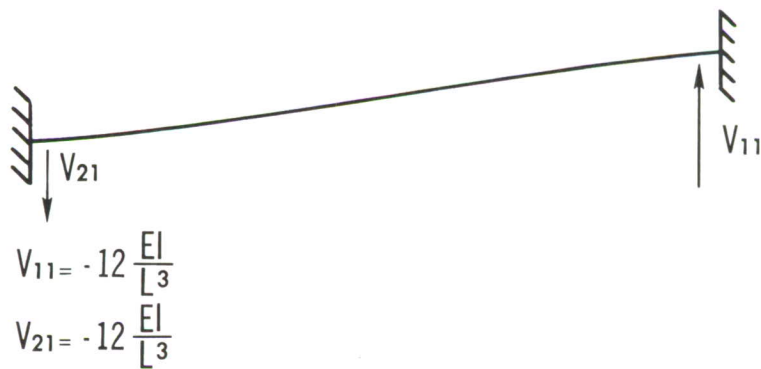


Figure 27. Stiffness Coefficients for Beam Elements in Example Problem Wing

$$A = 2 \text{ SQ. IN.}$$

$$E = 0.97 \times 10^7$$

$$\epsilon = \frac{\Delta L}{L} = \frac{1}{10}$$

$$\sigma = E\epsilon = 0.97 \times 10^6$$

$$N = EA\epsilon = 1.94 \times 10^6$$

STIFFNESS COMPUTATIONS

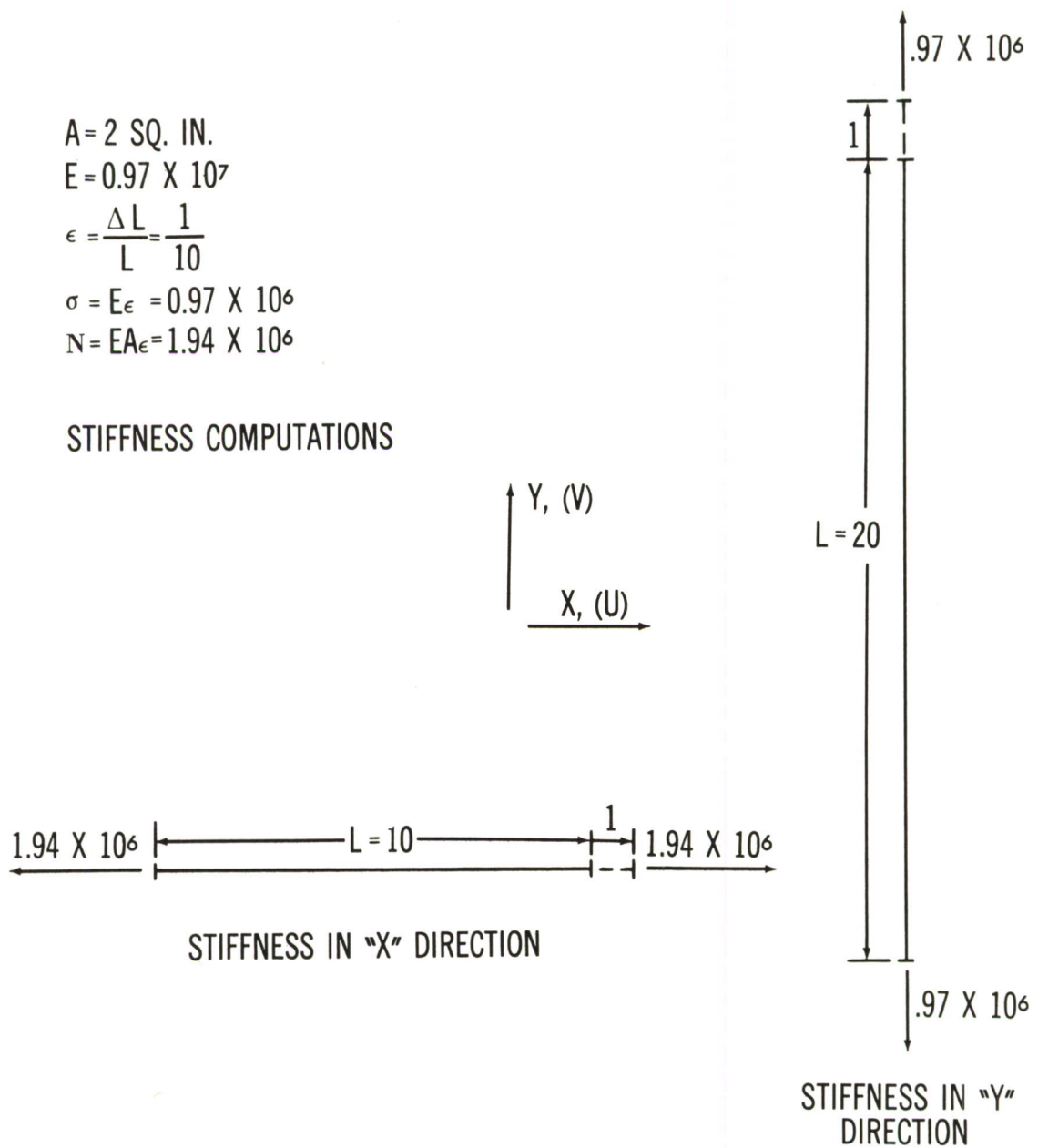


Figure 28. Stiffness Coefficients for Beam Elements in Example Problem Wing

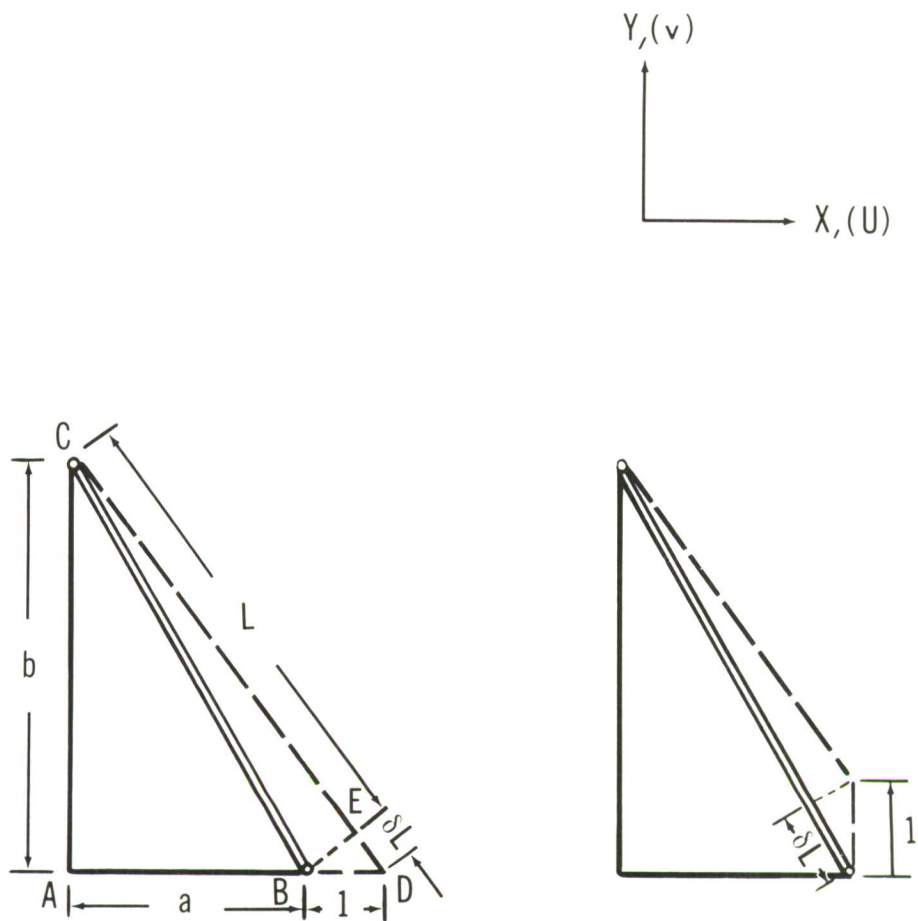
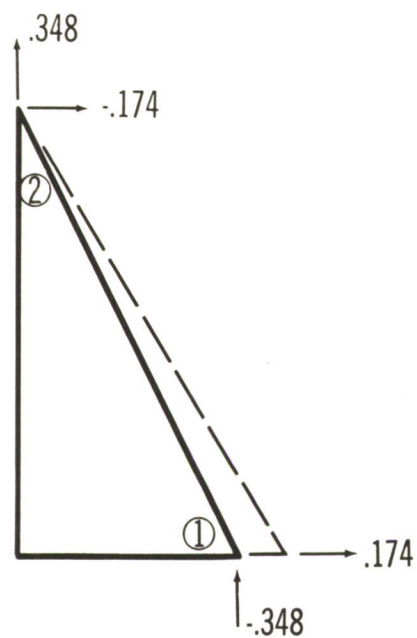
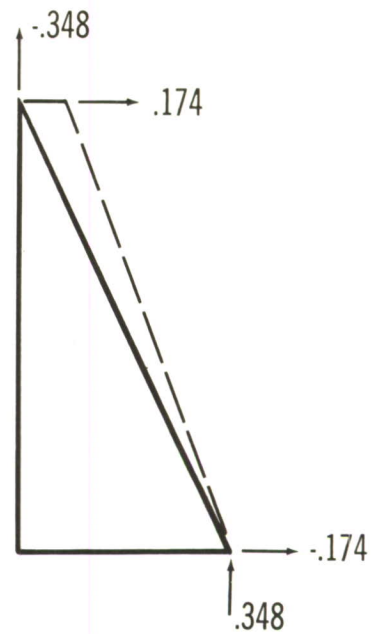


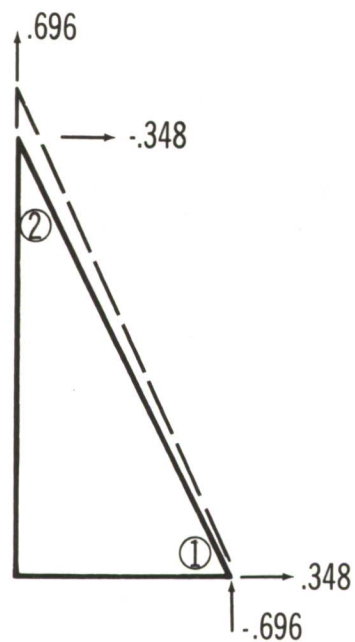
Figure 29. Oblique Frame Elements in Example Problem Wing



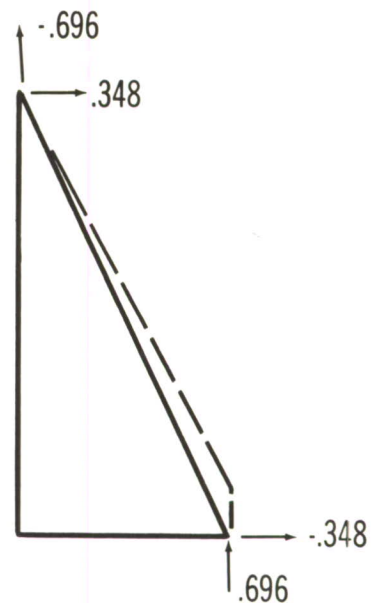
DISPLACEMENT $U_x = 1$



DISPLACEMENT $U_2 = 1$



DISPLACEMENT $V_2 = 1$



DISPLACEMENT $V_1 = 1$

Figure 30. Stiffness Coefficients for Front Spar (Oblique Bar) in Example Problem Wing

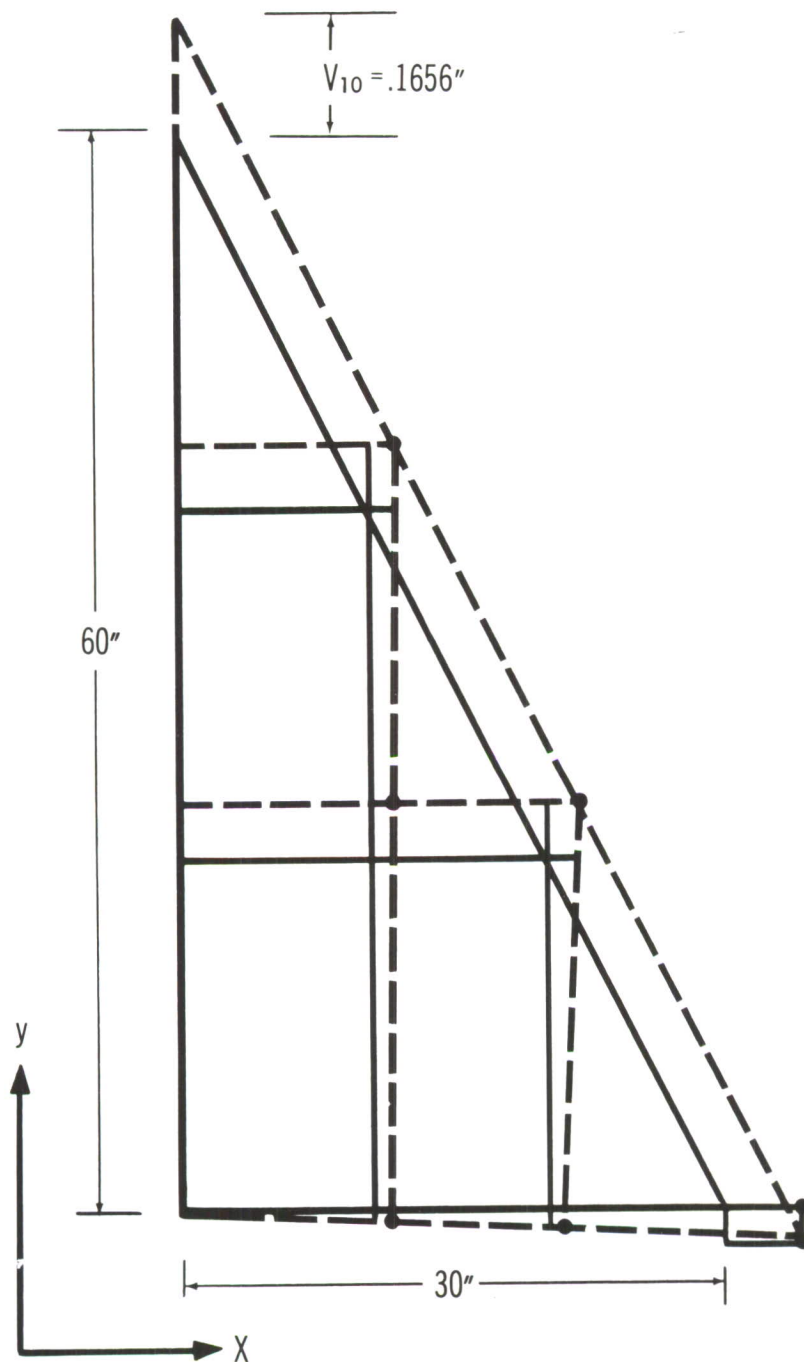


Figure 31. Mode of Displacement of Nodes of Example Problem Wing after Unlocking

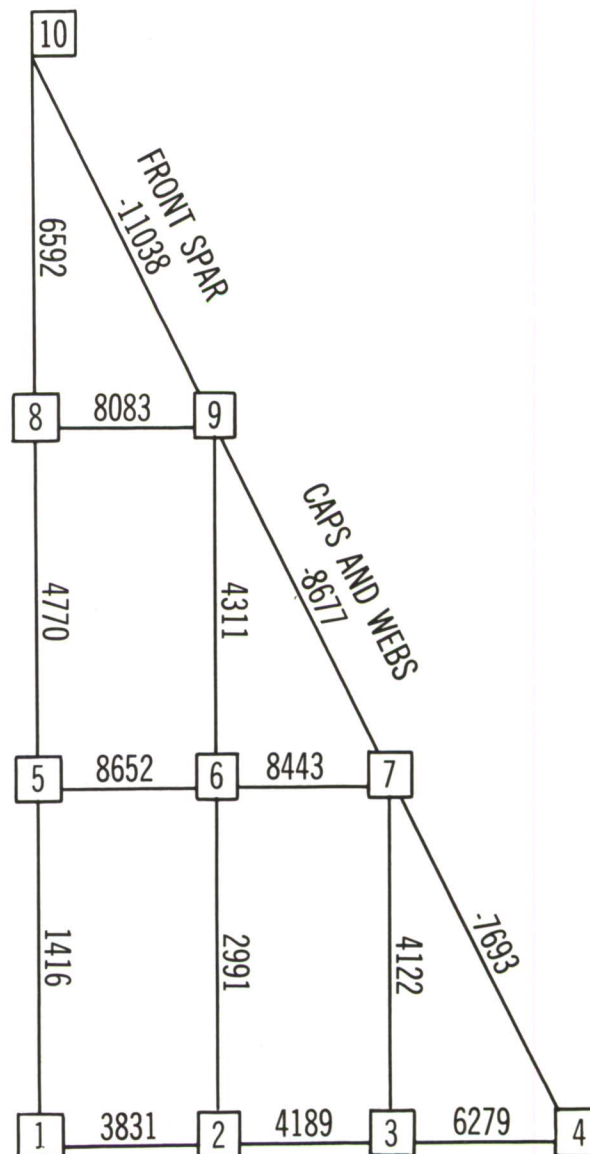


Figure 32. Thermal Stresses In Spar Caps of Example Problem Wing

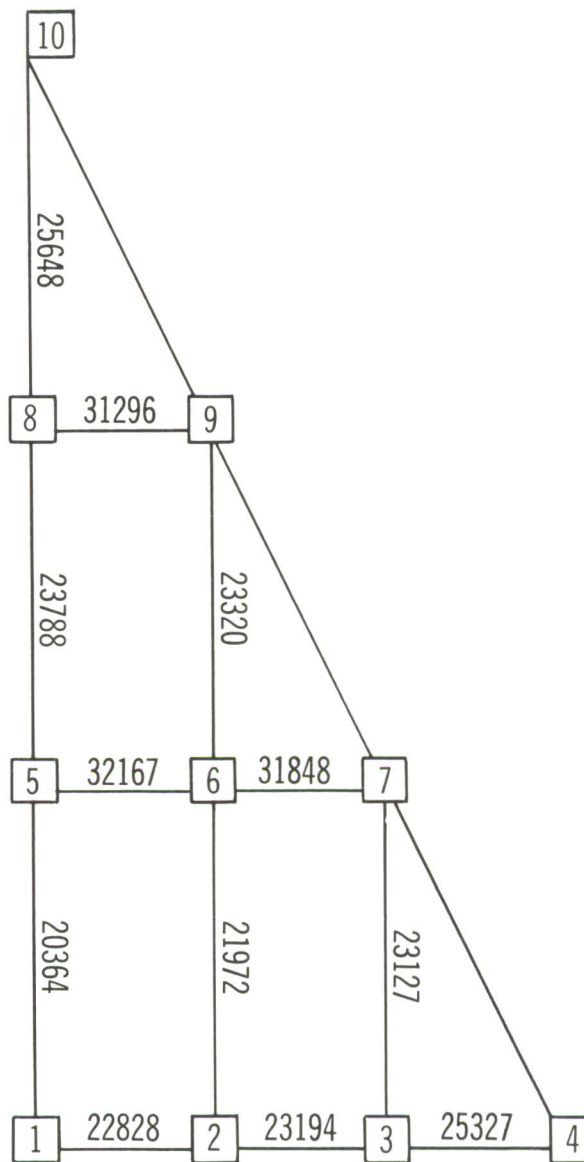


Figure 33. Thermal Stresses In Spar Webs of Example Problem Wing

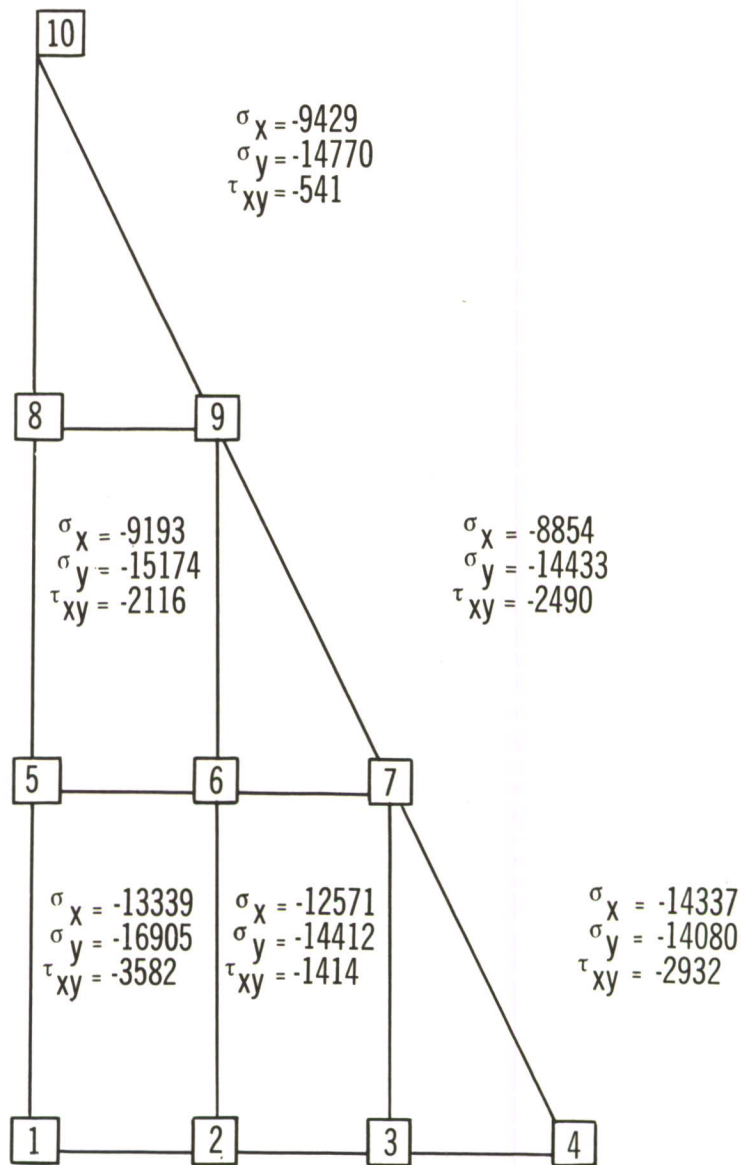


Figure 34. Thermal Stresses In Panels of Example Problem Wing

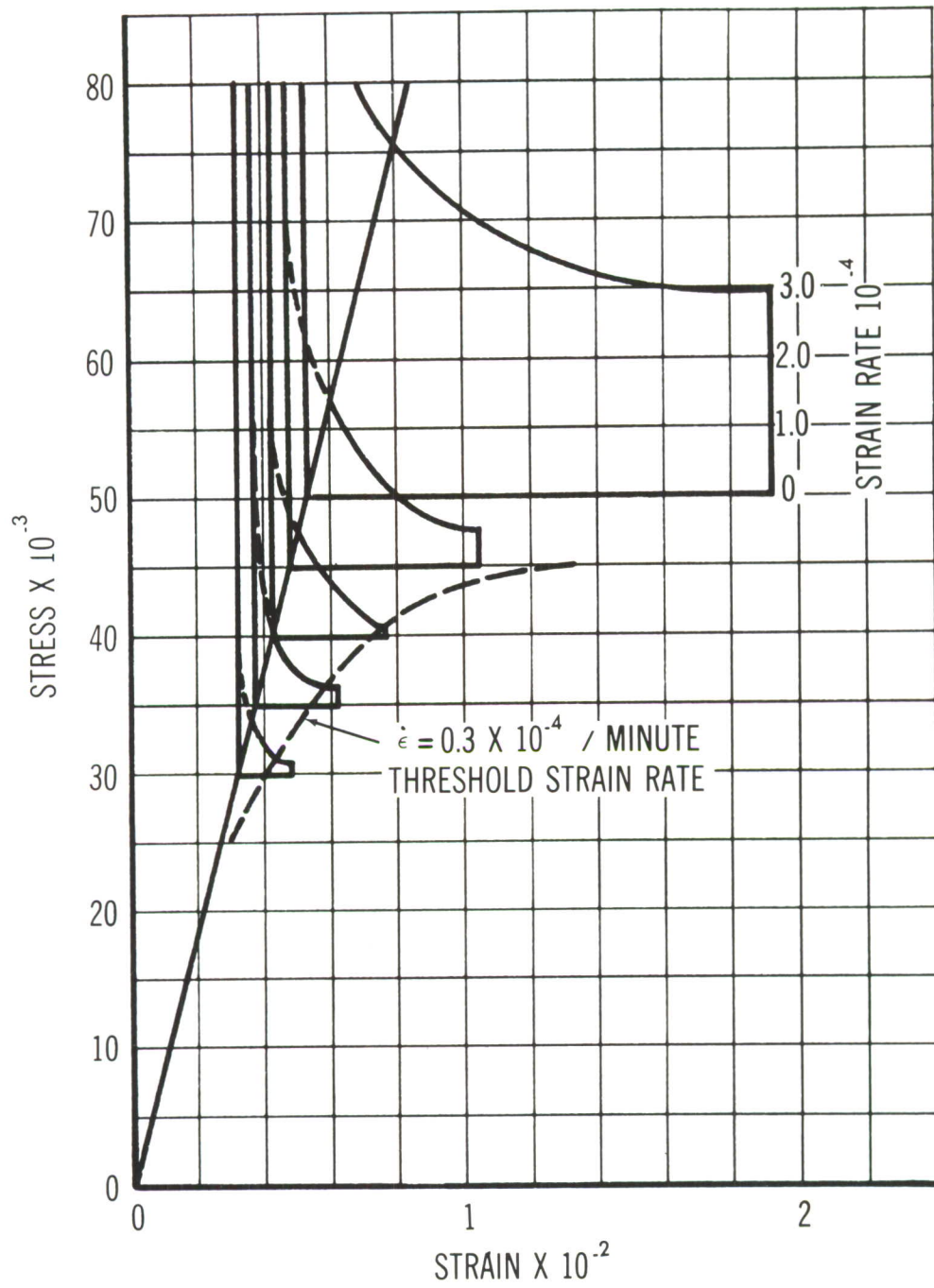


Figure 35. Creep Rates for 75 S-T Aluminum Alloy at 300°F

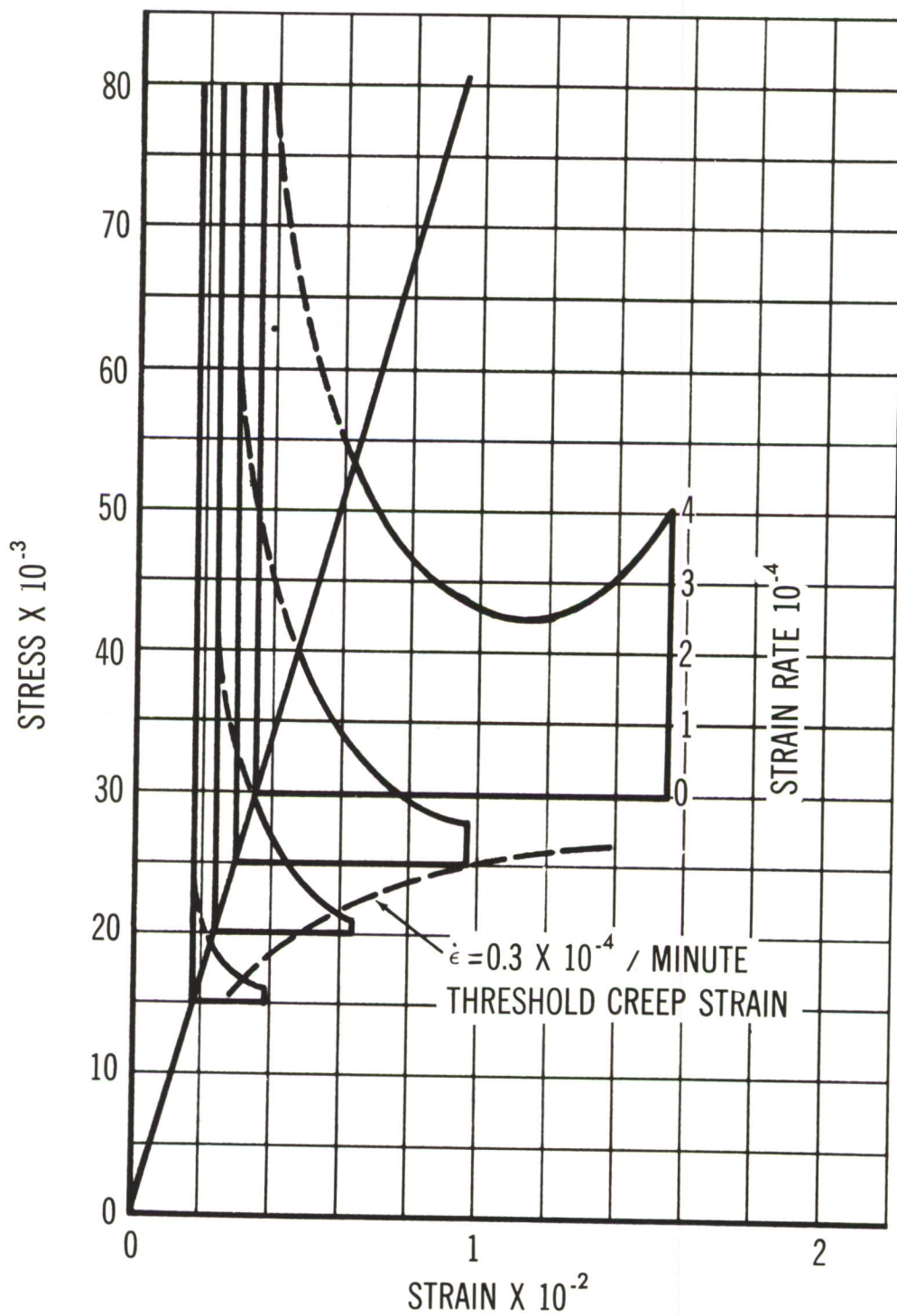


Figure 36. Creep Rates for 75 S-T Aluminum Alloy at 400°F



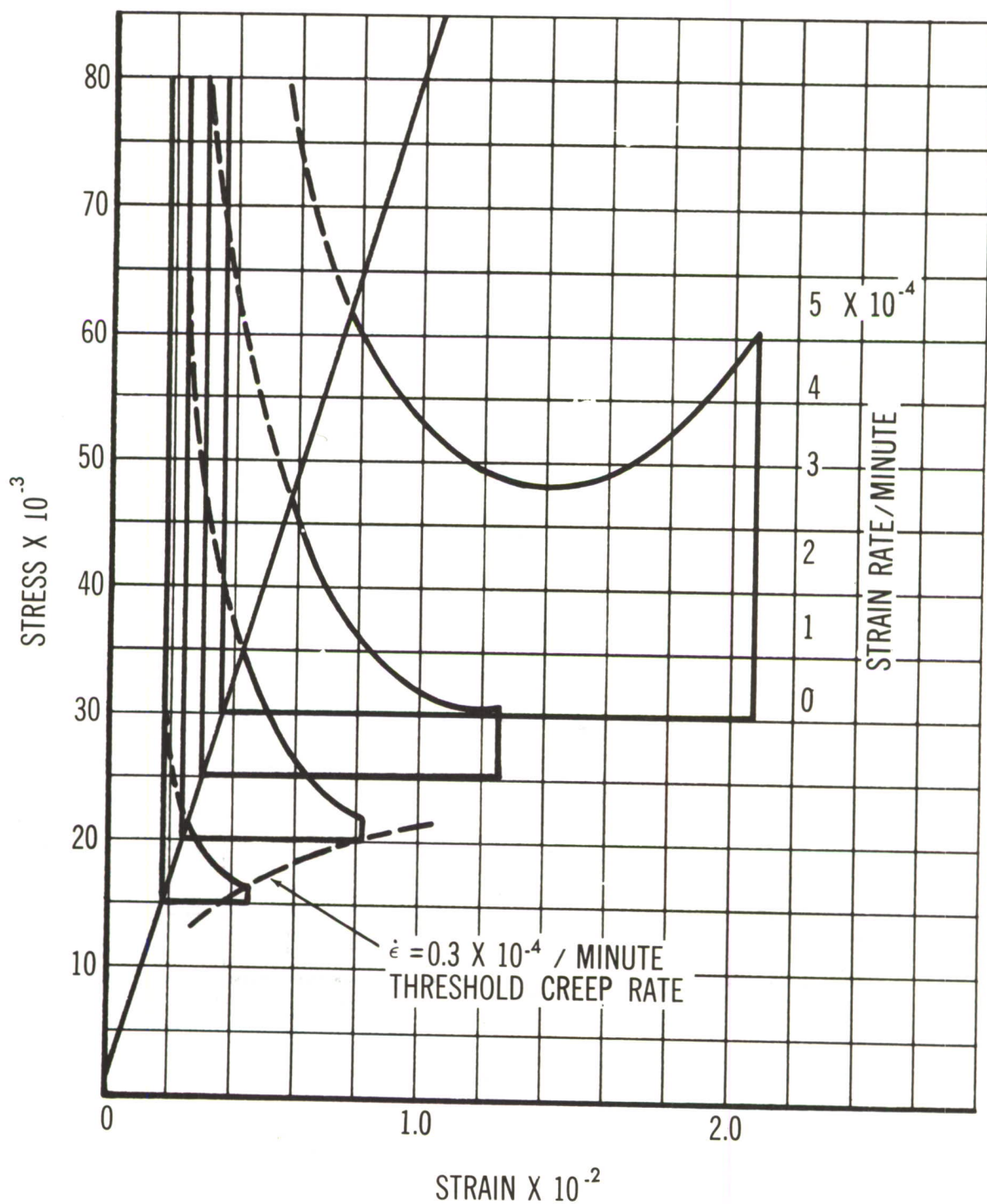


Figure 38. Creep Rates for 75 S-T Aluminum Alloy at 450°F

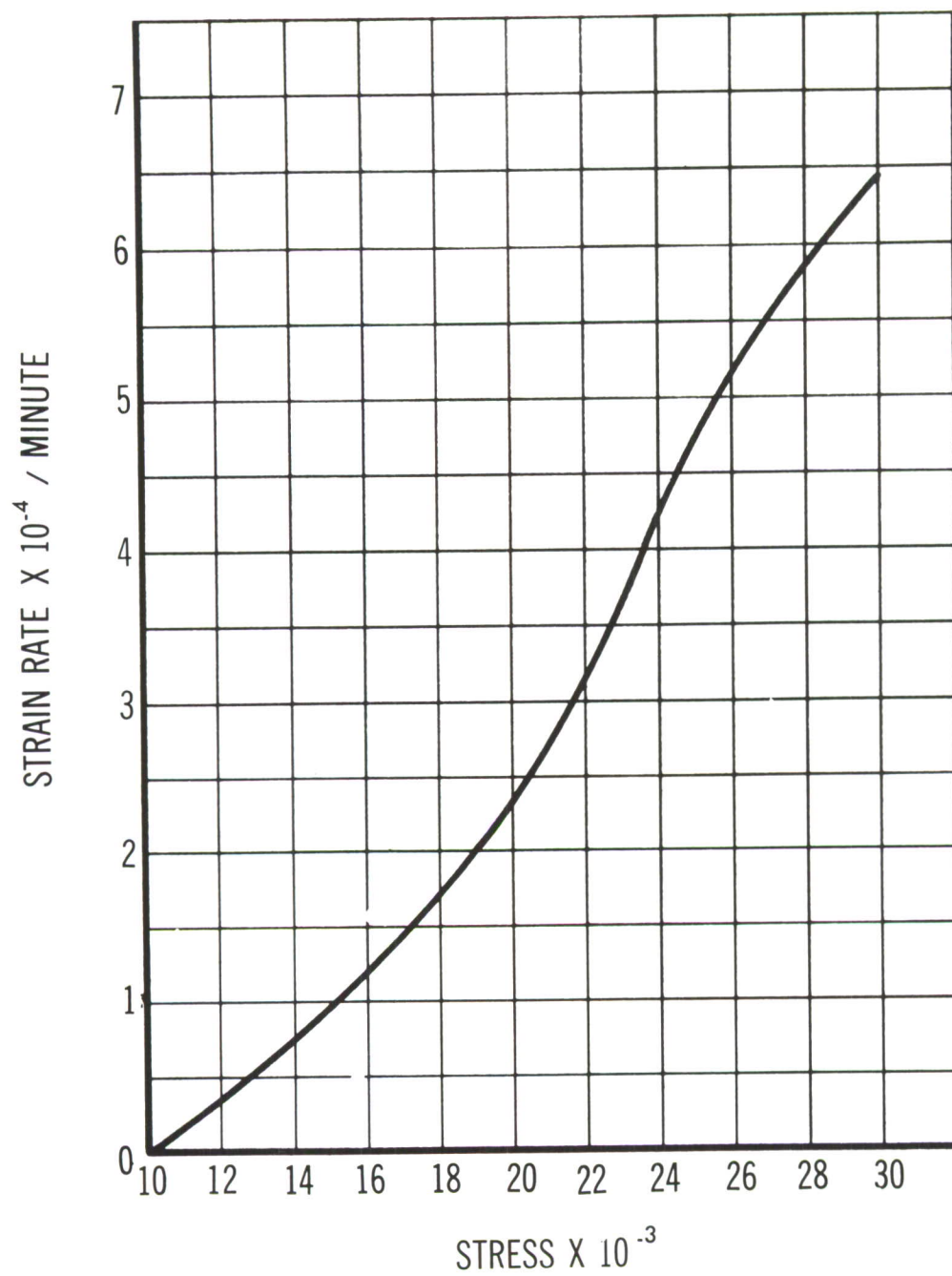


Figure 39. Creep Rate for 75 S-T Aluminum Alloy at 450°F at One Minute

PREDICTION OF CREEP EFFECTS

IN

AIRCRAFT STRUCTURES

PART IV

MATERIALS CHARACTERISTICS

IN RELATION TO CREEP

AND ITS PREDICTION

INTRODUCTION

In an examination of characteristics of aeronautical structural materials for use in elevated temperature structures, a re-consideration of basic governing conditions ruling uses of these materials in past, "conventional" temperature regimes is helpful.

In former efforts, great emphasis has been put upon strength capabilities of airframe constructional materials that their strength to weight ratios be kept low and thus promote efficient, light weight vehicles. This approach prevailed in a comparatively simple environment which involved a narrow range of temperatures centering around "room" conditions. In this environment uses of materials required high inherent stiffness, or moduli of elasticity and rigidity, and, the preservation of stable internal structures in the materials themselves to permit wide ranges of strength utilization without impairing their stiffness. In short low temperature operations permitted conditioning materials so that high proportional limits could be realized in them and, what is also important, could be depended upon to serve without detrimental change when subjected to service environments. Briefly the circumstances outlined allowed material use under conditions of elastic action and this coincided with structural design assuming small deflections, especially in structural elements susceptible to buckling effects where plastic action is deliberately restricted to small amounts.

In the presence of elevated temperatures, several occurrences take place which run counter to the fundamental ideas incorporated in previous effort, namely, restriction of advantages arising out of elastic action. Among these adverse happenings are:

1. Decay of moduli of elasticity and rigidity resulting simply from temperature increases.
2. Decay in proportional limits resulting simply from temperature increases which weaken base metal lattice structures.
3. Decay in proportional limits resulting from the deterioration of metal improvement steps, such as cold working, heat treat strengthening, etc. , resulting from thermal activation of adverse metallurgical mechanisms.

Viewing these things from the reverse side, it can be seen that the core idea of alloy design for elevated temperature materials involves steps seeking to retain moduli and proportional limit values inherent in base metals together with development of metal improvement schemes which require high temperatures to initiate deterioration.

SIGNIFICANT VARIABLES INFLUENCING MATERIALS PERFORMANCE IN HEATED ENVIRONMENTS

Four variables assert themselves in relation to structural design when materials

are gaged for performance in heated environments. They are load, temperature, time and deformation. Assuming that load and temperature are items which can be chosen, they may be classed as independent variables: the remaining two variables, time and deformation, then depend on the other two, load and temperature. It should be realized that the foregoing classification of variables is arbitrary and is chosen from convenience. It can readily be assumed also in a structural design problem that temperatures may be specified by vehicle velocity and time by service requirements and hence loads and deformations become dependent variables.

This example illustrates the point that although operative variables in a given situation may be readily recognized, this recognition quite possibly is of relative unimportance because of the many approaches that may conceivably be taken in putting them into use. Accordingly it becomes evident that interrelations of variables are over-riding in importance to variables themselves when the information utility is approached objectively.

THE DEFORMATION VARIABLE

In approaching interrelations of variables, knowing the relative importance of various factors entering into a complex is valuable in essaying effective interrelations. Inasmuch as loads, temperatures and time are measurable quantities in terms of pounds, degrees and seconds, direct implications of magnitudes are readily perceived. The deformation quantity, however, is directly measurable as a change in length. But because the stiffness of compression members, for example, is not directly proportional to length or length change, a simple and direct relationship cannot be assigned to deformation factors. Possibly the nearest approach to specification of deformation variables lies in statement of limiting amounts by which effects may be defined.

In a foregoing section it is stated that "No plastic component of strain was ever allowed previously in aircraft structures within limit load, except a residual 2×10^{-3} considered negligible". In the sense used above, the term limit load expresses working load imposed on a member and when limit load is multiplied by 1.5, the product expresses ultimate or failure load for the member.

Considering the foregoing, the deformation which takes place in a heated structure can be visualized as the combination of reversible and irreversible deformation actions consisting of the following:

1. Reversible actions.

- a. Elastic action taking place in accordance with Hooke's law which is regulated in magnitude by the temperature present, and, in extent by the condition of the material at hand combined with the extent to which combinations of time and temperature effect changes in the material condition.
- b. Thermal expansion taking place under conditions of negligible structural restraint. A condition of negligible structural restraint characterizes most tests aimed to assess materials properties. In short the thermal expansion term is cancelled out in tests but it must be reckoned into structural problems.

2. Irreversible actions

- a. Time independent plastic action which appears immediately upon imposition of a load on a structural element or structure. In current practice involving room temperature operations, "sets" arising from irreversible plastic action are commonly recognized in the term "permanent set". In the light

of current knowledge, irreversible plastic action is governed in magnitude by loads imposed upon members and in extent by the rate at which loads are applied.

- b. Time dependent plastic action which usually is observed immediately upon completion of time independent plastic action taking place upon loading. This action falls into three categories in order of their appearance with respect to time. They are termed "primary creep" wherein decreasing amounts of deformation occur as time progresses, "secondary creep" wherein deformation accumulates in direct proportion to time, and "tertiary creep" wherein increasing amounts of deformation appear as time elapses.

In view of both the structural significance of deformation effects and the involved deformation relationships occurring in actual operations of structures, the material tests to be described were studied with particular attention to singular effects of time, temperature and load upon deformation characteristics.

"STANDARD" CREEP TESTS

The "standard" creep tests presently described were performed with 0.025 in by 0.125 in by 15 in long strips of Armco PH 15-7 Mo Condition RH-950 stainless steel in a special creep testing machine. In the performance of these tests, the practice used involved conventional procedure of attaching specimens suitably equipped with temperature measuring thermocouples into the machine's grips, then rapidly applying heat to the specimen assembly until the desired temperature was attained, and, then maintaining this temperature throughout the duration of the test. Following application of heat and attainment of temperature equilibrium, loads were slowly applied so as to minimize adverse effects arising from momentum and impact. As soon as full load application was attained, the extension of specimens was observed as were extension increments subsequently appearing at twenty minute intervals throughout duration of the test.

A noteworthy item with this test procedure is the manner in which effects of thermal expansion are cancelled through application of load subsequent to heating. The test results, accordingly, reflect the effects of time, temperature and load in terms of stress and their effects upon only elastic and plastic deformations.

In the performance of these tests, temperatures for test were selected to represent (1) a condition (700°F) where small metallurgical change in the test material was expected; (2) a condition where experience indicated that creep effects would be marginal (800°F); (3) a condition where moderate metallurgical change in the material might be expected in a long run (900°F); and (4) a condition where severe metallurgical change in the material could be expected in a comparatively short run (1000°F). The loads (stresses) applied were estimated from Larson-Miller stress - rupture plots arbitrarily proportioned for estimating a time of about fifty hours required to produce about one percent total creep deformation. The specific conditions for individual tests are given in Table 40. Figures 40 to 55 show results from these tests. Figure 56 shows details of deformation patterns taken during these tests. Figure 57 shows the elastic recovery and permanent set patterns taken by the test specimens upon unloading. Figures 58 and 59 compare the total time independent deformation comprised of combined elastic and time independent inelastic deformation taking place upon loading with the elastic recovery appearing upon unloading.

LIMITING DEFORMATION: STRESS STRAIN DIAGRAM APPROACH

In the study of data showing deformation information confusion may arise in distinguishing between the importance of those deformations arising from the simple

application of load and those permanent deformations remaining after loads are released. In practice illustrated by ordinary stress strain curves, the actual deflections taking place upon loading, especially those occurring below the yield points, are of minor concern in that they do not serve to establish limits for material usages. The limiting factor is the "offset" or permanent set arising from plastic flow. In a sense loading deflections are indicative of causes and permanent sets are indicative of results.

In the study of creep curves the subtlety of the interrelations of cause and effect assert themselves, especially when such study is approached with a specific limiting permanent set, or what is analagous, plastic strain, in mind. The first thing that appears in creep testing is the deformation that occurs upon loading and is independent of time. Where a limiting plastic strain of .002 prevails, this limit can be attained almost instantaneously upon load application providing stresses are equivalent to the yield stress. In the event it should be desired that permanent sets arising from loading alone be eliminated, first thought would lead to use of loads that produce stresses at or below the proportional limit. By way of the example of Armco PH 15-7 Mo, Condition RH 950 tested at 800°F, the yield strength given by the producer is 149 K.S.I. and the proportional limit is 92.5 KSI. The difference in magnitude between these two values emphasizes the importance of good working stress level selection especially as a three way compromise between structural weight, the initial deformation upon loading and subsequent creep deformation is involved in the selection.

In relation to the foregoing example, it is of importance that the deformation present under actual load amounts to .040 (4.0% deformation) strain at the proportional limit and .079 (7.9% deformation) at yield stress as indicated by the Armco Technical Data Manual information referencing to tension test (stress-strain diagram) data.

LIMITING DEFORMATION: CREEP (TIME-DEFORMATION) DIAGRAM APPROACH

In relating creep curve information given in Figures 44 through 47 with observations given above and arrived at from study of the Armco Technical Data Manual, the disparity of deformation information from the two sources is evident. Whereas stress-strain diagrams from tension tests indicate .079 strain at 149 KSI yield stress, the creep diagrams showed about .028 and .025 strain at 170 KSI stress and about .029 and .026 strain at 175 KSI stress, both of which exceeded the yield stress and proportional limit stresses reported from Armco tension tests by wide margins. Although rigorous explanation of these differences is not immediately available, mode of loading suggests itself as a possible contributor to this situation. In tension testing the loads are gradually applied over an appreciable length of time, and, in creep tests loading is accomplished as rapidly as possible and in one increment. In passing it may be surmised that the strain differences observed upon loading the two pairs of creep specimens, .028 and .025 strain at 170 KSI stress and .029 and .026 at 175 KSI stress, arose from variations in speed of loading.

STRAIN MODES APPEARING IN CREEP TESTS

Figure 56 relates the outcome of attempts to assess creep curves in terms of strain modes, especially up to the time where secondary creep asserts itself. The elastic strain shown in Figure 56 is not elastic deformation taking place up to the proportional limit: it is the elastic component of total strain taking place upon loading. It is the quotient of the applied stress divided by that modulus of elasticity given for the appropriate temperature in the Armco Data Manual. The time independent plastic strain shown in Figure 56 is the plastic component of the total strain taking place upon loading. It is the difference between the total strain and the elastic strain component. The primary creep strain shown in Figure 56 is strain occurring between time of completion of loading to beginning of secondary creep.

Figure 57 shows results from unloading the creep specimens at the end of test run. The elastic recovery shown is the contraction in specimen length observed upon removal of the load. The permanent set indicated in Figure 57 is that dilation experienced by the specimen during test which remained unchanged after unloading.

Figures 58 and 59 compare the time independent deformations occurring upon loading with the elastic recovery observed after unloading. These charts show, in general, that the energy input into a specimen in the form of elastic and plastic action is not entirely converted into potential energy in the form of stored elastic action.

The energy losses suggested by the differences in height of the two bars representing each specimen represent a part of the energy input to specimens which was used up in plastic deformation action.

The point is that loading energy input is used up in both storage of potential energy in a test bar and in causing it to deform in a plastic manner. In other words part of the energy is recoverable and that which is not can contribute to structural damage prior to the onset of time - dependent creep damage as shown in Figures 60 and 61. In these figures the time independent (elastic and inelastic) deformation converted to permanent set upon loading represents the difference between the total permanent set arising from the combination of inelastic and creep deformation, and, the creep deformation. The charts depicted in Figures 60 and 61 show that at all four temperatures of test the portion of permanent set acquired during loading was generally of a magnitude that constituted structural damage conditions. Briefly, the pronounced tendency for time independent plastic strain to cause permanent set in excess of .002 (0.2% offset) strain was evidenced. In view of this, together with the fact that the loads used were greatly in excess of both the proportional and yield limits, the desirability for information relative to those loads which would result in negligible structural damage asserted itself.

INCREMENTAL LOADING TESTS

In view of the importance of stress level in creep tests, especially because this level influences magnitude of time independent plastic deformation experienced upon loading, incremental loading tests were made to determine approximate stress levels at which time independent plastic deformation asserts itself, its increase with respect to increasing stress, and, its repeatability upon complete recycling.

The incremental loading tests were made with Armco PH 15-7 Mo, Condition RH-950 stainless steel. These tests were run in Arcweld Model JE creep test machines using Arcweld Model 400 extensometers to observe deformations taking place. Tests were run under the limiting conditions of test shown in Table 40. Specific test performance was as follows: first, a specimen having a .505 in. wide x .025 in. thick x 2 in. gage length test section conforming to Federal Standard 151A was loaded to 10% of the limiting stress; then this load was released; in a second step the specimen was loaded to 20% of the limiting stress, and then this load was released. Following this, successive loadings at 30%, 40% and so on up to 100% of limiting stress were applied and released to complete a single "step" loading cycle. In each test run with a single specimen, five complete cycles were run in order to examine repeatability of performance under repetitive conditions of test.

INITIAL INCREMENTAL LOADING CYCLES

Figure 62 summarizes the findings from a single initial loading cycle. In this chart the line AB shows the total deflections obtained throughout the loading program. The line ACD shows the extensions observed upon release of each incremental load. The area ABCD shows a field wherein elastic action activity is manifested, the points along the line AB representing extension upon application of load and the line CD representing the residual extension accruing upon release of load. The

area CDE represents a field of permanent set accumulation wherein a portion of the energy input arising from loading is converted into set rather than into stored potential energy which is reflected in elastic recovery.

If the permanent set is considered as representing a plastic component of strain, it may be looked upon as damaging so far as an airframe structure is concerned. In the instance shown, the plastic component appears at a stress of about 92.5 KSI, the proportional limit stress shown in the Armco Technical Data Manual. In addition the stress required to produce 0.2% deformation is 166 KSI, a number in excess of the 149 KSI yield strength figure given by Armco for 700°F yield strength. This latter number, 166 KSI, suggests, in comparison with the former, 149 KSI, an effect arising from loading rate. In the case of incremental tests, loading was accomplished in about 5 to 10 seconds. In tension testing about 75 to 90 seconds are ordinarily required to attain the yield load.

SECONDARY INCREMENTAL LOADING CYCLES

In the sense used herein, the term, secondary incremental loading cycle, is used to denote any cycle exclusive of an initial incremental loading cycle. Figure 63 shows such a secondary cycle as an example. Specifically the cycle shown in Figure 63 immediately followed that shown in Figure 62 during test and both represent a single test run. In Figure 63 the zero deformation shown at the origin of coordinates actually represents final permanent set attained at the end of the initial incremental loading cycle. Also, the line AB indicates the total deflections observed throughout the secondary cycle loading program. The area ABC shows a field wherein elastic action activity is manifested. The points along the line AB represent extension upon application of load and the line AC represents the residual extension resulting from release of load. The area ACD represents a field of permanent set accumulation wherein a portion of the energy input arising from loading is converted into set rather than stored potential energy which is reflected in elastic recovery. The schematic nature of the line AC is to be noted and this circumstance arises from measurement of dimensions in the order of 0.0001 to 0.002 inch with mechanical instrumentation. Accordingly firm evidence is not believed to be presented in single secondary cycle results but trends may be roughly deduced from multiple cycle test trends.

In the example shown in Figure 63 the predominance of elastic action is fairly evident. The plastic action indicated appears as a more or less linear growth suggestive of secondary creep. Evidence of time independent plastic action or primary creep action is not suggested since the non-linear relations are not evidenced. The suggestion that presents itself however is that lattice displacements accomplished during initial cycle loadings were adequate to offset those displacements ordinarily expected in "normal" primary creep. Consequently the material may be "triggered" to go into secondary creep during the second cycle upon input of sufficient incremental energy to initiate secondary creep activation.

The interesting implication from the foregoing is a suggested mechanism for "stabilizing" a metal for "creep" service by hot stretching, for example. Second thought, however, suggests that such an operation implies conditioning fully hardened material. The prospects for fabricating such a material into airframe configurations appear remote and presently seem beyond ordinary fabricating capabilities.

INCREMENTAL LOADING TESTS: Repetitive Loadings

Figure 64 schematically diagrams the program approach used to obtain the results shown in Figures 65, 66 and 67. These tests were run at a constant temperature of 700°F with a full load of 185 KSI. Figures 68 and 69 display results from tests

run at 800°F with a full load of 175 KSI. The 800°F test condition is represented by a single test. Two tests were run but extensive extensometer slippage negated the second test run which was cast out during data reduction. The results from test run at 900°F and 135 KSI full load are given in Figures 70, 71 and 72 and those results from tests run at 1000°F and 77 KSI full load are shown in Figures 73, 74 and 75.

Figures 65, 66, 68, 70 and 71, and, 73 and 74 depict the deformation occurring during the loadings at 700°, 800°, 900° and 1000°F respectively. These curves resemble stress-strain curves and show the work hardening taking place during the initial cycle followed by elastic working of this cold worked material in subsequent cycles. The chief item of interest shown in these curves is the "modulus line" shown in the straight line portions of component portions of the several curves. In essence these "modulus" lines serve only to reiterate the well understood and evaluated inverse change of modulus of elasticity as temperature increases. Figures 67, 69, 72 and 75 show the deformations occurring upon unloading subsequent to each incremental loading. These curves reassert the damaging effect of an initial loading cycle and at least in the instance of the tests run at 700°F, 800°F and 900°F, all temperatures below the 950°F aging temperature used to produce Condition RH-950 in Armco PH 15-7 Mo, show the profound influence of the time independent plastic strain in the deformation outcome as it relates to the "secondary creep" taking place after the initial loading cycle has done its work.

Figure 76 compares loading strains developed by incremental loading to a pre-determined stress level at the end of an initial loading cycle with those developed at the end of a fifth incremental loading cycle. In actuality those strains shown as appearing at the end of the fifth loading cycle represent the permanent set accrued during the second, third, fourth and fifth loading cycles. The purpose of this comparison is to emphasize the strong influence exerted by original loading in relation to the somewhat minor influence exerted by succeeding loadings. For additional comparative information elastic action components calculated from published elastic modulus data are shown in Figure 76.

Figure 77 compares strains observed upon unloading the incremental loading tests and again it compares strains observed at the end of the first with those observed at the end of the fifth loading cycles. In this chart, the total deformation, which includes both permanent set and elastic recovery is compared with the elastic recovery observed in each test case. The high permanent set generation, especially at 700°, 800°F, and 900°F, certainly indicates the influence of high stress level in promoting early damage. However, as previously discussed, incremental step-loading tests indicate the ratio of permanent set to elastic recovery is possibly amenable to control providing low stress levels in the neighborhood of elastic limit stress are compatible with structure weights. In the comparisons shown in Figure 77 the important influence of the first loading is reasserted in that the permanent set produced in this step approached that produced in the succeeding four loading cycles.

Figures 78 and 79 compare the total strain observed as a result of incremental loading with the elastic recovery observed upon load removal. These charts also compare the calculated elastic action strain component anticipated upon loading with the strain recovery observed upon unloading. In these charts effects arising in the first loading cycle are shown separately from those accrued in the second, third, fourth and fifth loading cycles. This was done to reassess the importance of initial loading action. This point is brought out by the charts which essentially show that severe elastic-plastic deformation experienced in initial loading serves to condition material by a work hardening process to subsequently serve as an elastic material when subjected to additional loadings. Clean-cut comparisons relating elastic action input and output are not shown in these charts. It is felt

that to obtain these comparisons, which appear fundamental to a sound understanding of the efficiency of elastic action and "frictional" effects encountered in its operation, critical experiment with highly refined apparatus is required. This approach appears highly desirable because in repeated loading situations it seems quite probable that in addition to gliding movement usually associated with creep observed in conventional tests, an additional "friction" or hysteresis entering with re-cycled loadings is suggested. This implies desirability for knowledge of mode and rate of accrual of these "run-down" factors.

REPEATED LOADING TESTS

In the performance of incremental loading tests the gradual build-up of stress level was considered a means for accumulating "cold-working" effects at a slow rate. On the other hand the sudden build-up of stress level in a single loading was considered a means for accumulating "cold work" at a greater rate than that experienced in incremental load build-ups. Also, because of singular importance asserted by initial incremental loading cycles in relation to subsequent loading cycles, time suggested itself as an influence and it appeared desirable to learn from repeated loading tests whether rapidity of load application was conducive to build-up of "cold working" effects in load cycles other than the initial one.

The repeated loading tests discussed here were made with Armco PH 15-7 Mo, Condition RH 950 stainless steel. These tests were run in Arcweld Model J.E. creep machines using Arcweld Model 400 extensometers to observe deflections. Tests were run under the conditions shown in Table 40. Specific test performance consisted of the following: first, a specimen with a 0.505" dia. x 0.025" thick x 2" long gage length conforming to Federal Standard 151A was loaded to the limiting stress; then the load was released. In each run with a single specimen, five complete loadings were successively applied and released to provide for data for examining repeatability of performance in the various specimens under repetitious loading.

Figure 80 schematically diagrams the approach used to obtain the results shown in Figures 81 through 84 inclusive. In these charts the curves drawn are faired and do not reflect observations except at the data points indicated. Figures 85 through 88 reflect the conditions obtaining with respect to permanent set-elastic recovery relations at the end of each loading cycle throughout the entire series of tests. The permanent set shown in these charts is cumulative set acquired as tests proceeded through cycling. The amounts of permanent set shown are large and, as the charts show, disproportionate with the elastic recovery. As mentioned in discussion relative to incremental loading tests, the indications are that to arrive at tolerable amounts of permanent set low stresses are necessary.

Figures 89 through 92 chart changes in permanent set and elastic recovery observed throughout repeated loading tests. These charts reiterate the observation that initial loading produced the greatest and determining set observed in each test case studied. The data charted in Figures 89 through 92 do not clearly show whether loadings subsequent to initial loading cause definite increases or decreases in either permanent set or elastic recovery. The intimation of the data, however, is that at least a slight tendency for both permanent set and elastic recovery to increase as load cycling progresses is present. The outcome of these tests suggests two things: the need for critical experiment in order to more accurately define the trends for change in permanent set and elastic recovery magnitudes; and, the need for extended experiment to determine whether the simultaneous increase in permanent set and elastic recovery persist beyond a primary

creep phase of action. Figures 93 and 94 show comparisons attempting to relate permanent set and elastic recovery observed subsequent to sequenced load applications with the temperatures at which the load applications were made. Because the stresses under which these tests were carried out apparently have little relation to each other, clean-cut interpretation of these charts is difficult. The striking impression gleaned from these charts is that in order to effect correlation of test variable interrelations a base line of departure in the form of some physical event is required to supplant arbitrary test variable selection.

TRANSIENT HEATING TESTS

The introduction of repeated heatings into creep tests is recognized as the introduction of a complex rather than a simple variable. This situation distinguishes tests of this nature from those made at a constant temperature for several reasons, among which are:

1. Decay in the modulus of elasticity in direct proportion to temperature increase
2. Decay in the elastic limit in direct relation to temperature increase
3. Introduction of displacements arising from thermal expansion effects which vary from linearity with respect to temperature ranges present.
4. Non-linearity of the heat or temperature increase which apparently proceeds in accordance with an exponential law.

The transient heating tests described were made with 0.025" thick x 0.125" wide x 3" long gage length strips of Armco PH 15-7 Mo, Condition RH 950 stainless steel. In the conduct of these tests, the desired stress level was obtained by dead weight loading cold specimens prior to any heating. After loading heat was applied by resistance heating a 0.500" outside diameter x 0.010 wall Inconel tube surrounding the specimen. This arrangement provided a combination of radiant and convective heat transfer for specimen heating and resulted in a requirement for from about 2.75 to 4.0 minutes to heat an individual specimen from room to test temperature. Upon attainment of desired temperature in a specimen, the heater was de-energized and allowed to cool to room temperature. This cooling consumed about 55 minutes in each test case. In each test case the heating program involved five successive heatings and coolings.

Figure 95 schematically describes the procedure used to obtain the data shown in Figure 96. This chart shows plots of data points obtained at 20-second intervals during initial transient heating of each test specimen. Aside from display of heating curves falling into a scatter band delineated in the greater part by curves governed by the temperature level and corresponding heating rates, this data plot yields little information. Figures 97 and 98 are replots of the data shown in Figure 96. These plots by throwing the data into logarithmic form bring out the duplex nature of the curves shown in Figure 96 and thus bring out indication of a transition which suggests change in the mode of response of the material to its environment. At this stage of investigation it does not appear wise to attempt assessment of this transition in terms of the stress, times and temperatures involved. However it does appear that the transition points may be viewed as an indication of shift from a state where elastic action predominates to one

where plastic action predominates. Figure 99 attempts to relate transition points with temperatures at which they occurred. Because of the undetermined relation between the indicated transition and an "effective elastic limit," it is difficult to discern trends from the meager data at hand. However, judging from the fact that the strain at which the elastic limit occurs as temperatures increase in conventional short time tension tests, it is surmised that the data imply a downward trend as indicated in Figure 99.

Figure 100 displays data similar to that shown in Figure 96 and represents transient heating tests run at 700°F at various stress levels. These data also present the confused situation reflected in Figure 96 which is discussed above. Figures 101 and 102 display replots of the data shown in Figure 100. These logarithmic plots also show the existence of transition points in the time-deformation curves which suggest the shift from elastic to plastic action fields already discussed. Figure 103 relates the occurrence of the transition points with respect to the strains at which they occur at differing stress levels. The upward trend indicated in Figure 103 appears to be consistent with observations connected with short time tension test data.

The foregoing experimentation indicates in its way a requirement for critical experiment which provides continuous records of concurrently occurring strains and temperatures which appear in transient heating tests. Such experiment will lead to the determination of "effective elastic limits" operative under these environmental conditions.

Figures 104 through 110 display results obtained from five cycle transient heating runs. In all of these charts, the dominant position of the initial heating cycle stands out both as it affected the deformations appearing upon loading and upon release of load. A general tendency for a steady permanent set condition to establish itself in the initial cycle is generally evidenced in these curves. The permanent set observed beyond the initial cycle accumulated in a linear manner in general. However the outcome shown in Figure 107 was such that it suggested the possible influence of a "primary" creep action. This primary creep action first occurred at the highest stress level used at 700°F and is of extreme interest because it hints at possibility of a "strain aging" mechanism coming into play. In general, however, the deformations occurring upon "loading" appeared to coincide in curve form, shape and trend with the permanent set curves. The gradual strain increase indicated both upon "loading" and in permanent set observed upon "load" release was indicative of an action akin to secondary creep action and probably reflected a time effect introduced in the normal course of heating and cooling.

PULSED CYCLE HEATING TESTS

The complex conditions arising from heatings of specimens maintained at a constant stress level in pulsed cycle heating tests are the same as those that apply in transient heating cycles. The pulsed cycle heating tests were accomplished under the same conditions as those used for transient heating tests. The distinguishing difference between the two series of tests appeared in the maintenance of the pulsed cycle tests at temperature for specific time intervals prior to initiation of cooling. Figure 111 schematically diagrams the procedure followed in pulsed cycle heating tests and Figures 112 through 115 plot the permanent set trends for each test.

Figures 116, 117, and 118 compare the effects of differing stress level at the various temperatures used in the 5-minute pulse pulsed heating tests. These curves reiterate the generalities found in "conventional" creep tests in that they show the existence of primary and secondary stages of creep together with the tendency for higher stresses to accelerate both primary and secondary creep. Figure 119 displays the effects of differing stress level at 1000°F upon tests using a 25-minute heating pulse. Figures 120, 121 and 122 show the same kind of comparative data for those tests run with a 125-minute heating pulse. The curves shown in Figures 119 through 122 reiterate the generalizations given in relation with Figures 116 through 118.

Figures 123 through 126 compare the effects of varying pulse time periods at equivalent stress levels and temperatures. The characteristic shown in these comparisons is the tendency for creep strains to increase markedly together with an accelerating creep rate as the time pulse duration increases. Ready explanation of this feature does not appear to arise from total energy input since the number of cycles of heating at the 125 minute pulse interval are less than those at a 5 minute pulse interval. This arises because the charts show time only in terms of pulse times exclusive of the times during the heatings-up and cooling-down where variable heat input is present. About the only surmise that can be advanced without detailed study is that a finite time subsequent to the attainment of a given temperature is required to activate the creep processes and set them in motion at a maximum steady rate consistent with the environmental conditions at hand.

Figures 127 and 128 compare the effects of the various temperatures at equivalent pulse times upon the observed strain. Largely because of the lack of comparability between the various stress levels used at the differing temperature levels, these charts do not serve to reveal contrasting features.

COMPARISON OF EFFECTS OF "CONVENTIONAL" CREEP WITH THOSE OF "PULSED STEP-LOAD" CREEP

These test were made to compare the effects of conventional creep, that is, creep which takes place under conditions of steady stress application at constant temperature, with those effects observed as a result of creep under pulsed step loading at constant temperature. The pulsed step loading used consisted of applying a 50KSI load, a stress level slightly above that at which creep activation was expected at the temperature used, maintaining this stress for fifteen minutes and then, without load release, increasing the stress to 70KSI. Upon reaching the 70KSI stress, this stress level was maintained for fifteen minutes whereupon the loads were released to complete a single step load pulse cycle. In the test programming the effects resulting from sixteen step load pulses which were equivalent to eight hours of creep exposure were sought. These effects were for comparison with those arising from four hours' exposure, separately applied, at each of the two stress levels mentioned. In the interpretation of test outcomes, comparisons of effects arising from four hours to 70KSI added to those arising from four hours at 50KSI were to be made with those arising from eight hours of pulsed loadings.

The tests mentioned were run in a Tinius Olsen Electromatic Universal Testing Machine Olsen S-1 recording extensometers acting in conjunction with an Olsen Model 1050 recorder were used to observe the strains taking place. The universal testing machine itself employs a Thymotrol speed control unit which provides

infinitely variable speeds and this control provided means for slowing the testing machine motor to a point where only enough "take up" to accomplish constant load maintenance was obtained. This control also provided means for rapidly changing from one load level to another and finally for releasing loads rapidly without introducing undue shock and inertial effects. Figure 40 shows a schematic representation for the constant temperature-constant load test program and Figure 129 shows a similar representation for a pulsed step-load test program.

Figure 130 displays and compares the results obtained from the above tests. Those tests run at 70KSI load and 1000°F temperature resulted in the steeply rising creep curves-identified Mark A and Mark B in Figure 130. These particular tests were not run for the full four hours planned, but they were run out to the limit of extension measurable by the equipment used. The tests run at 50KSI load and 1000°F resulted in the flat creep curves identified Mark C and D in Figure 130. Those creep curves identified Mark E and Mark F in Figure 130 show creep curves resulting from the pulsed step-load tests also run at 1000°F under the loading conditions described above.

In comparing results from "continuous" creep with those obtained from "pulsed" creep, the coordinates representing the terminal observations from the two tests run at 70KSI and 1000°F (Mark A and Mark B) were added to the terminal observation obtained in the first 50KSI, 1000°F creep test (Mark C). This resulted in locating the summation points shown by Mark G and Mark H. Likewise the coordinates representing the terminal observations from the two tests run at 70KSI and 1000°F (Mark A and Mark B) were added to the terminal observations obtained in the second 50KSI, 1000°F creep test (Mark D). This resulted in locating the summation points shown by Mark J and K.

In consideration of the data shown in Figure 130 the following observations can be made:

- A. The first (Mark C) 50KSI, 1000°F constant stress test acquired 0.15% strain in 245 minutes and the first (Mark A) 70KSI, 1000°F constant stress test acquired 3.15% strain in 100 minutes. These outcomes sum up to 3.30% strain acquired in 345 minutes by constant stress loadings. This compares with the lesser 2.35% strain acquired in 355 minutes through pulsed step-loading.
- B. The first (Mark C) 50KSI, 1000°F constant stress test acquired 0.15% strain in 245 minutes and the second (Mark B) 70KSI, 1000°F constant stress test acquired 3.56% strain in 130 minutes. These outcomes sum up to 3.71% strain acquired in 385 minutes by constant stress loadings. This compares with the lesser 2.65% strain acquired in 385 minutes through pulsed step-loadings.
- C. The second (Mark D) 50KSI, 1000°F constant stress test acquired 0.54% strain in 255 minutes and the first (Mark A) 70KSI, 1000°F constant stress test acquired 3.15% strain in 100 minutes. These outcomes sum up to 3.69% strain in 355 minutes by constant stress loadings. This compares with the lesser 2.53% strain acquired in 355 minutes through pulsed step-loading.
- D. The second (Mark D) 50KSI, 1000°F constant stress test acquired 0.54% strain in 255 minutes and the second Mark B 70KSI, 1000°F constant stress test acquired 3.56% strain in 130 minutes. These outcomes sum up to 4.10% strain acquired in 385 minutes by constant stress loadings. This compares with the lesser 2.76% stress obtained in 385 minutes through pulsed step-loading.

Figure 131 compares the several numbers obtained by summing outcomes of constant stress tests and comparing them with outcomes of pulsed step-load tests. The suggested trend lines intimate that constant stress loading induces greater amounts of creep than pulsed step-loading because the strain it produces accumulates more rapidly. These trend lines bring focus on the relaxation effects observed in preceding test studies wherein both a "work-hardening" effect which tended to reflect in increasing amounts of elastic action and in a partition of loading input energy into elastic recovery and permanent set on strain was observed. In view of the unrefined test techniques used together with the high stress levels and temperatures also used to bring focus on phenomenon trends, a need for critical and refined experiment is expressed in the foregoing outcome. This approach bears consideration because, on one hand, evaluations of "material constants" necessary to the practical operation of creep prediction procedures will of necessity need be gathered rapidly under simplified experimental approaches, and, on the other hand, the cyclic nature of aircraft loadings require realistic assessments to permit correlations of "materials evaluation test data" with actualities of material performance under flight service conditions in order to render utility into the prediction schemes.

SUMMARY OF TEST FINDINGS

Those tests which isolated the stress variable for study repeatedly asserted the importance of initial load application in establishing deformation patterns. The deformation attained upon initial load application is comprised of elastic and inelastic or plastic components. The elastic component, within limits, operates under conditions of reversibility whereas the inelastic component does not. The reversible action appears related in extent and perhaps is limited to the elastic limit established by the temperature at which the material is operated. The plastic or irreversible action taking place in initial loading appeared to be somewhat time dependent since loading rates appeared to influence its extent. Beyond the initial loading, the extent of the deformation, which is inelastic in nature, is dependent upon the temperature and stress at which loads are applied for the establishment of the rate of accumulation of irreversible deformation, and, the times for which these rates are allowed to accumulate.

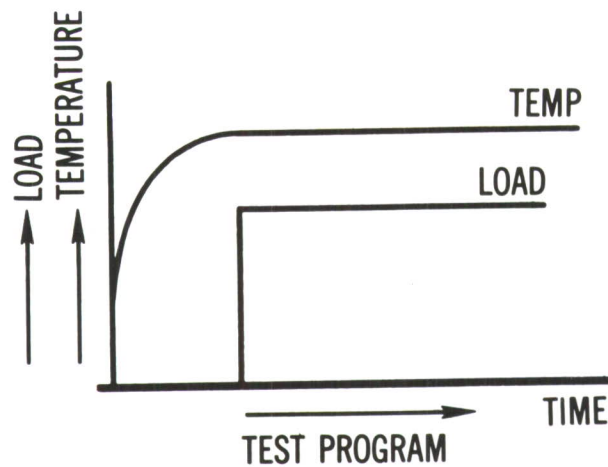
Those tests which isolated the temperature variable for study asserted the complexity of events taking place upon heating to temperatures and a need for understanding of these so that the extent of reversible action taking place could be assessed. The plastic action taking place upon attainment of temperature appeared to be dependent also on the temperature and stress at which loads are applied for establishment of rate of the accumulation of the irreversible deformation, and, the times for which these rates are allowed to accumulate.

The test findings assert need for critical or precise study of (1) the effect of load rate in initial load applications upon the partition of deformation action into elastic and inelastic parts especially with respect to the temperature present and the elastic limit of given materials; (2) the interrelations existing between times and strains appearing with varying stress levels at given temperatures as a result of accumulation of plastic movements; (3) the interrelations existing between times and temperatures required to produce equivalent strains at specific stress levels; and (4) the combining of the cumulative distribution of strain function (step 2) with the exponential growth pattern (step 3) to produce a tool for prediction of inelastic or plastic action increase. This in combination with

considered relations derived from loading rate relations can result in a comprehensive basis for predicting basic material deformation patterns under conditions of elastic and inelastic behavior anticipated with varying loading rates, stress levels of operation, temperature and times of use.

TABLE 40 CONDITIONS OF TEST AND PERTINENT DATA POINT VALUES
FOUND IN "STANDARD" CREEP TESTS

TEMP °F	STRESS KSI	ELASTIC MODULUS PSI x 10 ⁶	ELASTIC STRAIN %	TIME INDEPENDENT PLASTIC STRAIN %	PRIMARY CREEP STRAIN %	ELASTIC RECOVERY %
700	180	25.2	0.714	1.686	0.40	2.05
"	"	"	"	1.966	0.32	2.14
"	182	25.2	0.722	1.638	0.38	1.84
"	"	"	"	1.718	0.30	1.97
800	170	24.5	0.695	2.115	0.57	2.24
"	"	"	"	1.805	0.56	1.90
"	175	"	0.714	2.186	0.68	--
"	"	"	"	1.826	0.56	2.01
900	130	23.6	0.551	1.159	0.27	1.58
"	"	"	"	1.329	0.30	1.73
"	135	"	0.572	1.268	0.33	1.56
"	"	"	"	1.178	0.31	1.58
1000	55	22.5	0.245	0.425	0.34	0.65
"	"	"	"	0.395	0.38	0.63
"	77	"	0.342	0.578	0.38	0.92
"	"	"	"	0.658	0.42	0.86



MATERIAL: ARMCO PH 15-7 MO-RH 950
 TEMPERATURE: 700° F
 LOAD: 180 KSI.

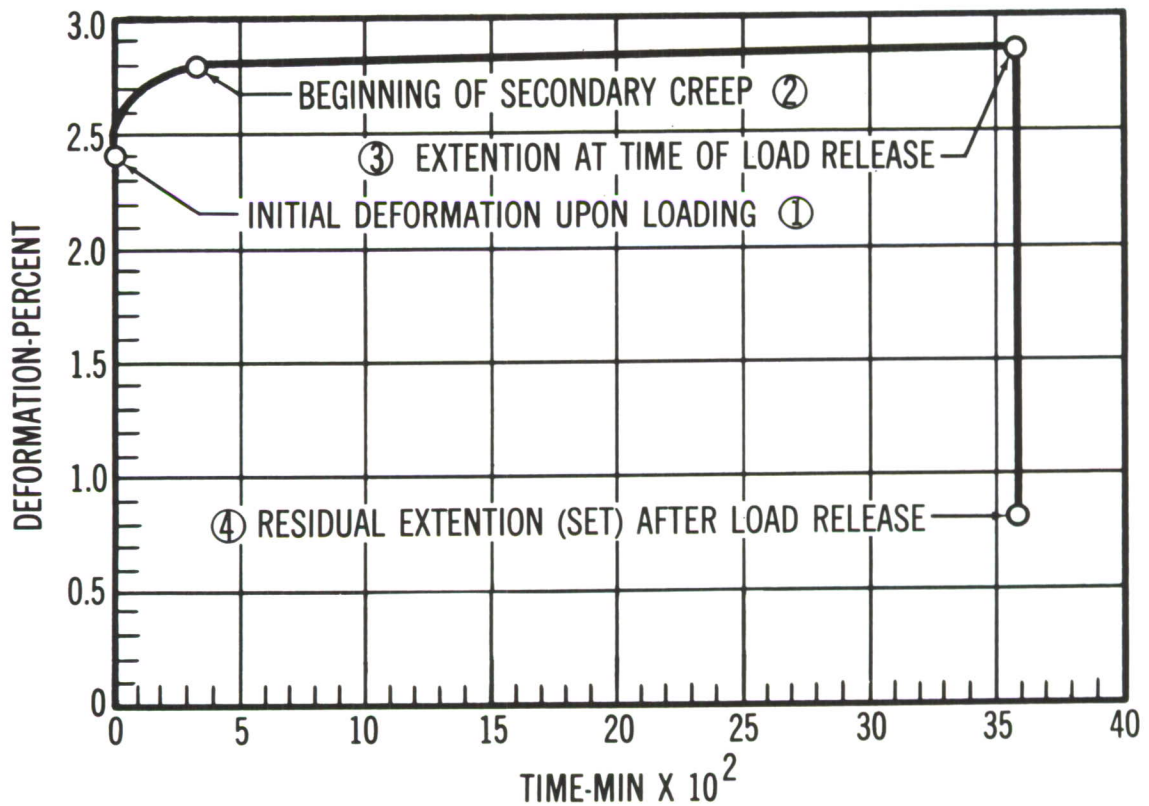


Figure 40. Time-Deformation Data, Armco PH 15-7 Mo 700°F., 180 KSI, "Standard" Creep Test

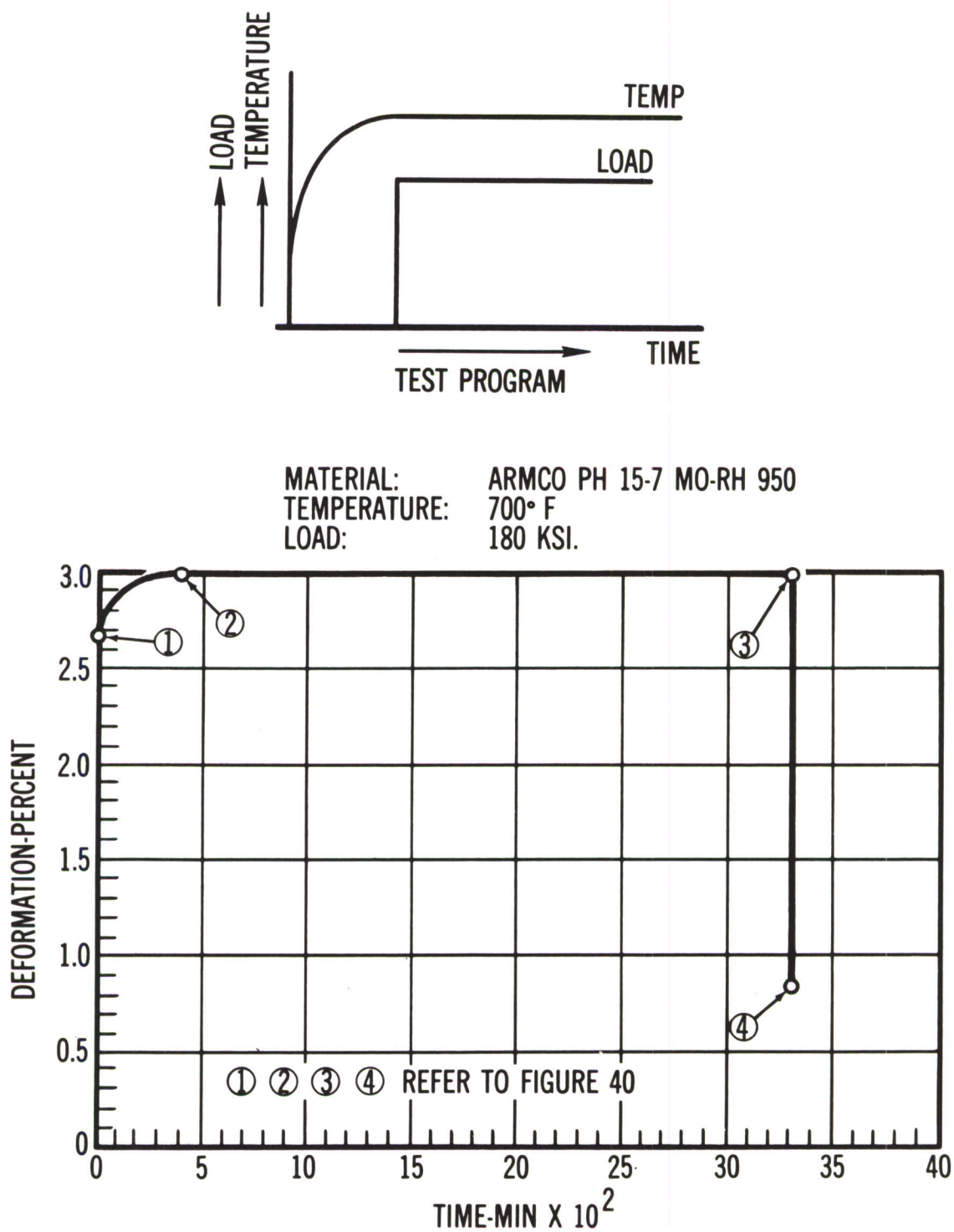


Figure 41. Time-Deformation Data, Armco PH 15-7 Mo 700°F., 180 KSI, "Standard" Creep Test

MATERIAL: ARMCO PH 15-7 MO-RH 950
 TEMPERATURE: 700° F
 LOAD: 182 KSI.

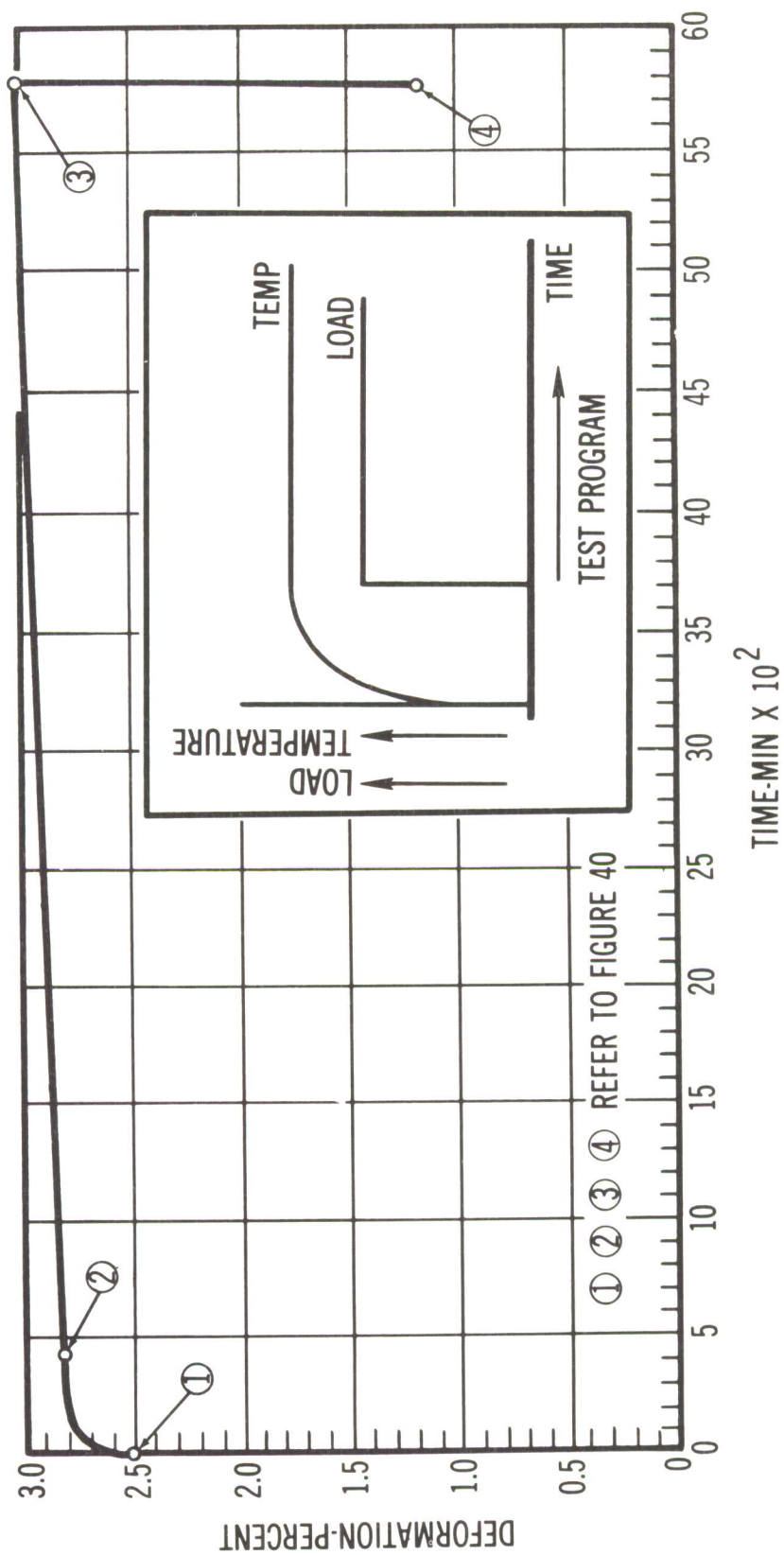
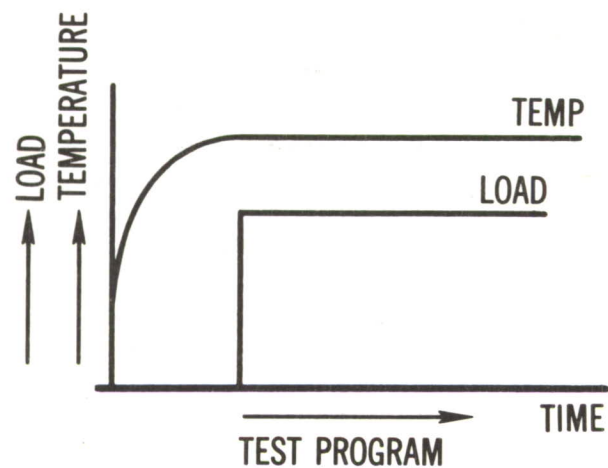


Figure 42. Time-Deformation Data, Armco PH 15-7 Mo 700°F., 182 KSI, "Standard" Creep Test



MATERIAL: ARMCO PH 15-7 MO-RH 950
 TEMPERATURE: 700° F
 LOAD: 182 KSI.

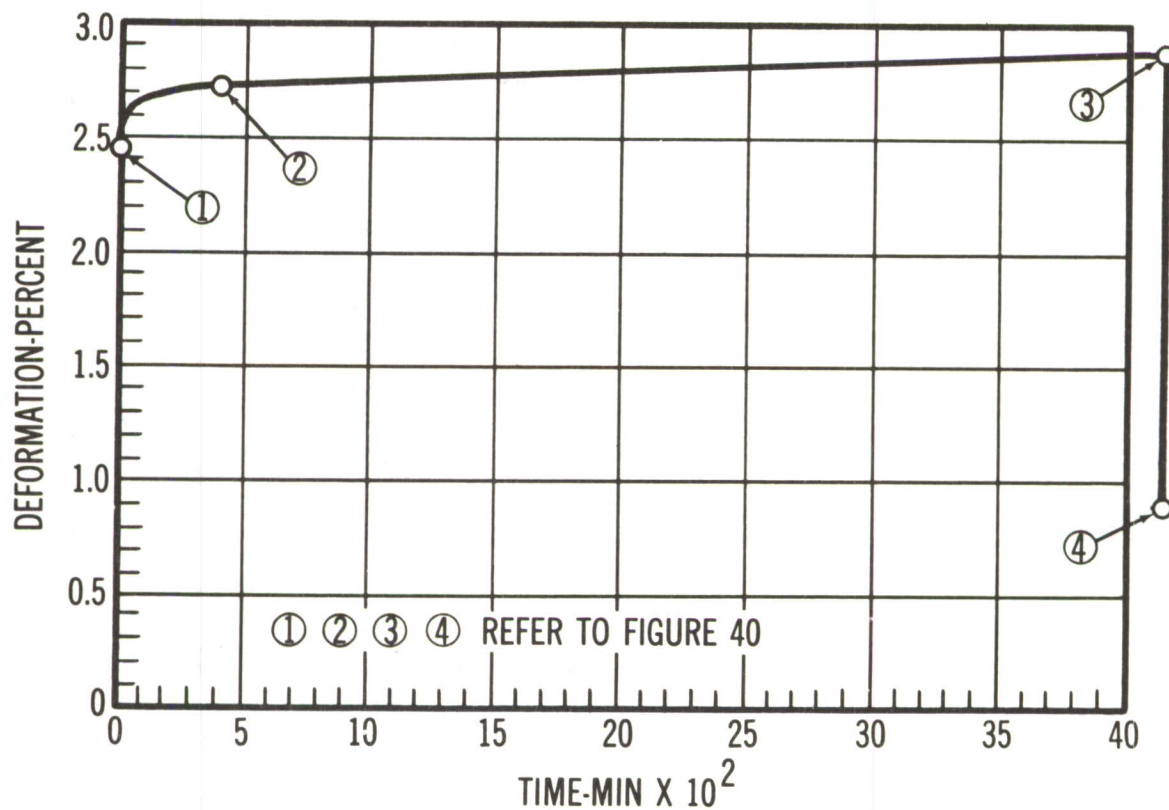


Figure 43. Time-Deformation Data, Armco PH 15-7 Mo 700°F.,
 182 KSI, "Standard" Creep Test

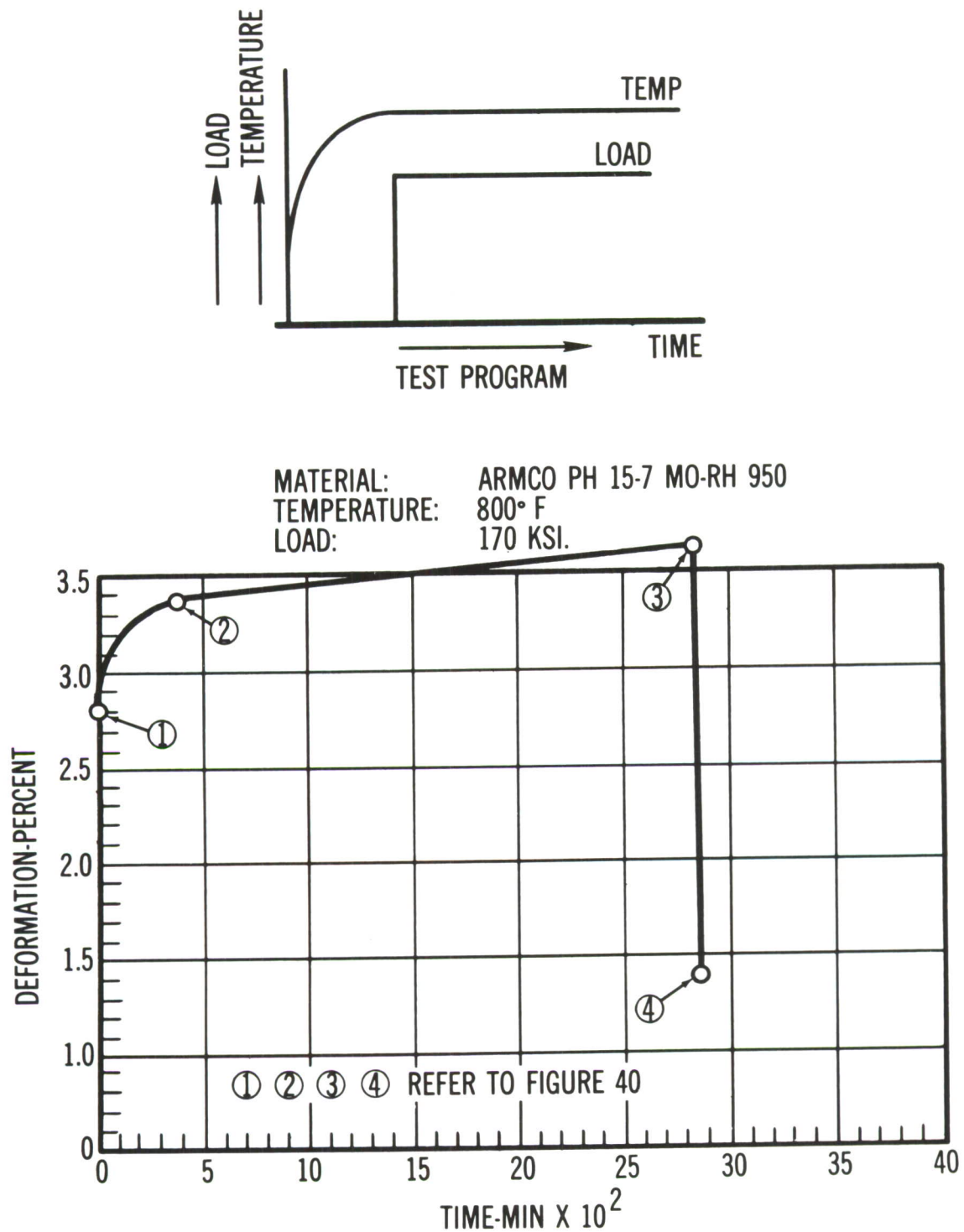


Figure 44. Time-Deformation Data, Armco PH 15-7 Mo 800°F., 170 KSI, "Standard" Creep Test

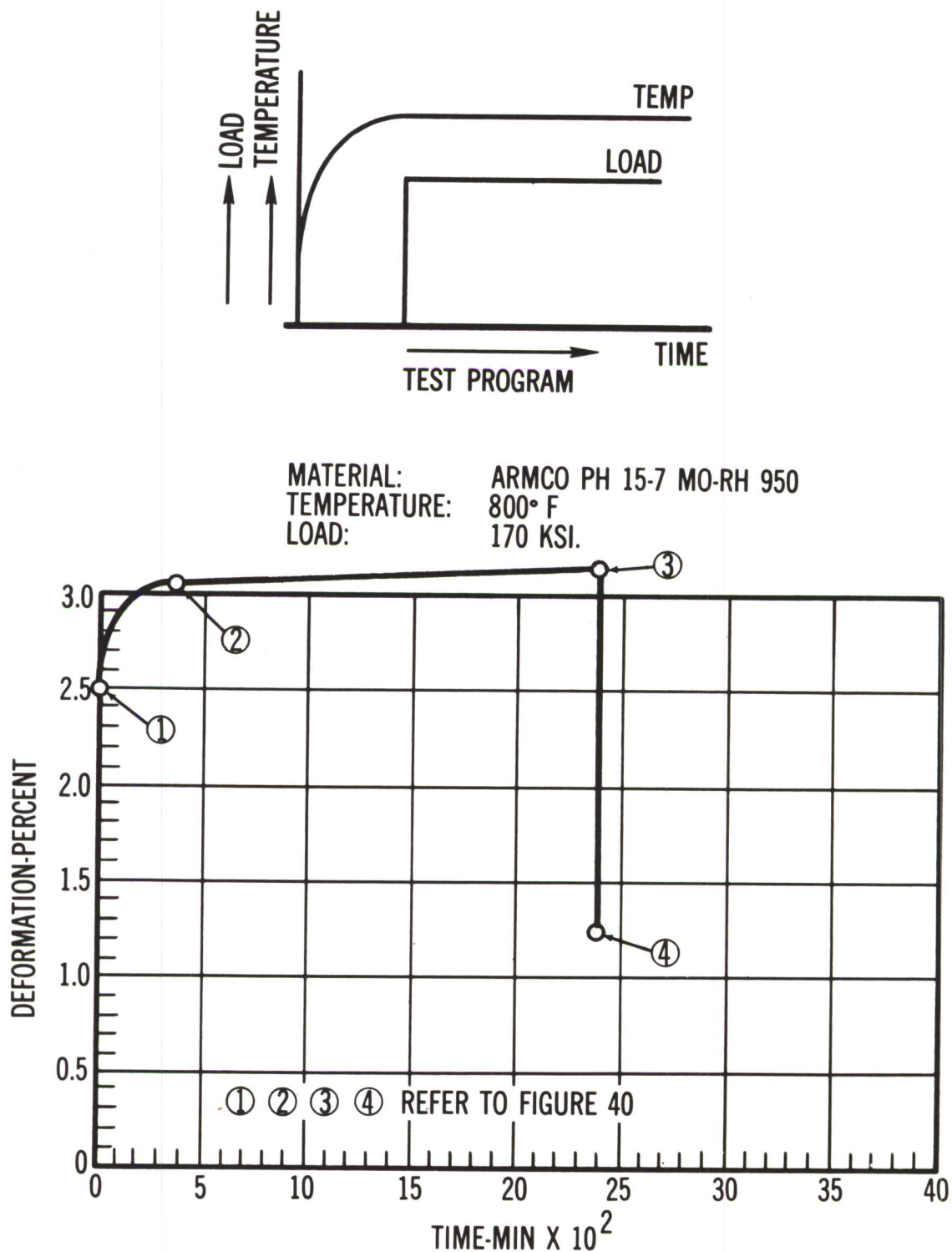


Figure 45. Time-Deformation Data, Armco Ph 15-7 Mp 800°F., 170 KSI, "Standard" Creep Test

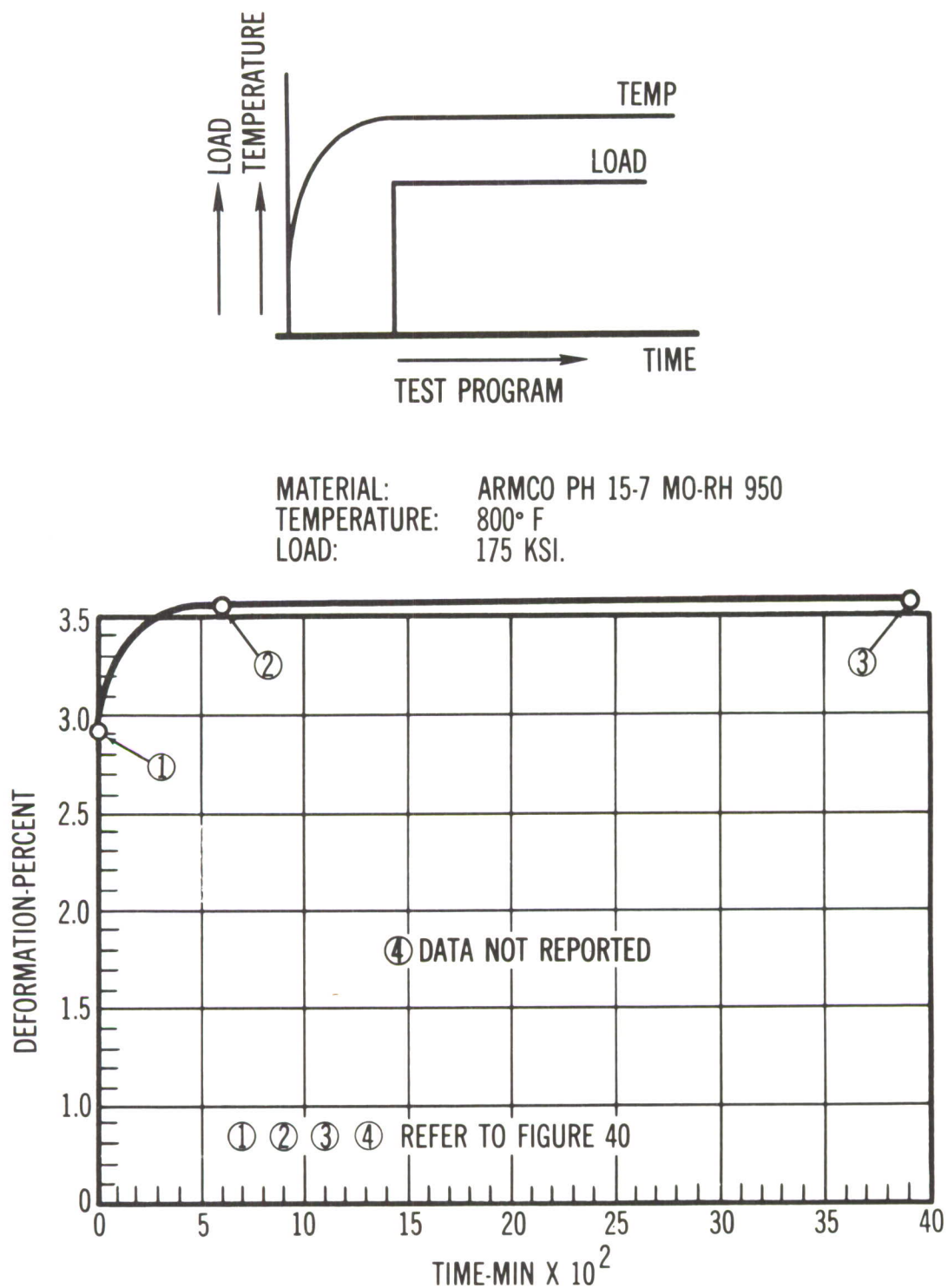
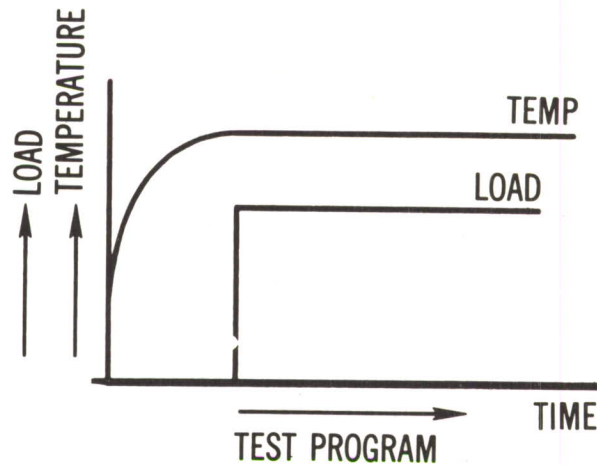


Figure 46. Time-Deformation Data, Armco PH 15-7 Mo 800°F., 175 KSI, "Standard" Creep Test



MATERIAL: ARMCO PH 15-7 MO-RH 950
 TEMPERATURE: 800° F
 LOAD: 175 KSI.

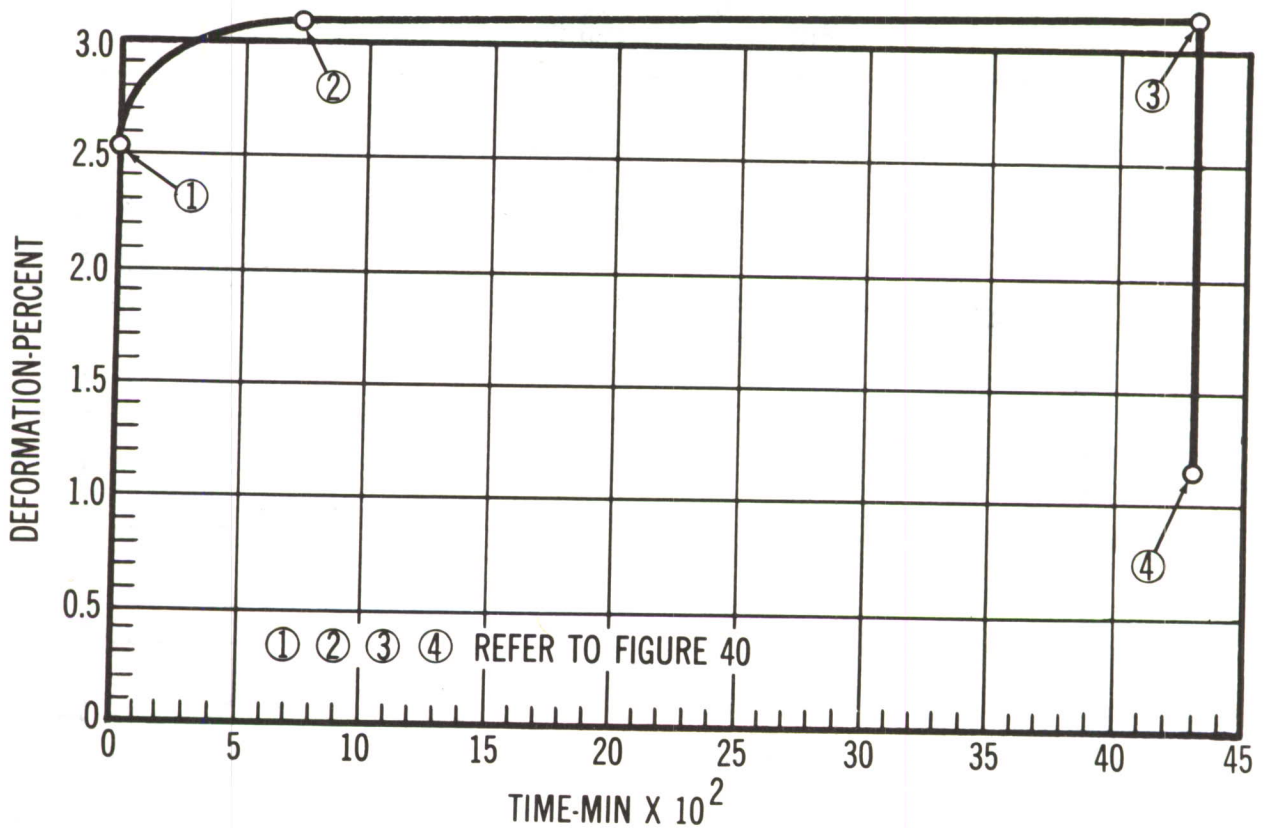
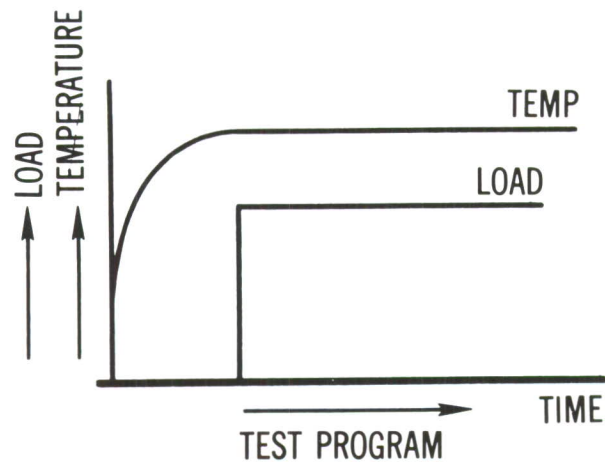


Figure 47. Time-Deformation Data, Armco PH 15-7 Mo 800°F., 175 KSI, "Standard" Creep Test



MATERIAL: ARMCO PH 15-7 MO-RH 950
 TEMPERATURE: 900° F
 LOAD: 130 KSI.

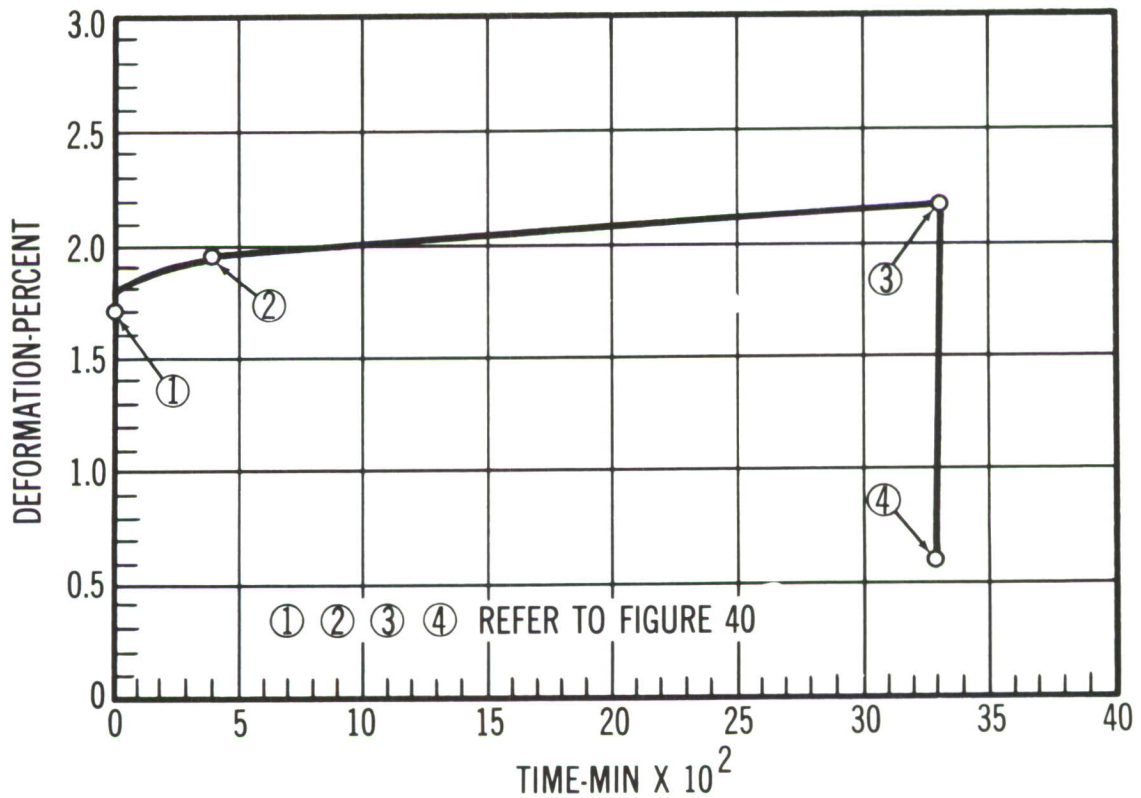


Figure 48. Time-Deformation Data, Armco PH 15-7 Mo 900°F., 130 KSI, "Standard" Creep Test

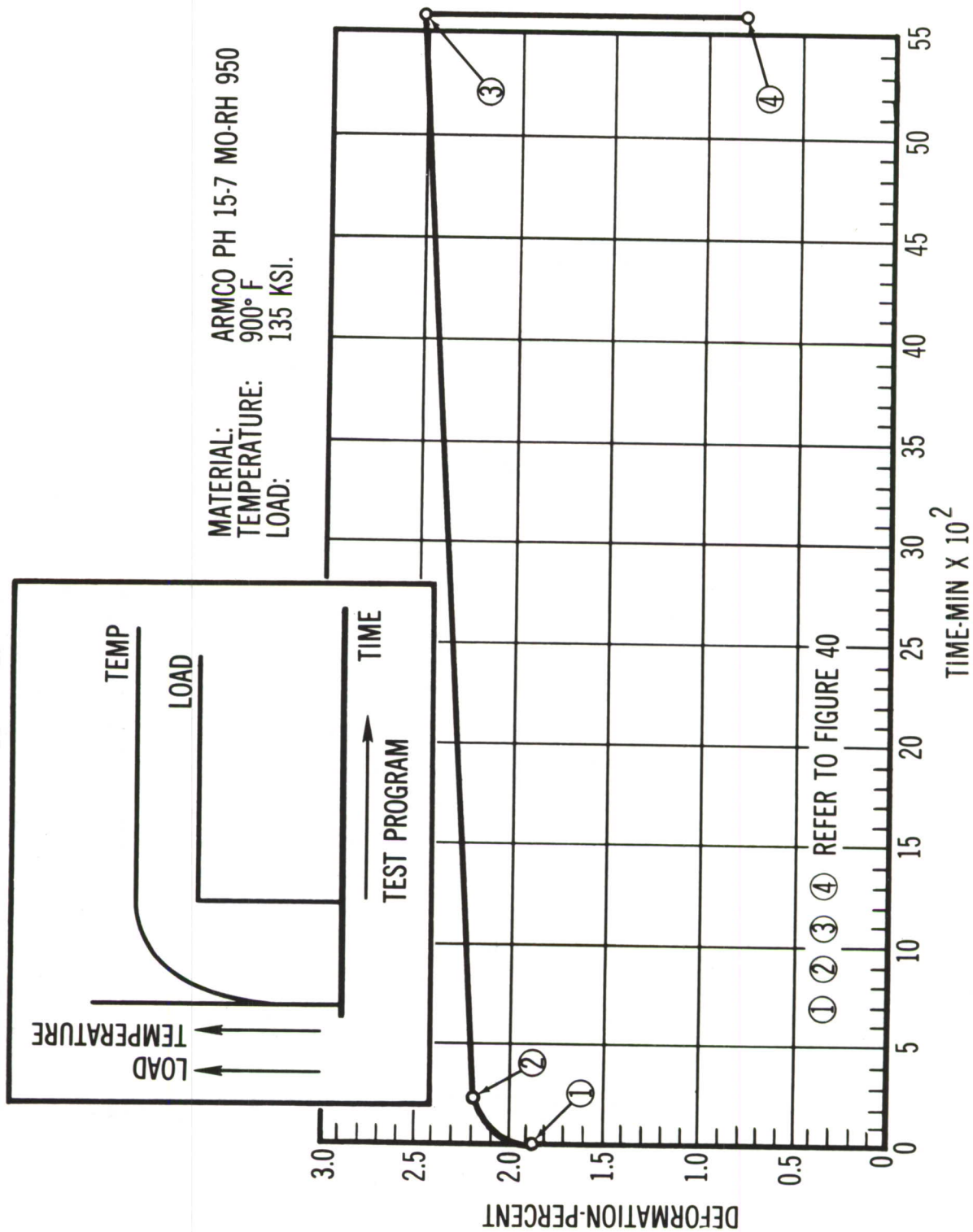


Figure 49. Time-Deformation Data, Armco PH 15-7 Mo 900°F., 130 KSI, "Standard" Creep Test

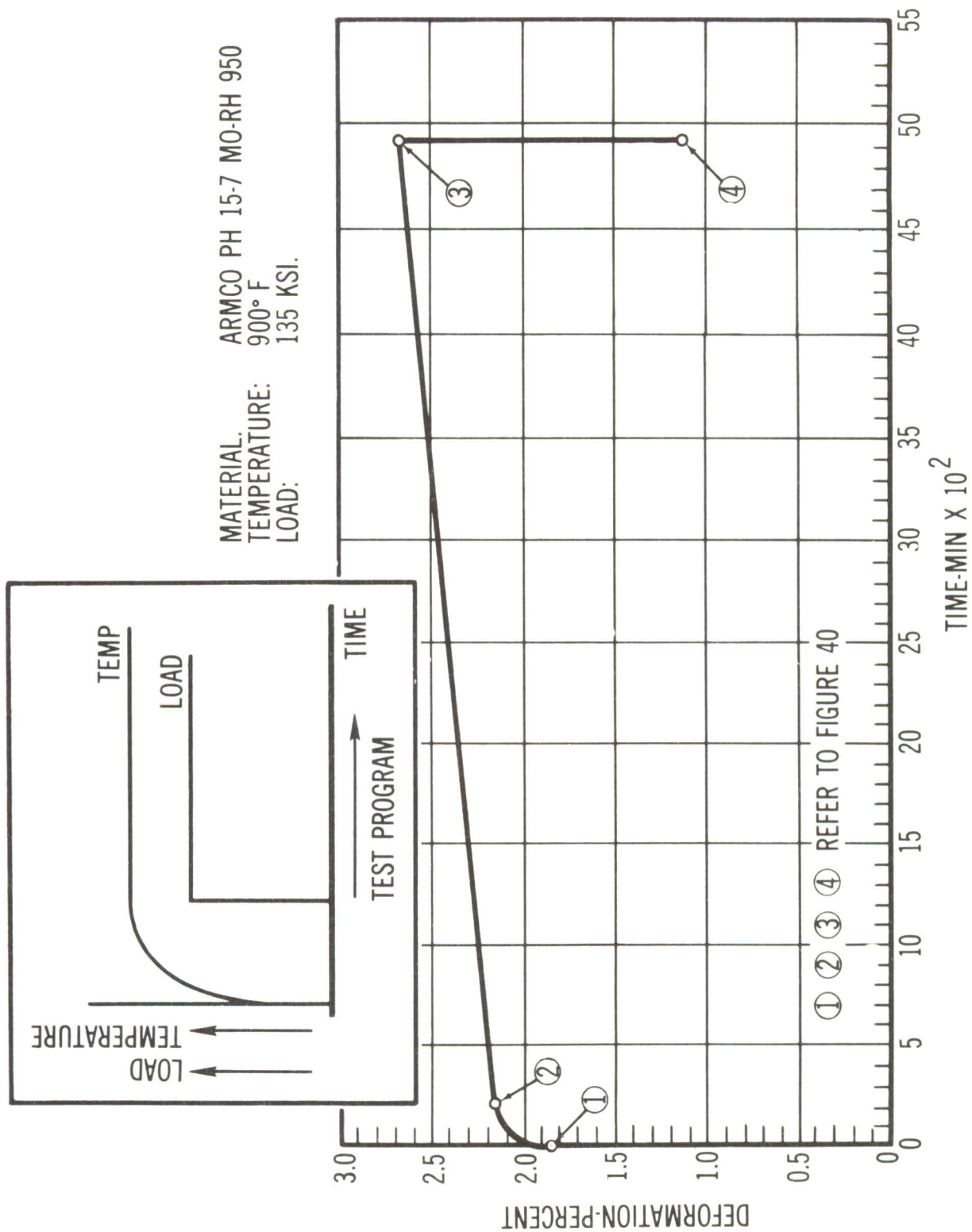


Figure 50. Time-Deformation Data, Armco PH 15-7 Mo 900°F., 135 KSI, "Standard" Creep Test

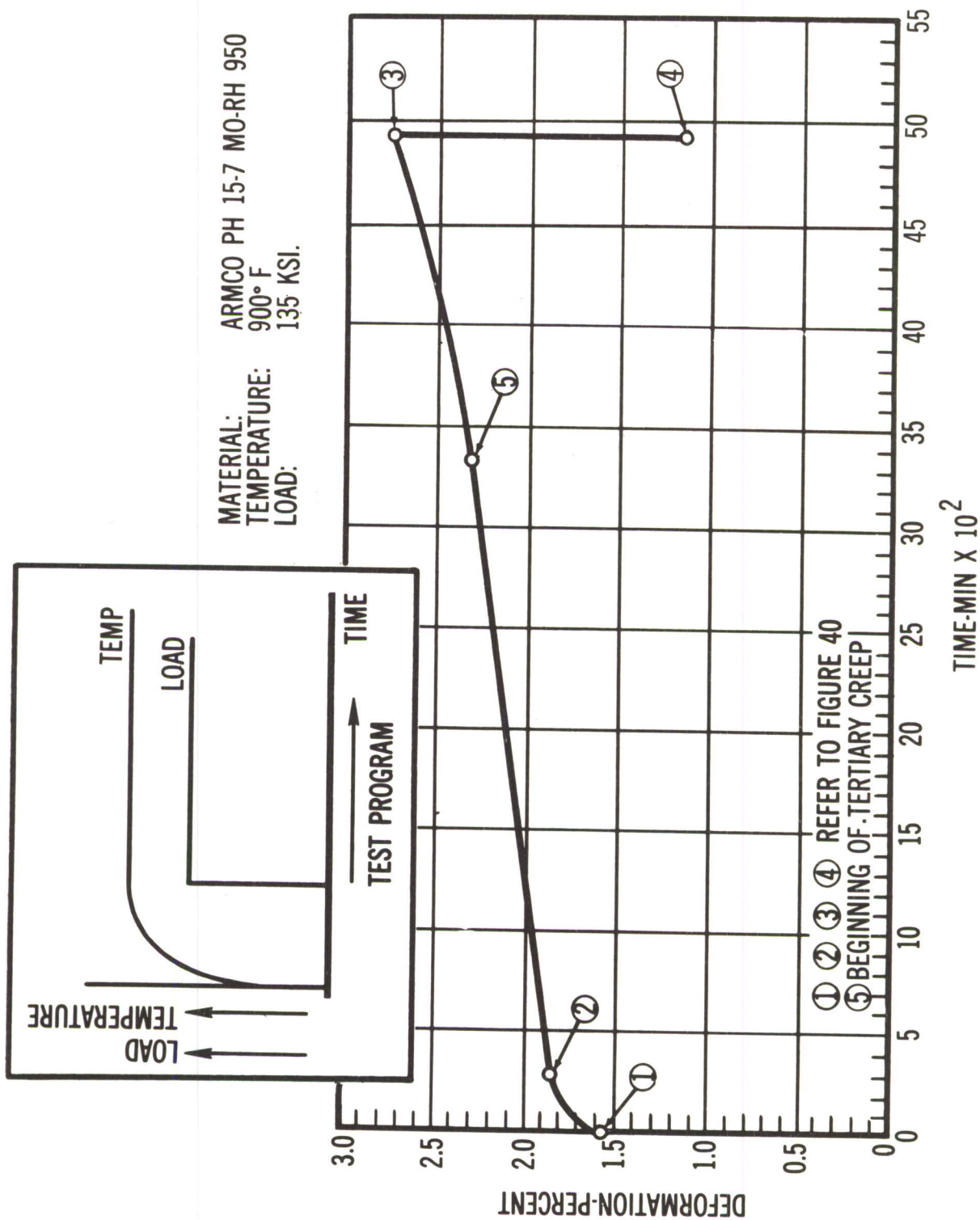
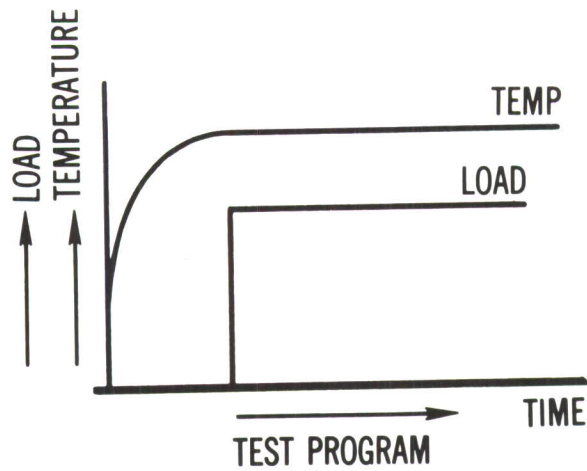


Figure 5L. Time-Deformation Data, Armco PH 15-7 Mo 900°F., 135 KSI, "Standard" Creep Test



MATERIAL: ARMCO PH 15-7 MO-RH 950
 TEMPERATURE: 1000° F
 LOAD: 55 KSI.

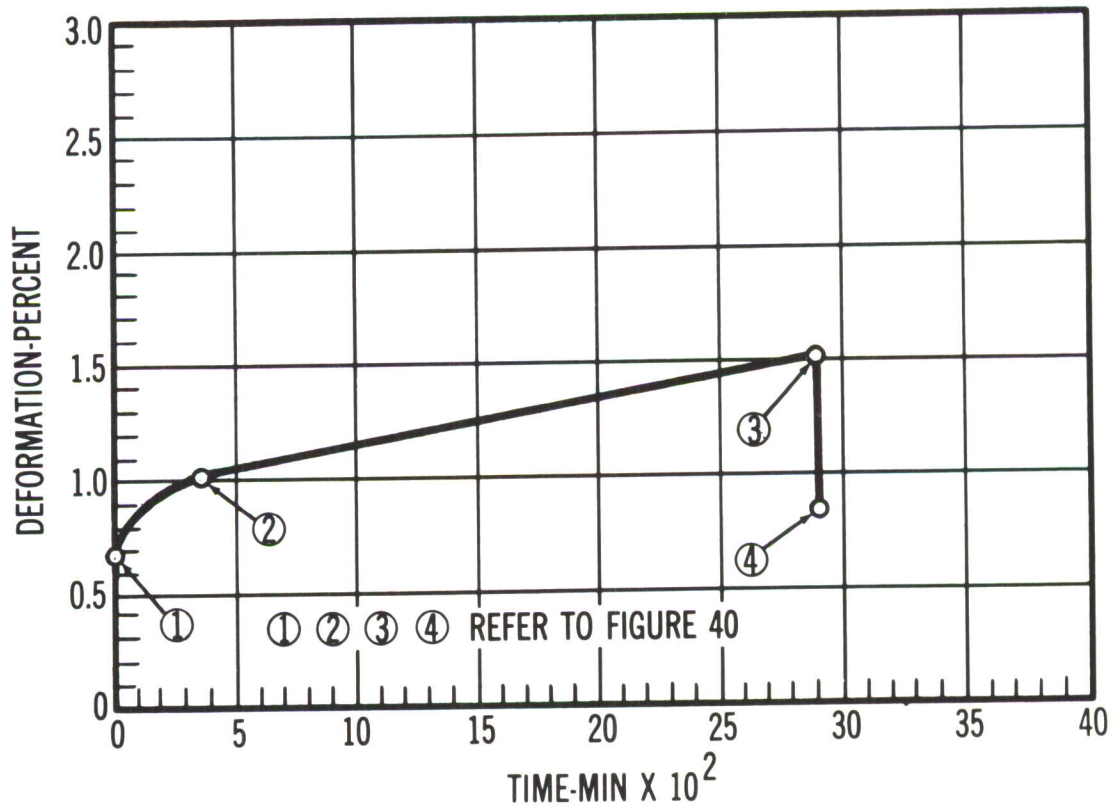


Figure 52. Time-Deformation Data, Armco PH 15-7 Mo 1000° F., 55 KSI "Standard" Creep Test

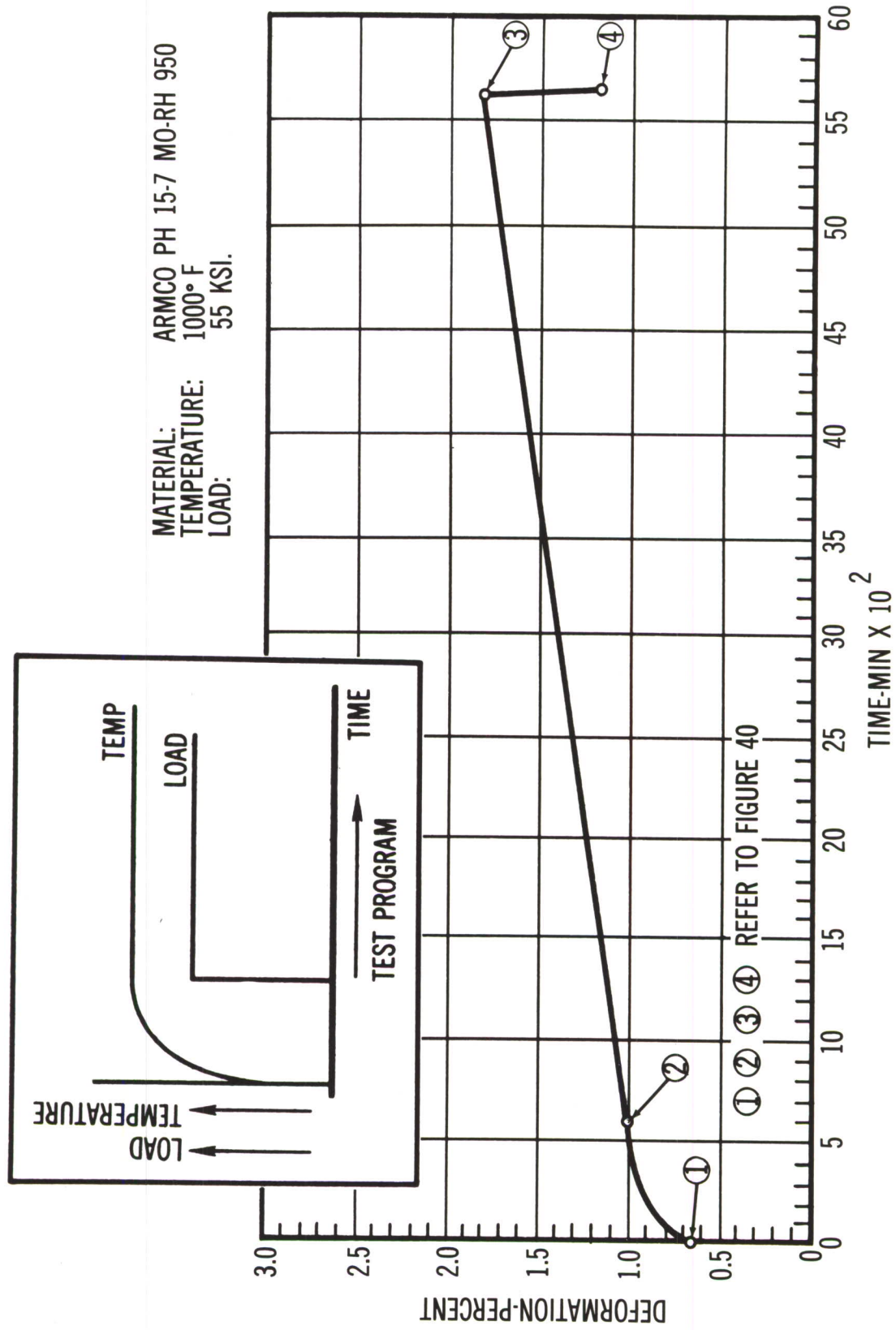


Figure 53. Time-Deformation Data, Armco PH 15-7 Mo 1000°F., 55 KSI, "Standard" Creep Test

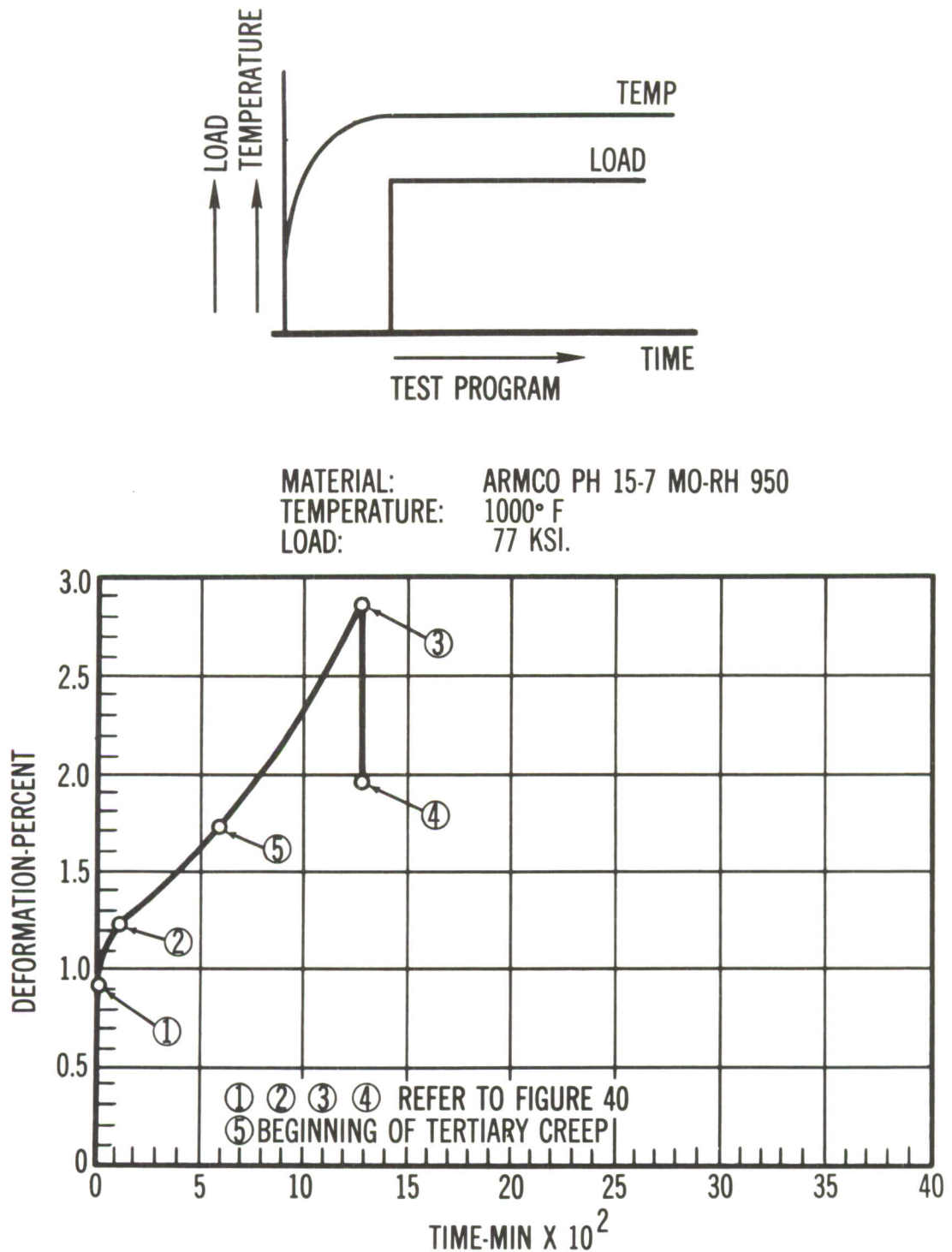
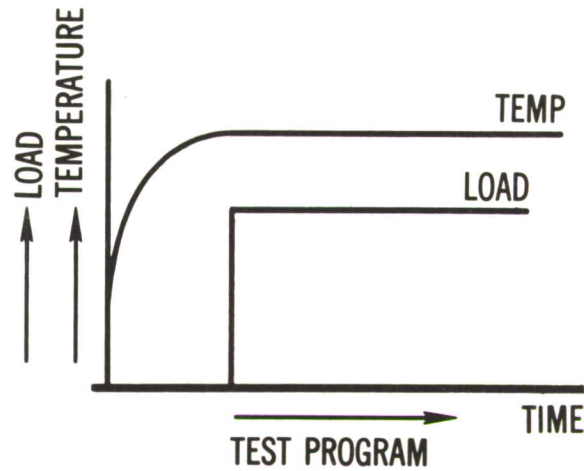


Figure 54. Time-Deformation Data, Armco PH 15-7 Mo 1000° F., 77 KSI "Standard" Creep Test



MATERIAL: ARMCO PH 15-7 MO-RH 950
 TEMPERATURE: 1000° F
 LOAD: 77 KSI.

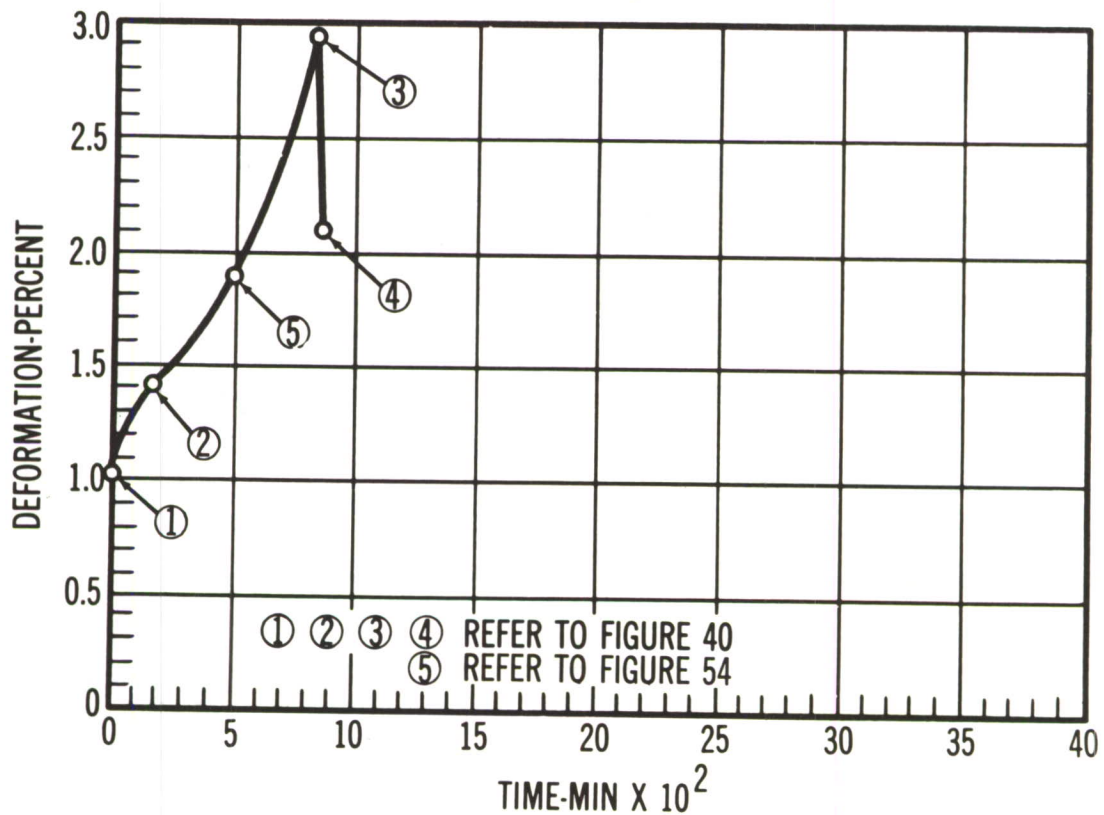


Figure 55. Time-Deformation Data, Armco PH 15-7 Mo 1000° F., 77 KSI "Standard" Creep Test

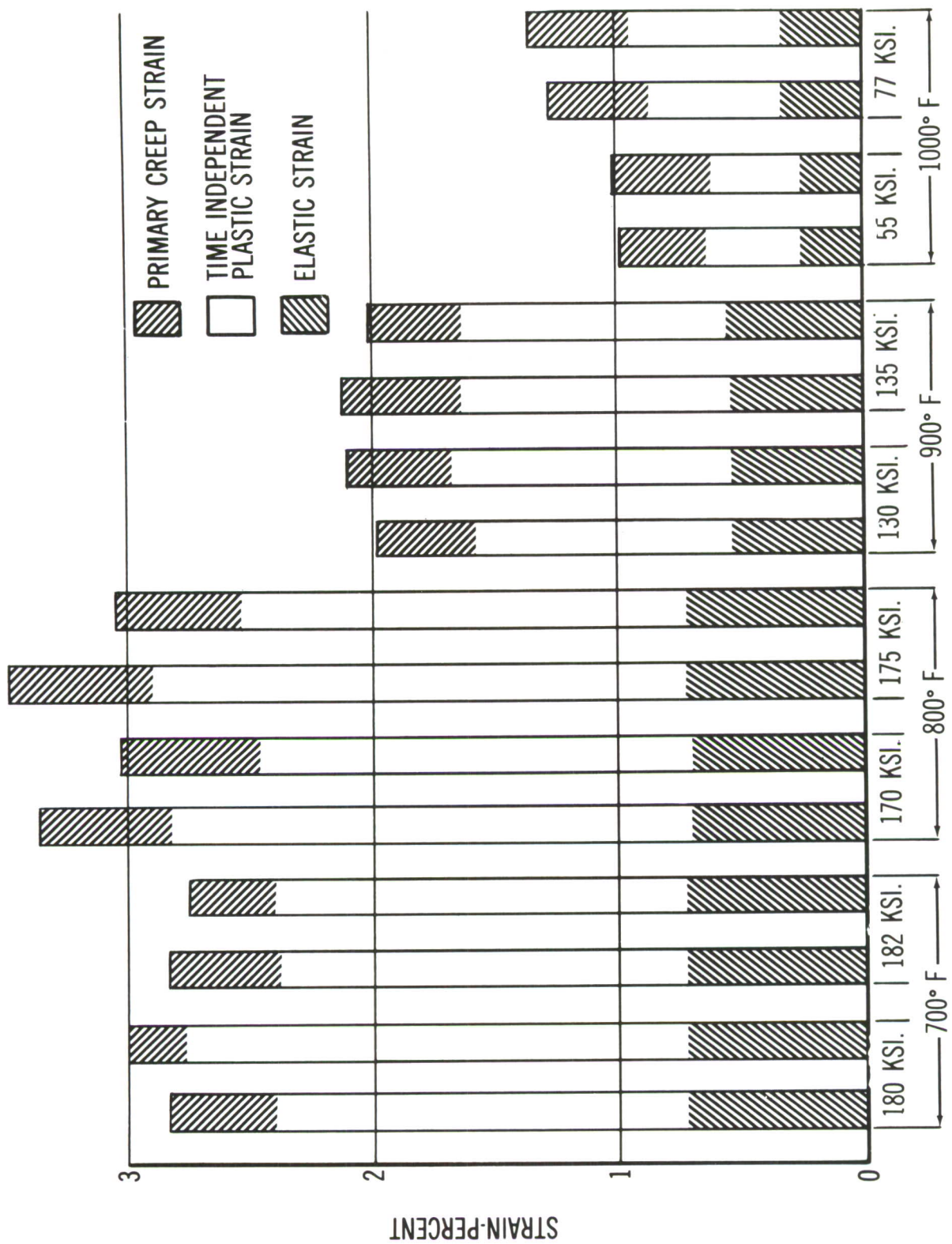
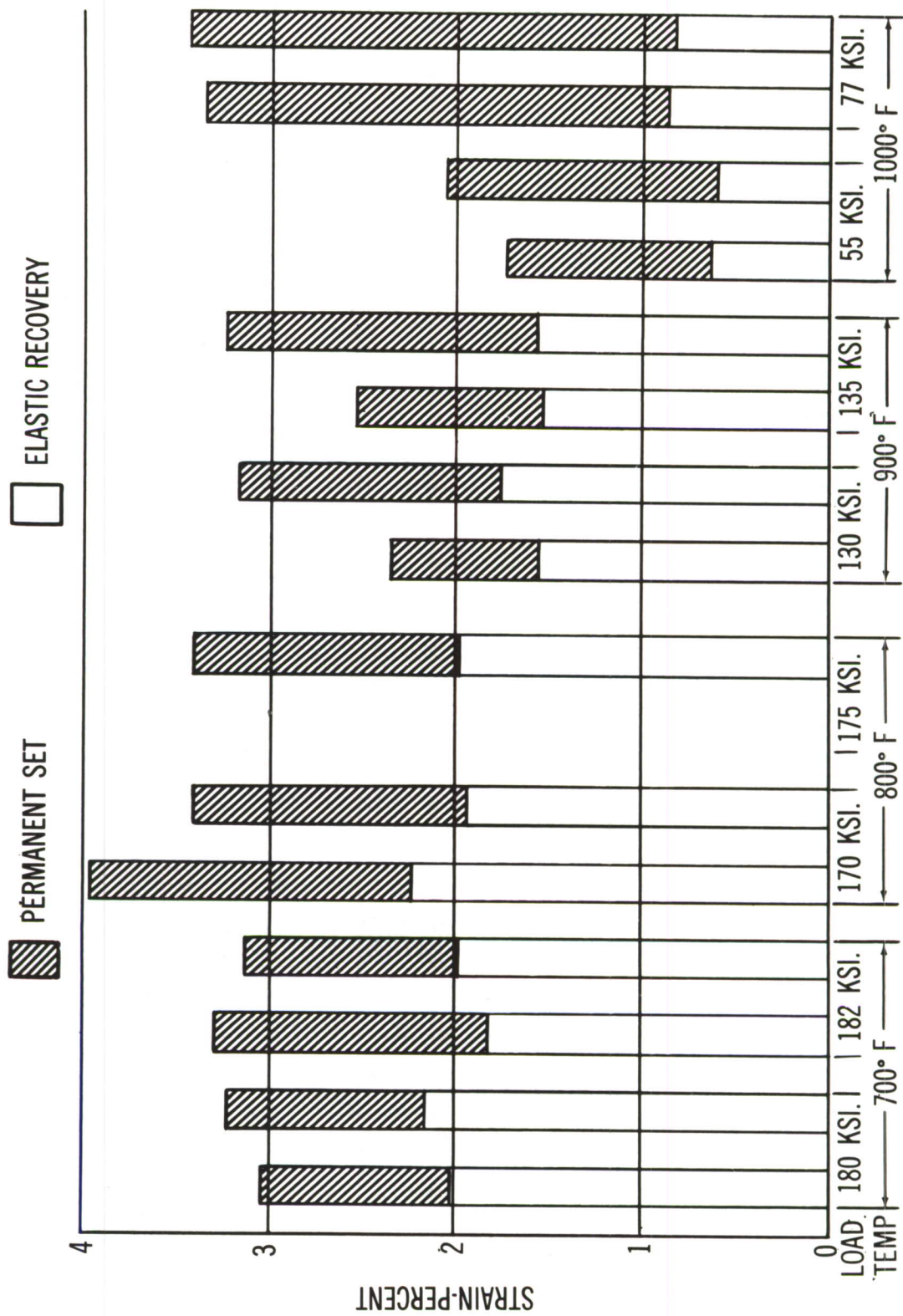


Figure 56. "Make-up" of Loading Strains in "Standard" Creep Tests with Armco PH 15-7 Mo.



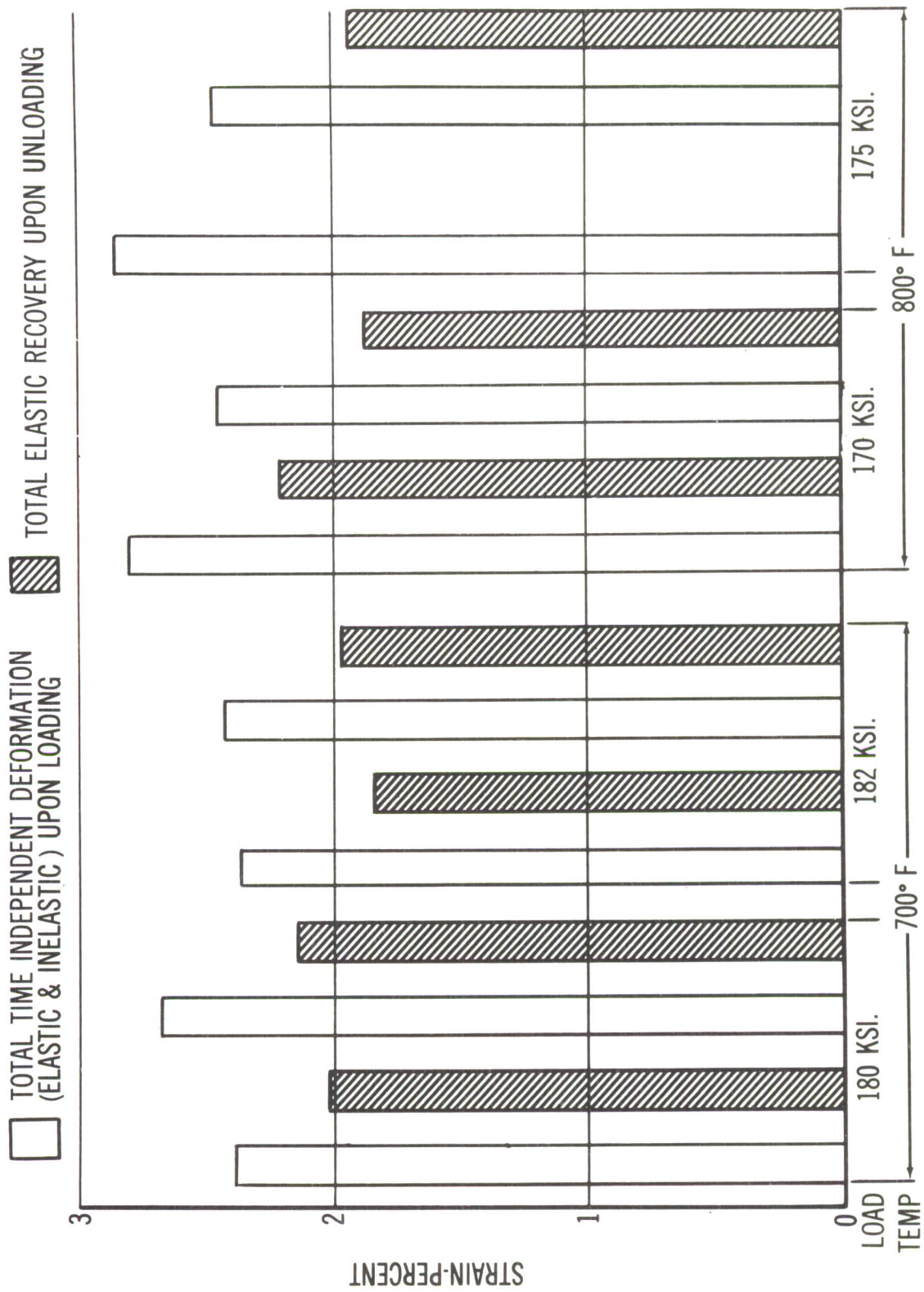


Figure 58. Comparison of Time Independent Strains Observed upon Loading and Unloading "Standard" Creep Tests with Armco PH 15-7 Mo at 700°F and 800°F.

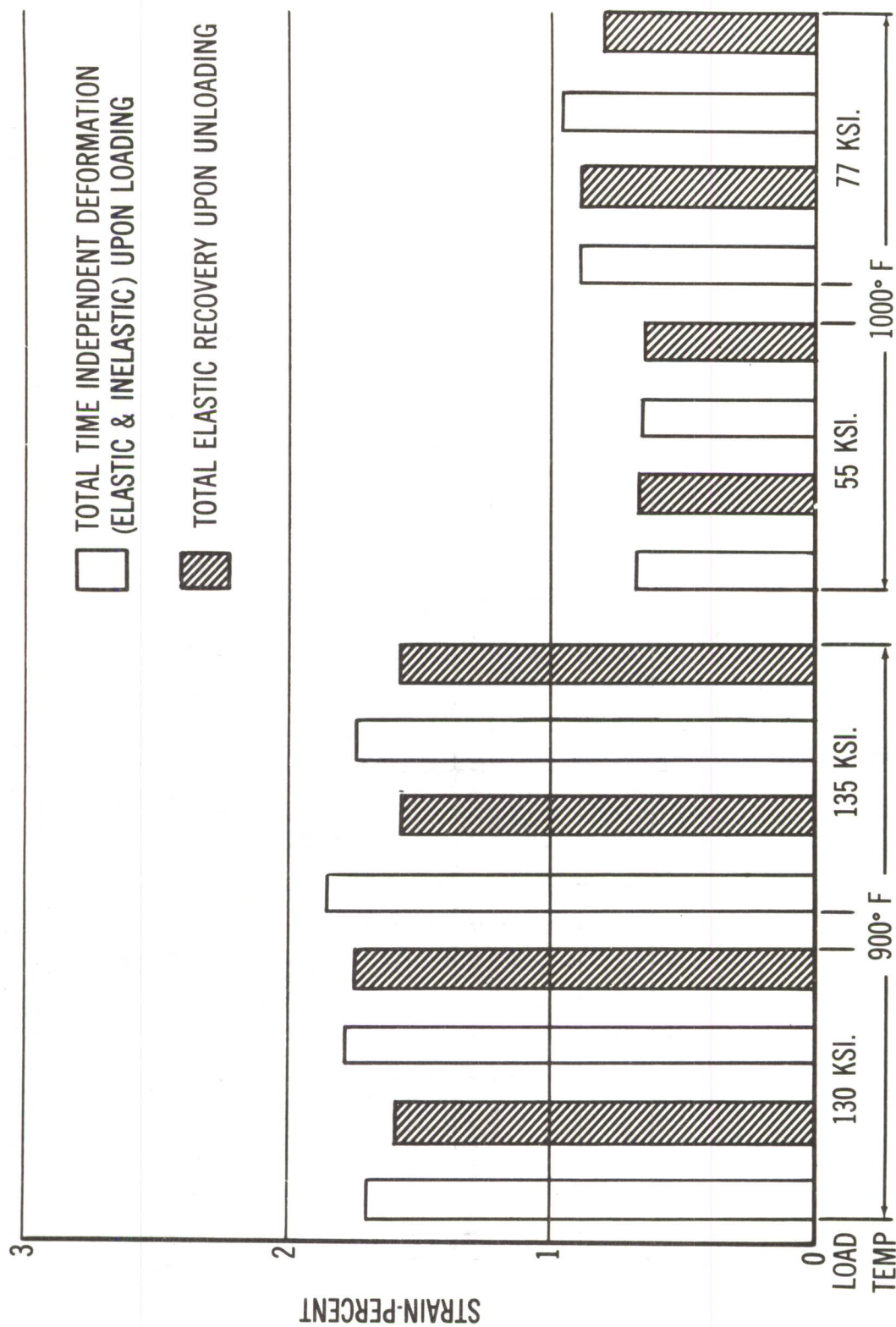


Figure 59. Comparison of Time Independent Strains Observed upon Loading and Unloading "Standard" Creep Tests with Armco PH 15-7 Mo at 900°F and 1000°F.

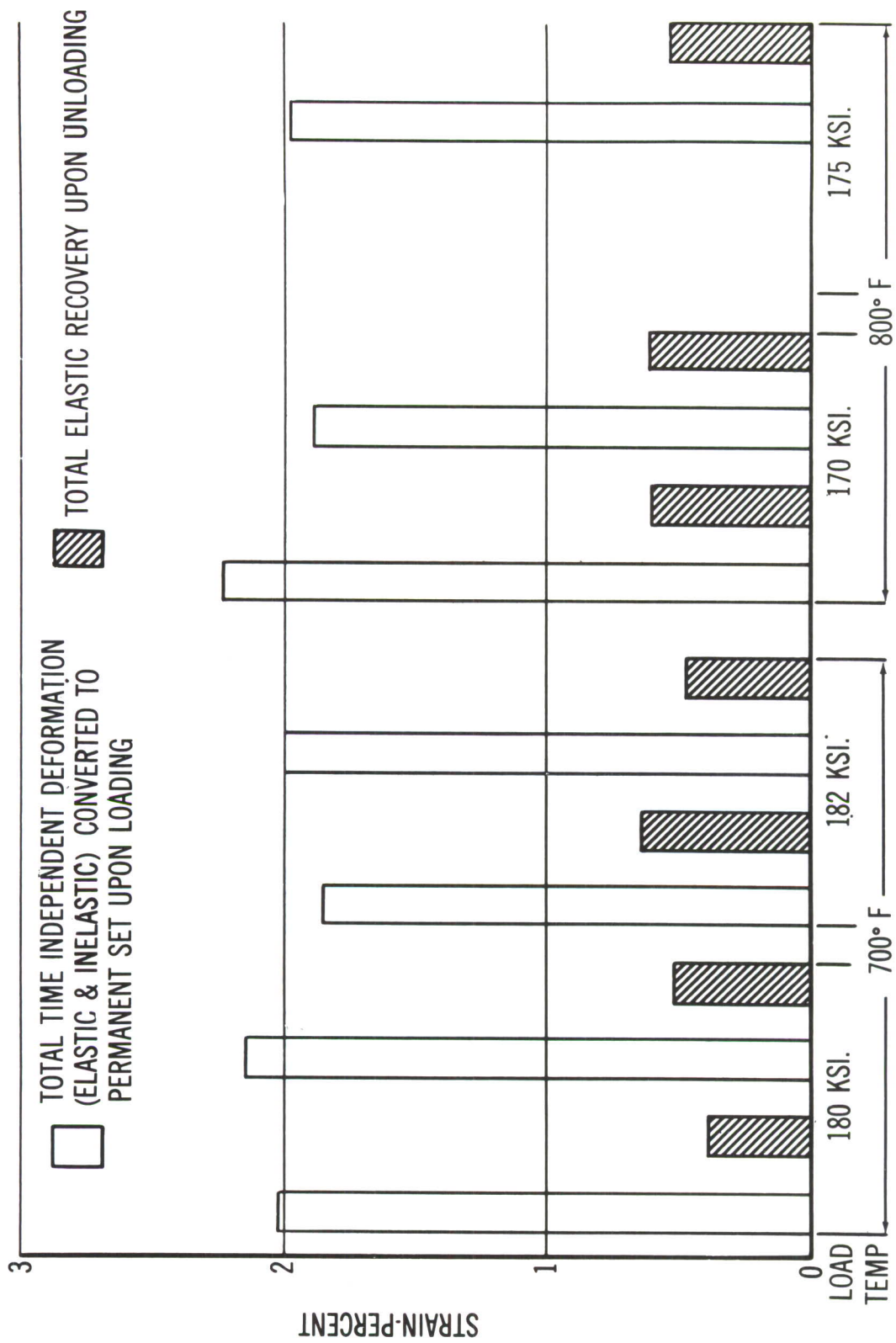


Figure 60. Comparison of Total Elastic Recovery Observed upon Unloading "Standard" Creep Tests with Armco PH 15-7 Mo at 700°F and 800°F with the Input Strain Converted into Permanent Set upon Loading

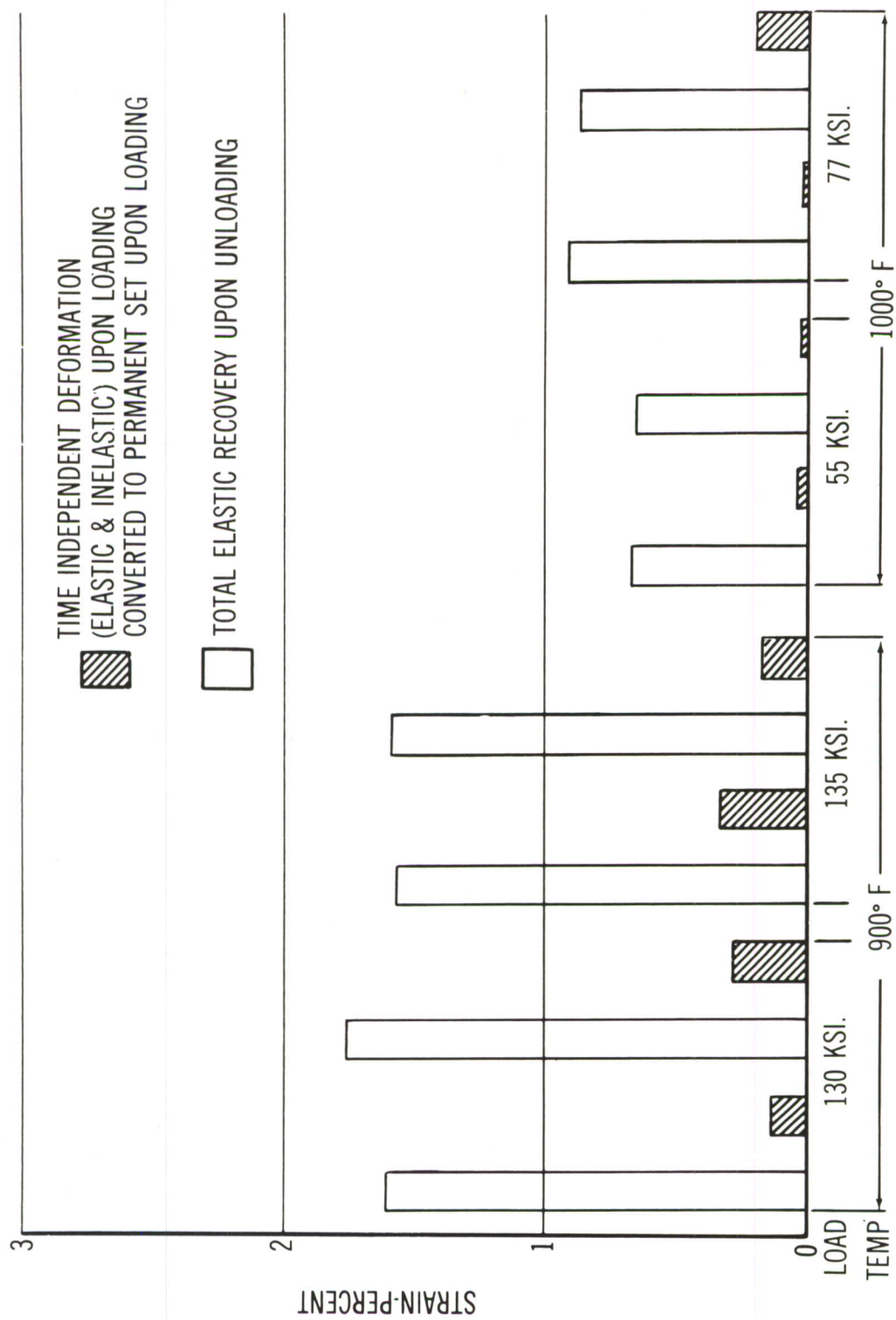


Figure 6L. Comparison of Total Elastic Recovery Observed upon Unloading "Standard" Creep Tests with Armco PH 15-7 Mo at 900°F and 1000°F with the Input Strain Converted into Permanent Set upon Loading

TEMPERATURE-700° F
FULL LOAD STRESS-185 KSI.

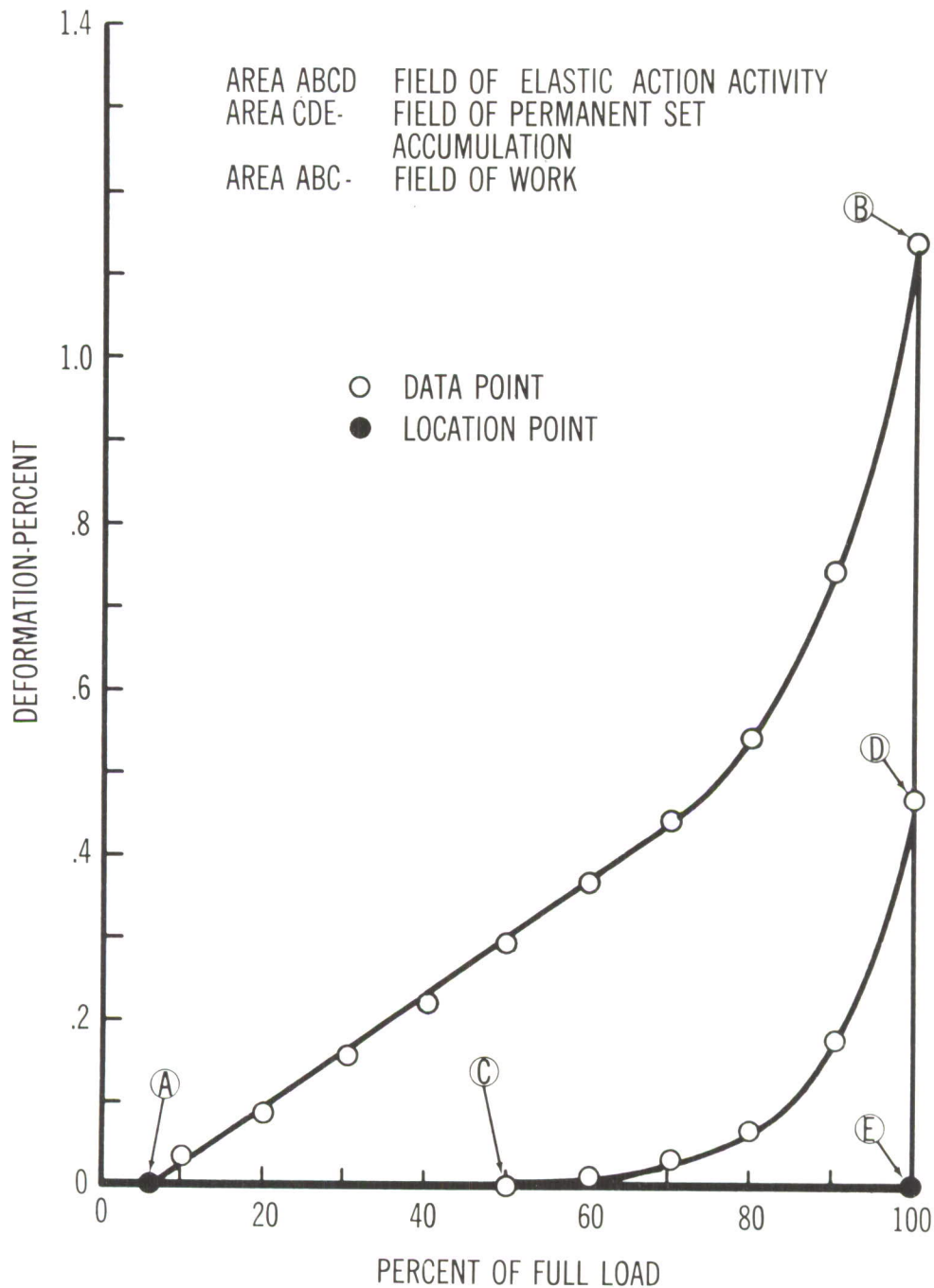


Figure 62. Typical Field of Deformation Activity Observed upon Incremental Step Loading Armco PH 15-7 Mo at Elevated Temperature

TEMPERATURE-700° F
FULL LOAD STRESS-185 KSI.

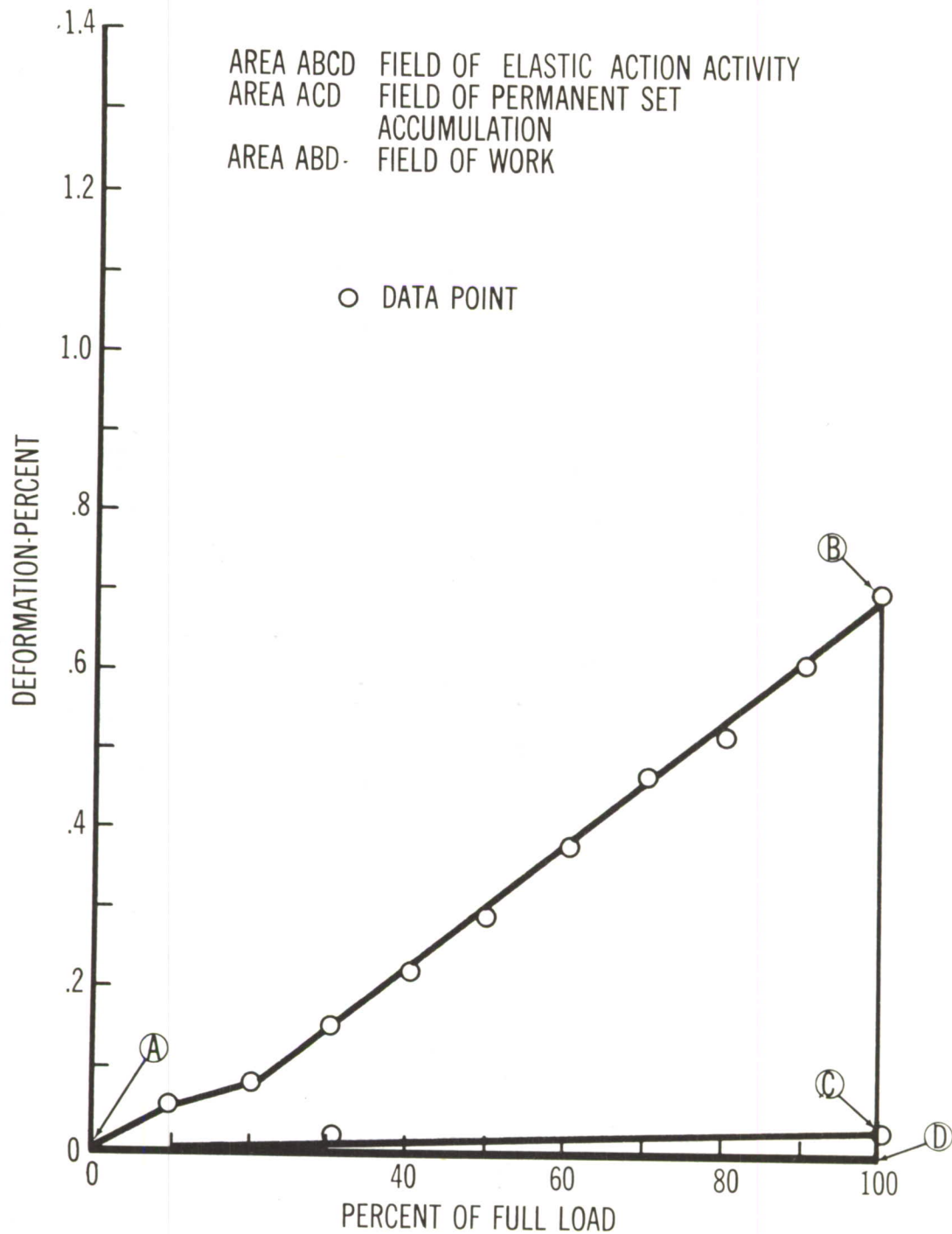
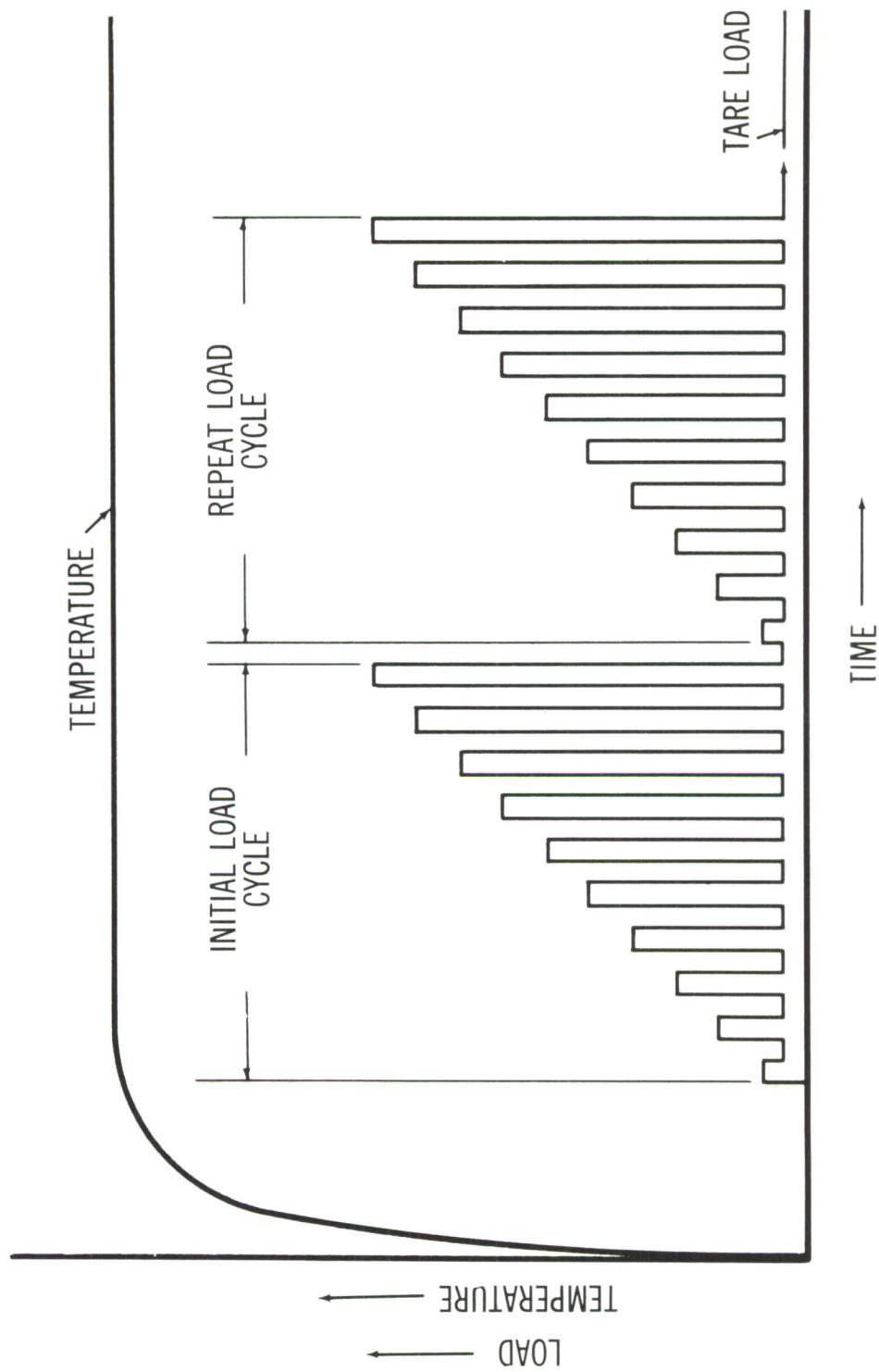


Figure 63. Typical Field of Deformation Activity Observed upon Unloading Incremental Step Loaded Armco PH 15-7 Mo at Elevated temperatures



CONDITION OF TEST: CONSTANT TEMPERATURE AND INTERRUPTED INCREMENTAL TRANSIENT LOAD CYCLE SEQUENCE.

Figure 64. Program for Incremental Step Loaded Test (Schematic)

MATERIAL: ARMCO PH 15-7 MO. COND. RH 950
 TEMPERATURE: 700° F
 FULL LOAD: 185 KSI.
 ○ -LOAD POINT
 □ -LOAD RELEASE POINT

DEFORMATION OCCURRING UPON LOADING

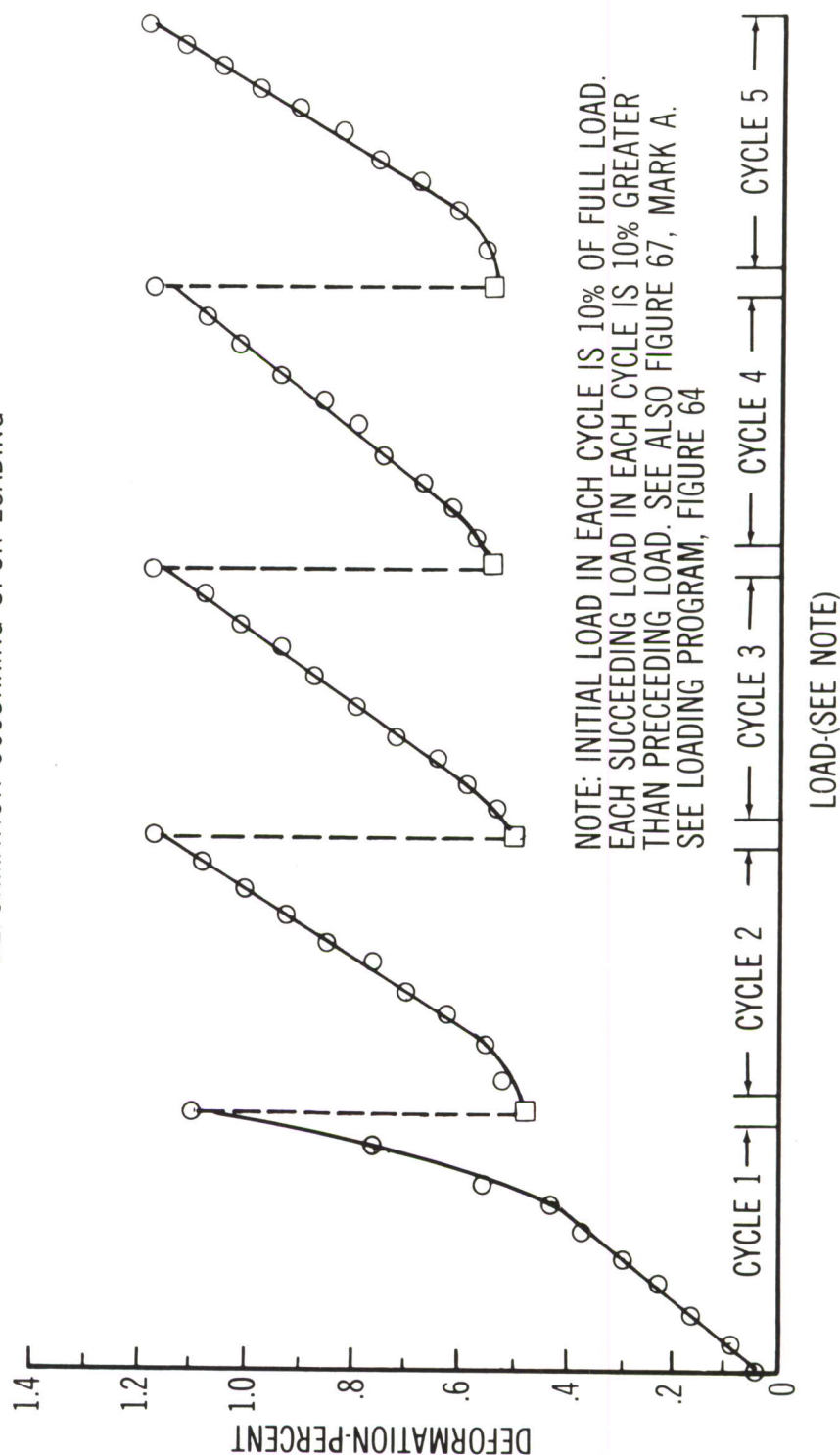


Figure 65. Time-Deformation Data, Armco PH 15-7 Mo 700° F., 185 KSI Incremental Step Loading.
 (Loading Condition)

MATERIAL: ARMCO PH 15-7 MO. COND. RH 950
 TEMPERATURE: 700°F
 FULL LOAD: 185 KSI.
 ○ LOAD POINT
 □ LOAD RELEASE POINT

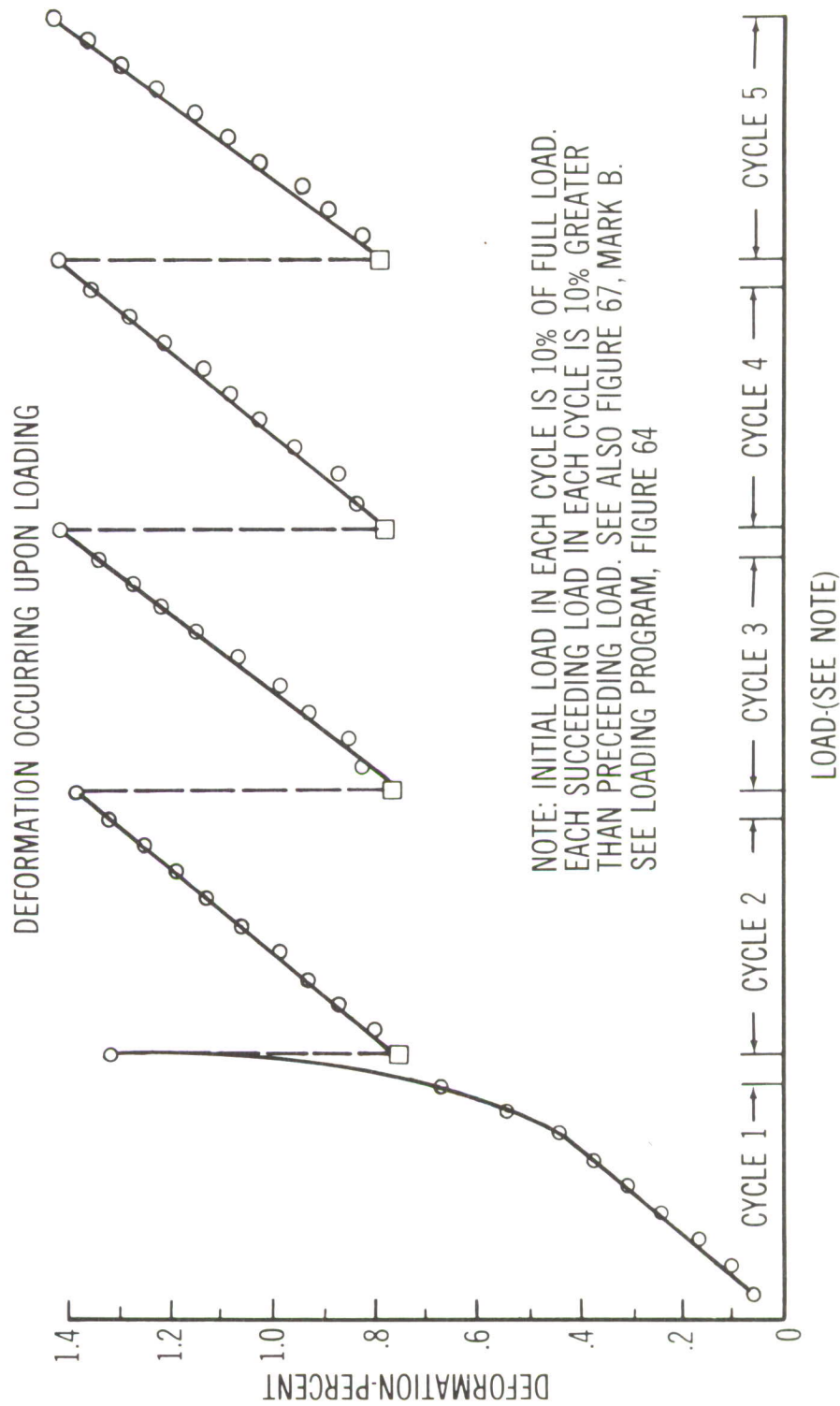


Figure 66. Time Deformation Data, Armco PH 15-7 Mo 700°F., 185 KSI, Incremental Step Loading (Loading Condition)

MATERIAL: ARMCO PH 15-7 MO. COND. RH 950 FULL LOAD: 185 KSI.
 TEMPERATURE: 700° F

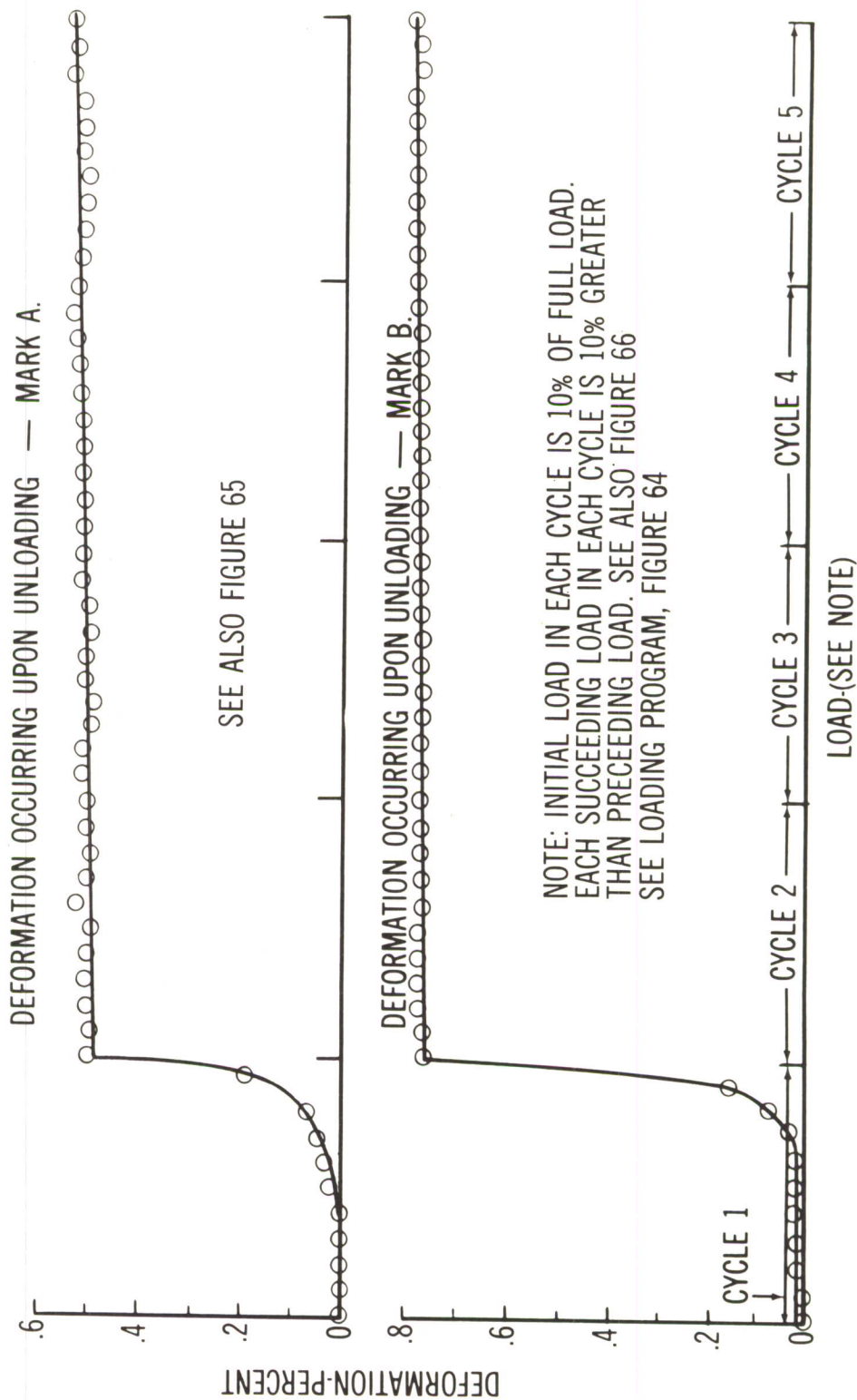


Figure 67. Time Deformation Data, Armco PH 15-7 Mo 700°F., 185 KSI. Incremental Step Loading (Unloading Condition)

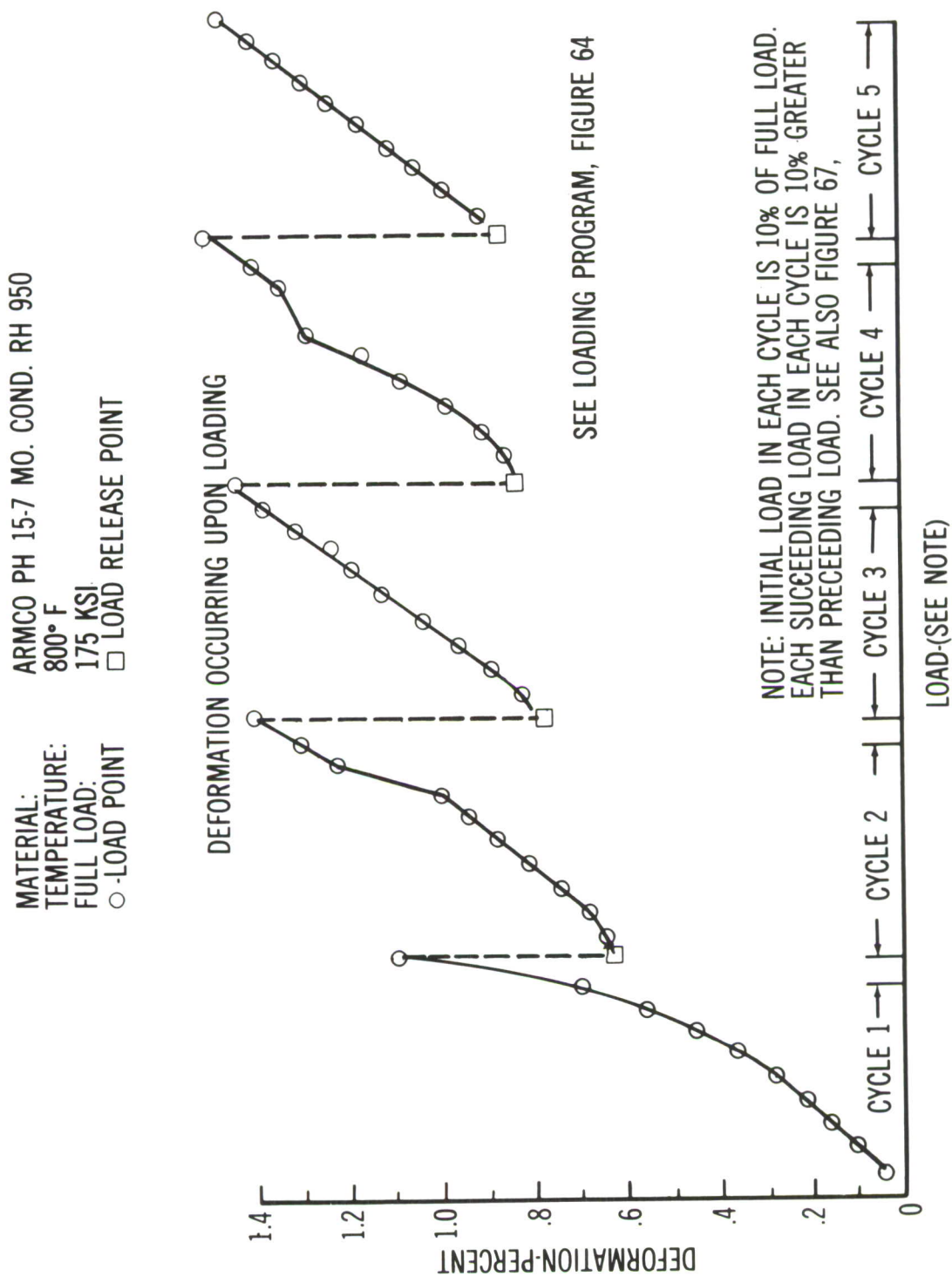


Figure 68. Time Deformation Data, Armco PH 15-7 Mo 800°F., 175 KSI. Incremental Step Loading (Loading Condition)

MATERIAL: ARMCO PH 15-7 MO. COND. RH 950
 TEMPERATURE: 800°F
 FULL LOAD: 175 KSI.

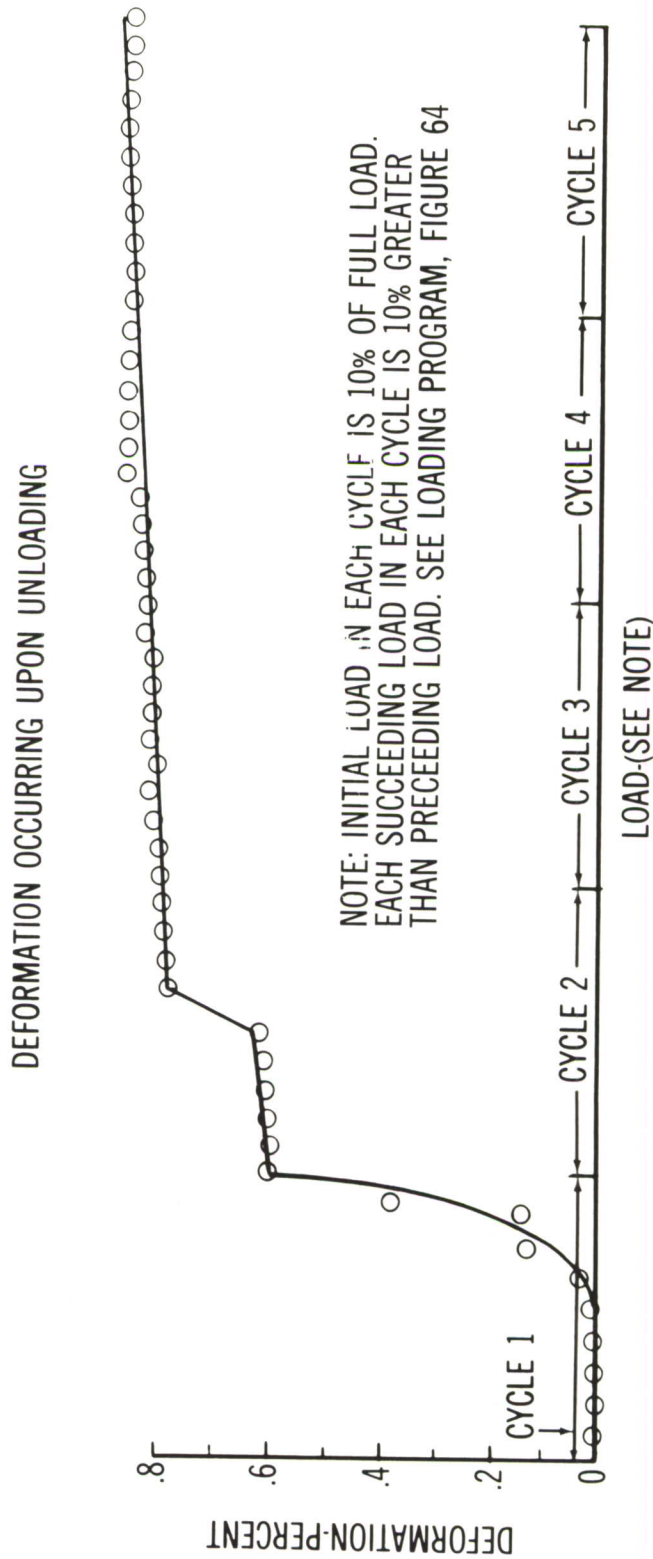


Figure 69. Time-Deformation Data, Armco PH 15-7 Mo 800°F., 175 KSI. Incremental Step Loading (Unloading Condition)

MATERIAL: ARMCO PH 15-7 MO. COND. RH 950
 TEMPERATURE: 900° F
 FULL LOAD: 135 KSI.
 ○ LOAD POINT
 □ LOAD RELEASE POINT

DEFORMATION OCCURRING UPON LOADING

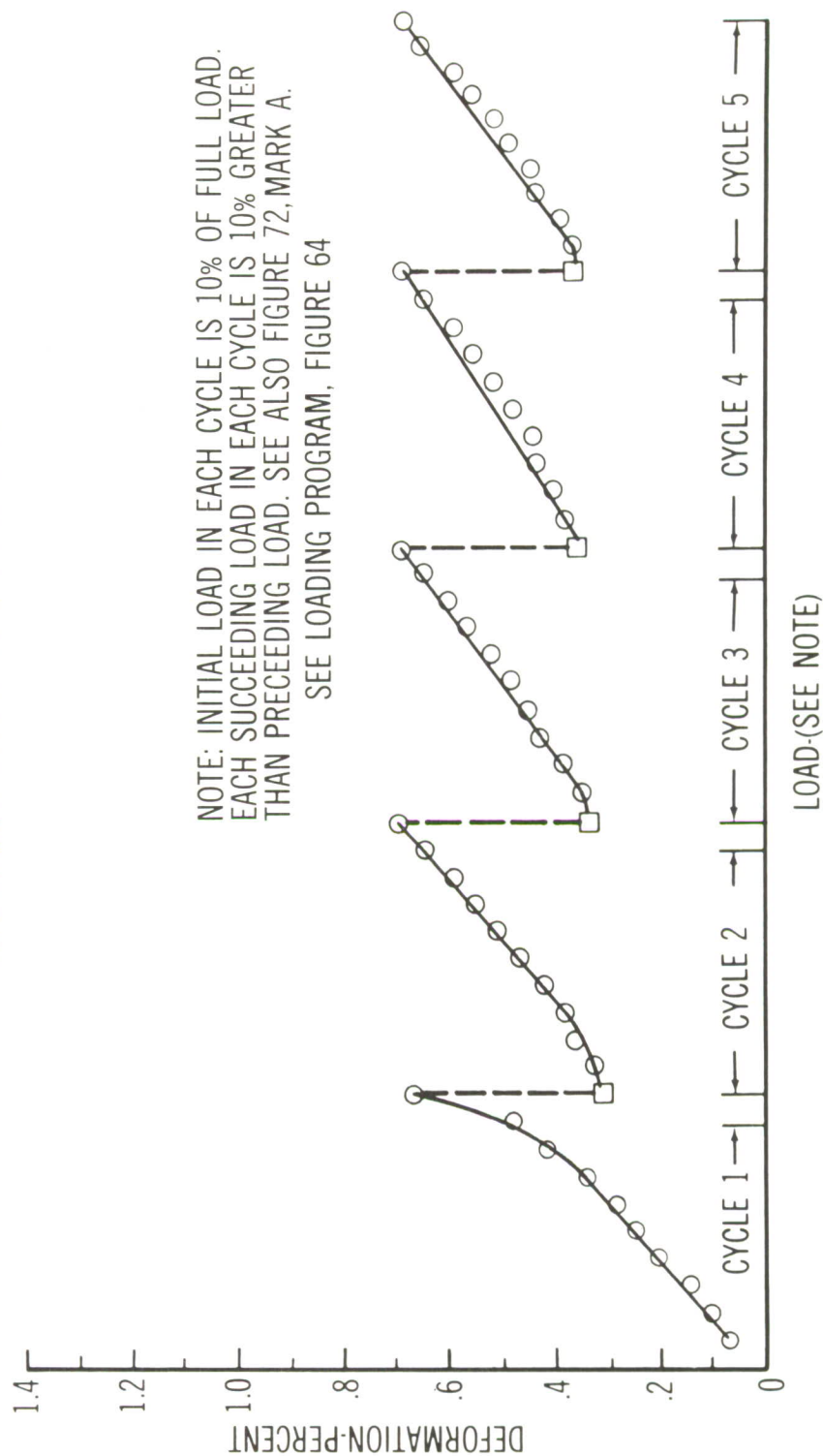


Figure 70. Time-Deformation Data, Armco PH 15-7 Mo 900°F., 135 KSI. Incremental Step Loading (Loading Condition)

MATERIAL: ARMCO PH 15-7 MO. COND. RH 950
 TEMPERATURE: 900° F
 FULL LOAD: 135 KSI.
 ○ LOAD POINT
 □ LOAD RELEASE POINT

DEFORMATION OCCURRING UPON LOADING

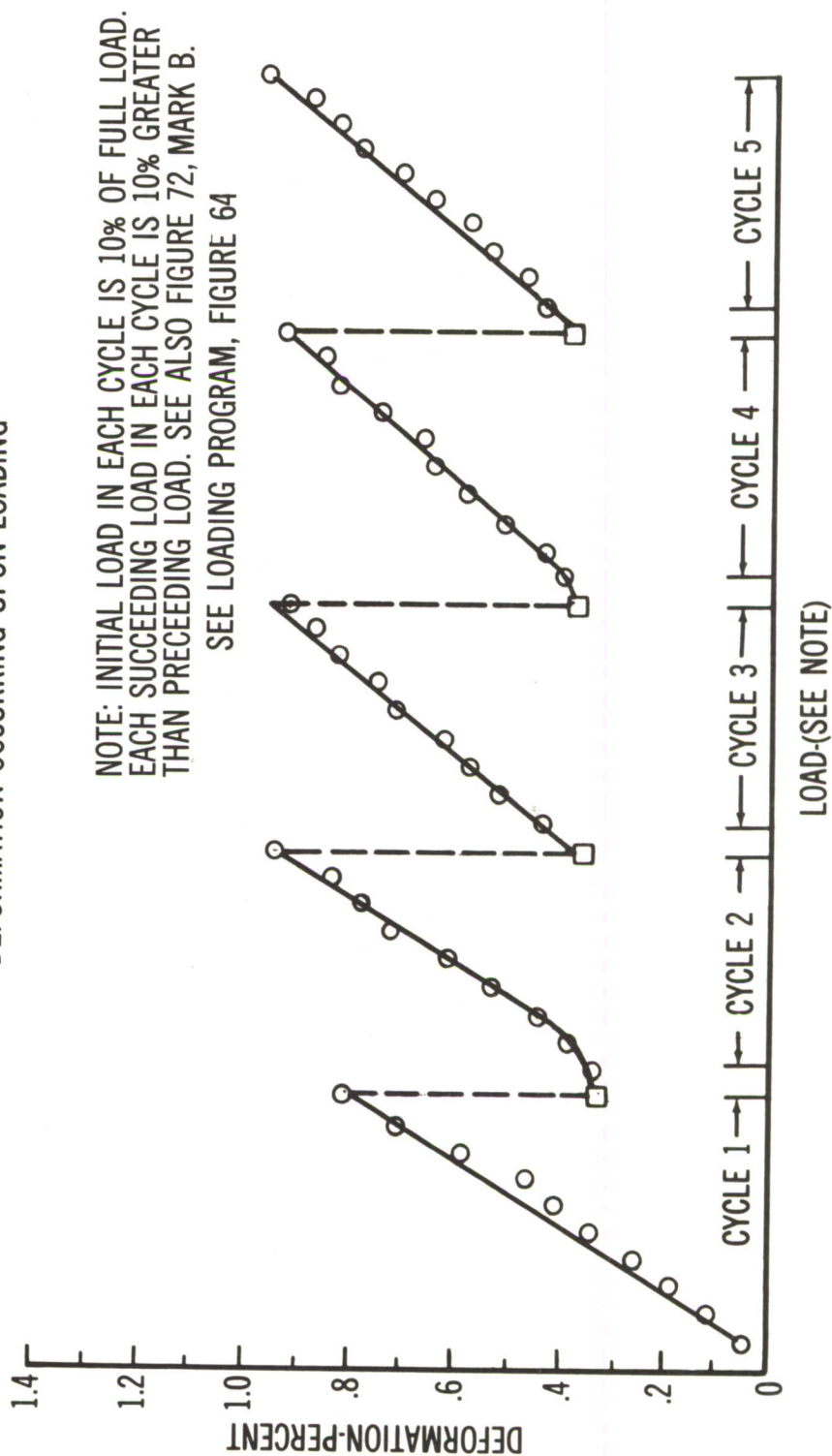
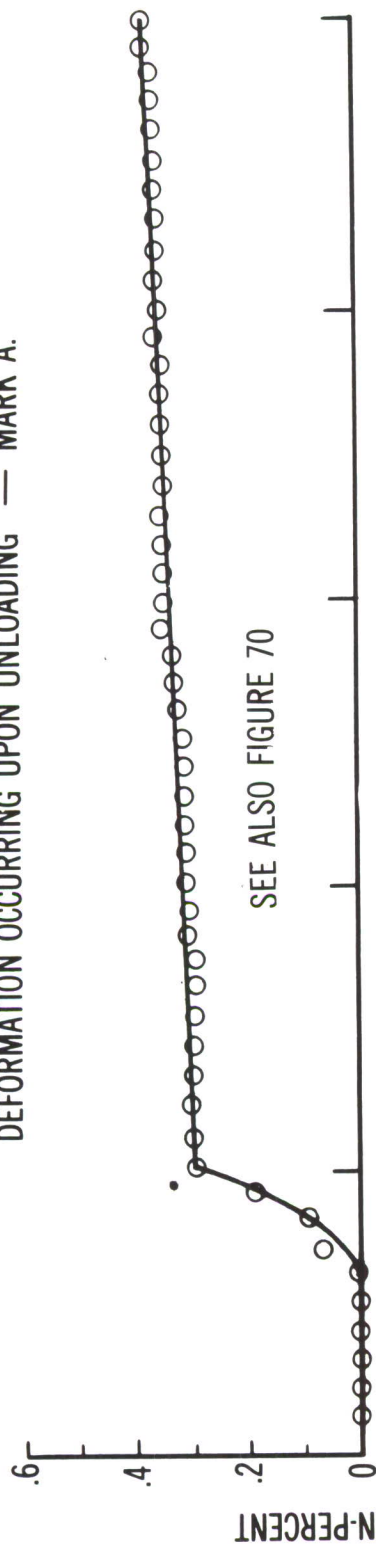


Figure 7L. Time-Deformation Data, Armco PH 15-7 Mo 900°F., 135 KSI. Incremental Step Loading (Loading Condition)

MATERIAL: ARMCO PH 15-7 MO. COND. RH 950 FULL LOAD: 135 KSI.
 TEMPERATURE: 900° F

DEFORMATION OCCURRING UPON UNLOADING — MARK A.



DEFORMATION OCCURRING UPON UNLOADING — MARK B.

NOTE: INITIAL LOAD IN EACH CYCLE IS 10% OF FULL LOAD. EACH SUCCEEDING LOAD IN EACH CYCLE IS 10% GREATER THAN PRECEDING LOAD. SEE ALSO FIGURE 71 SEE LOADING PROGRAM, FIGURE 64

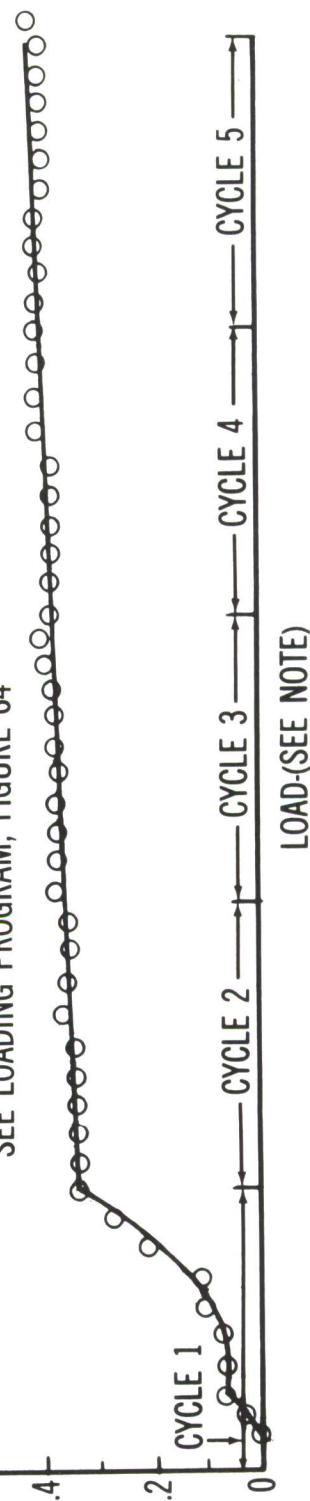


Figure 72. Time-Deformation Data, Armco PH 15-7 Mo 900°F., 135 KSI. Incremental Step Loading (Unloading Condition)

MATERIAL: ARMCO PH 15-7 MO. COND. RH 950
 TEMPERATURE: 1000° F
 FULL LOAD: 77 KSI.
 ○ LOAD POINT
 □ LOAD RELEASE POINT

DEFORMATION OCCURRING UPON LOADING

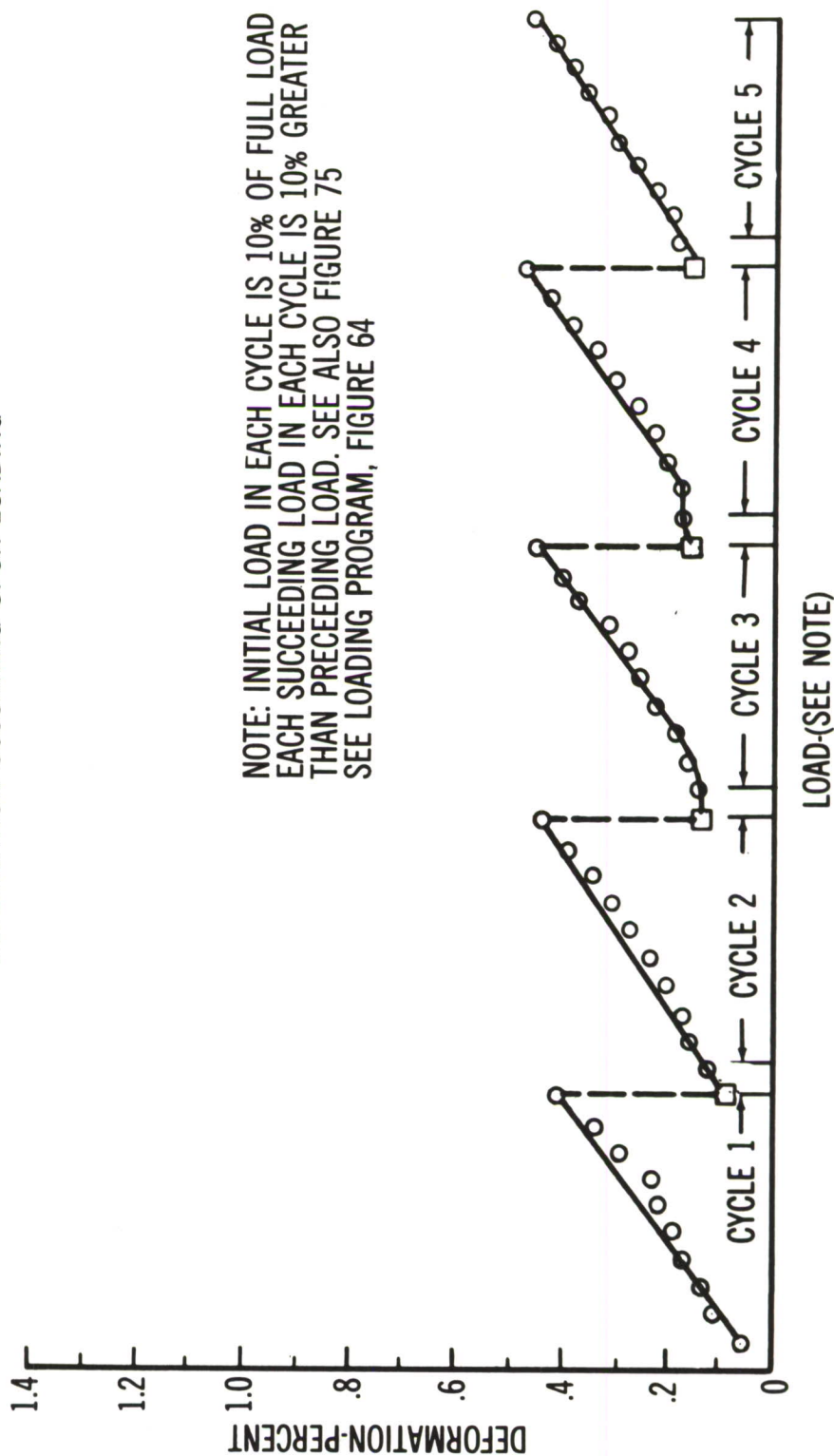


Figure 73. Time-Deformation Data, Armco PH 15-7 Mo 1000°F., 77 KSI. Incremental Step Loading (Loading Condition)

MATERIAL: ARMCO PH 15-7 MO. COND. RH 950
 TEMPERATURE: 1000° F
 FULL LOAD: 77 KSI.
 ○ -LOAD POINT
 □ -LOAD RELEASE POINT

DEFORMATION OCCURRING UPON LOADING

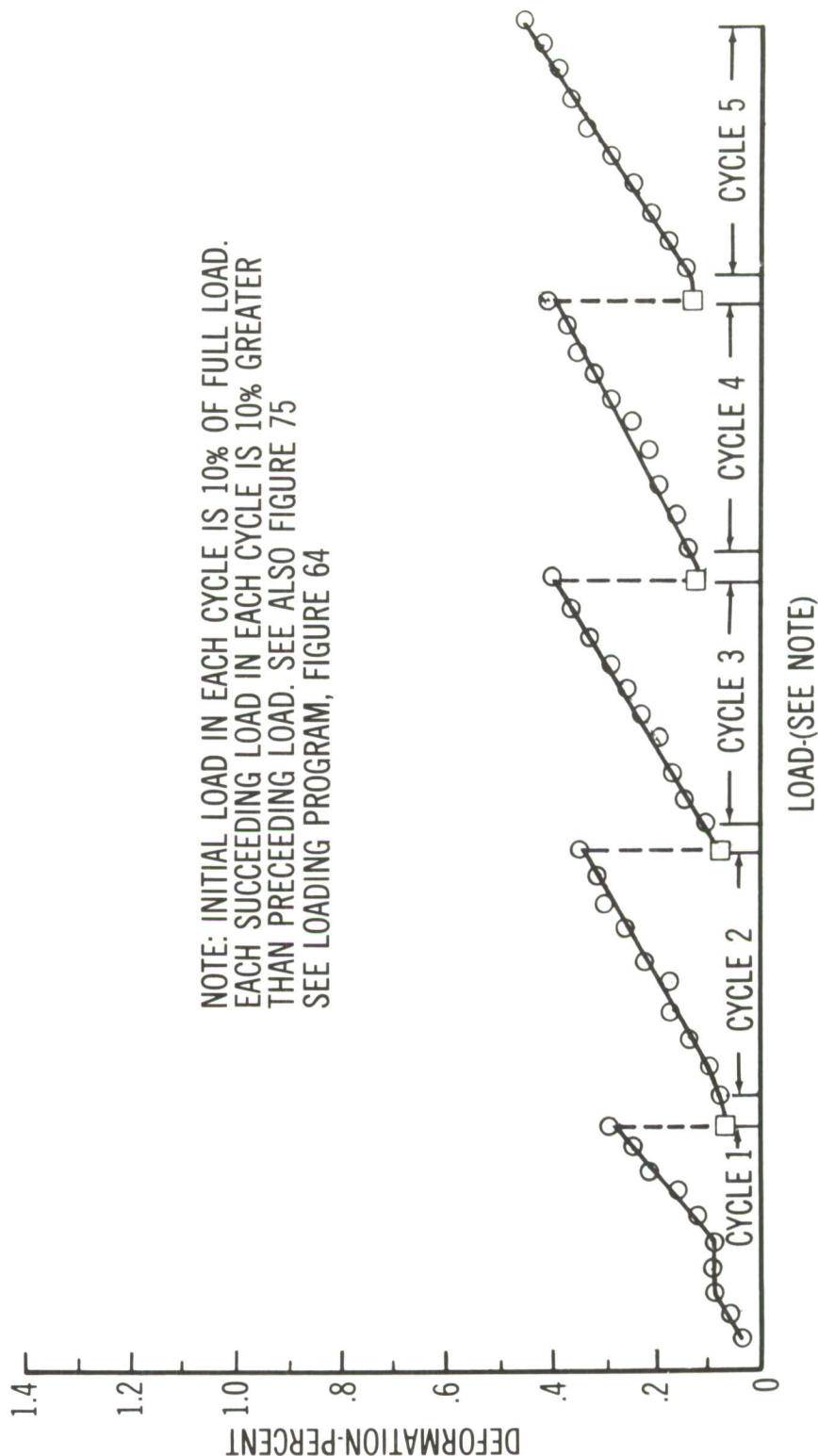
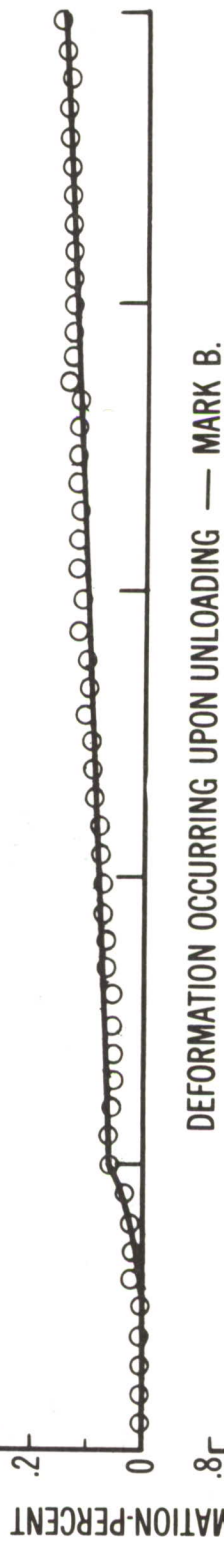


Figure 74. Time-Deformation Data, Armco PH 15-7 Mo 1000°F., 77 KSI. Incremental Step Loading (Loading Condition)

MATERIAL: ARMCO PH 15-7 MO. COND. RH 950 FULL LOAD: 77 KSI.
 TEMPERATURE: 1000° F

DEFORMATION OCCURRING UPON UNLOADING — MARK A.

SEE ALSO FIGURE 73



NOTE: INITIAL LOAD IN EACH CYCLE IS 10% OF FULL LOAD.
 EACH SUCCEEDING LOAD IN EACH CYCLE IS 10% GREATER
 THAN PRECEDING LOAD. SEE ALSO FIGURE 74
 SEE LOADING PROGRAM, FIGURE 64

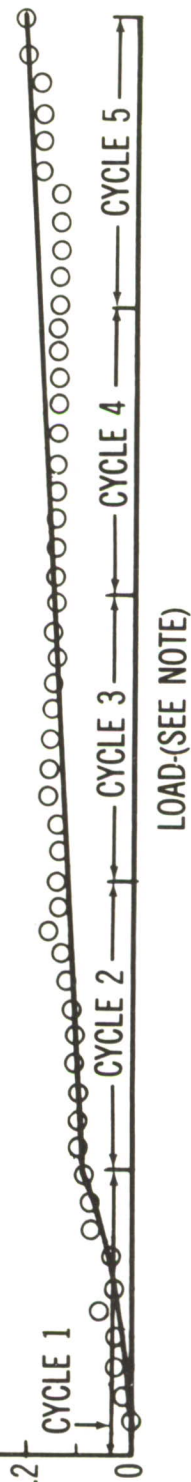


Figure 75. Time-Deformation Data, Armco PH 15-7 Mo 1000° F., 77 KSI. Incremental Step Loading (Unloading Condition)

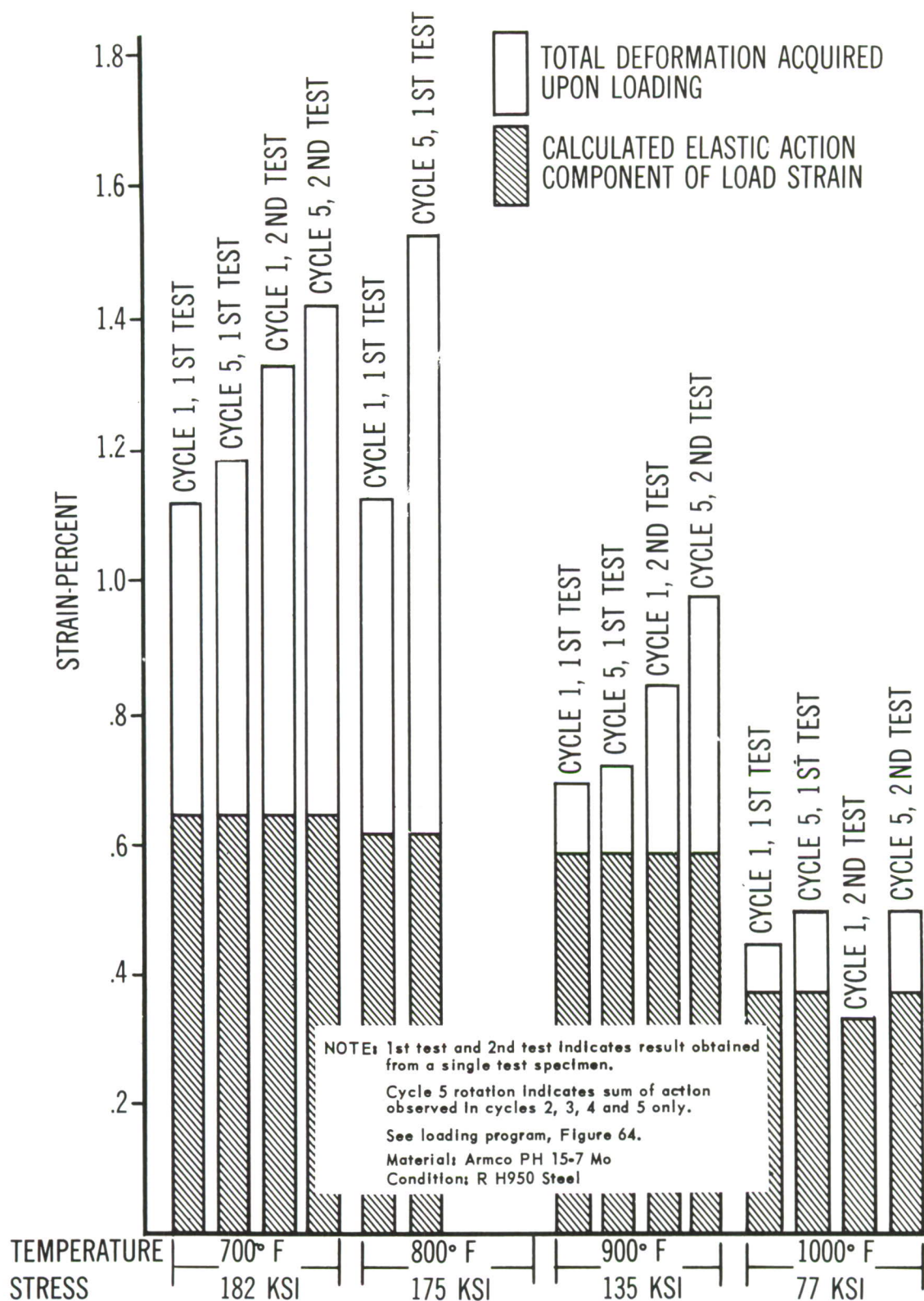


Figure 76. "Make-up" of Loading Strains in Increment Loaded Creep Tests with Armco PH15-7 Mo.

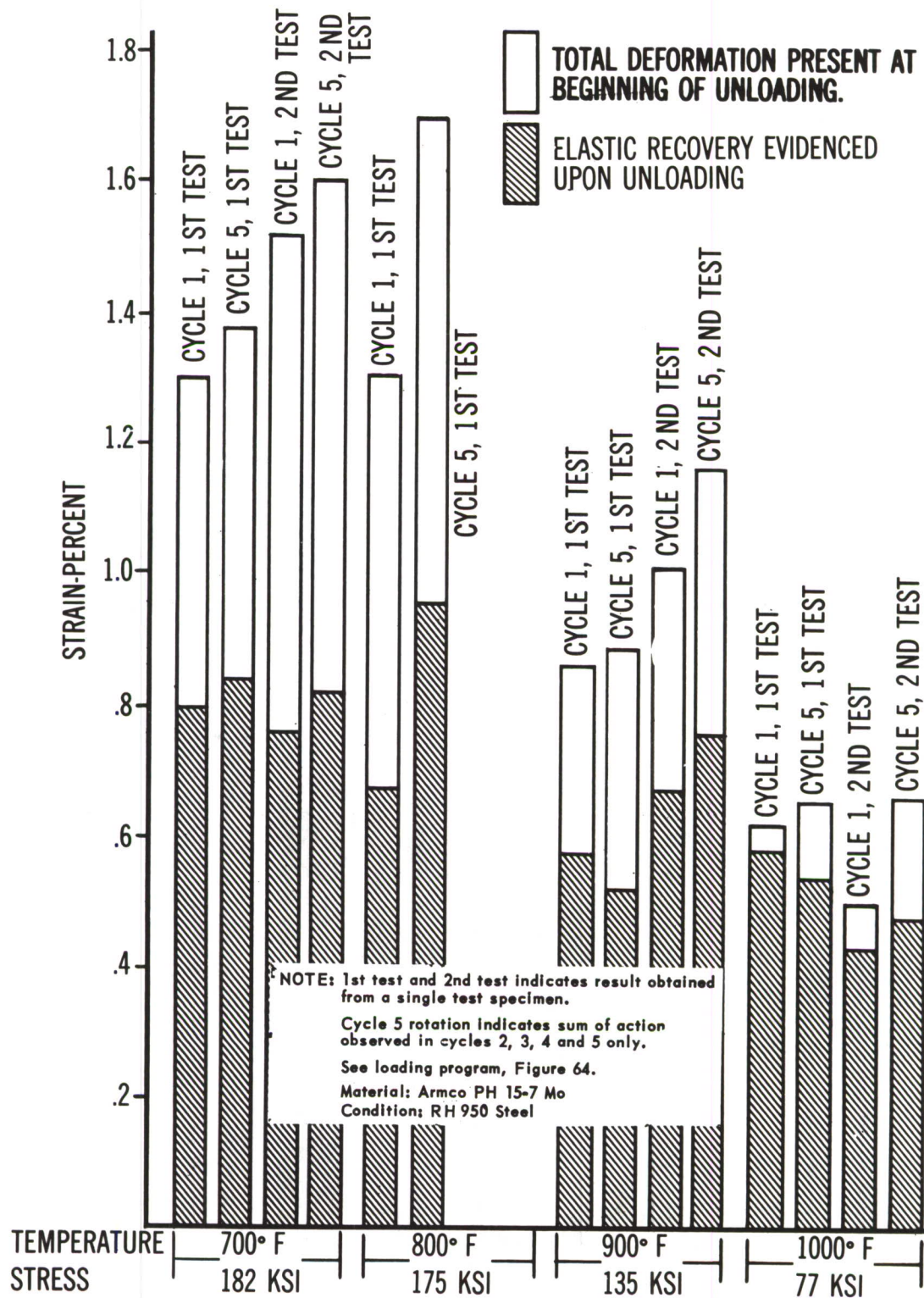


Figure 77. "Make-up" of Unloading Strains in Increment Loaded Creep Tests with Armco PH15-7 Mo.

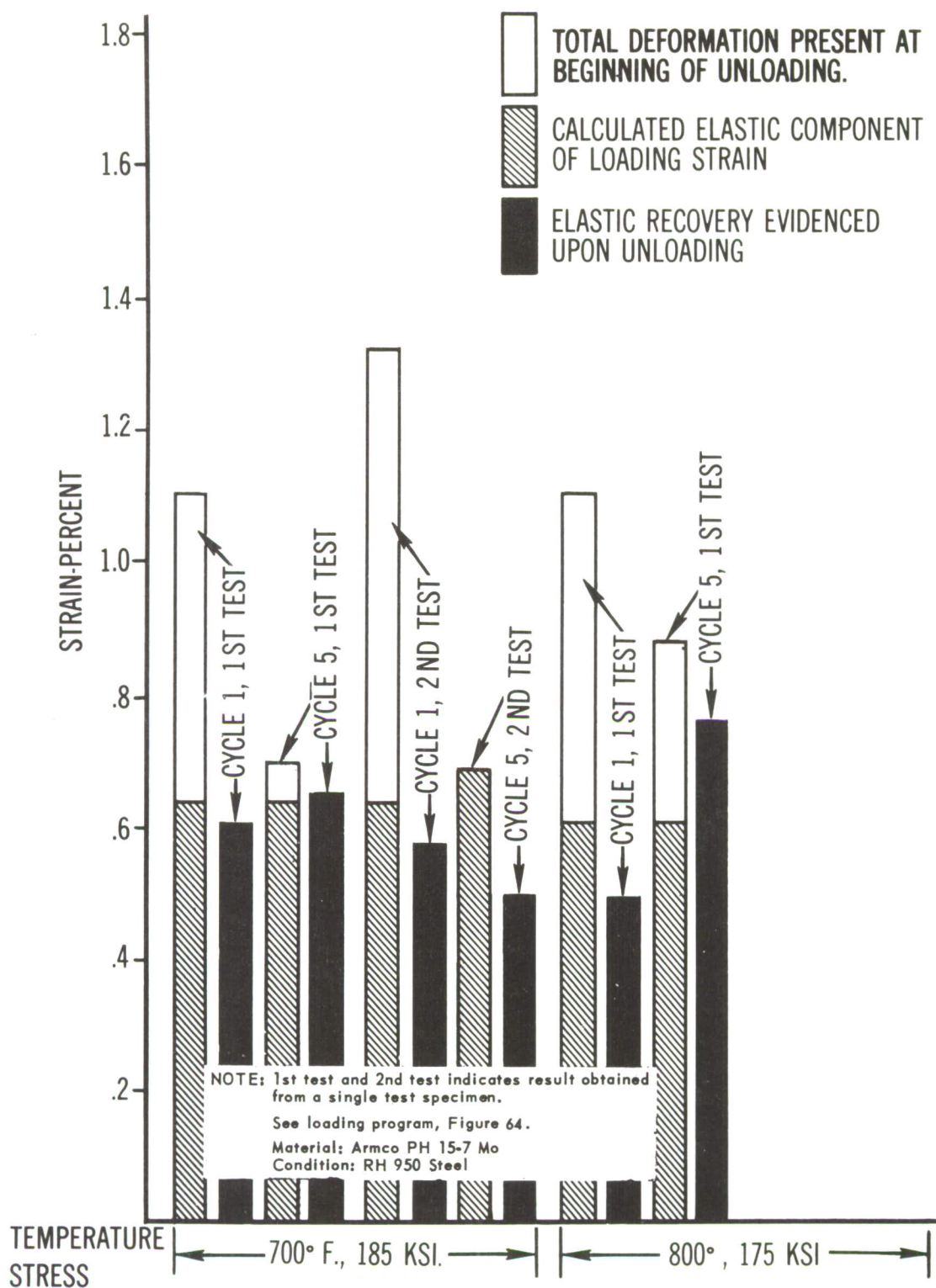


Figure 78. Comparison of Strains Incidental to Loading With Elastic Strain Recovery Occurring Upon Load Release (700°F and 800°F).

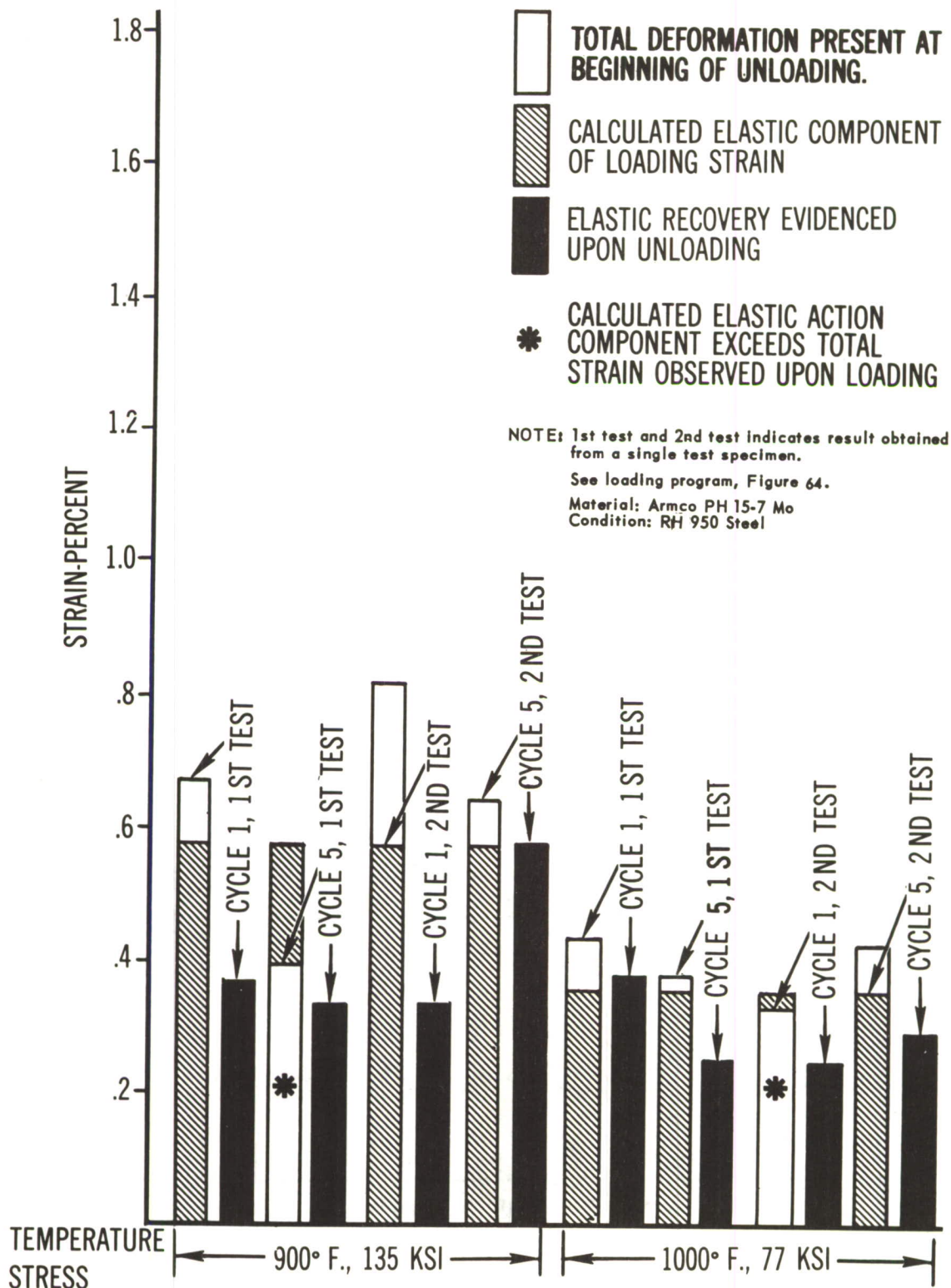


Figure 79. Comparison of Strain Incidental to Loading with Elastic Strain Recovery Occurring Upon Load Release (900°F & 1000°F)

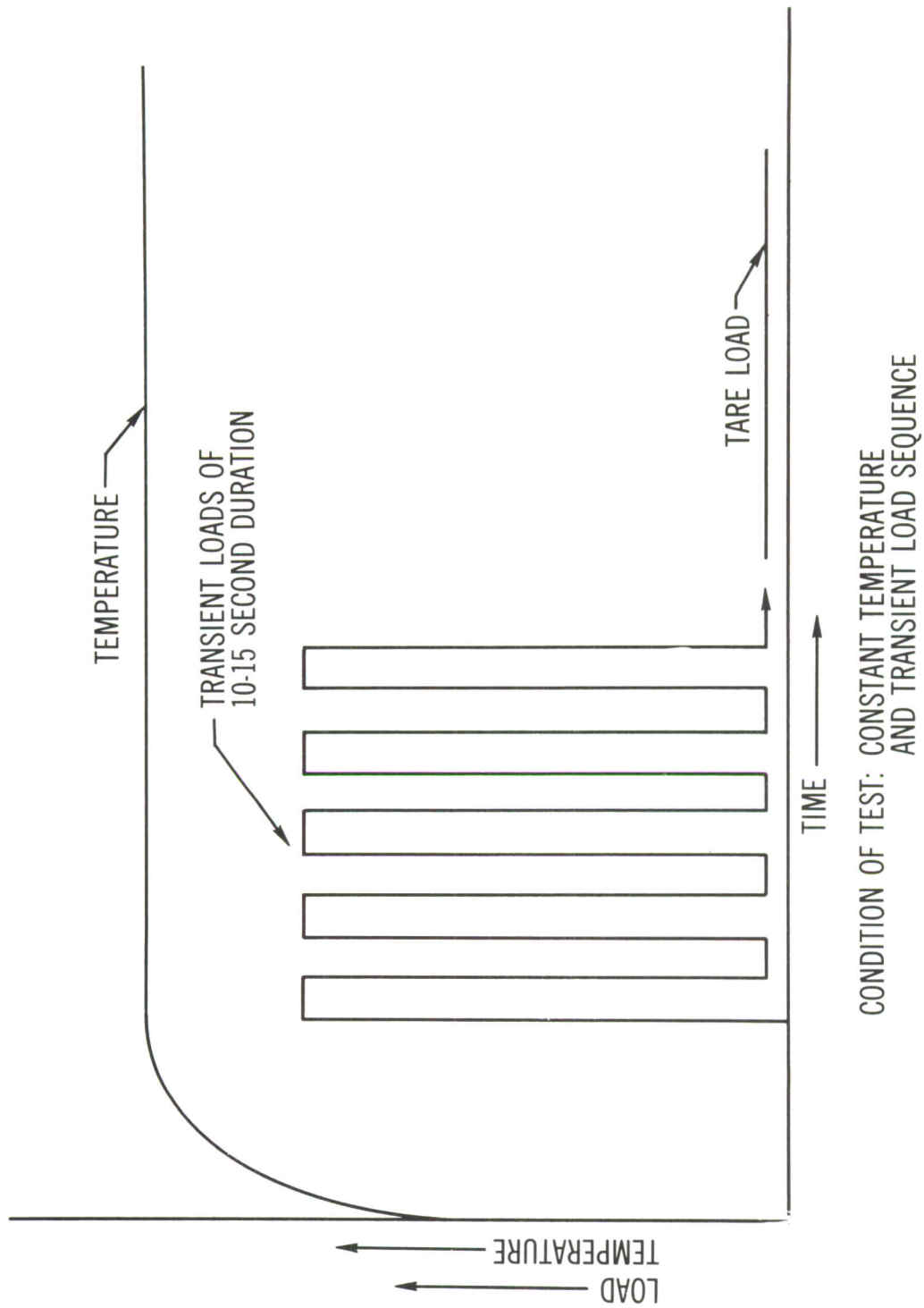


Figure 80. Program for Repeated Load Tests.

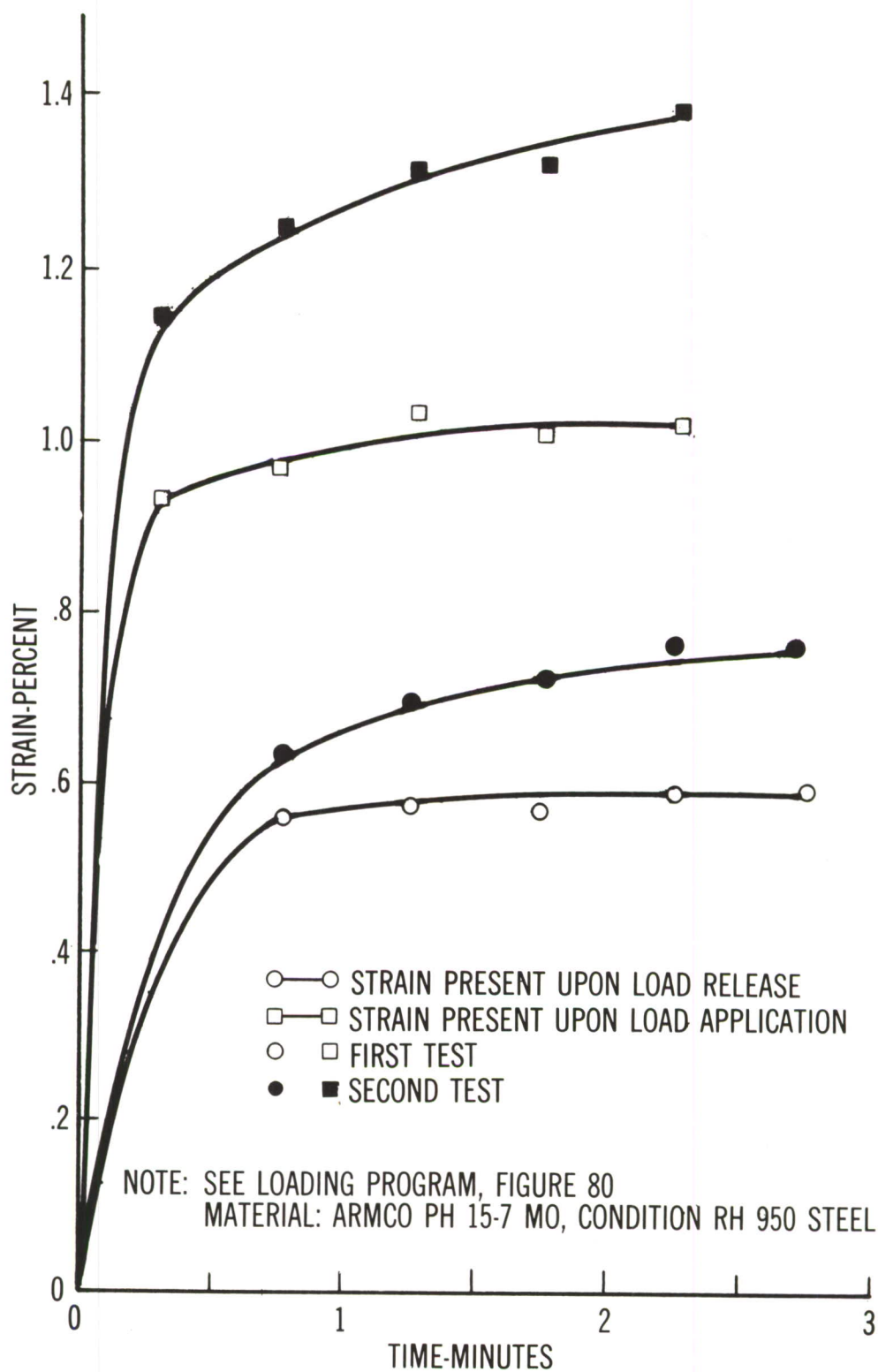


Figure 81. Strains Resulting From Successive Applications of 182 KSI Load to Armco PH15-7 Mo at 700°F.

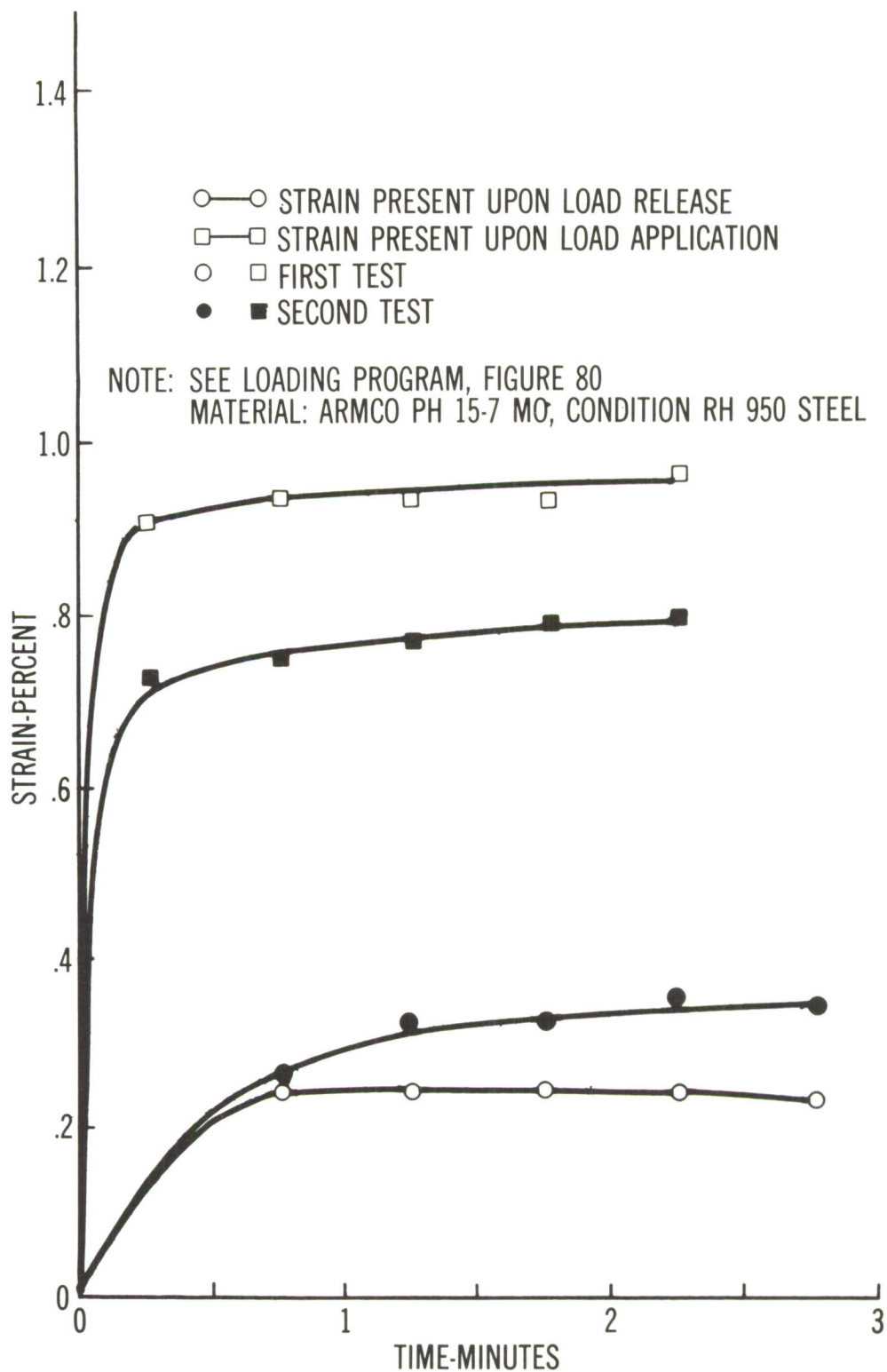


Figure 82. Strains Resulting from Successive Applications of 175 KSI Load to Armco PH15-7 Mo at 800°F.

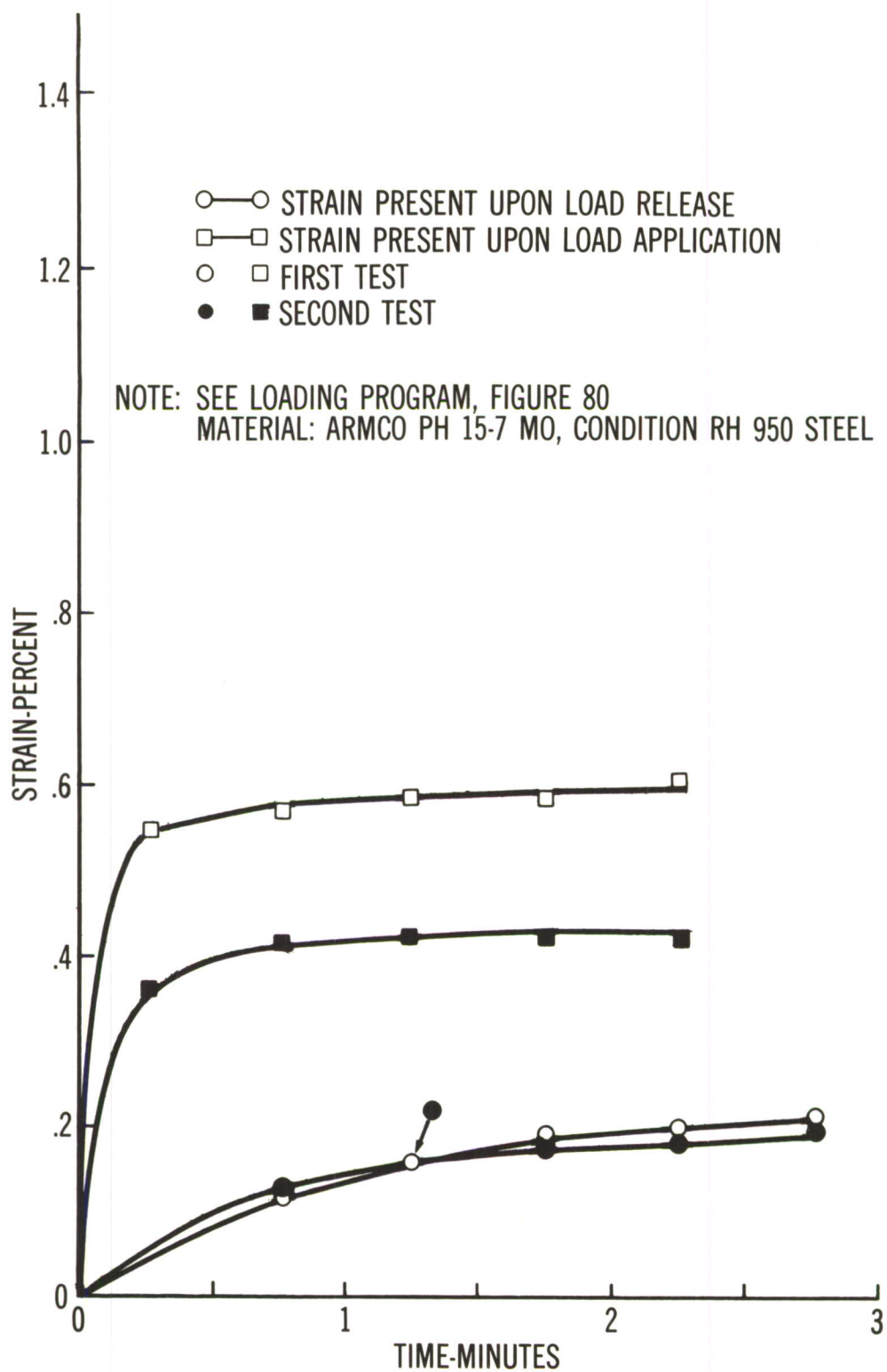


Figure 83. Strains Resulting from Successive Applications of 135 KSI Load to Armco PH15-7 Mo at 900°F.

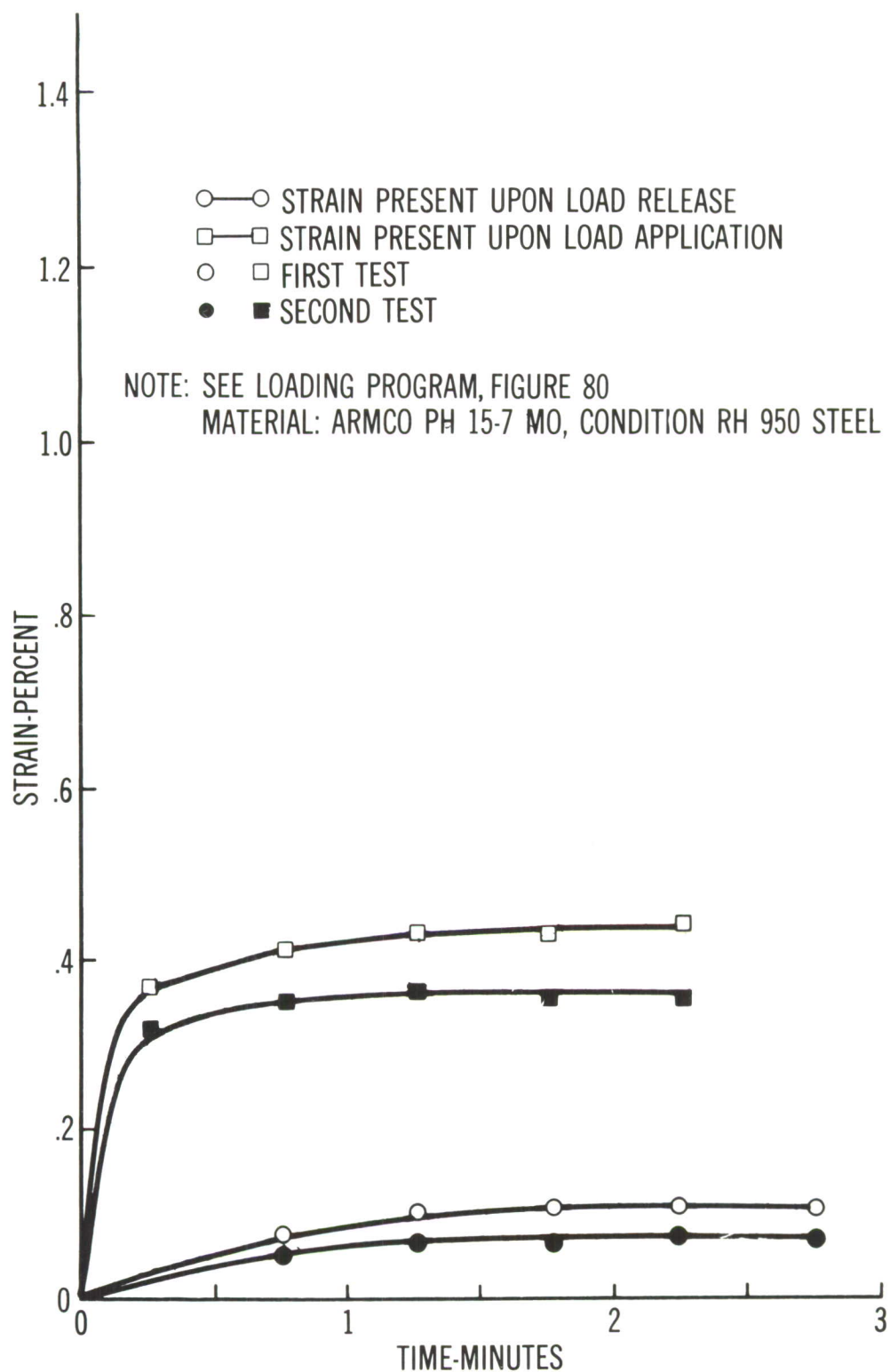


Figure 84. Strains Resulting From Successive Applications of 77 KSI Load to Armco PH15-7 Mo at 1000°F.

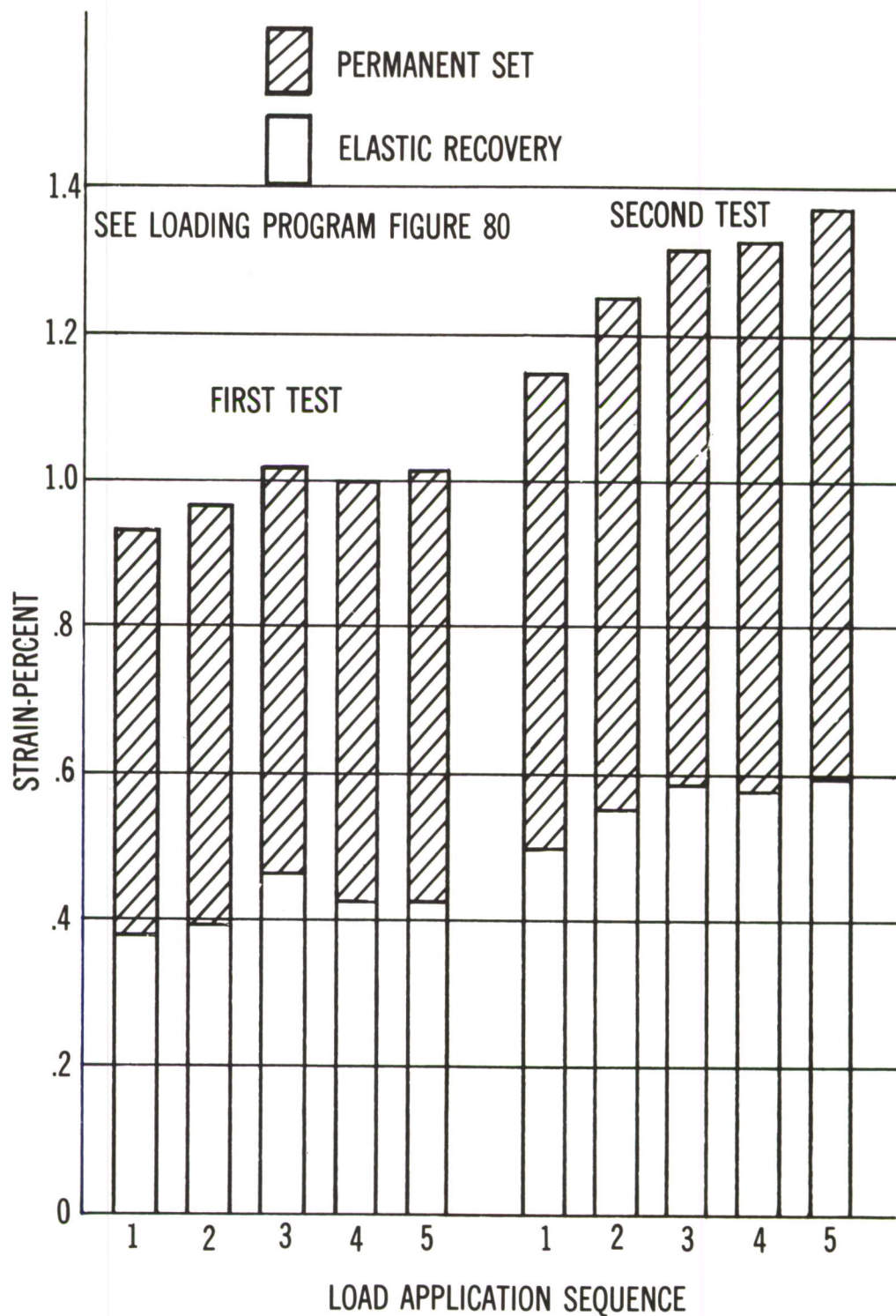


Figure 85. "Make-up" of Strain Patterns Occurring Upon Load Release in Repeated Loading Tests (700°F 182 KSI Stress).

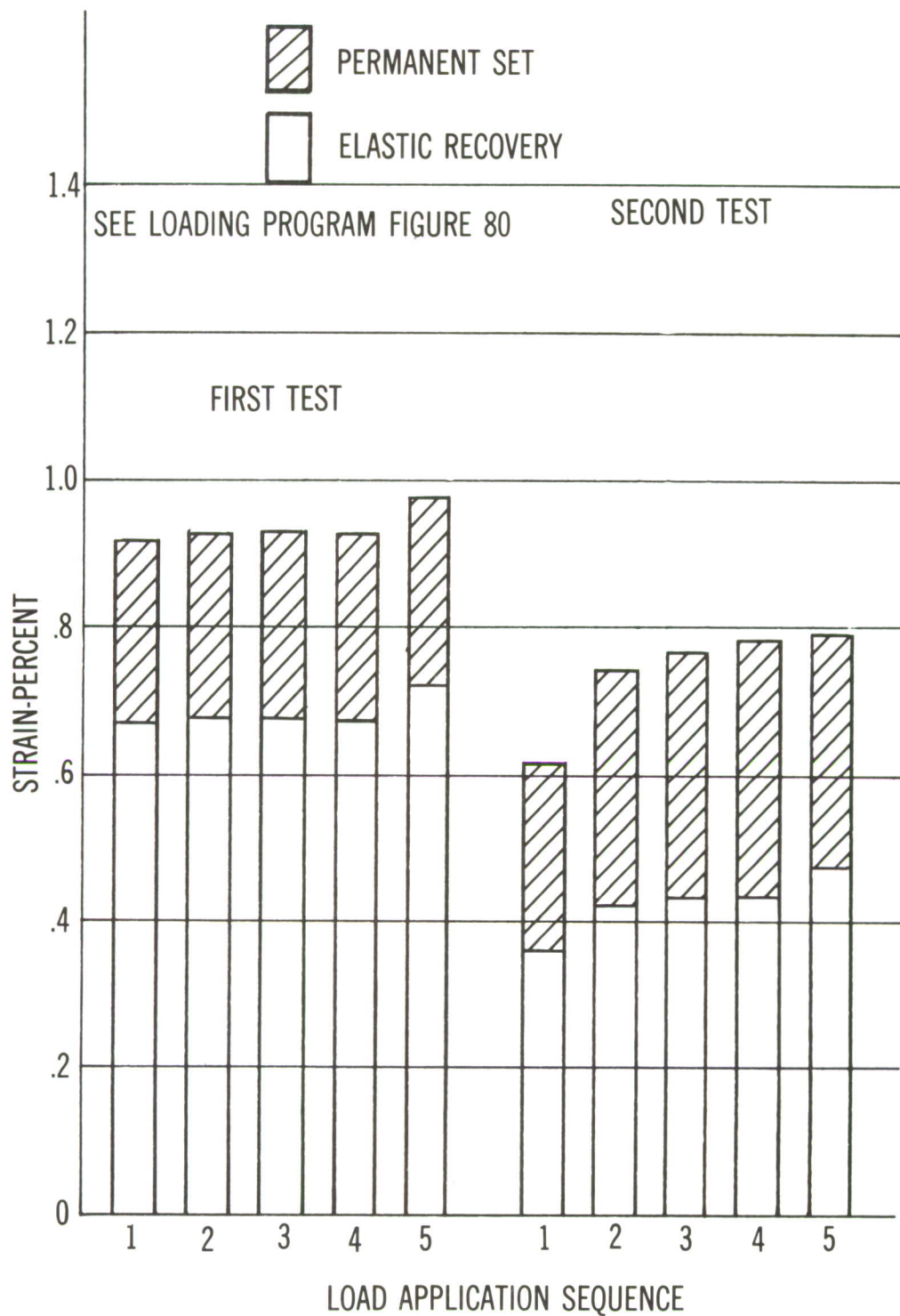


Figure 86. "Make-up" of Strain Patterns Occurring Upon Load Release in Repeated Loading Tests (800°F 175 KSI Stress).

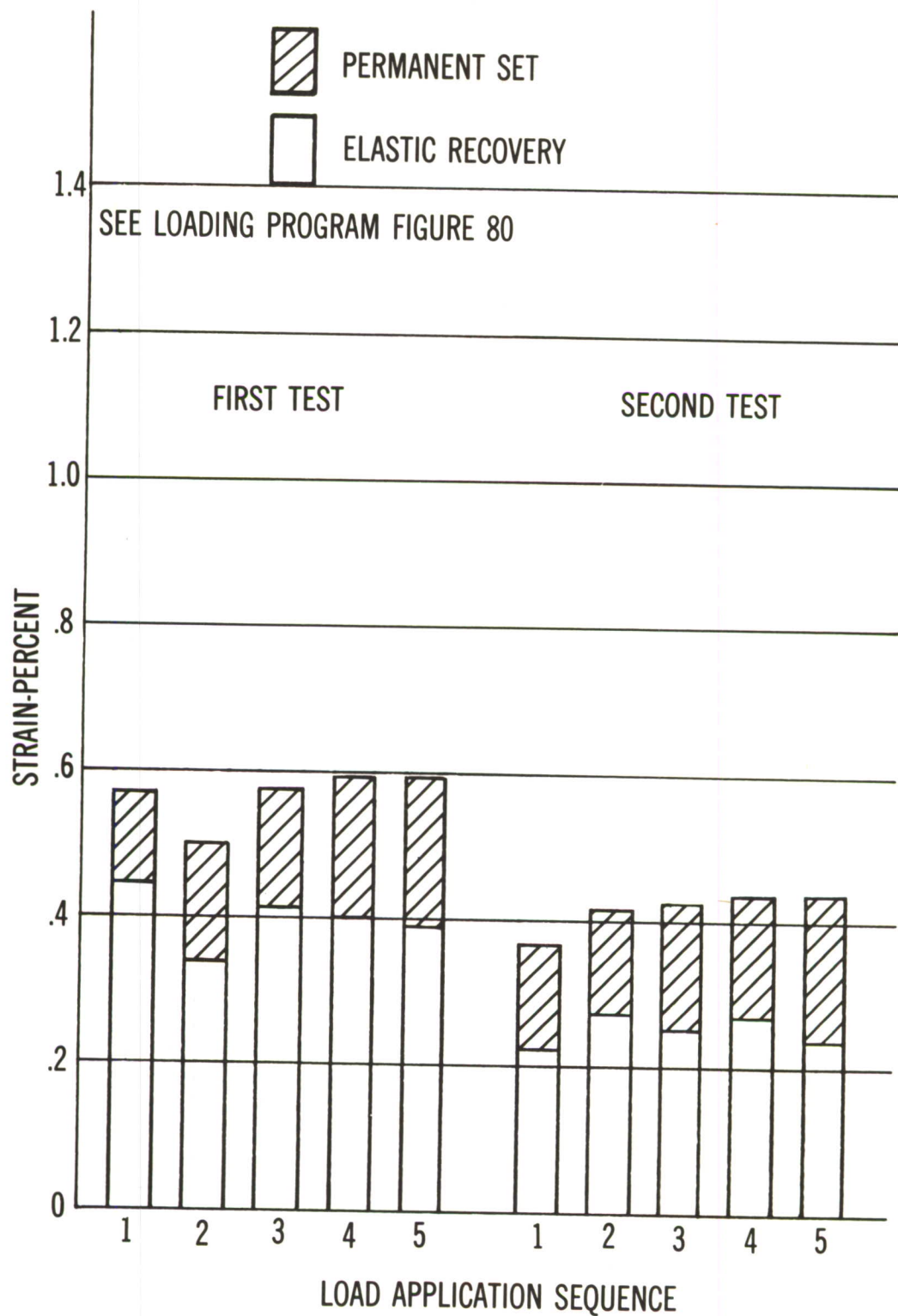


Figure 87. "Make-up" of Strain Patterns Occurring Upon Load Release in Repeated Loading Tests (900°F 135 KSI).

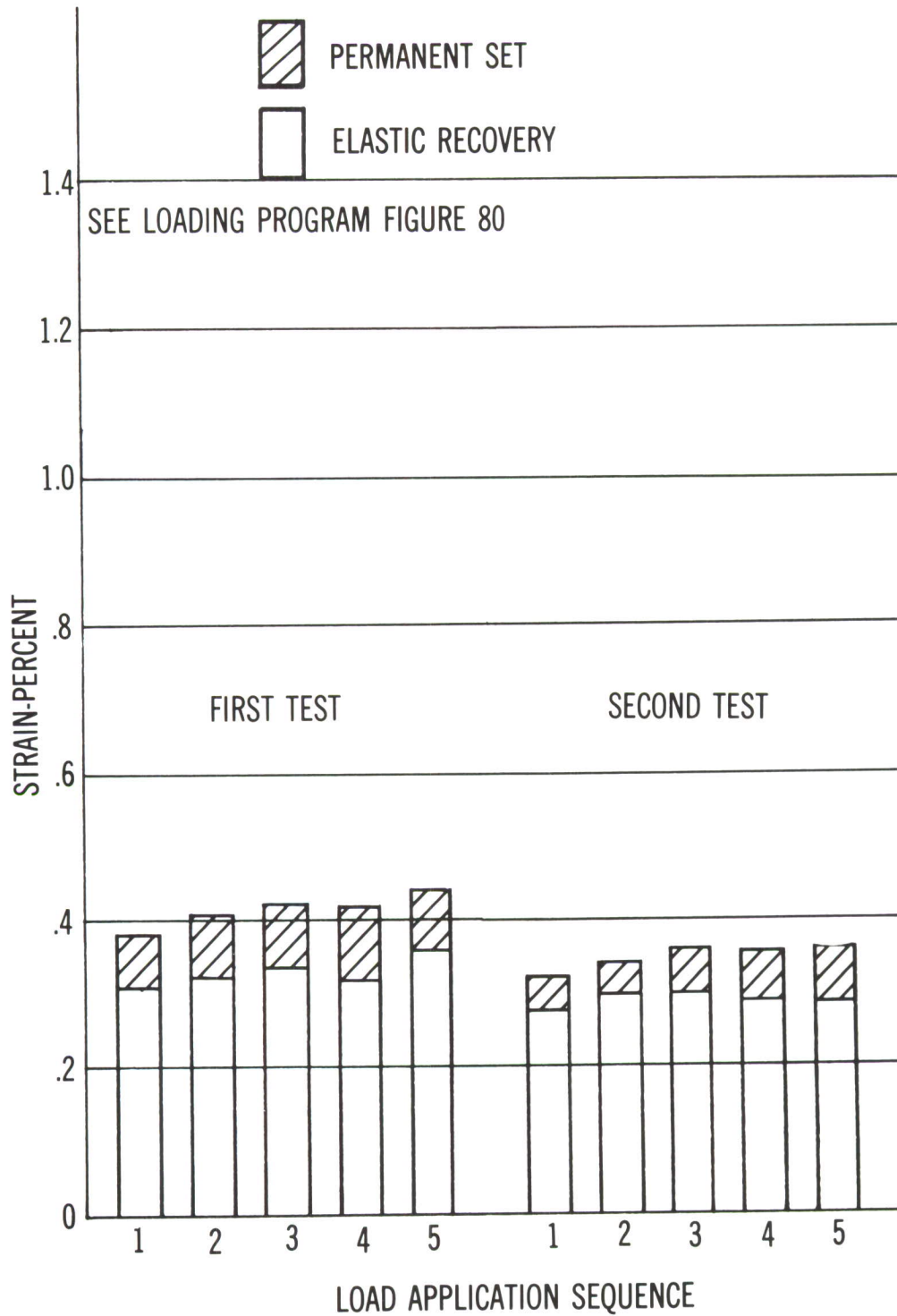


Figure 88. "Make-up" of Strain Patterns Occurring Upon Load Release in Repeated Loading Tests (1000°F 77 KSI).

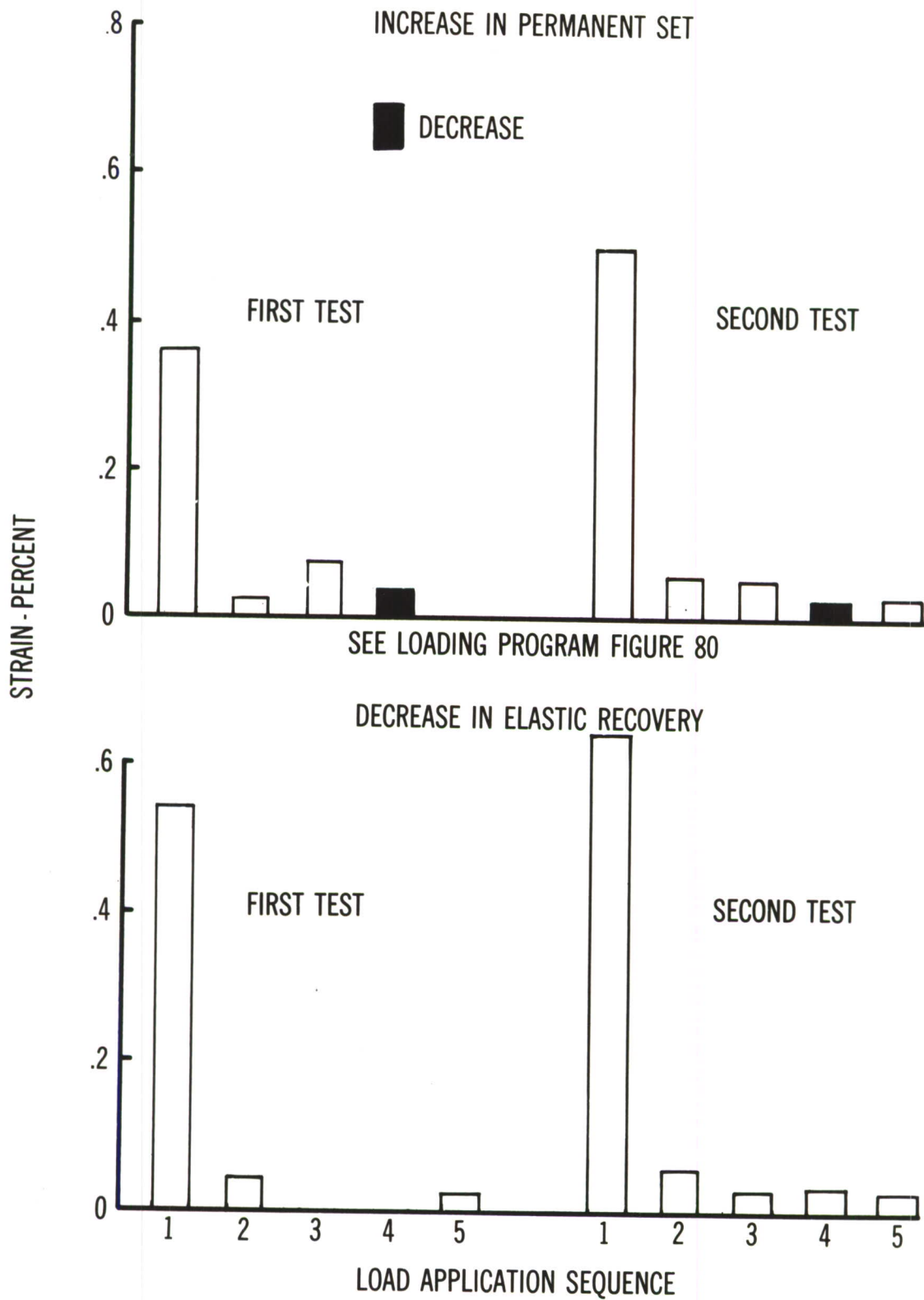


Figure 89. Strain Changes Incident to Repeated Load Tests (700°F, 182 KSI).

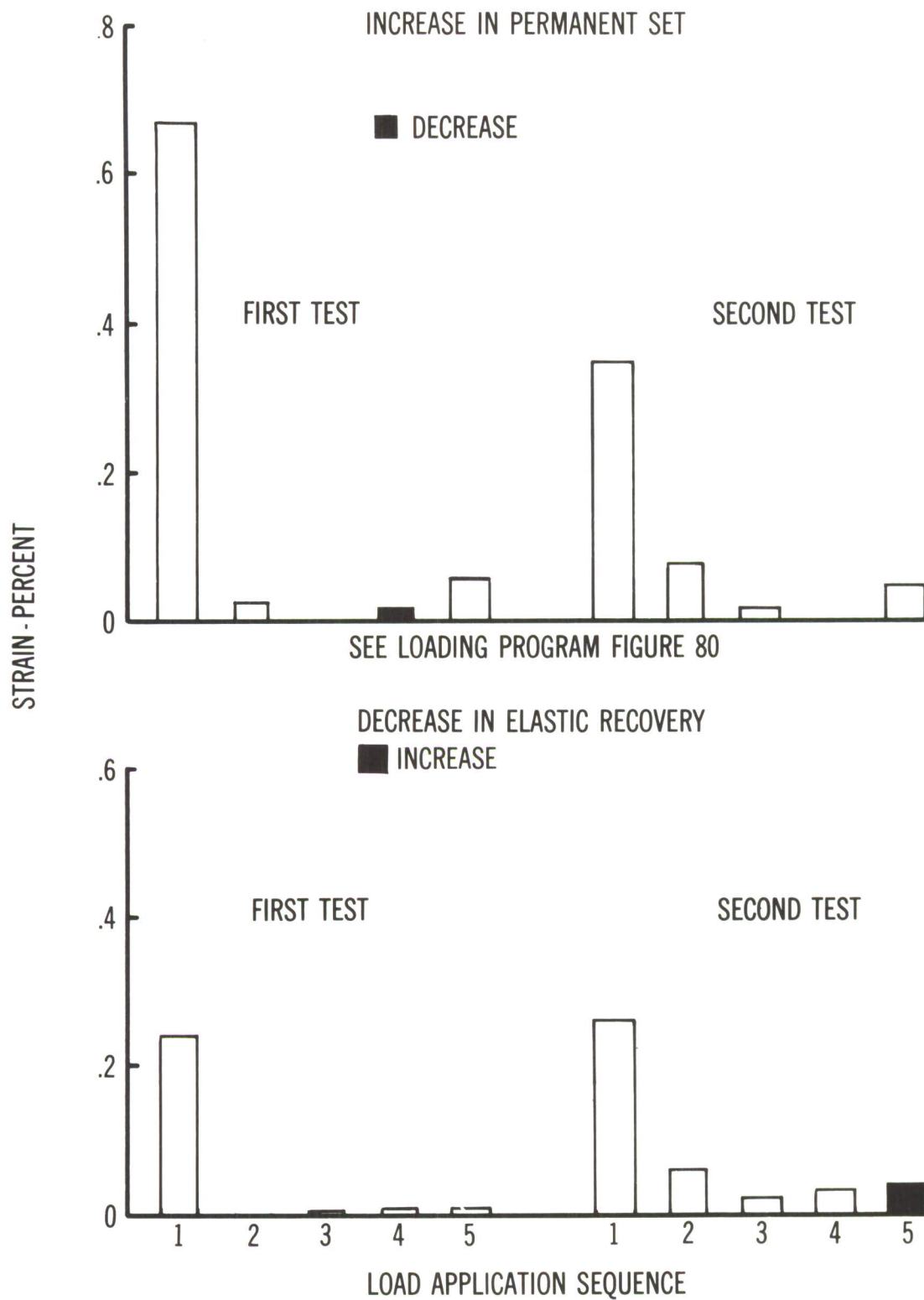


Figure 90. Strain Changes Incident to Repeated Load Tests (800°F, 175 KSI).

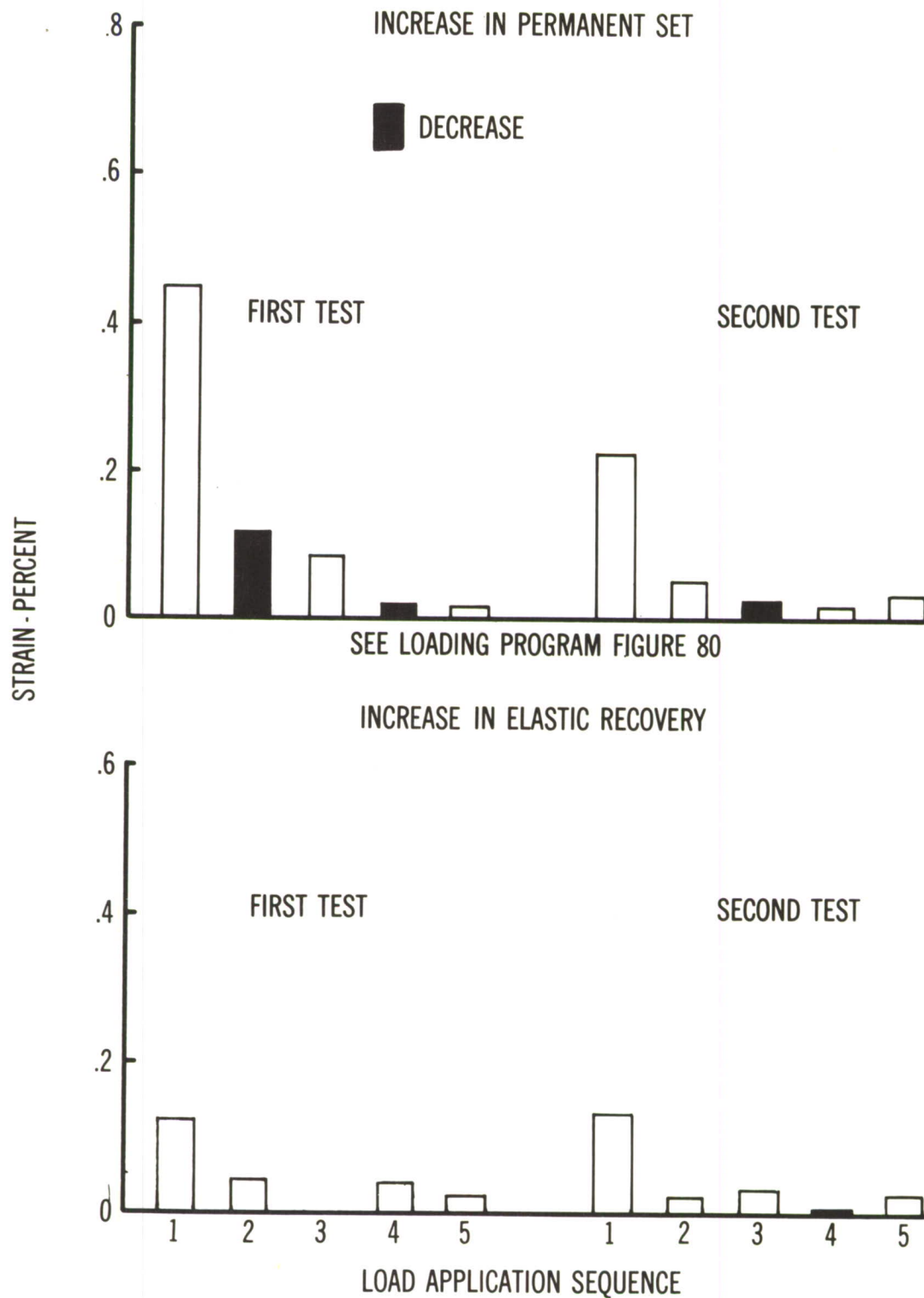


Figure 91. Strain Changes Incidental to Repeated Load Tests (900°F, 135 KSI).

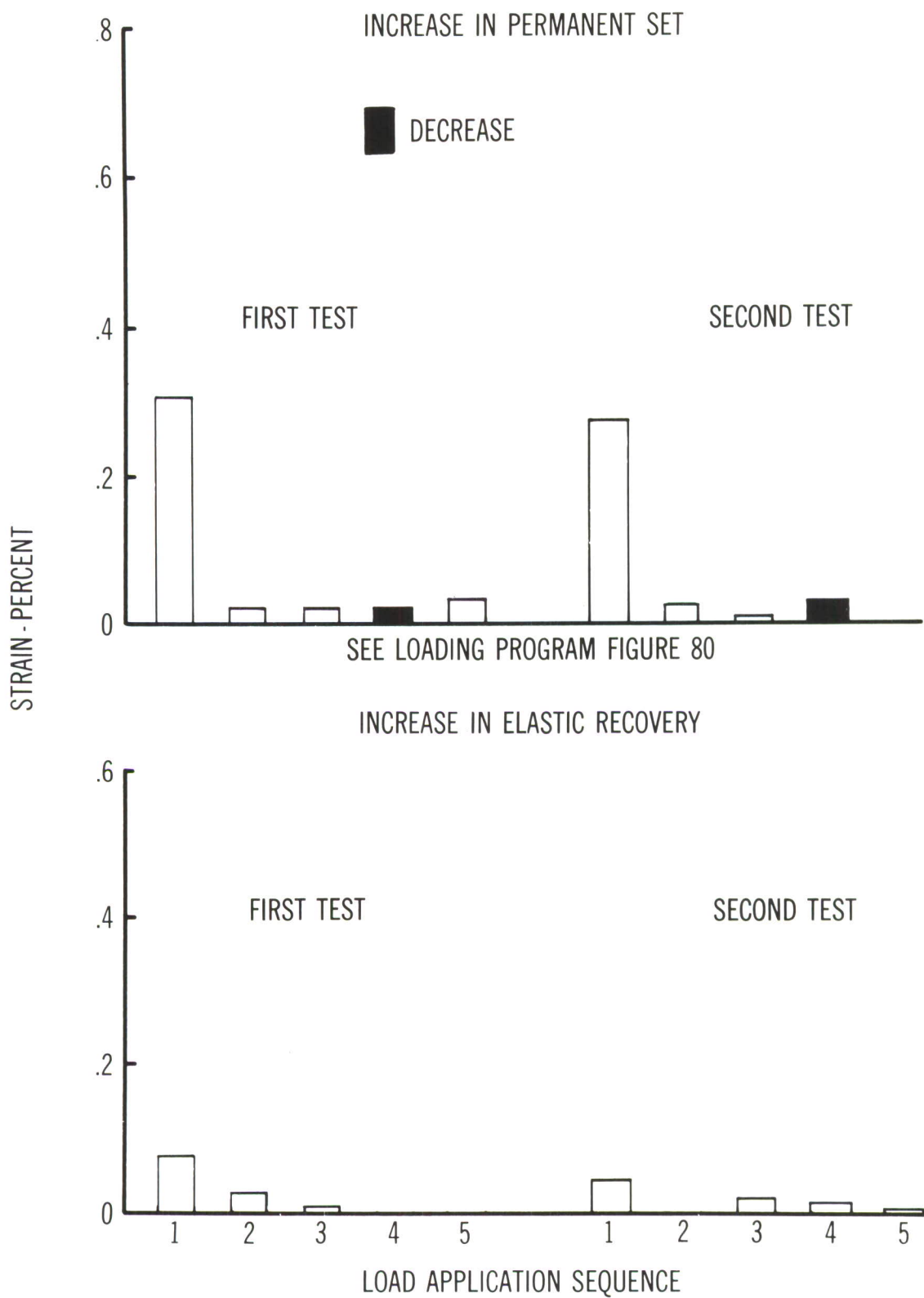


Figure 92. Strain Changes Incidental to Repeated Load Tests (1000° F, 77 KSI).

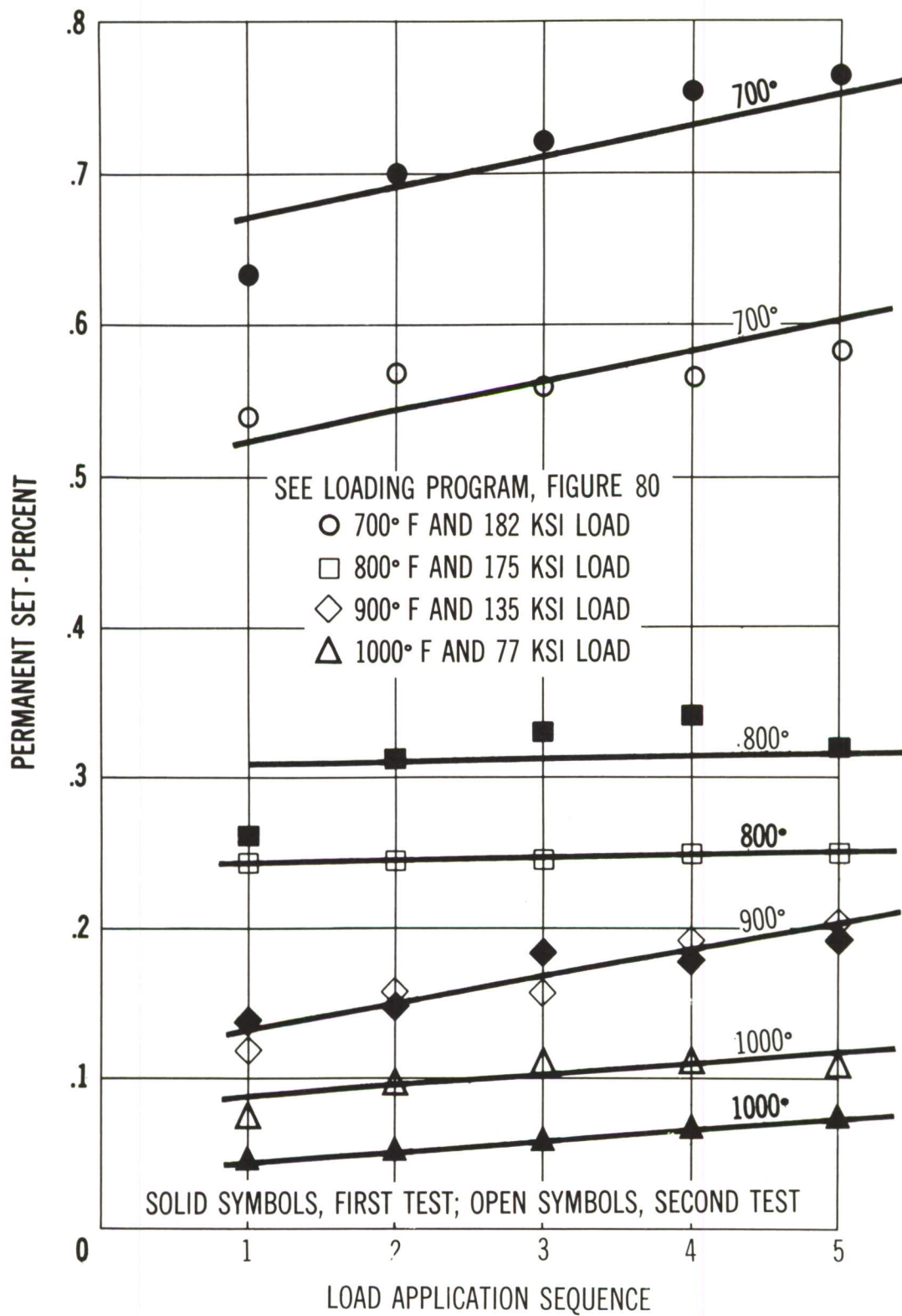


Figure 93. Permanent Set Accumulation Observed in Repeated Load Tests Run at Various Temperatures.

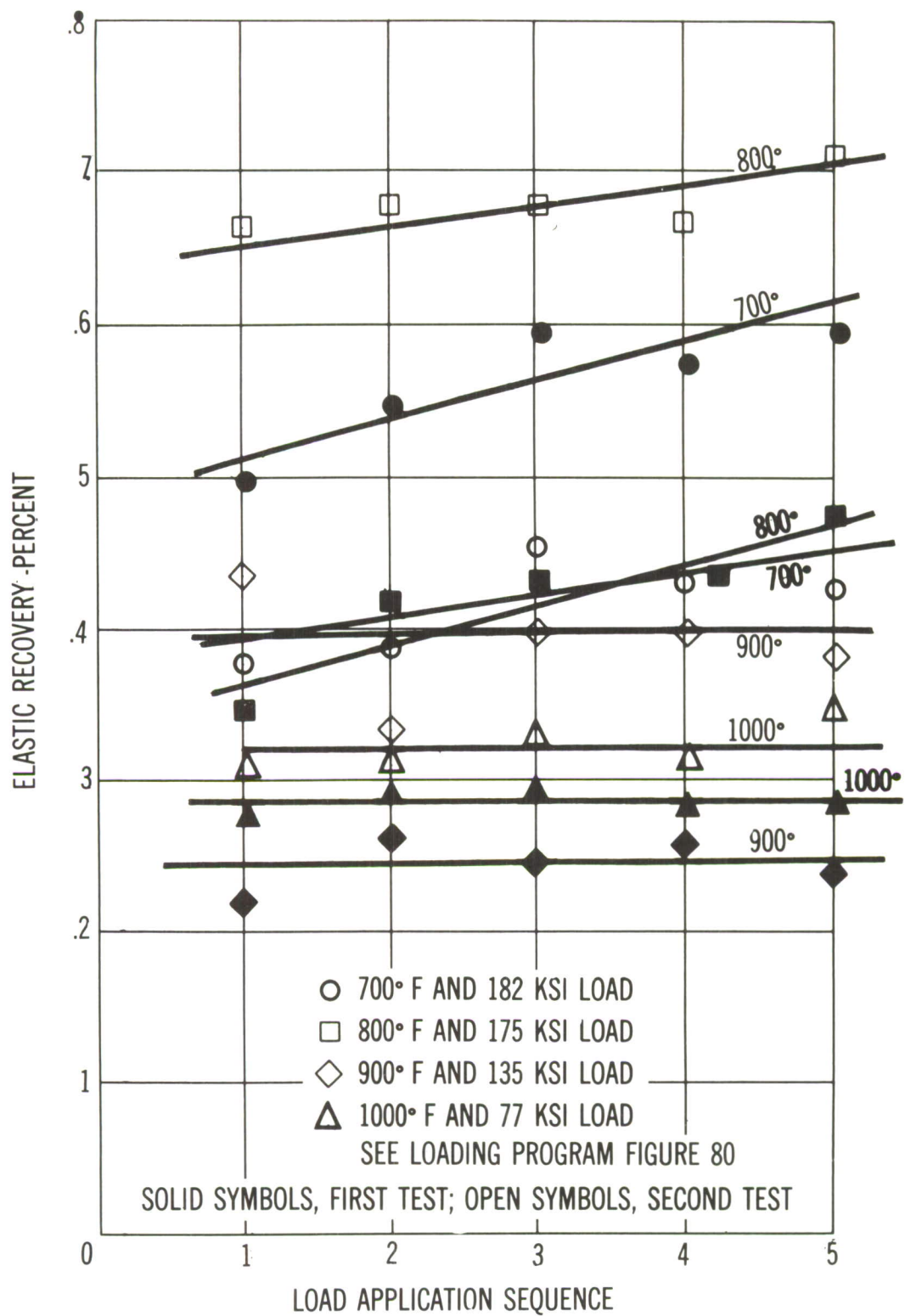


Figure 94. Elastic Recovery Accumulation Observed in Repeated Load Tests Run at Various Temperatures.

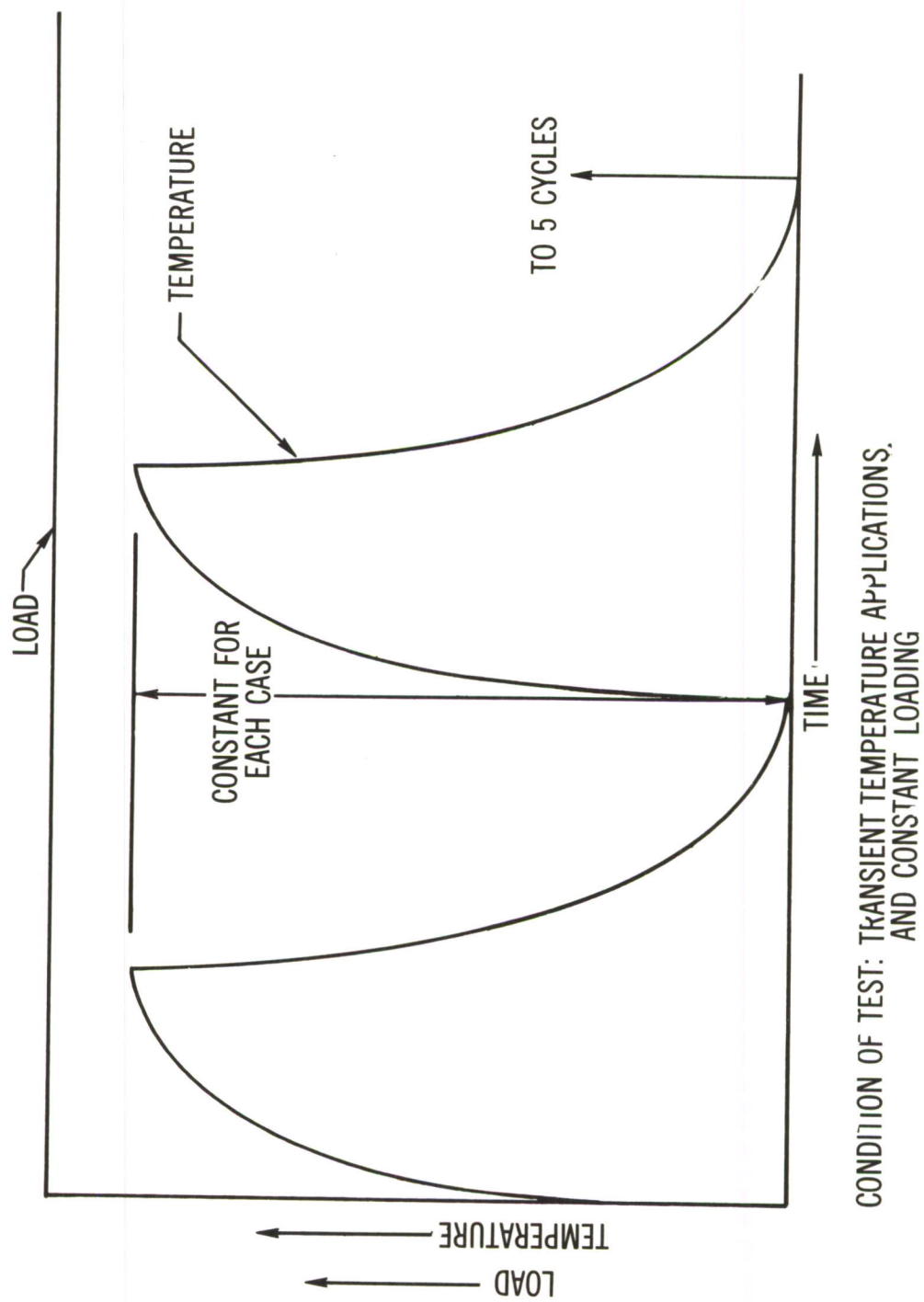


Figure 95. Program for Transient Heating Tests.

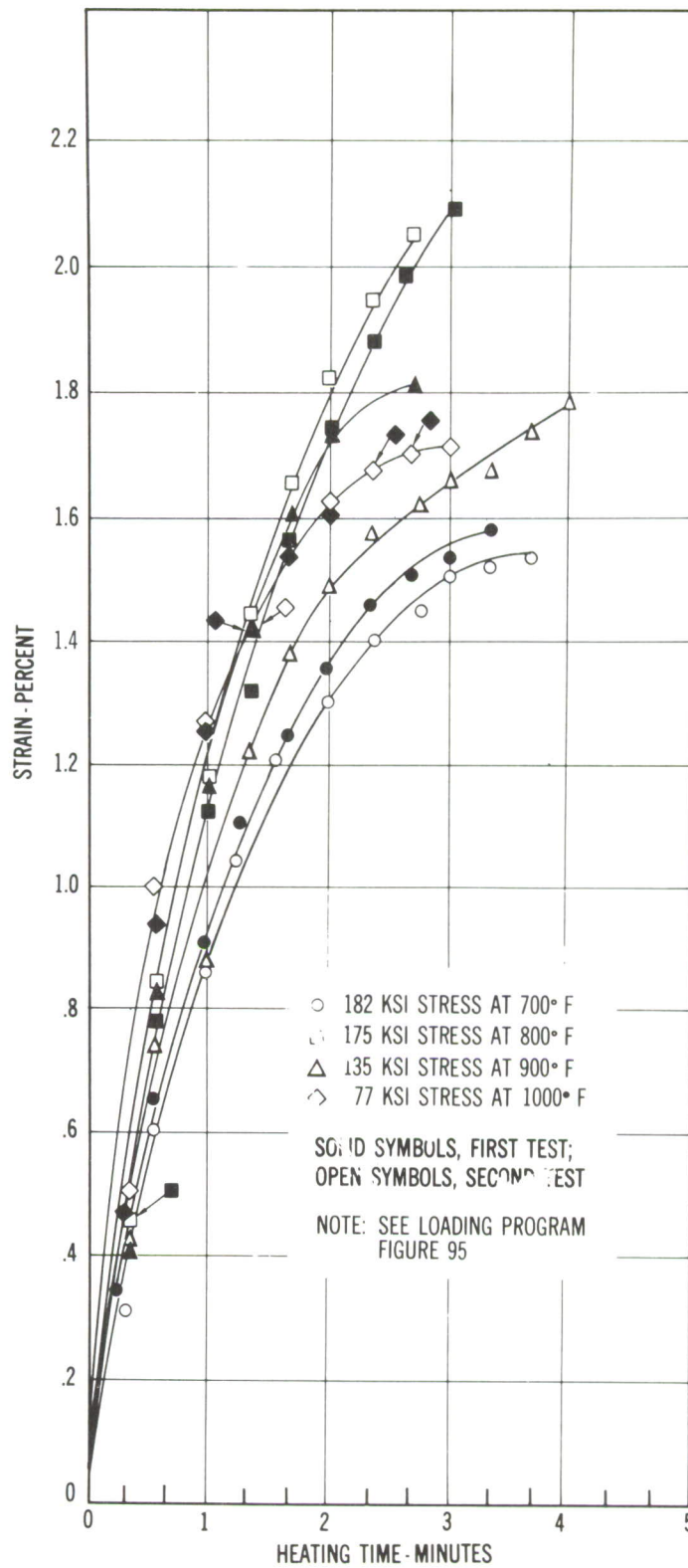


Figure 96. Initial Cycle, Transient Heating Creep Curves.

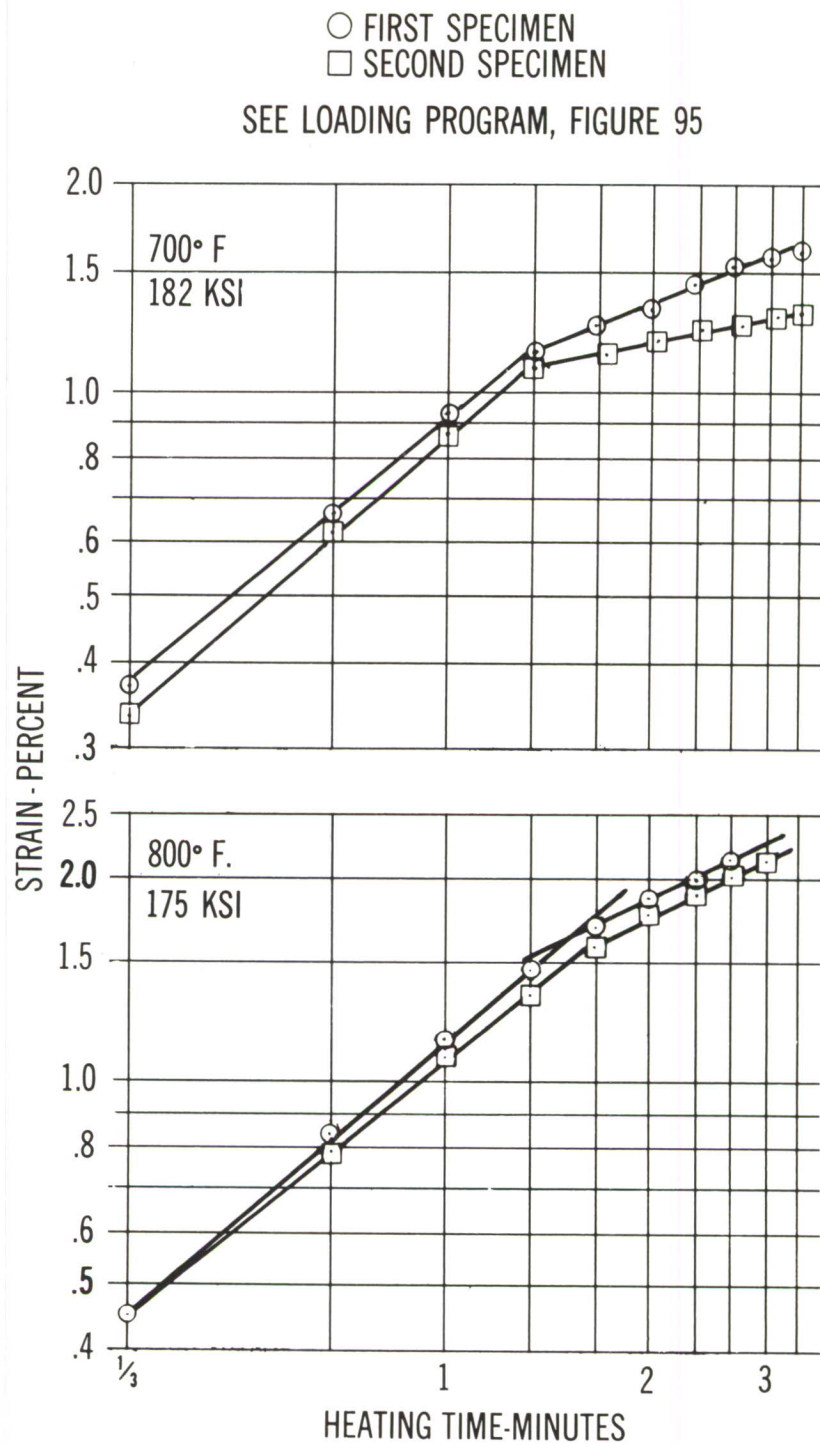


Figure 97. Initial Cycle, Transient Heating Creep Curves (Logarithmic 700° and 800°F).

○ FIRST SPECIMEN
 □ SECOND SPECIMEN

SEE LOADING PROGRAM FIGURE 95

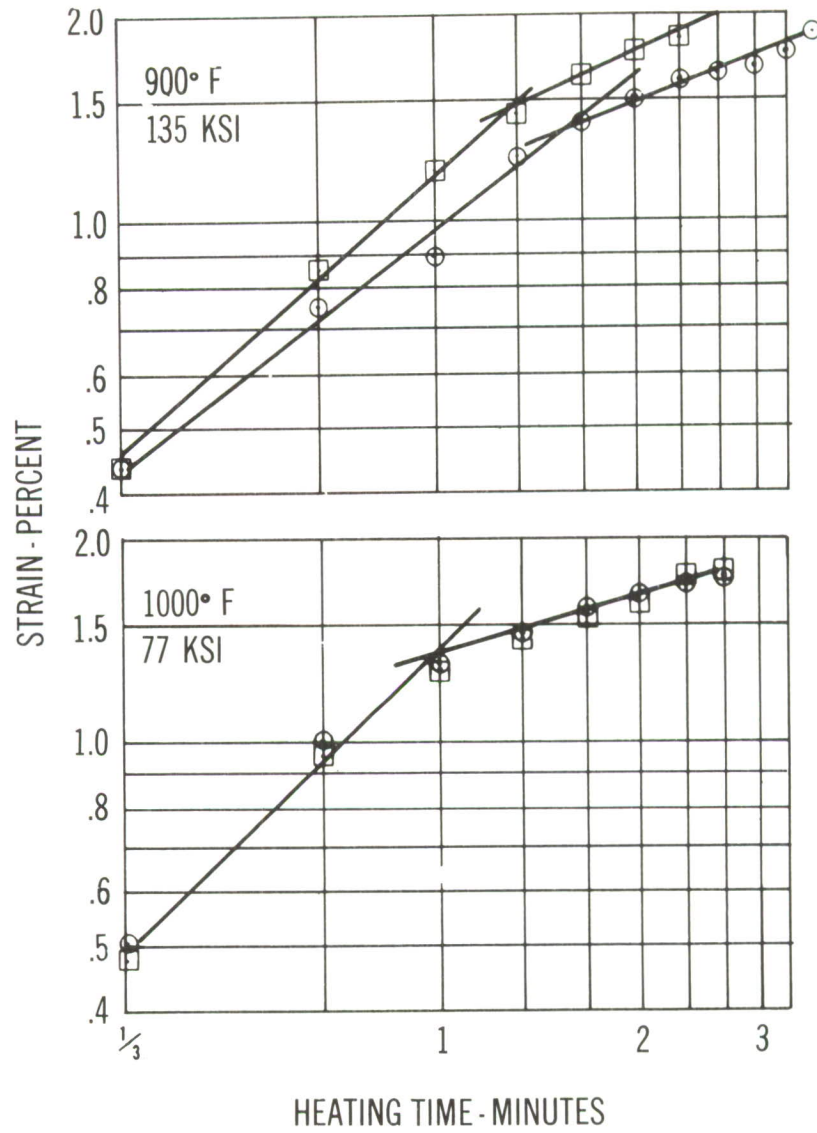


Figure 98. Initial Cycle Transient Heating Creep Curves (Logarithmic 900° and 1000° F)

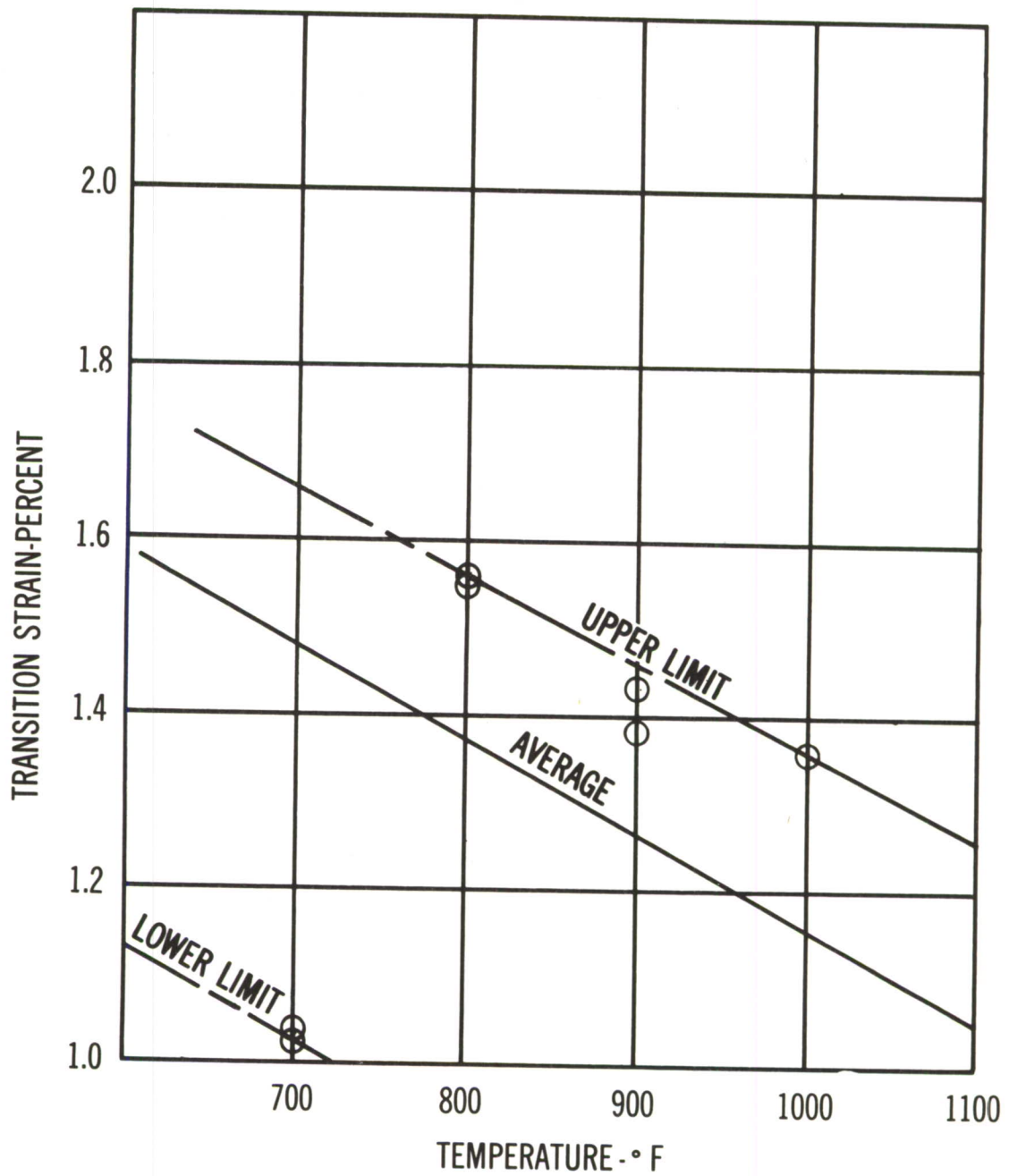


Figure 99. Strain Transition - Temperature Relations in Initial Transient Heating Cycles.

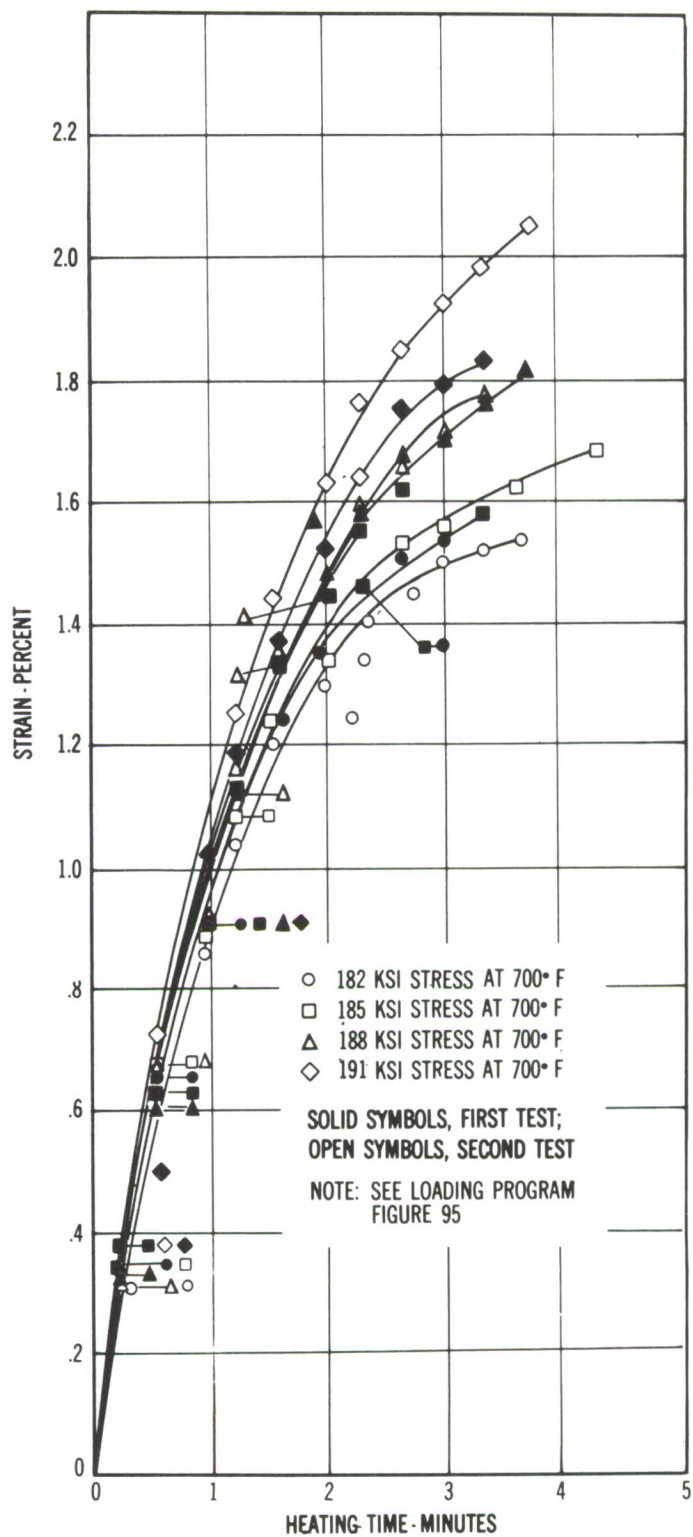


Figure 100. Initial Cycle Transient Heating Creep Curves for Constant Temperature, Varying Stress Conditions.

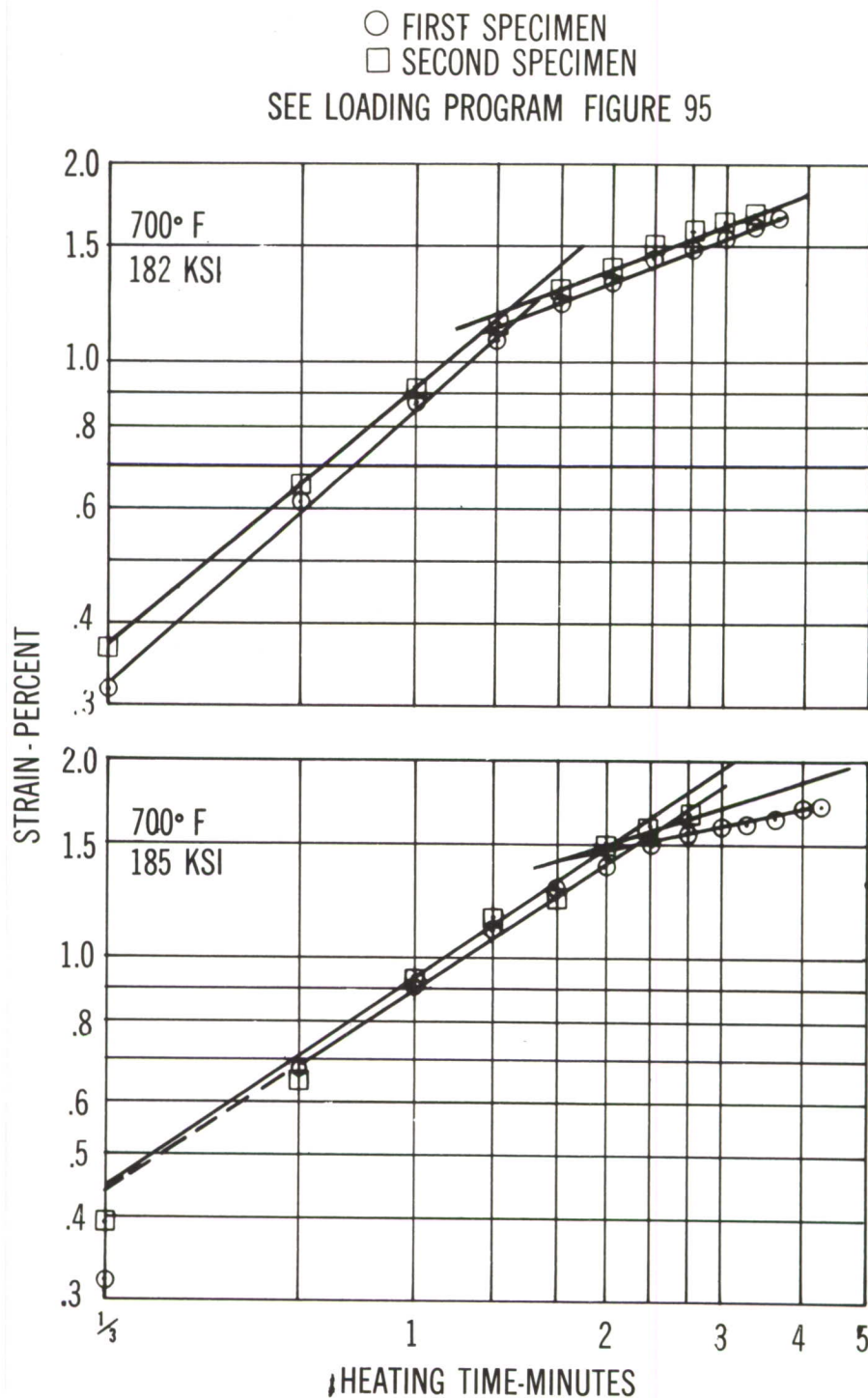


Figure 101. Initial Cycle Transient Heating Creep Curves for Constant Stress, Varying Temperature Conditions (700° F, 182 & 185 KSI).

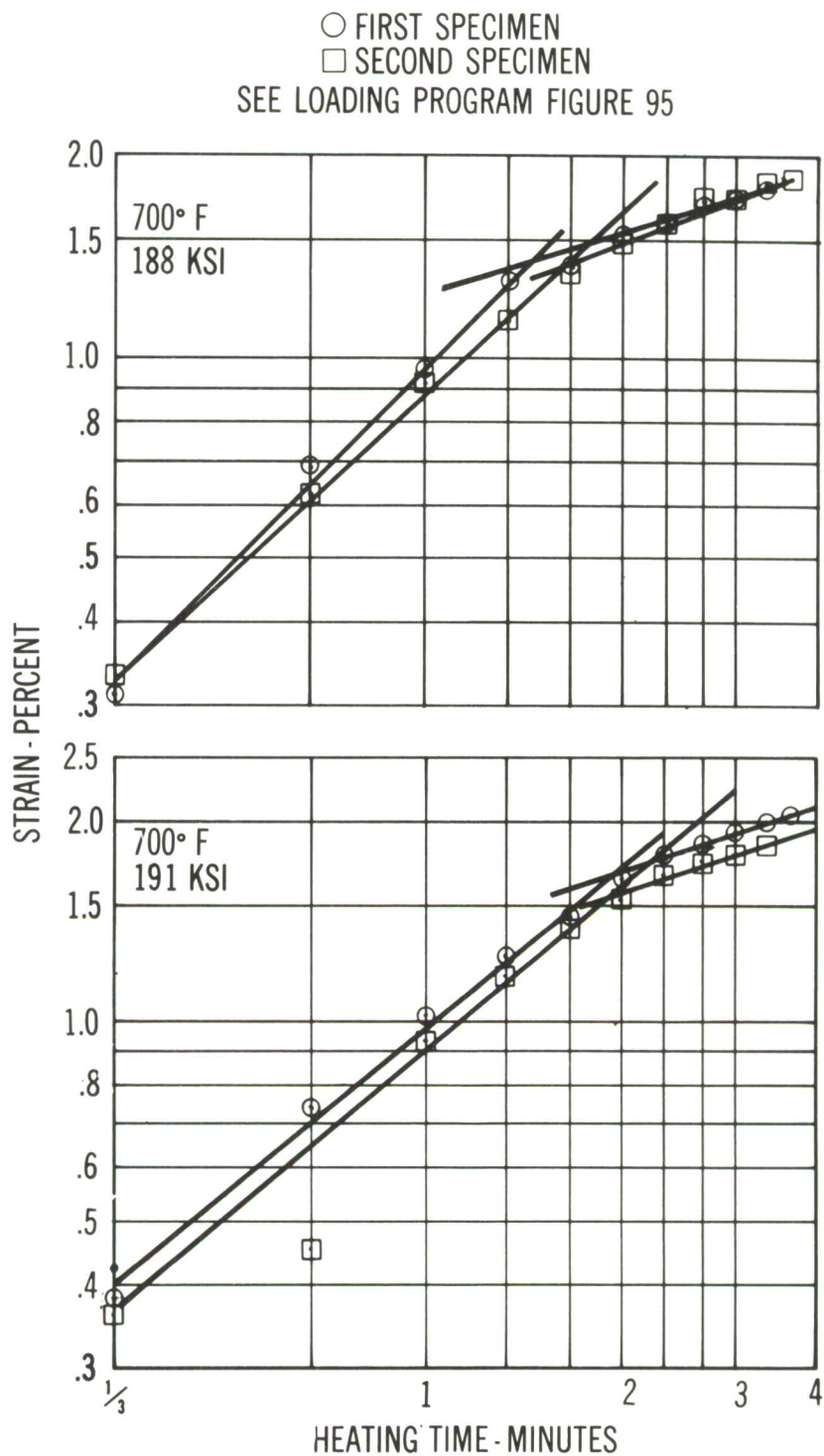


Figure 102. Initial Cycle Transient Heating Creep Curves for Constant Stress, Varying Temperature Conditions (700°F, 188 & 191 KSI).

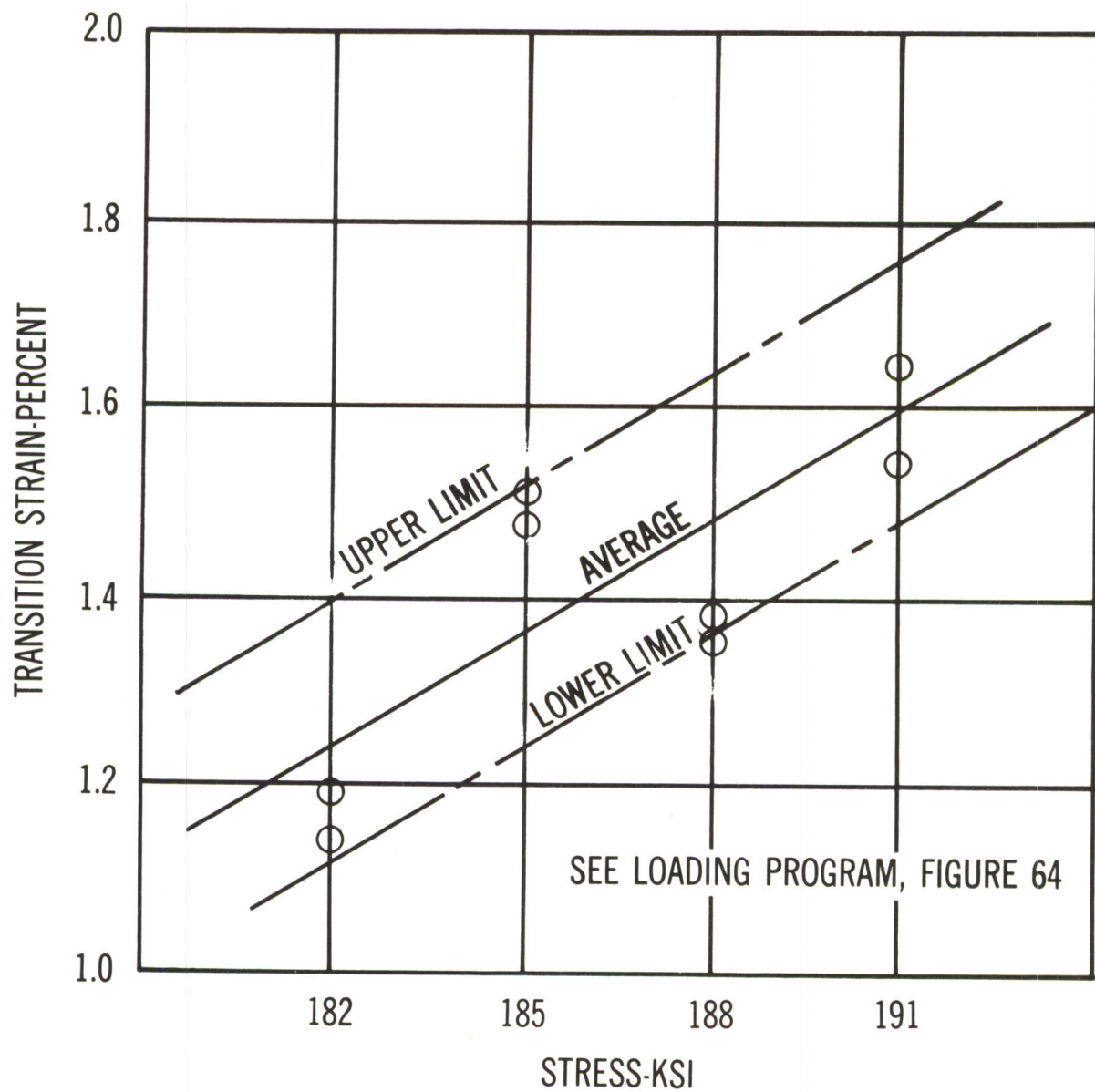


Figure 103. Strain Transition - Temperature Relations in Initial Transient Heating Cycles.

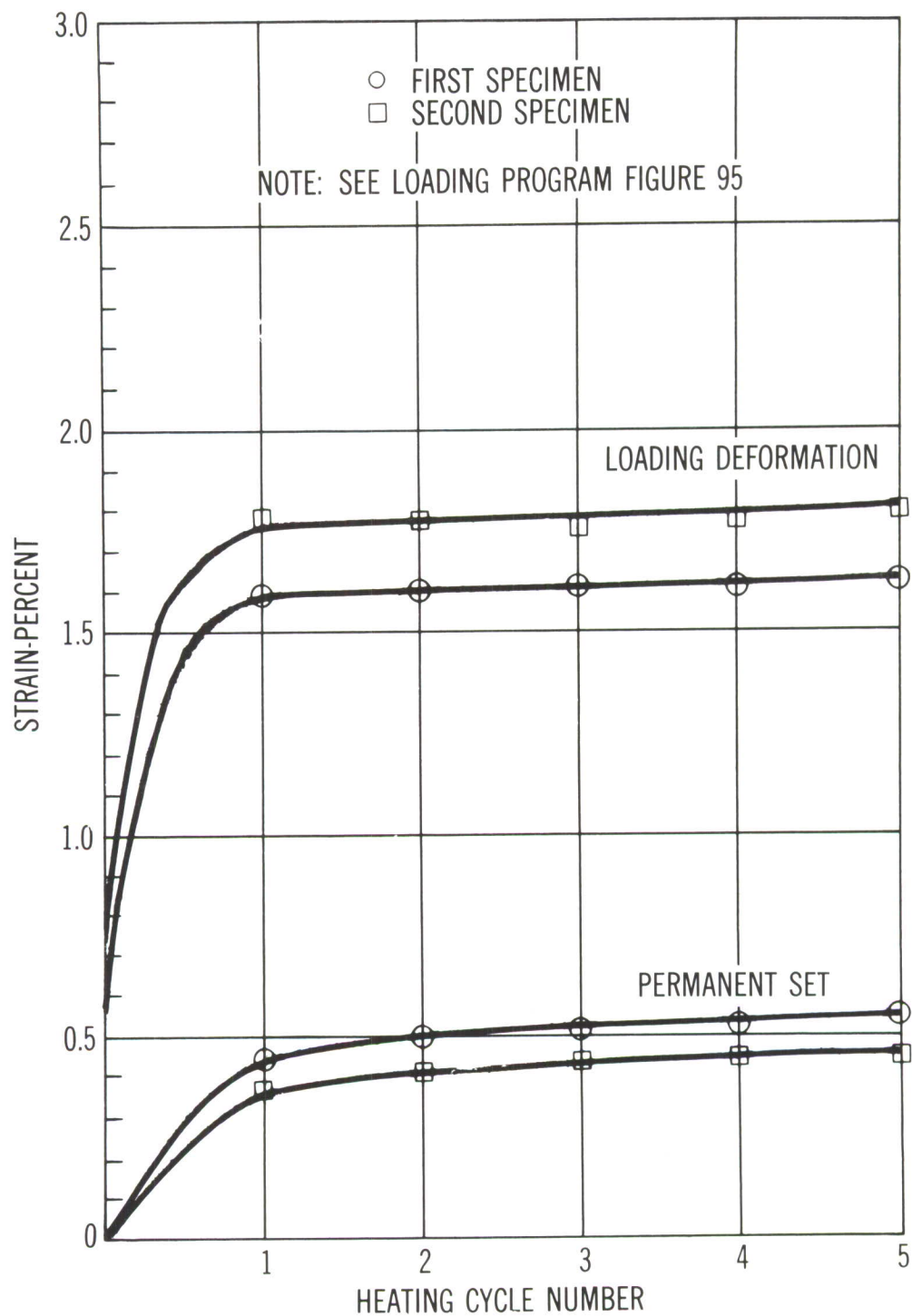


Figure 104. Transient Heating Creep Curves (700°F, 182 KSI)

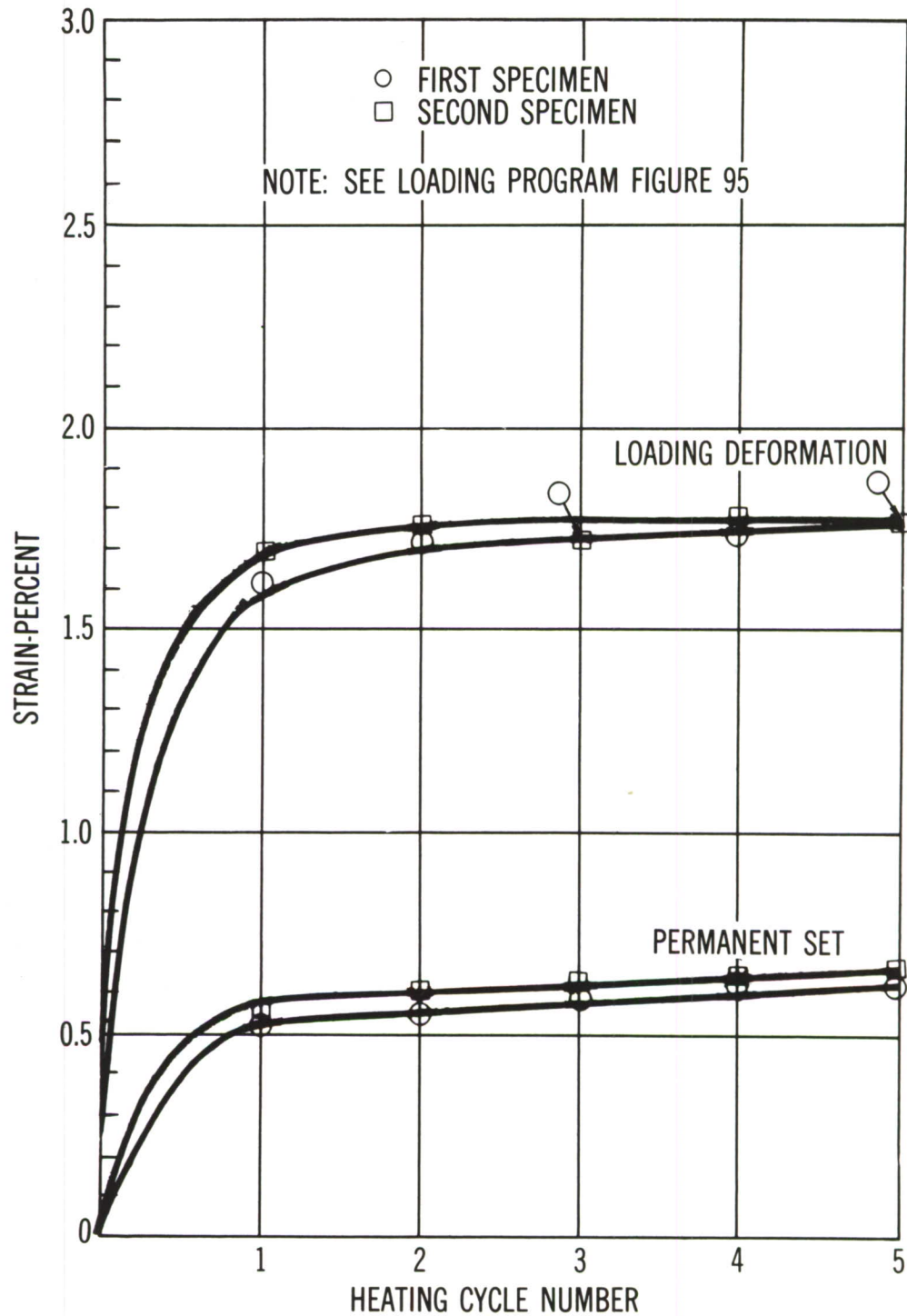


Figure 105. Transient Heating Creep Curves (700°F, 185 KSI)

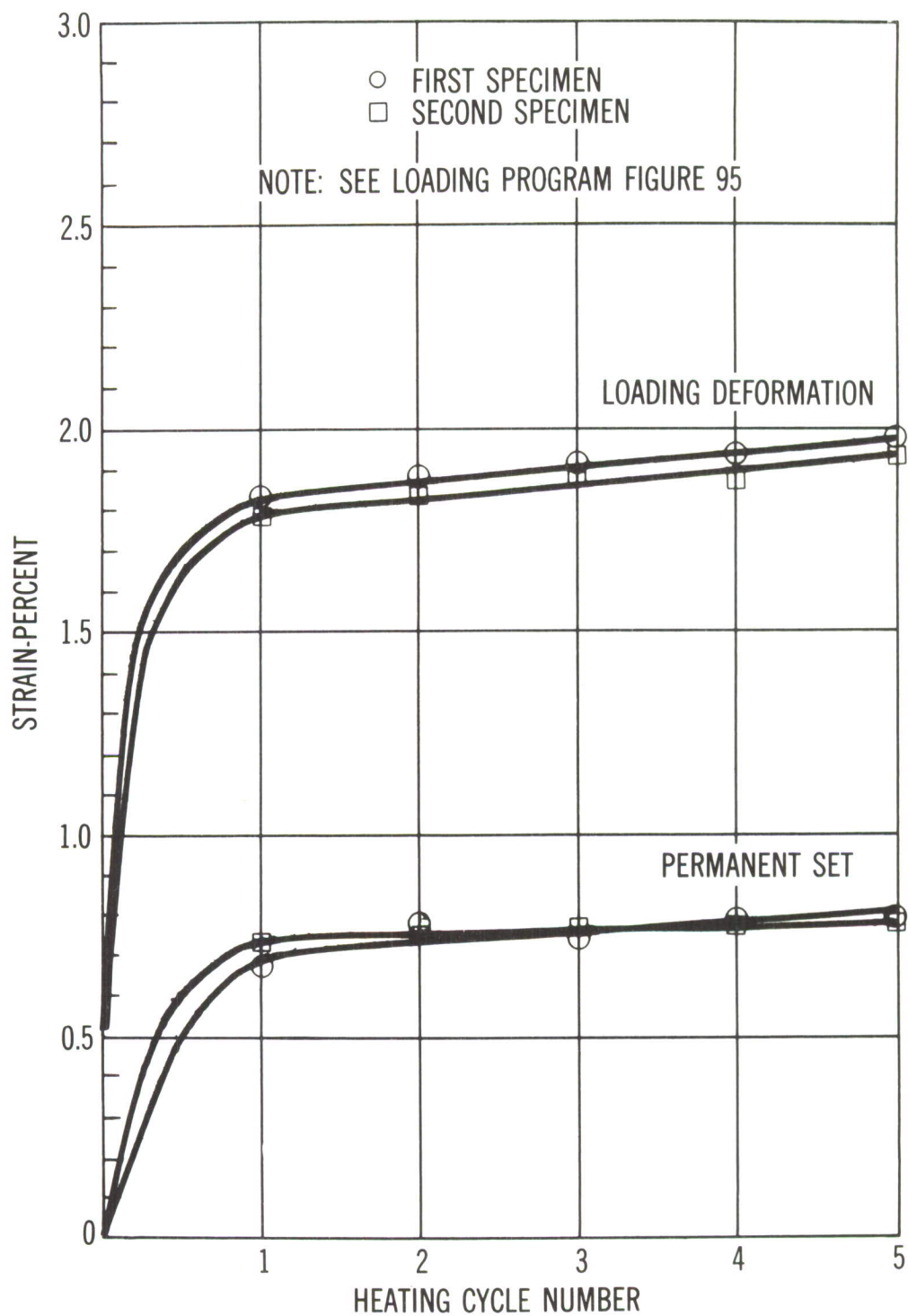


Figure 106. Transient Heating Creep Curves (700°F, 188 KSI)

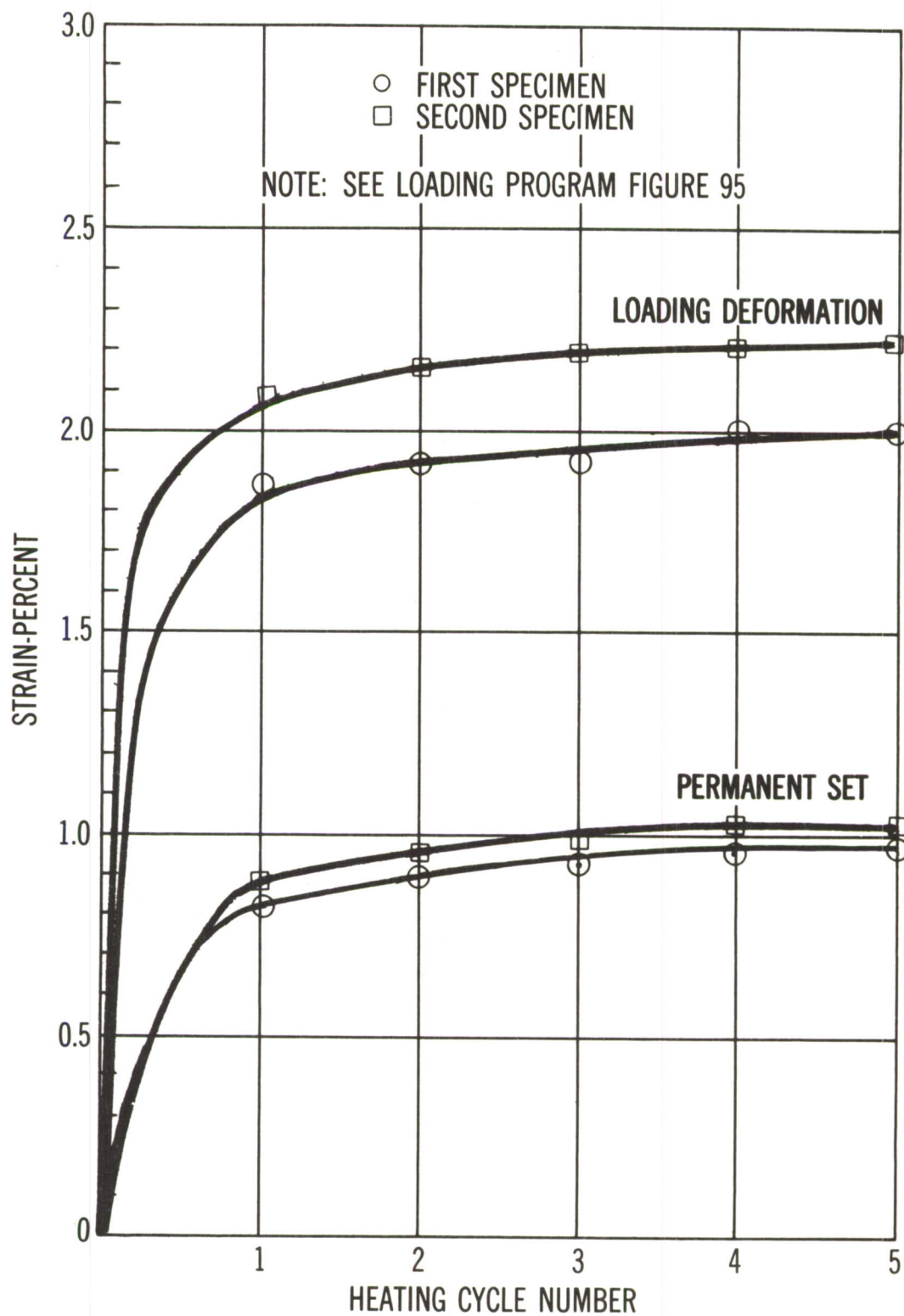


Figure 107. Transient Heating Creep Curves (700°F, 191 KSI)

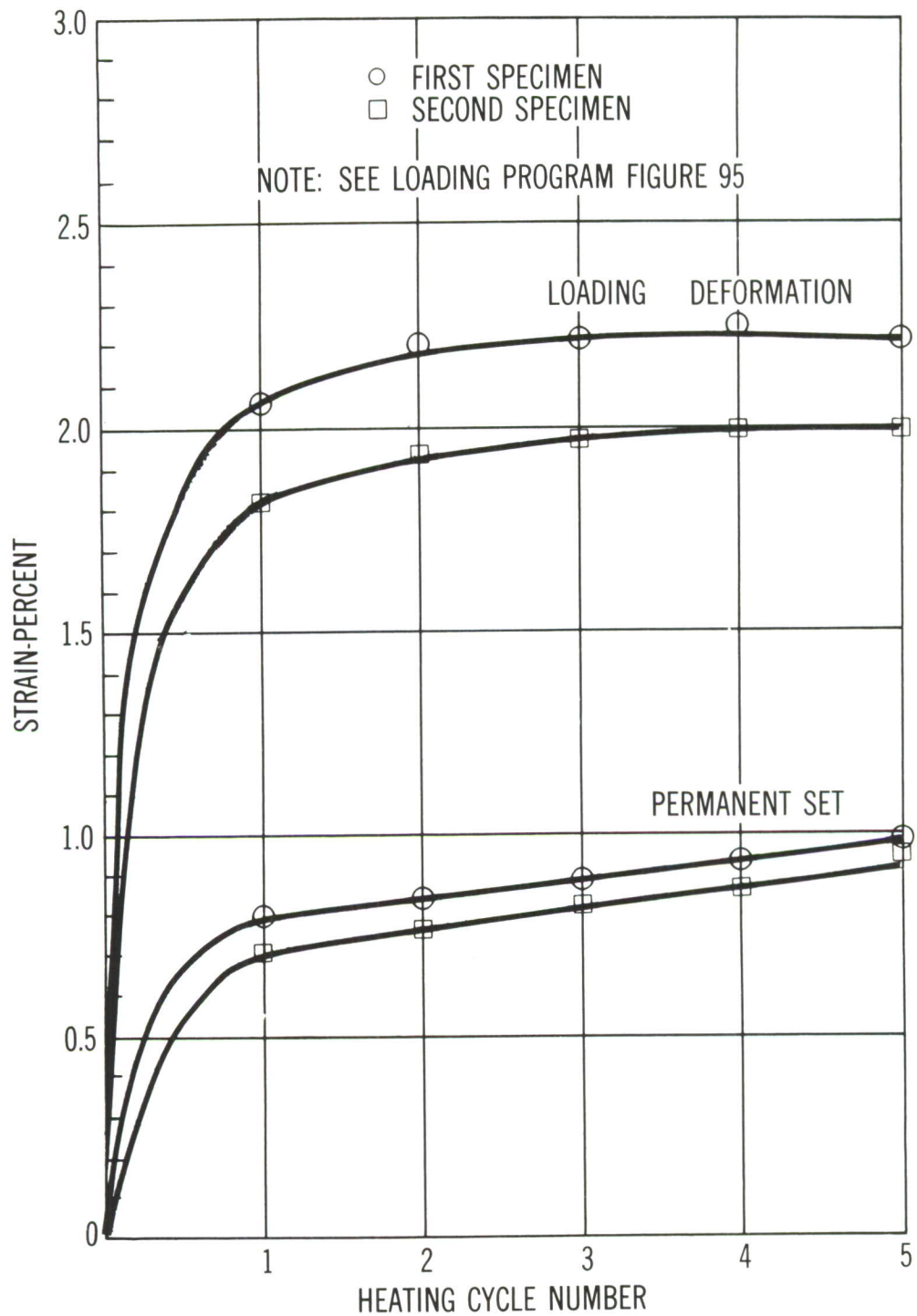


Figure 108. Transient Heating Creep Curves (800°F, 175 KSI)

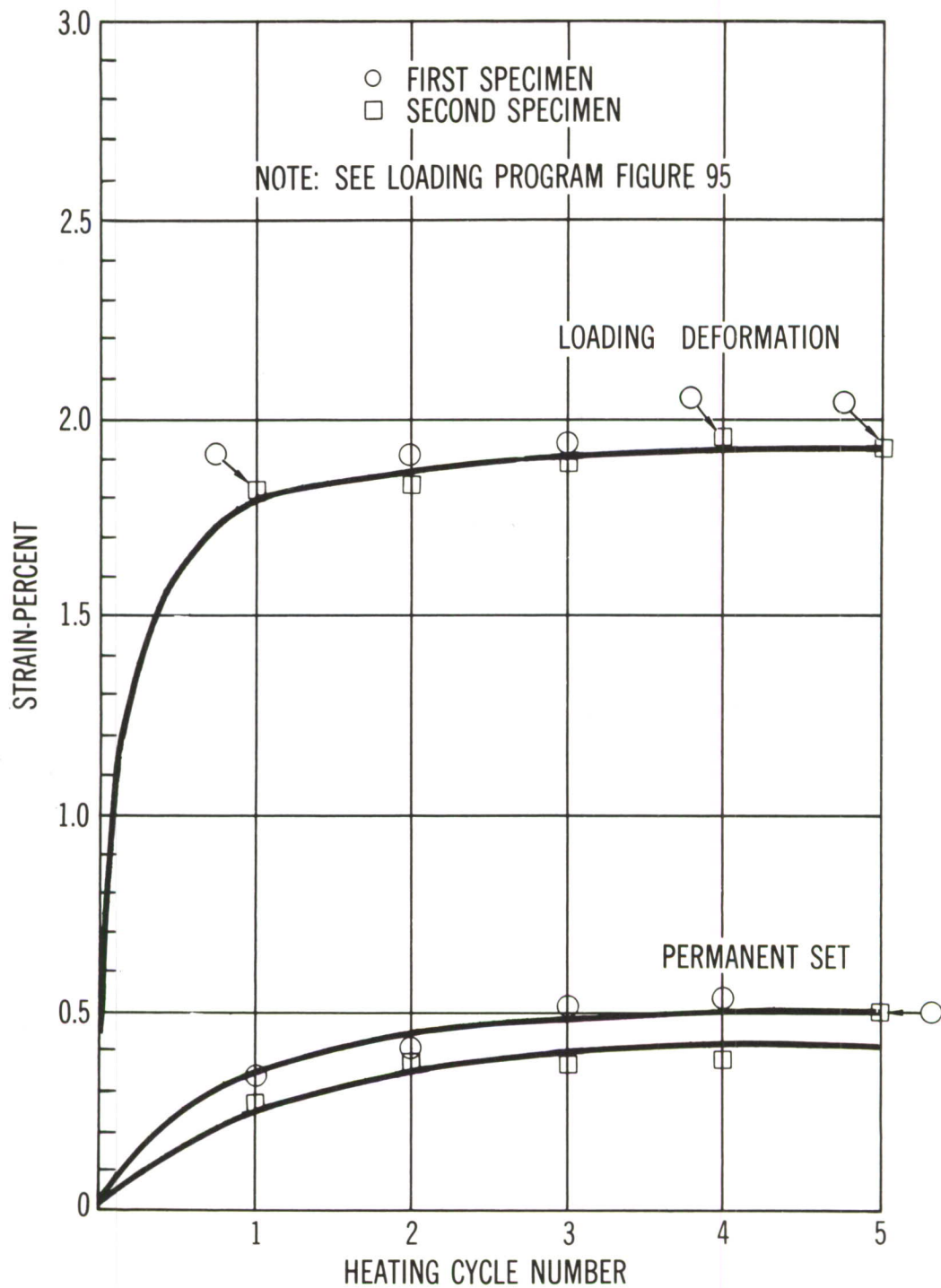


Figure 109. Transient Heating Creep Curves (900°F, 135 KSI)

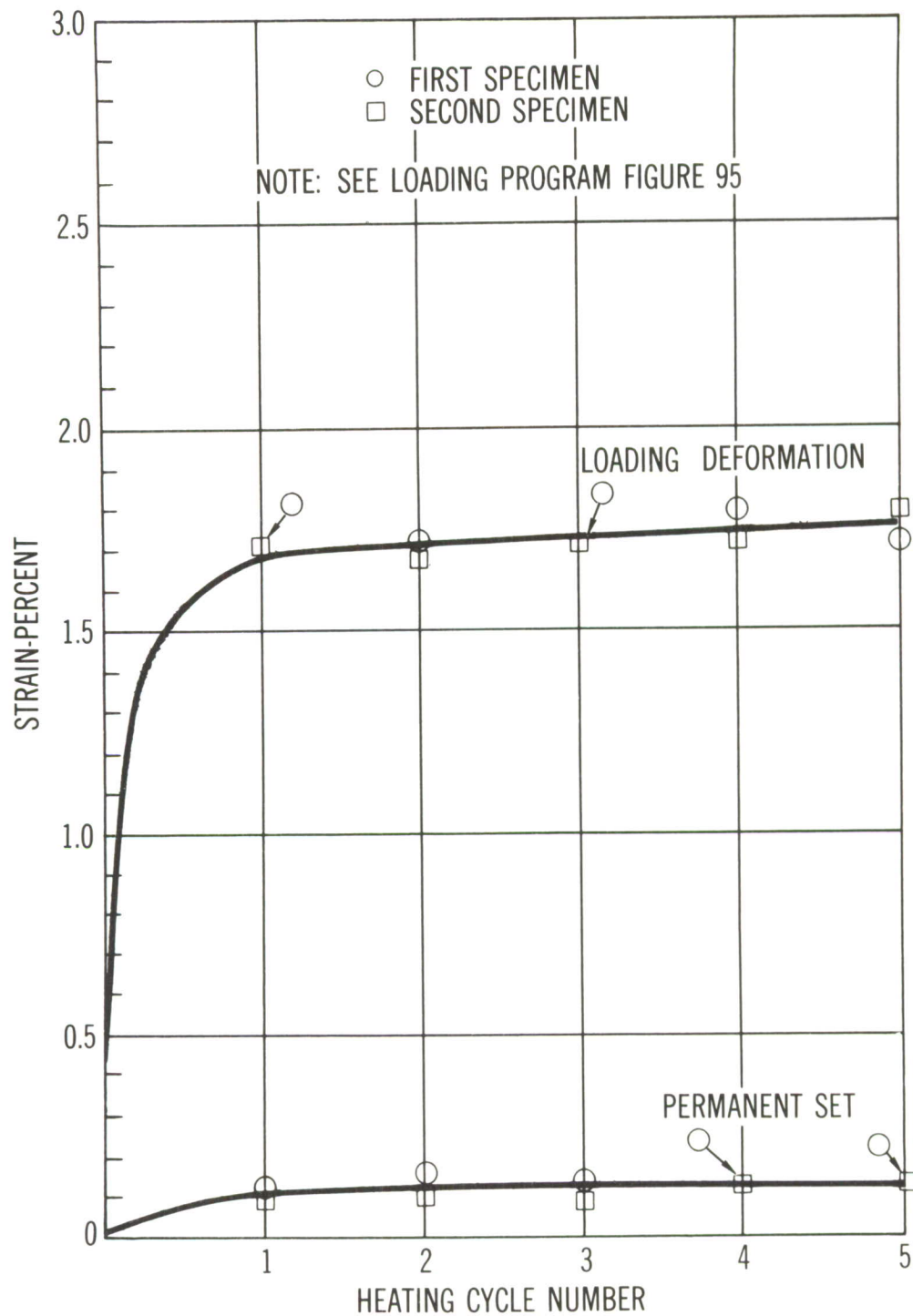
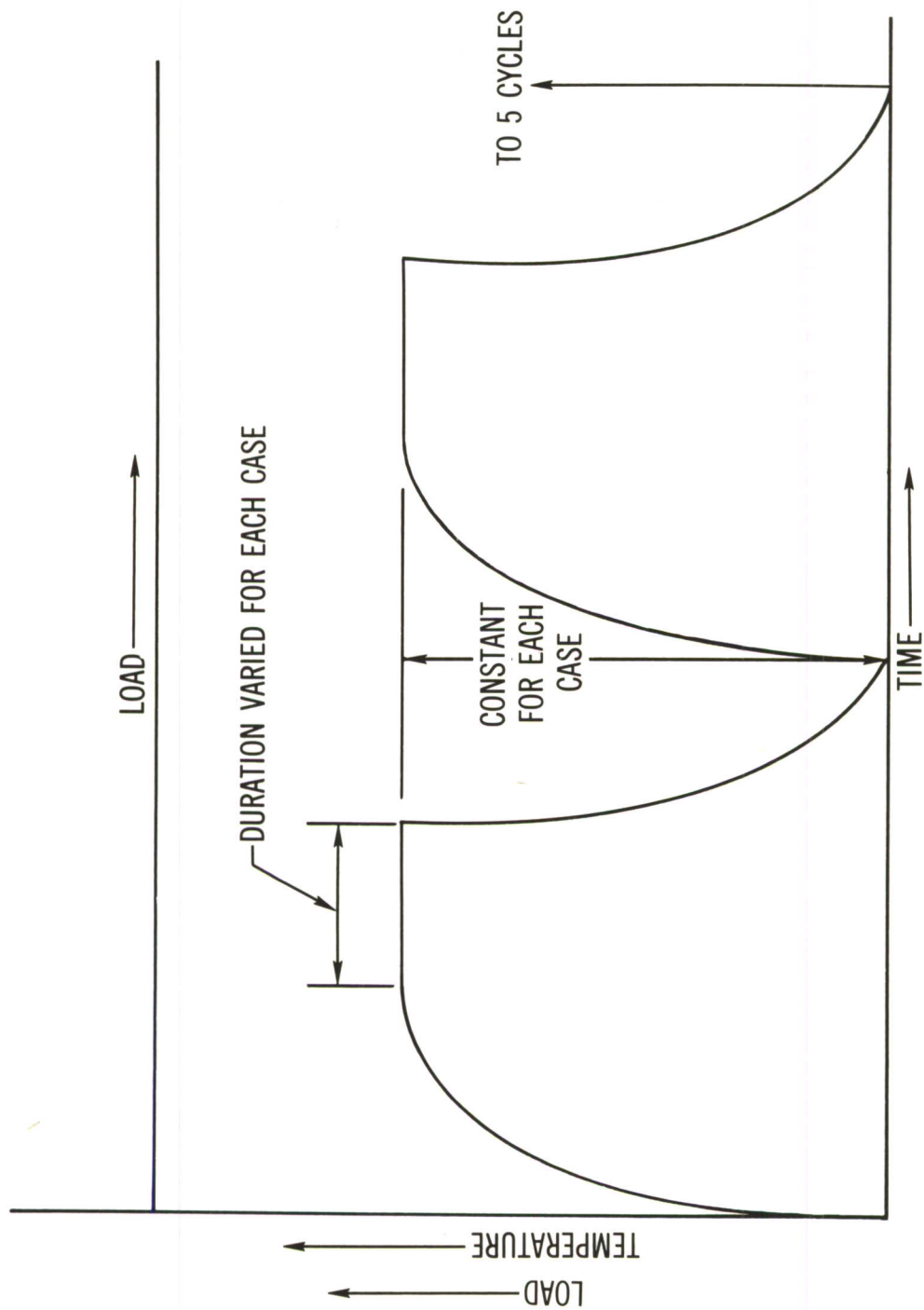


Figure 110. Transient Heating Creep Curves (1000°F, 77 KSI)



CONDITION OF TEST: PULSED TEMPERATURE APPLICATIONS
AND CONSTANT LOADING

Figure 111. Program for Pulsed Heating Tests.

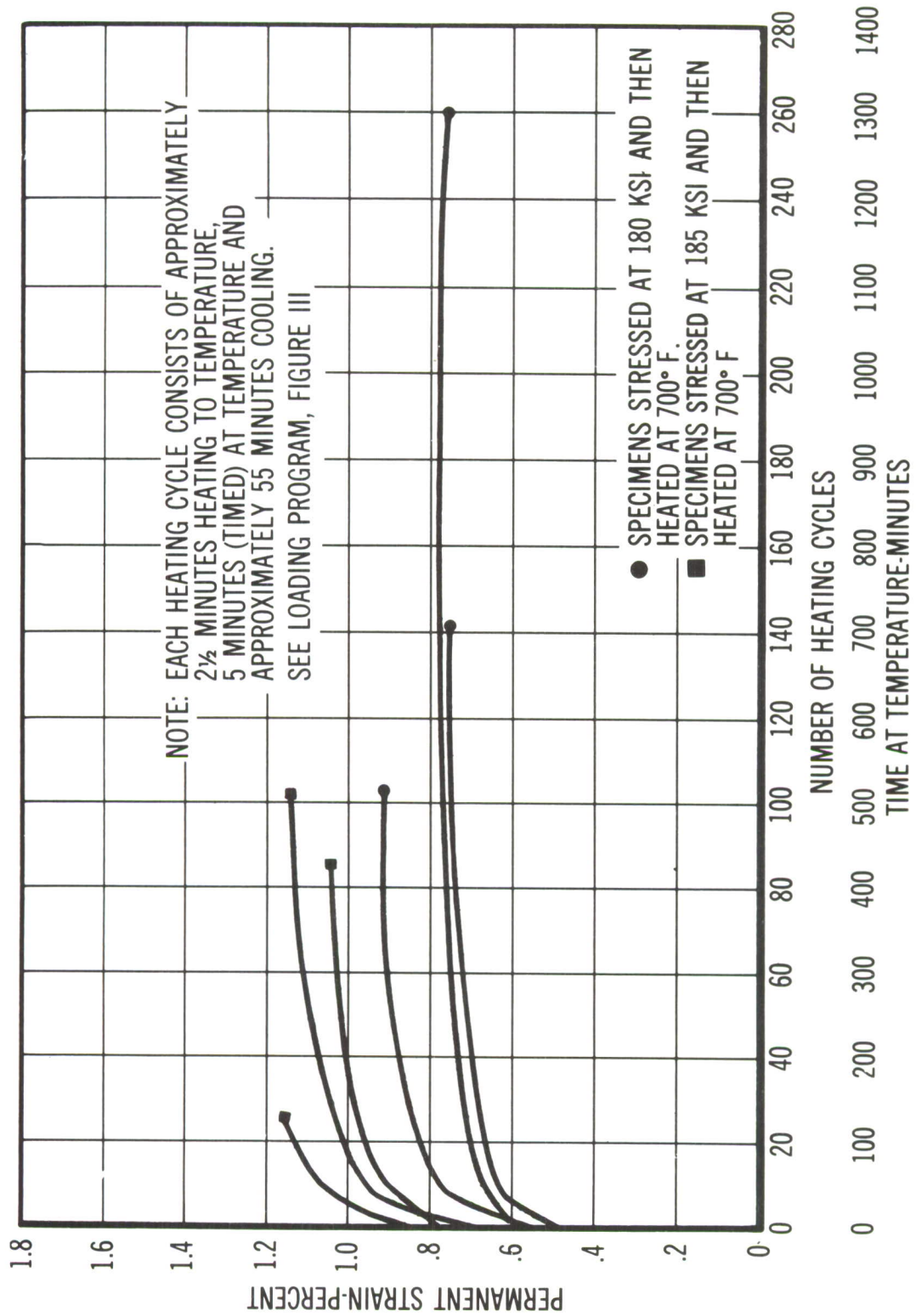


Figure 112. Pulsed Heating Creep Curves (700°F).

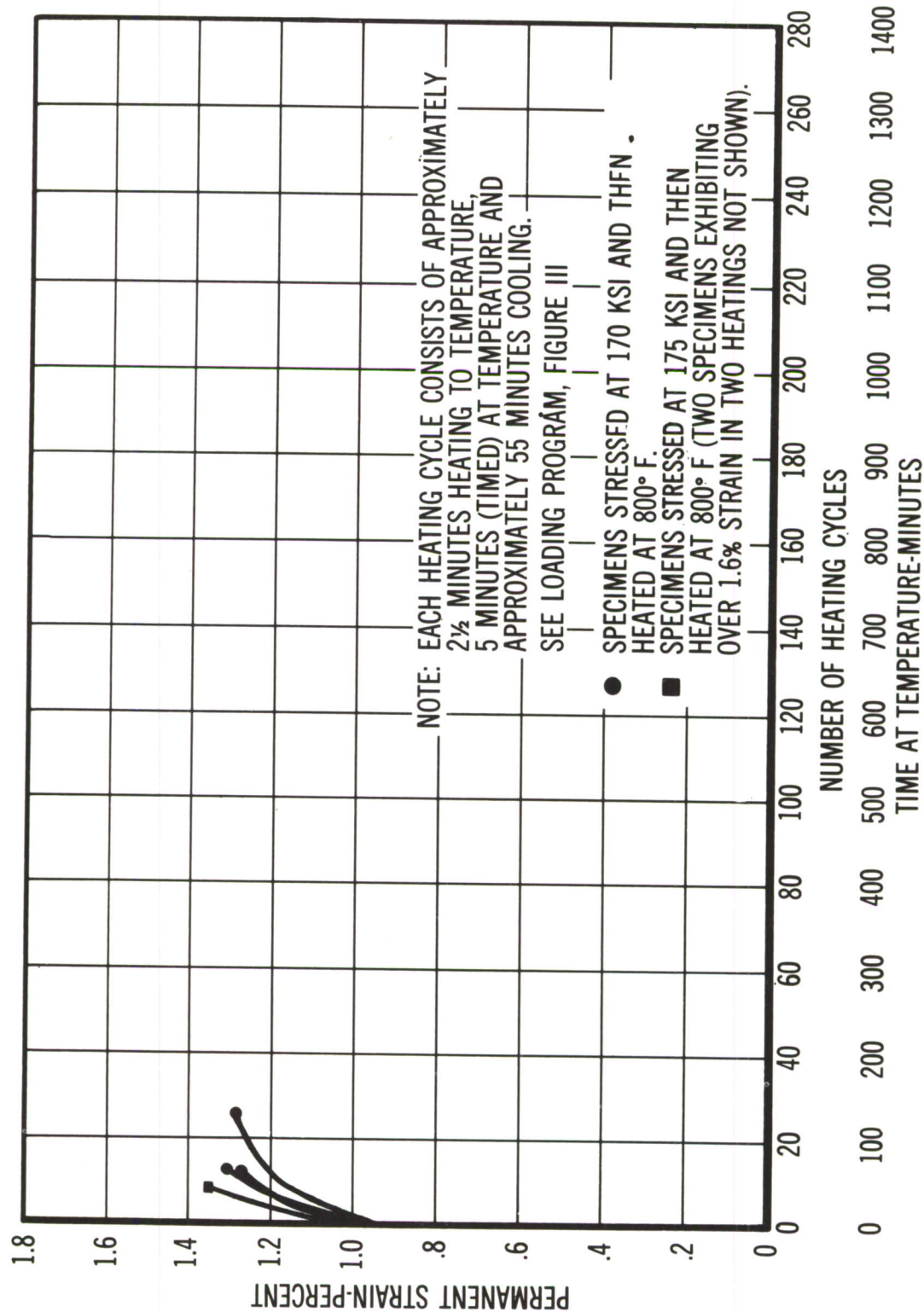


Figure 113. Pulsed Heating Creep Curves (800°F).

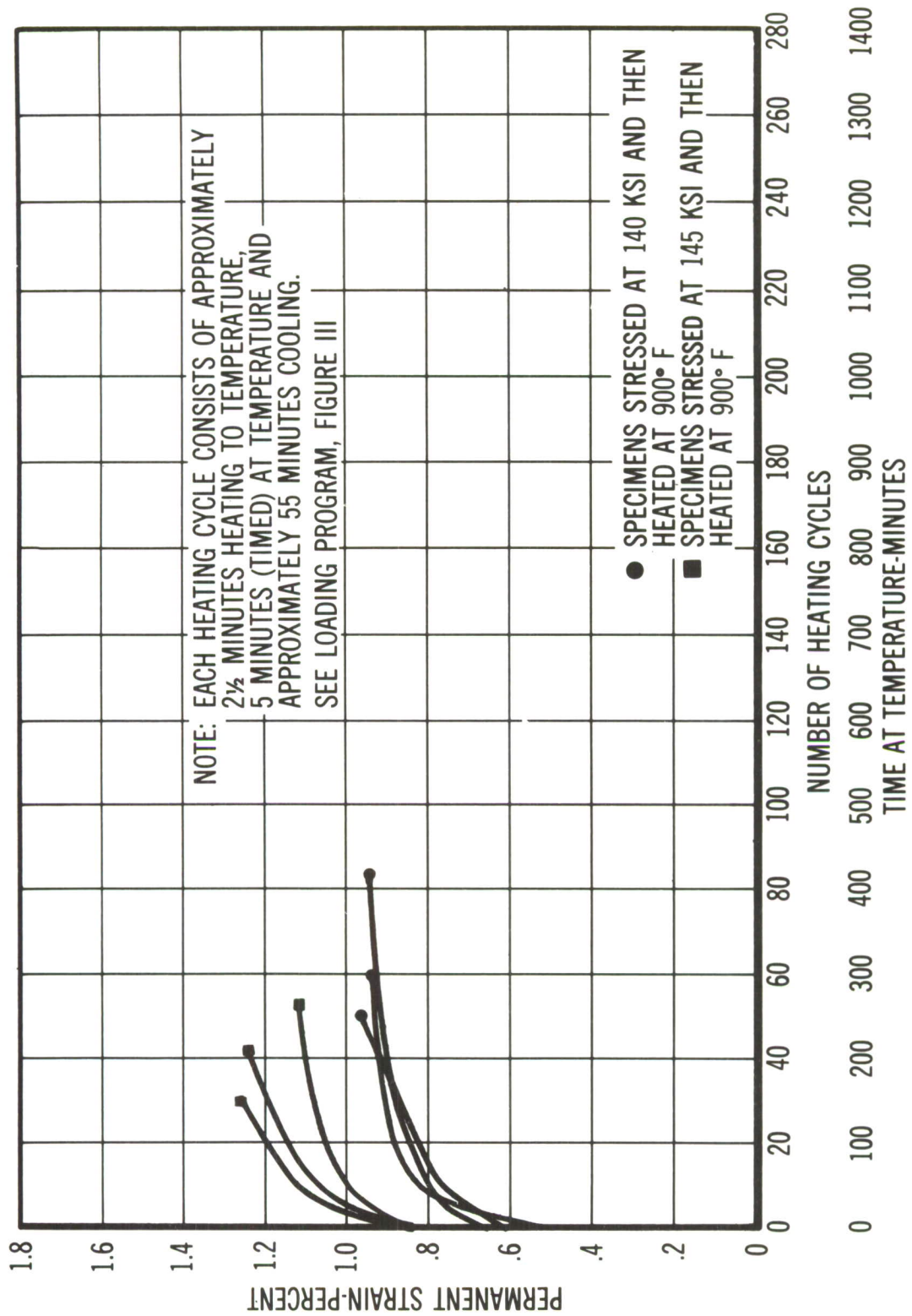


Figure 114. Pulsed Heating Creep Curves (900°F).

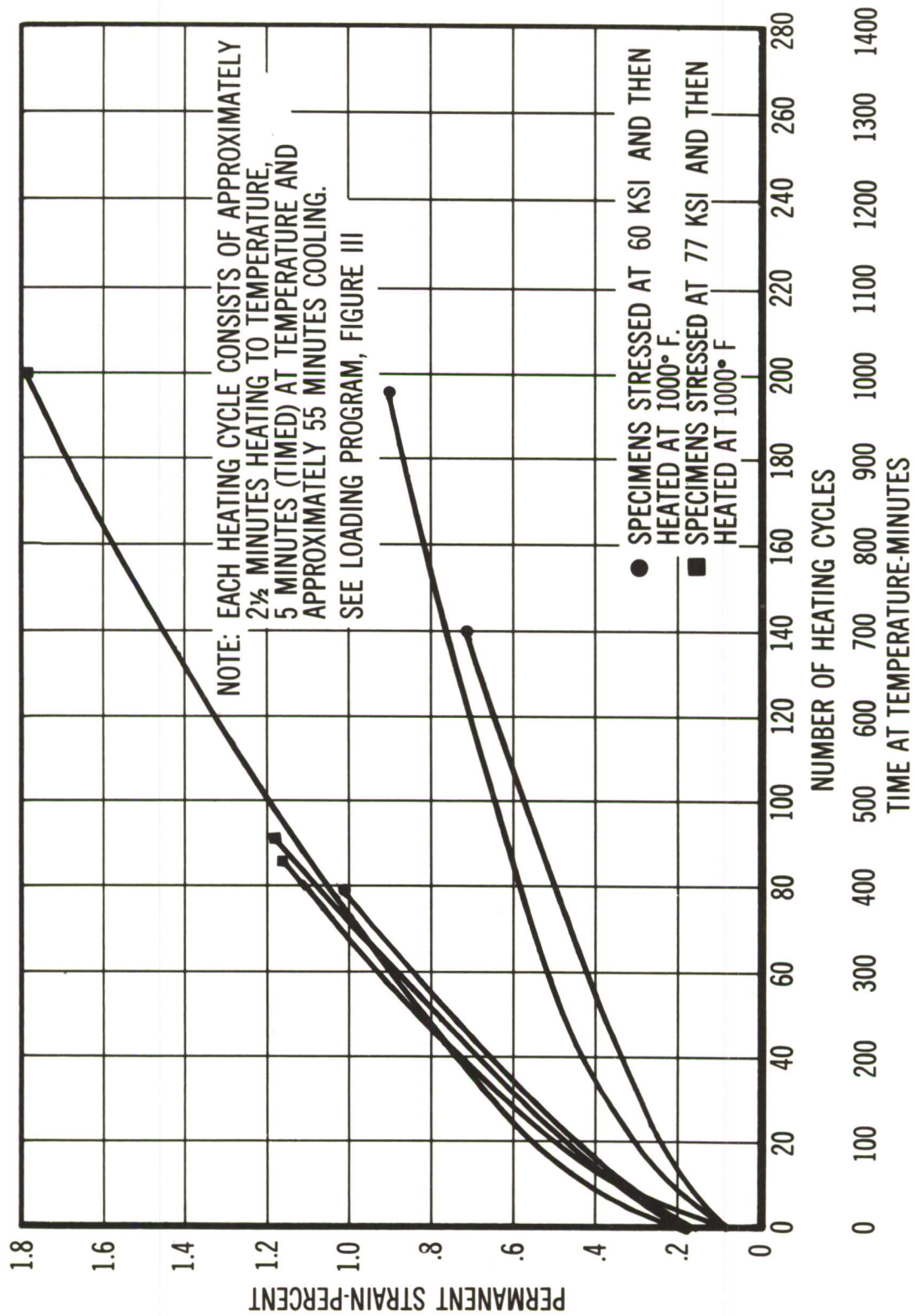


Figure 115. Pulsed Heating Creep Curves (1000°F)

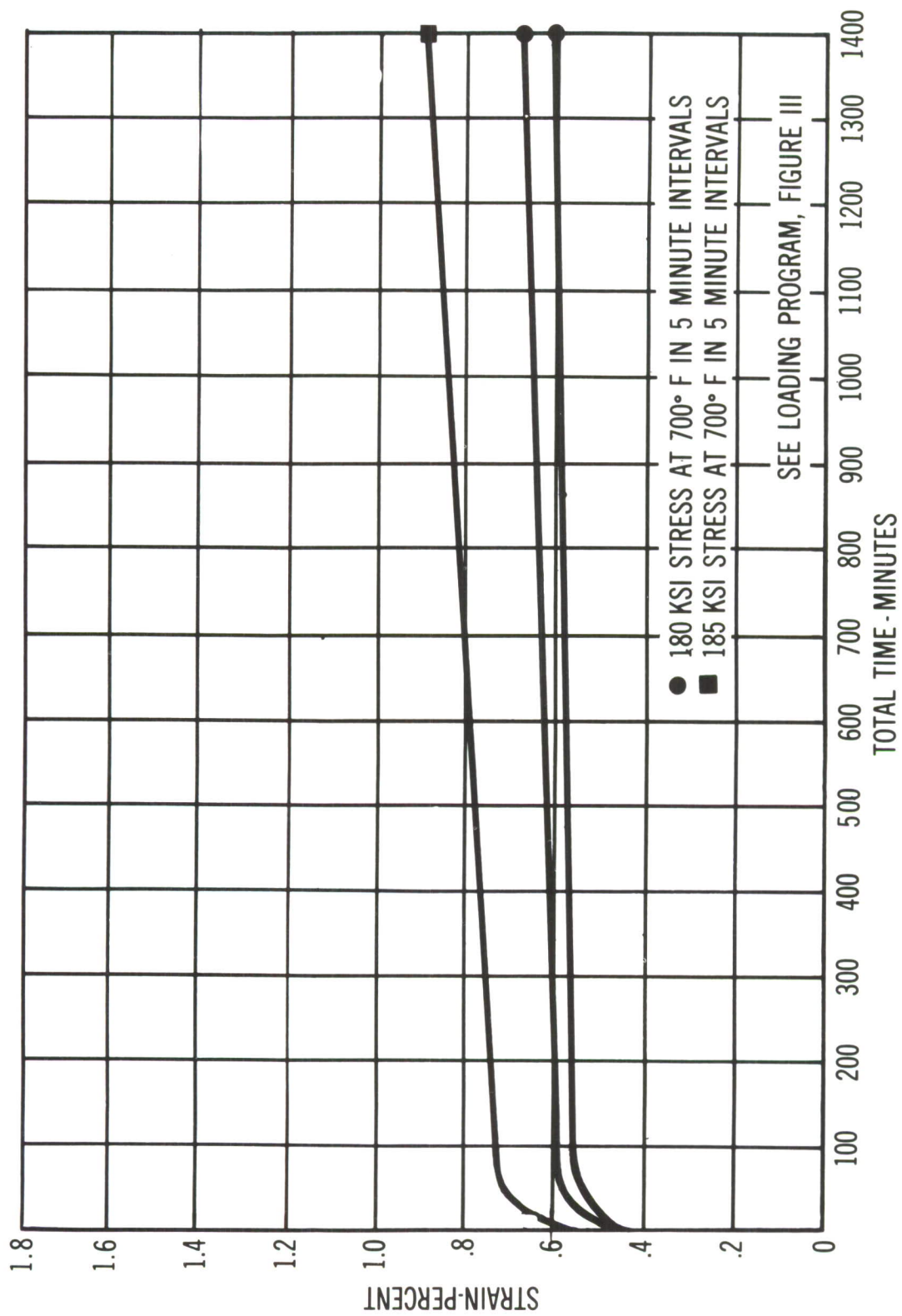


Figure 116. Effect of Stress Variation at 700°F Upon 5 Minute Pulsed Heating Creep.

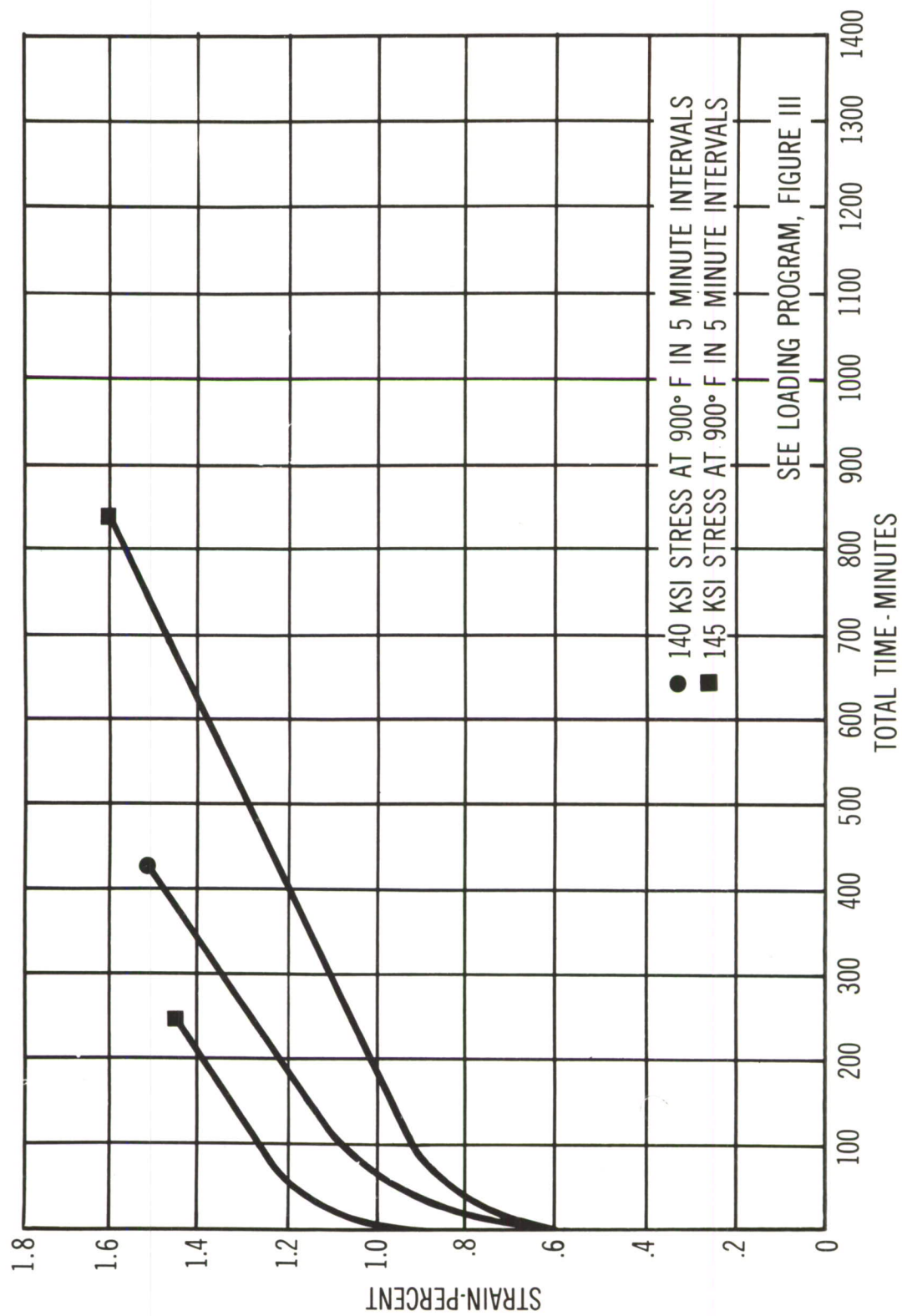


Figure 117. Effect of Stress Variation at 900°F Upon 5 Minute Pulsed Heating Creep.

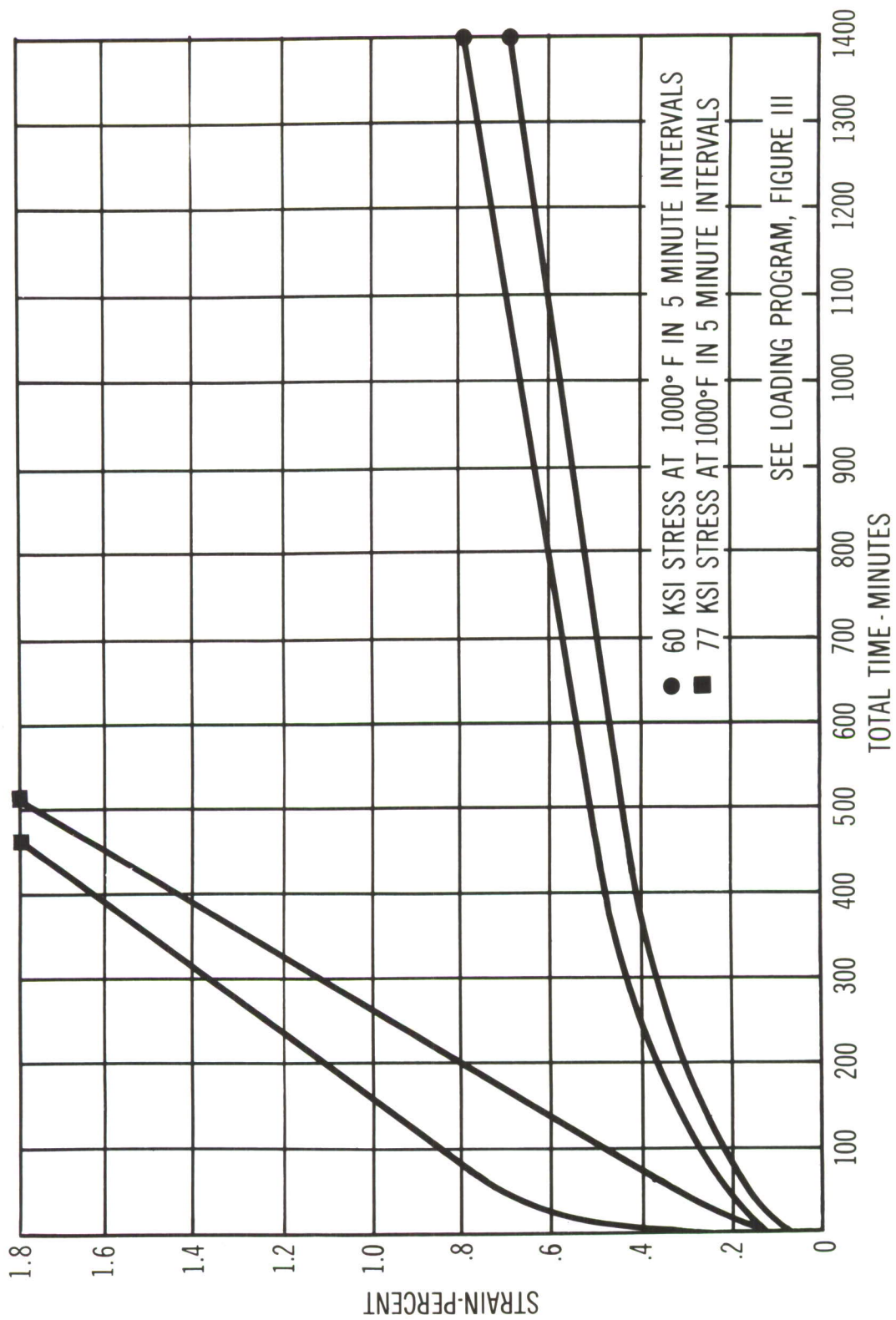


Figure 118. Effect of Stress Variation at 1000°F Upon 5 Minute Pulsed Heating Creep.

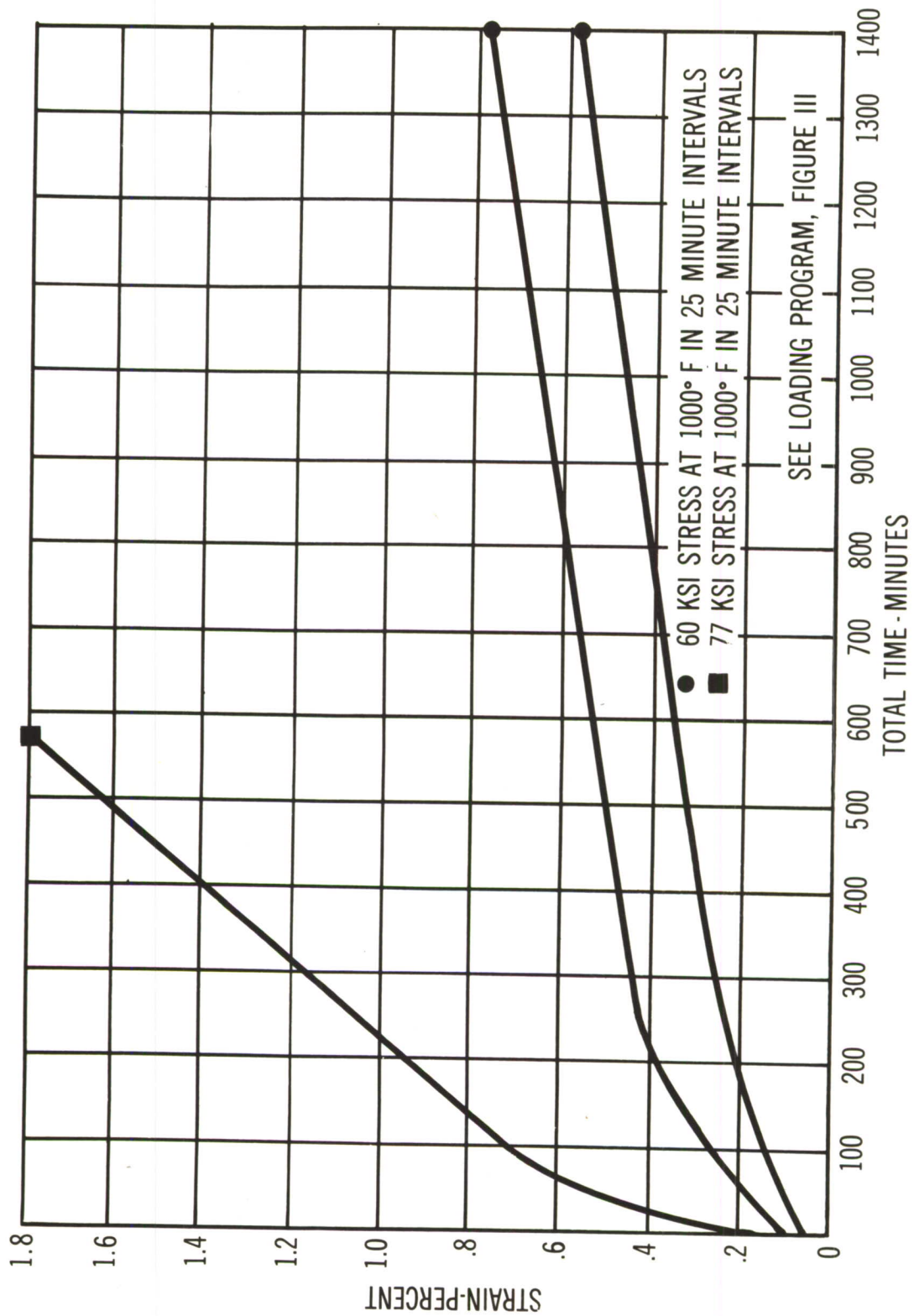


Figure 119. Effect of Stress Variation at 1000°F Upon Pulsed Heating Creep.

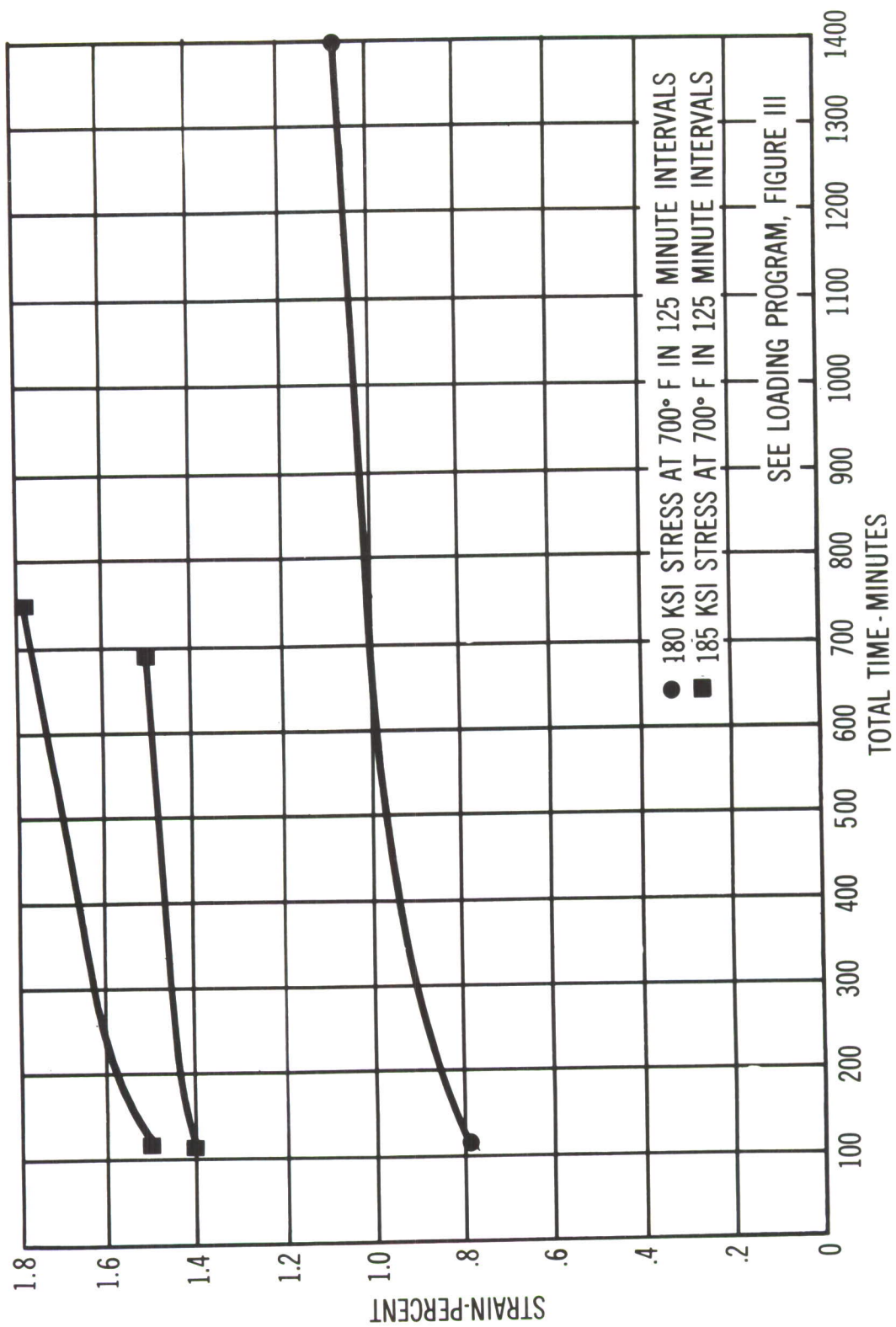


Figure 120. Effect of Stress Variation at 700°F Upon 125 Minute Pulsed Heating Creep.

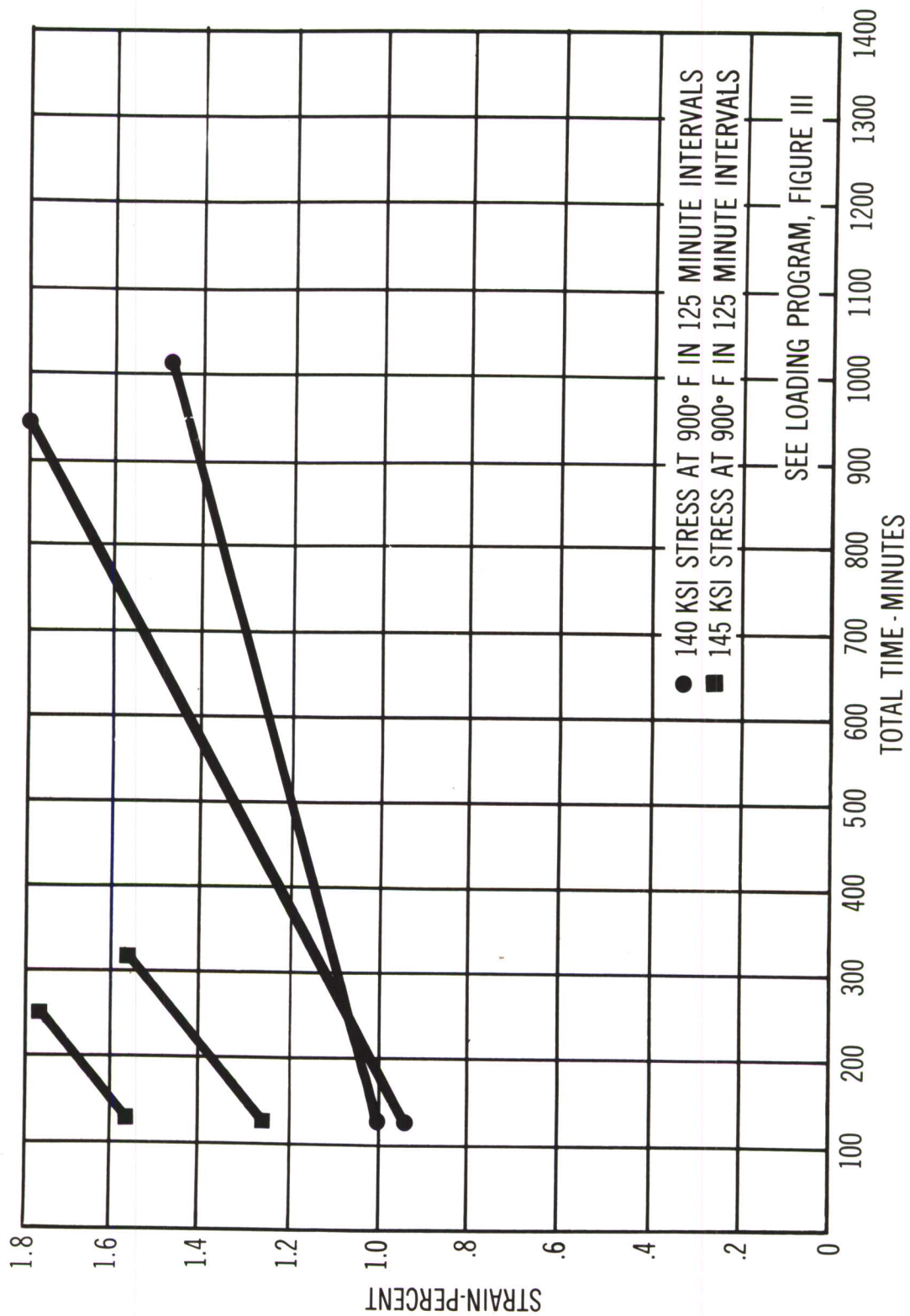


Figure 121. Effect of Stress Variation at 900°F Upon 125 Minute Pulsed Heating Creep.

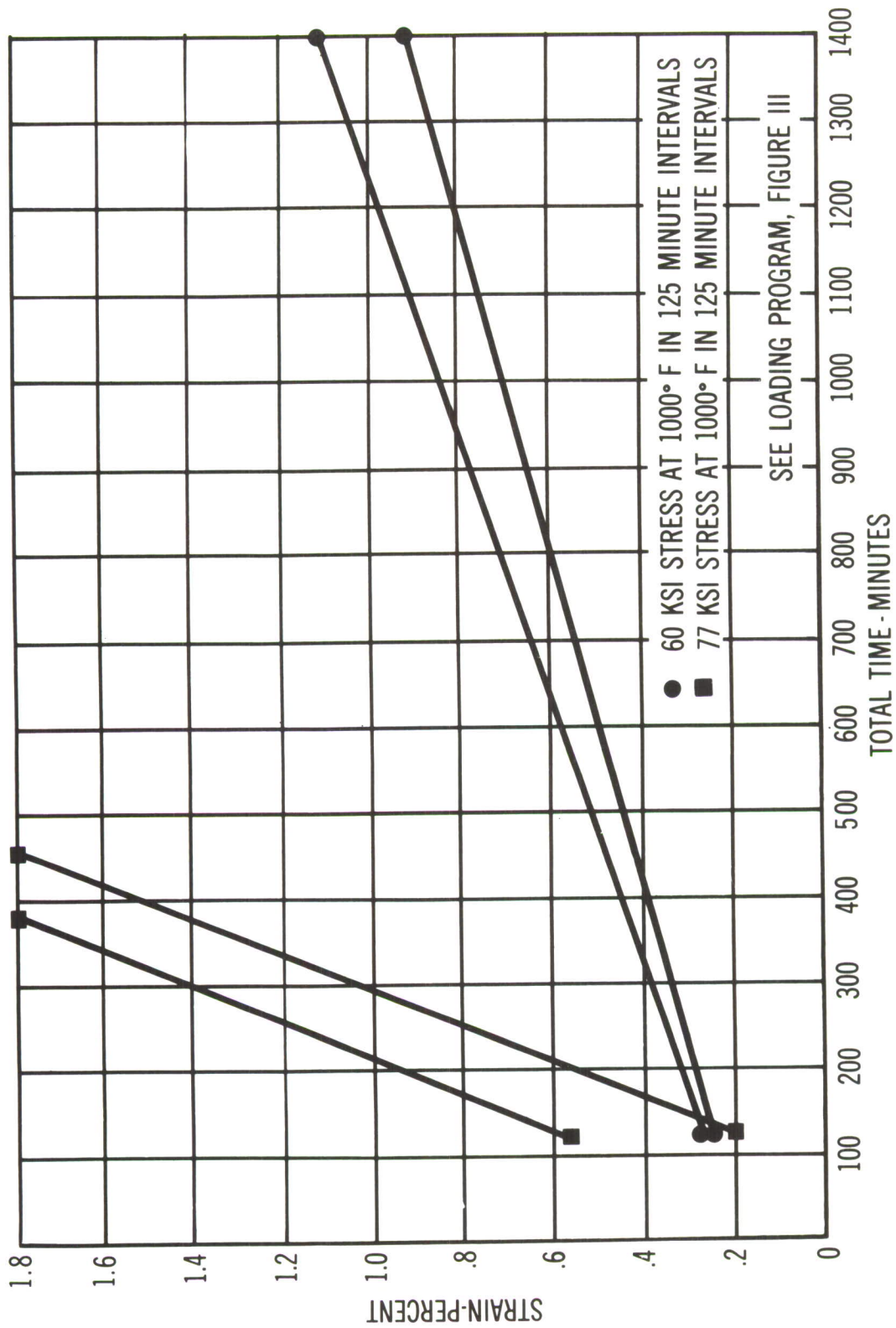


Figure 122. Effect of Stress Variation at 1000°F Upon Pulsed Heating Creep at Various Stress Levels.

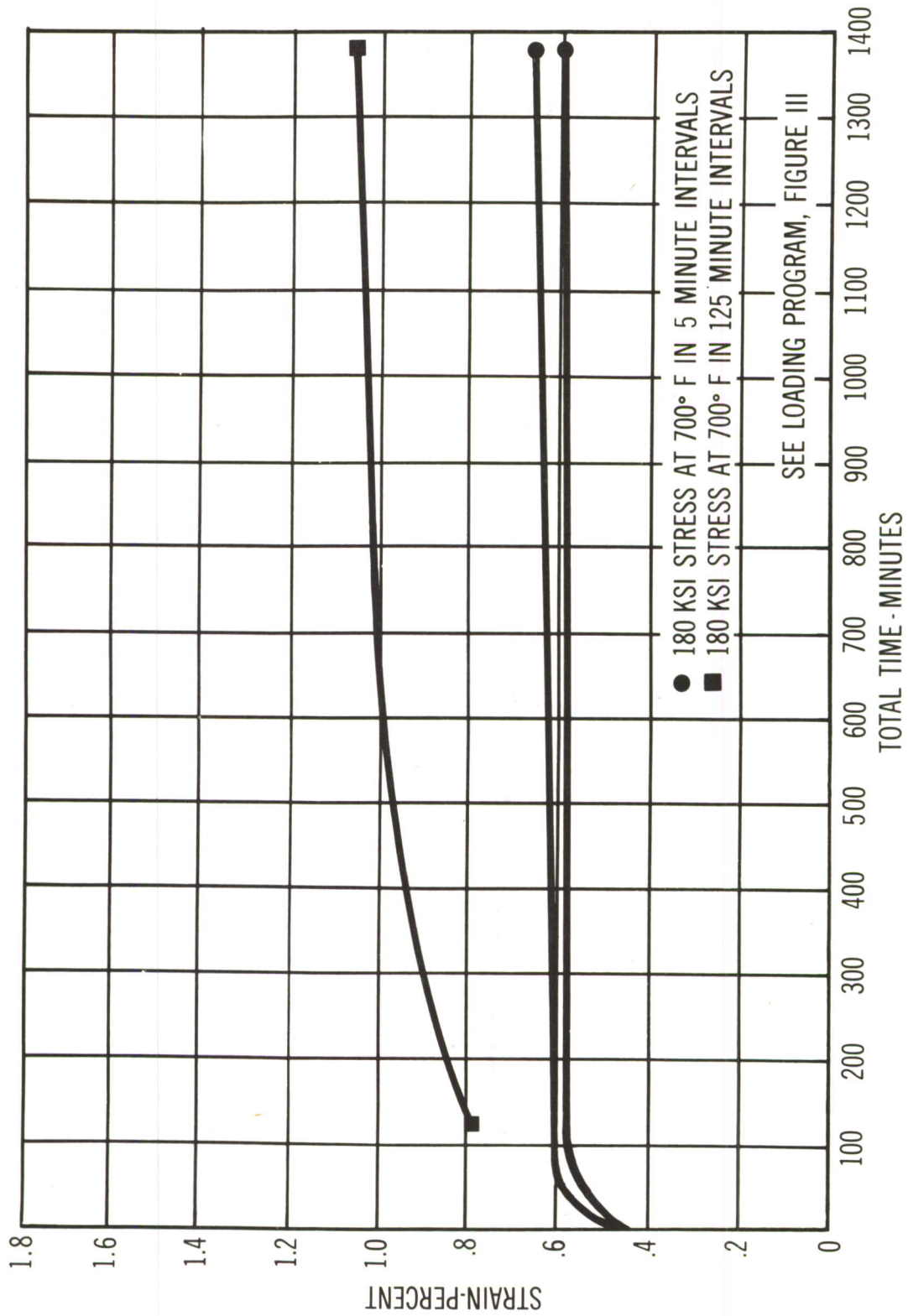


Figure 123. Effect of Pulse Time Variation at Constant Stress at 700°F on Pulsed Creep (180 KSI).

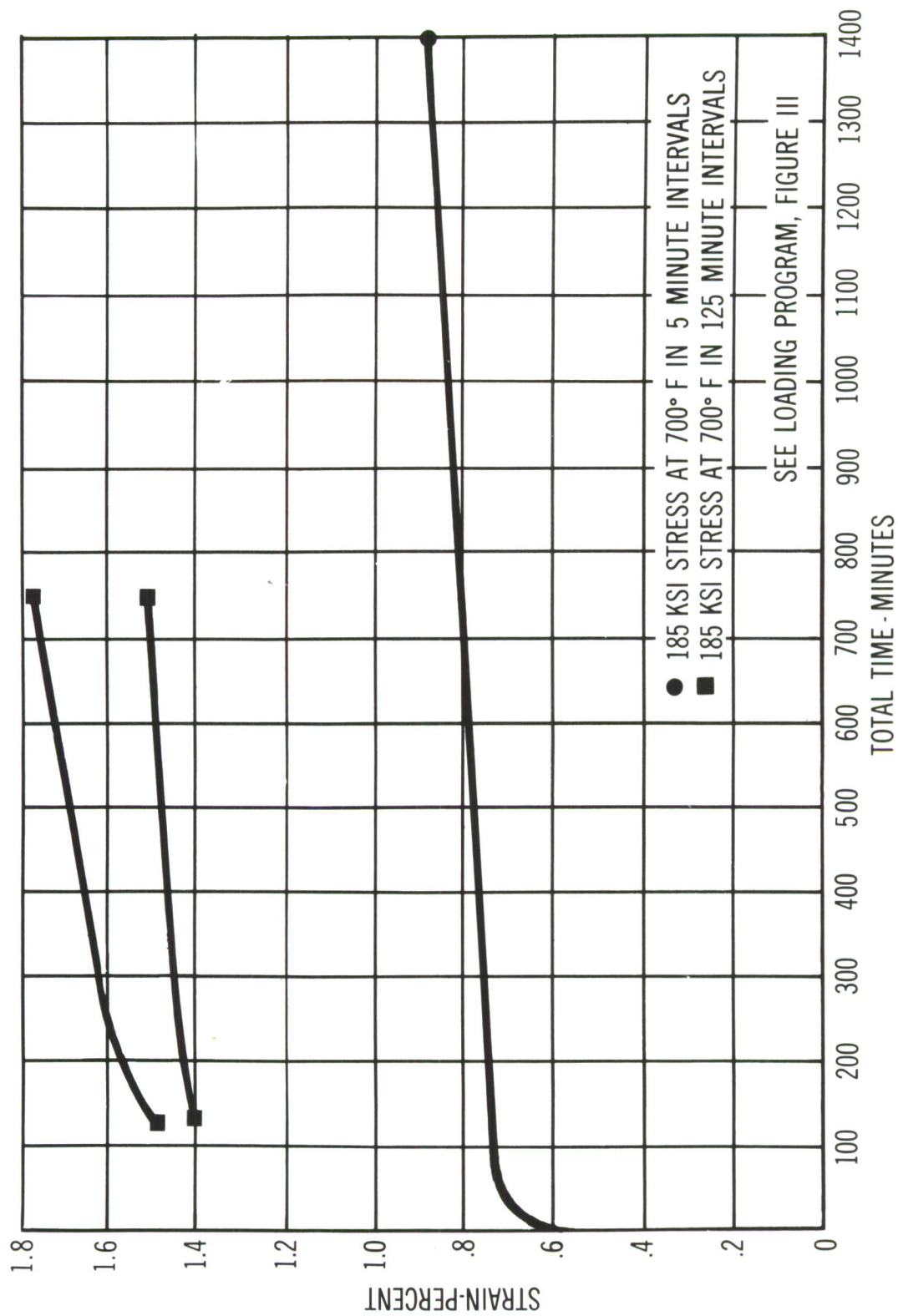


Figure 124. Effect of Pulse Time Variation at Constant Stress at 700°F on Pulsed Creep (185 KSI).

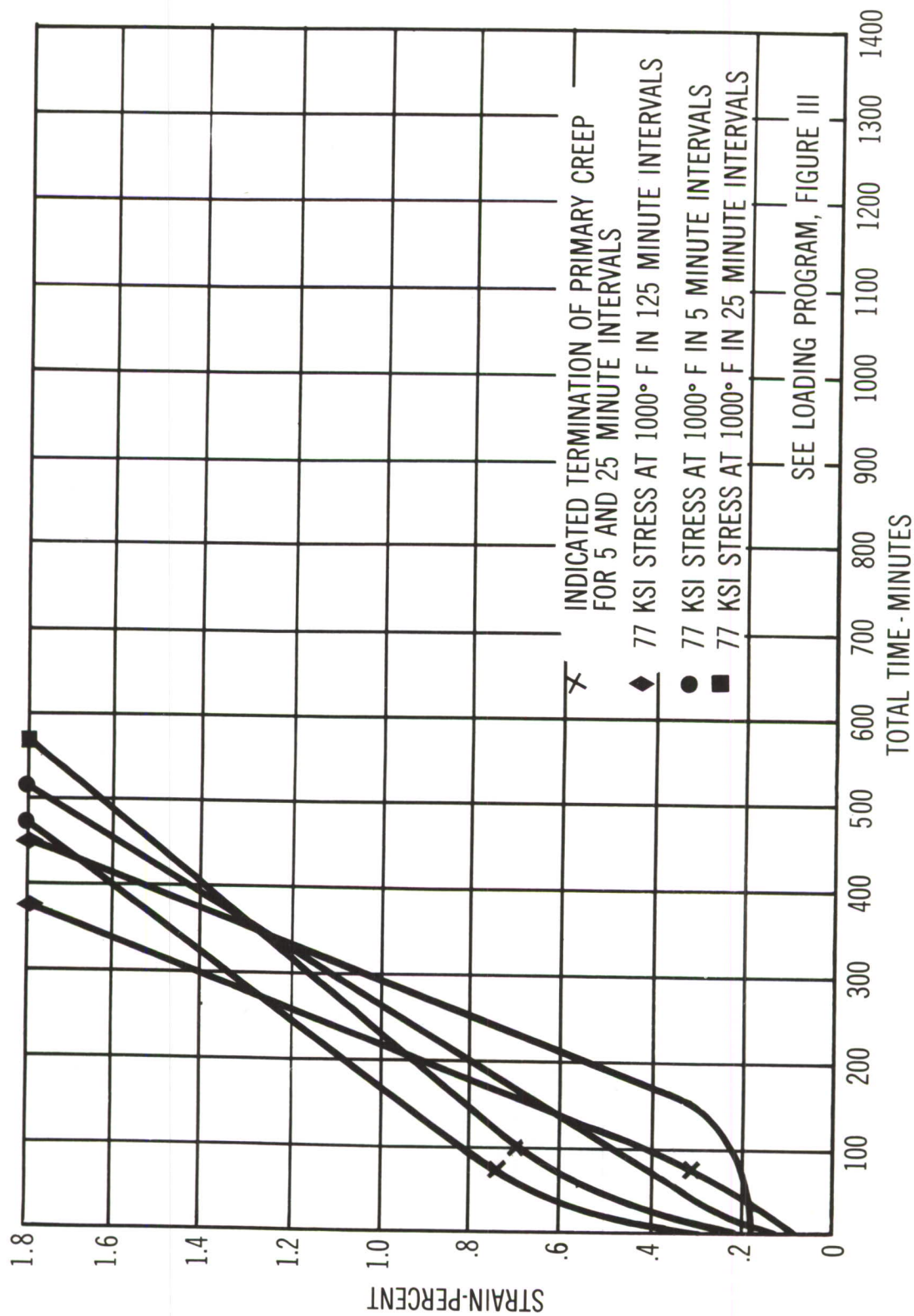


Figure 125. Effect of Pulse Time Variation at Constant Stress at 1000°F on Pulsed Heating Creep (77 KSI).

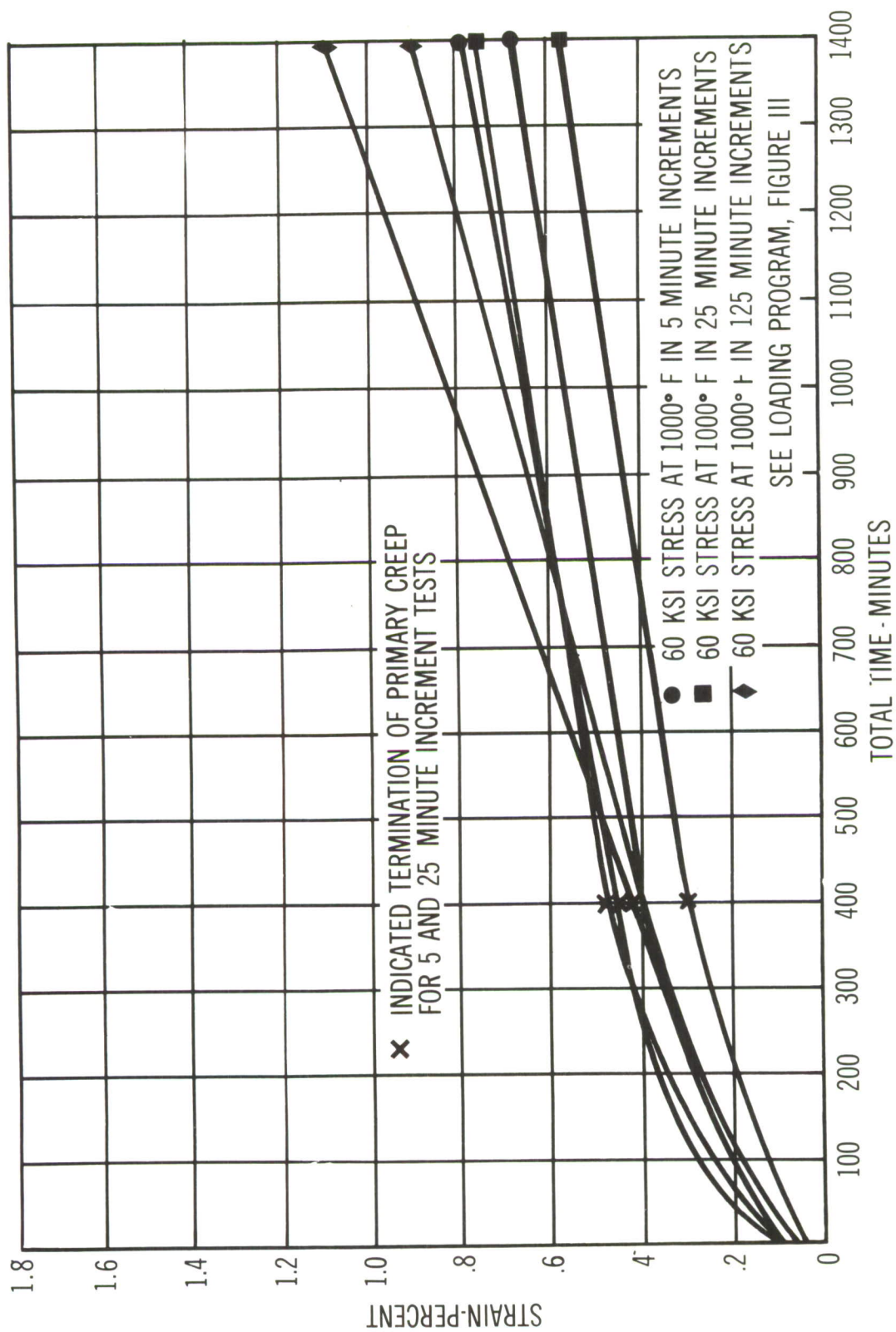


Figure 126. Effect of Pulse Time Variation at Constant Stress at 1000°F on Pulsed Heating Creep (60 KSI).

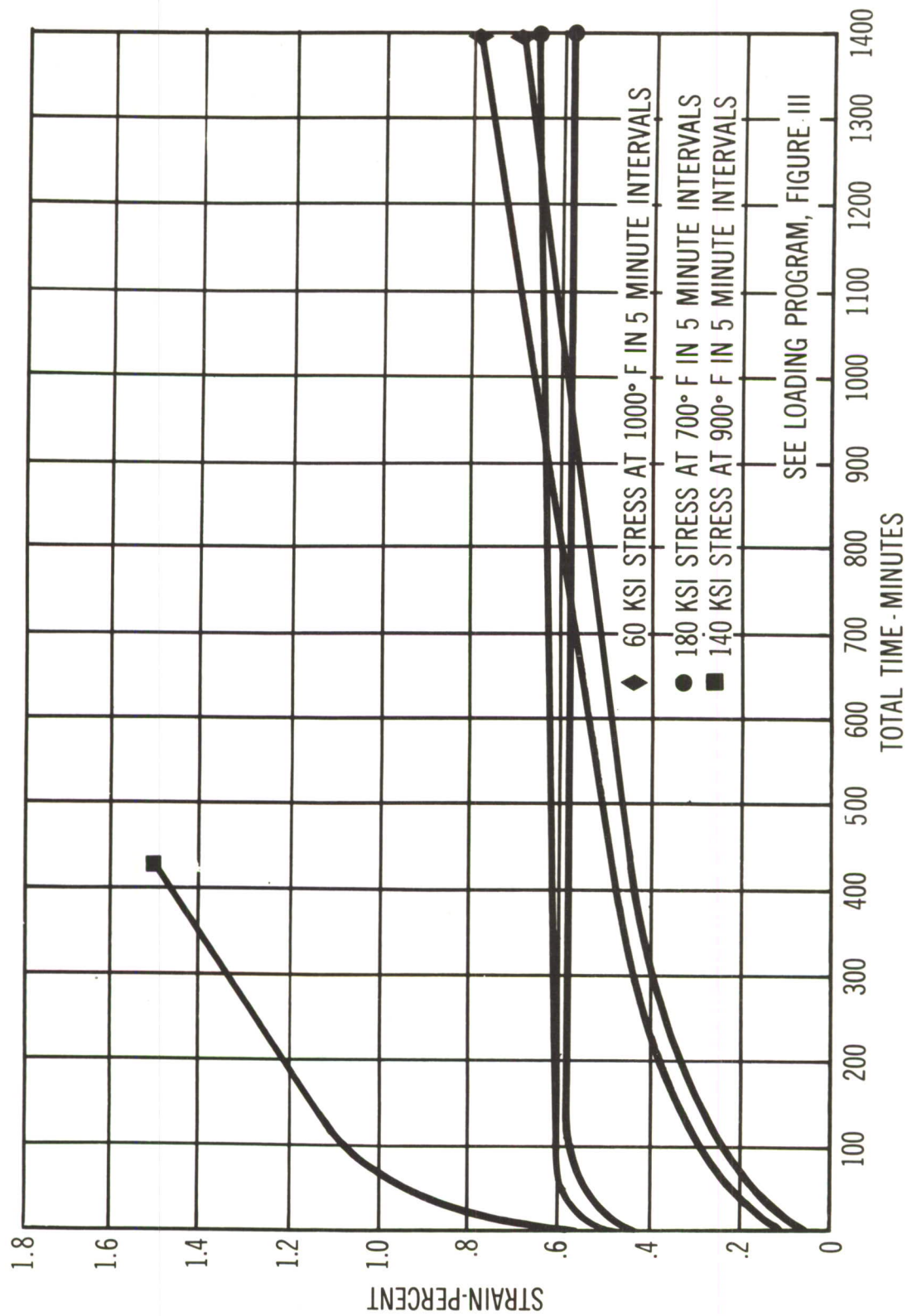


Figure 127. Effect of Stress and Temperature Variation at 5 Minute Pulse Intervals Upon Creep.

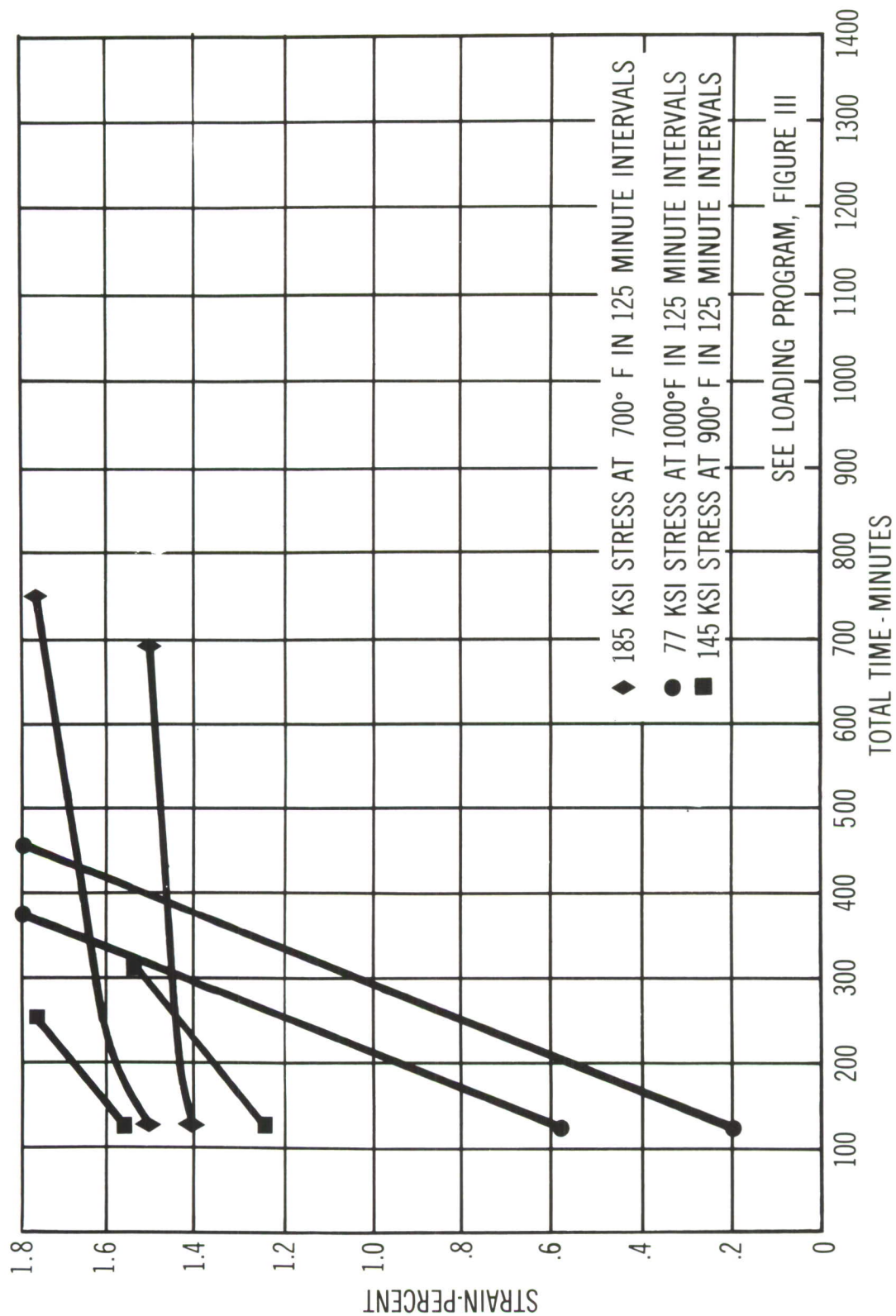


Figure 128. Effect of Stress and Temperature Variation at 125 Minute Pulse Intervals Upon Creep.

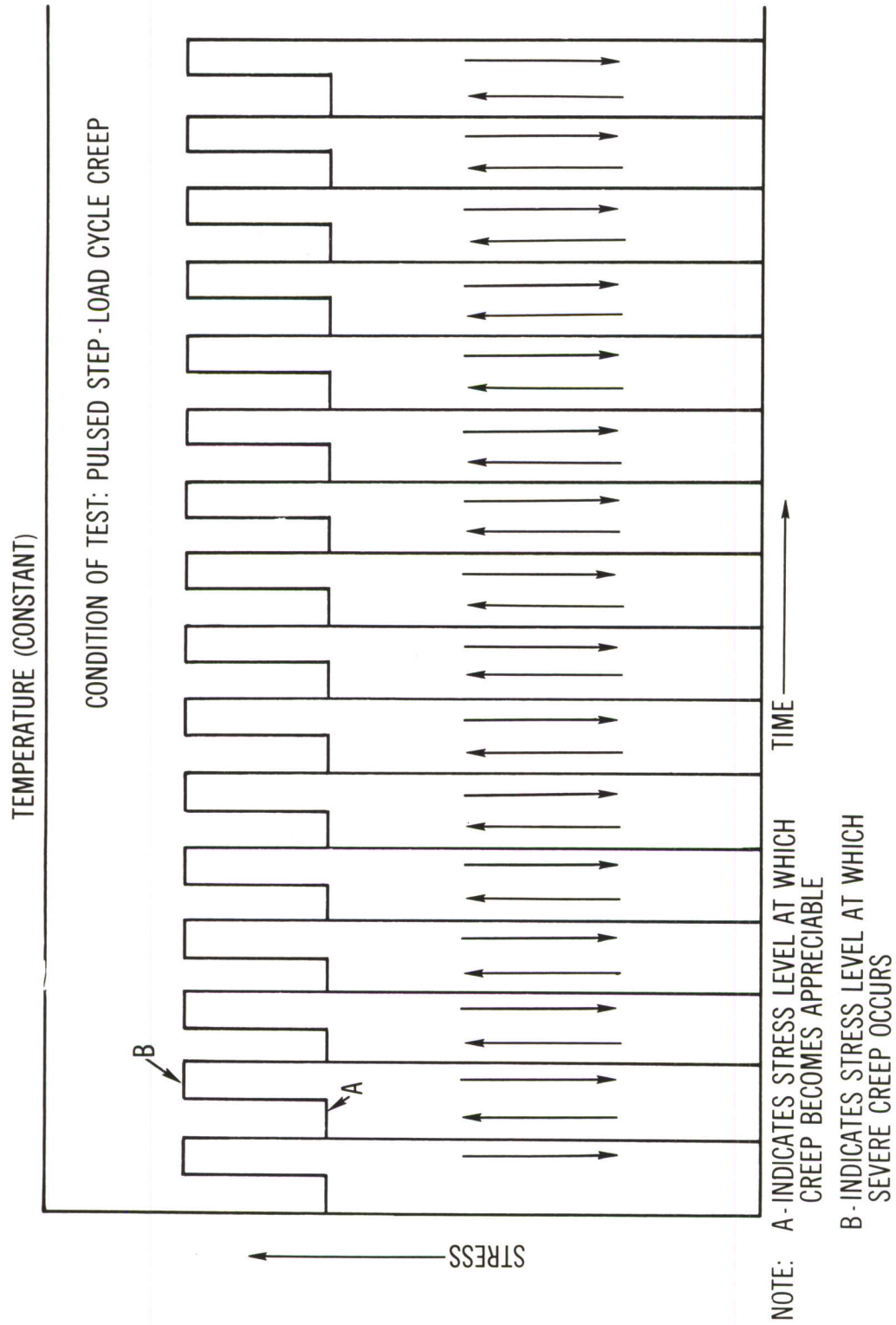


Figure 129. Program for Pulsed Step Load Tests.

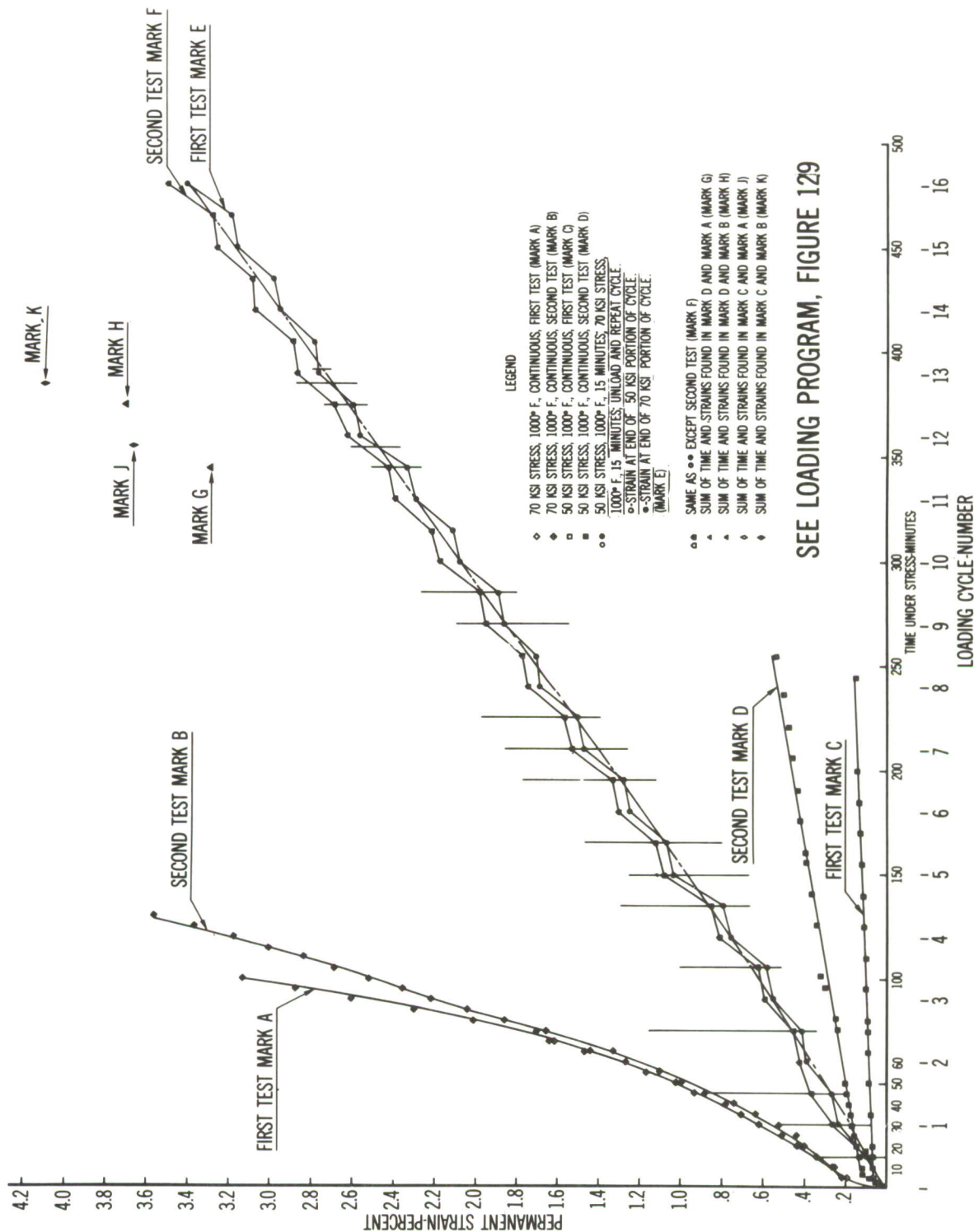


Figure 130. Comparisons of Creep Resulting From Constant Stress - Constant Temperature and Pulsed Step Loading - Constant Temperature Applications.

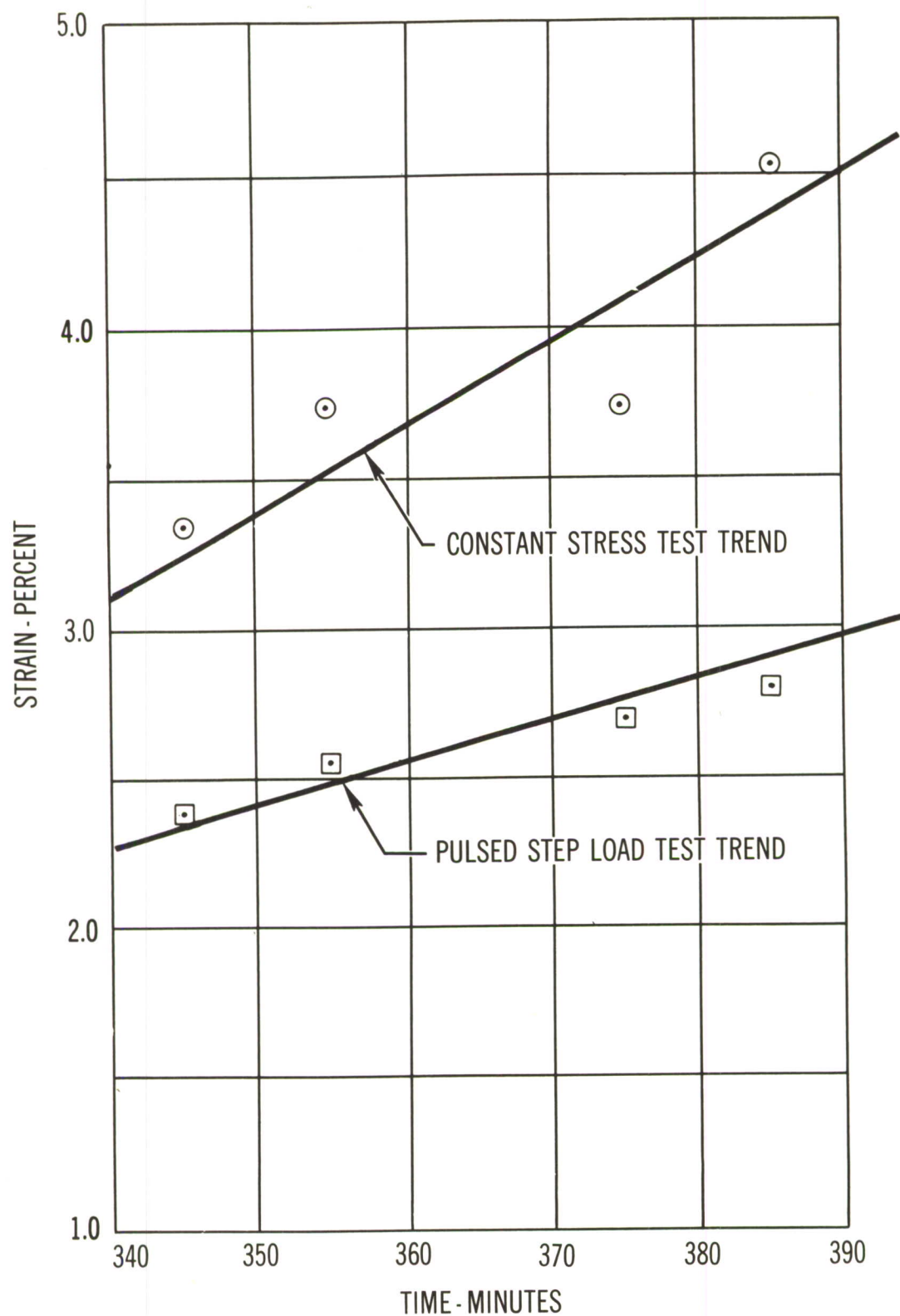


Figure 131. Comparison of Creep Trends in Constant Stress and Pulsed Step Load Tests.

PREDICTION OF CREEP EFFECTS
IN
AIRCRAFT STRUCTURES
APPENDIX I - BIBLIOGRAPHY

PERIODICALS

1. Aleksandrian, R. A., "Torsion of Thin-walled Rods with Closed Sections Subject to Transient Creep". Journal of Applied Mathematics and Mechanics. Vol 22, 1958, pp 1089-1107.
2. Aucker, B., et al., "Relationship between Small-angle Dislocation Boundaries and Creep". Journal of Applied Physics. Vol 27, April 1956, pp 333-334.
3. Bailey, W. H., et al., "Creep Properties of Austenitic Nickel-Chromium Steels Containing Columbium". Proceedings of the Institute of Mechanical Engineers. Vol. 34, 1957, pp 911-917.
4. Boyce, A. E., et al., "Effect of Stress on the Creep of Aluminum in the Dislocation Climb Range". Metal Progress. Vol 76, October 1959, p 284 (abstract).
5. Besseling, J. F., "A Theory of Elastic, Plastic and Creep Deformations of an Initially Isotropic Material Showing Anisotropic Strain-Hardening Creep-Recovery and Secondary Creep". Journal of Applied Mechanics, Vol 25, December 1958, pp 529-536.
6. Bleakely, H. H., "An Evaluation of the Recovery Theory of Creep" Canadian Journal of Technology, January 1955, p. 56.
7. Boettner, R. C. and W. D. Robertson, "Constant Stress Creep Apparatus". Review of Scientific Instruments. Vol 27, No. 12, December 1956, pp 1039-1041.
8. Borch, N. R., et al., "Activation Energies for Creep of an Alpha Solid Solution of Magnesium in Aluminum". Metal Progress. Vol. 76, No. 11, November 1959, p. 156 (abstract).
9. Bozajian, J. M., "Inelastic Stability Theory for Creep Buckling of Plates and Shells Under Transient Loading". Journal of the Aerospace Sciences. Vol. 25, December 1958, pp 795-796.
10. Carlson, R. L., "Time-Dependent Tangent Modulus Applied to Column Creep Buckling". Journal of Applied Mechanics. Vol. 23, September 1956, pp 390-394.
11. Charwat, A. F., "Contribution of Thermal Creep to the Skin Friction in Slip Flow". Journal of the Aerospace Sciences. Vol. 26, February, 1959, pp 120-121.
12. Christy, R. W., "Theory of Creep Limited by Self Diffusion". Journal of Applied Physics. Vol. 30, May 1959, pp 760-764.
13. Congleton, J. and R. N. Parkins, "Simple Creep Strain Recorder for use with Wire Specimens". Journal of Scientific Instruments. Vol. 35, October 1958, pp 379-380.

14. Cuff, F. B. and N. J., "Effect of Cold Work on the Creep-Rupture Properties of a Series of Simple 18-8 Stainless Steels". Journal of the Iron and Steel Institute. Vol. 186, June 1957, pp 188-197.
15. Cuthill, J. R., et al., "Effect of a Ceramic Coating on the Creep Behavior of Some High Temperature Alloys". Bulletin of the American Ceramic Society. Vol. 38, January 15, 1959, pp 4-12.
16. Davies, P. W. and Dennison, J. P., "Review of Intergranular Fracture Processes In Creep". Journal of the Institute of Metals. Vol. 87, 1958-1959, pp 119-125.
17. Feltenham, P., "On the Activation Energy of High Temperature Creep in Metals" Philosophical Magazine (Eighth Series). Vol. 2, May 1957, pp 584-588.
18. Feltenham, P., "On the Mechanism of High Temperature Creep in Metals with Special Reference to Polycrystalline Lead". Proceedings of the Physical Society, Section B, Vol. 69, December 1956 pp 1173-1188.
19. Feltenham, P., "Relation Between the Initial Instantaneous Extention in Creep and the Yield Stress and Coefficient of Work-hardening in Polycrystalline Metals". Nature Vol. 177. March 13, 1956, p. 632.
20. Finnie, I., "Creep Instability of Thin Walled Tubes Under Internal Pressure". Journal of the Aerospace Sciences. Vol. 26, April 1959, pp 248-249.
21. Finnie, I., "Creep Buckling of Tubes in Tension". Journal of the Aeronautical Sciences. Vol. 25, January 1958, pp 66-67.
22. Fountain, R. W. and Korchynsky, M., "Phenomenon of Negative Creep in Alloys" Metal Progress. Vol. 74, October 1958, p. 252.
23. Fox, D. K. and Reichenecker, W. J. "Creep and Tensile Data on Sand Cast Aluminum". Materials in Design Engineering. Vol. 50, November 1959, p. 184.
24. Garofalo, F., et al., "Validity of Time-Compensated Temperature Parameters for Correlating Creep and Creep-Rupture Data". Transactions of the American Society of Mechanical Engineers. Vol. 78, October 1956, pp 1423-1429.
25. Gemmell, G. D. and Grant, N. J., "Effects of Solid Solution Alloying on Creep Deformation of Aluminum". Journal of Metals. Vol. 9, Transactions, April 1957, pp 417-423.
26. Gerard, G. and Gilbert, A. C., "Critical Strain Approach to Creep Buckling of Plates and Shells". Journal of the Aerospace Sciences. Vol. 25, July 1958, pp 429-434.
27. Gerard, G. "Mechanical Behavior After Creep". Journal of the Aeronautical Sciences. Vol. 25, June 1958, pp 397-398.
28. Gerard, G., "Note on Mechanical Behavior After Creep". Journal of the Aeronautical Sciences, pp 397-398.
29. Gefkins, R. C., "Recrystallization of Lead During Creep". Journal of the Institute of Metals. Vol. 87, 1958-1959, pp 255-261.

30. Glen, J., "Effect of Alloying Elements on Creep Behavior". Journal of the Iron and Steel Institute. Vol. 190, October 1958, pp 114-135.
31. Glen, J., "New Approach to the Problem of Creep". Journal of the Iron and Steel Institute. Vol. 189, August 1958, pp 333-343.
32. Goldin, R., "Thermal Creep Design Criteria". Aeronautical Engineering Review. Vol. 16, December 1957, pp 36-41.
33. Goldin, R., "Thermal Creep Design Criteria". Machine Design. Vol. 29, October 17, 1957, p. 166.
34. Gomez, M. P., "Correlation and Extrapolation Methods of Creep Data". Trends in Engineering at the University of Washington, July 1959, p. 9.
35. Goodey, W. J., "Creep Deflection and Stress Distribution in a Beam". Aircraft Engineering. Vol. 30, June 1958, pp 170-172.
36. Griffith, J. E. and Marice, J., "Creep Relaxation for Combined Stresses". Journal of the Mechanics and Physics of Solids. Vol. 4 August 1956, pp 283-292.
37. Guard, R. W., "Creep and High Temperature Alloys". Steel Vol. 140, May 27, 1957, p. 108.
38. Habraken, L. and de la Motte, A., "Structural Hardening in the Low Alloyed Steels for Creep at High Temperatures". Metal Progress. Vol. 71, February 1957, p. 182.
39. Harris, G. T., et al., "Recent Developments in Creep Testing by the Cantilever Bending Method". Journal of the Iron and Steel Institute. Vol. 190, October 1958, pp 136-143.
40. Hilton, H. H., "Representation of Non-linear Creep by a Linear Viscoelastic Model". Journal of the Aerospace Sciences. Vol. 26, May 1959, pp 311-312.
41. Hoff, N. J., "Approximate Analysis of Structures in the Presence of Moderately Large Creep Deformations". Quarterly of Applied Mathematics. Vol. 12, April 1954, p. 49.
42. Hoff, N. J., "The Necking and the Rupture of Rods Subjected to Constant Tensile Loads". Journal of Applied Mechanics. Vol. 20, March 1953, p. 105.
43. Hoff, N. J., "On Primary Creep". Journal of the Mechanics and Physics of Solids Vol. 5, March 1957, pp 150-151.
44. Hoff, N. J., "Rapid Creep in Structures". Journal of the Aeronautical Sciences Vol. 22, October 1955, p. 661.
45. Hoff, N. J., et al., "Study of Creep Collapse of a Long Circular Cylindrical Shell Under Uniform External Pressure". Journal of the Aerospace Sciences. Vol. 26, October 1959, pp 663-669.
46. Huang, H. I., et al., "Activation Energy for High Temperature Creep of High Purity Aluminum". Journal of Metals. Vol. 8, October 1956, pp 1385-1388.

47. Jacobowitz, J. L. and Mader, K. "Steady State Creep Analysis of the Weight Loadings of Furnace Tubes on Multiple Supports". Transactions of the American Society of Mechanical Engineers Series B, Journal of Engineering for Industry. Vol. 81, May 1959, pp 115-125.
48. Jenkins, C. H. M. and Jenkinson, E. A. "Investigation of the Behavior of Metals Under Deformation at High Temperatures". Journal of the Iron and Steel Institute. Vol. 185, January 1957. pp 23-46.
49. Jenkins, W. D. and Johnson, C. R., "Creep of Annealed Nickel, Copper and Two Nickel Copper Alloys". Journal of Research of the National Bureau of Standards Vol. 60, March 1958, pp 173-191.
50. Jenkins, W. D. and Johnson, C. R., "Creep of Cold Drawn Nickel". Journal of Research of the Bureau of Standards. Vol. 63, July 1959, pp 1-18.
51. Johnson, A. E., et al., "Complex Stress Creep Relaxation of Metallic Alloys at Elevated Temperatures". Aircraft Engineering. Vol. 31, March-April 1959, pp 75-79 and 113-118.
52. Johnson, A. E., et al, "Creep Under Changing Complex Stress Systems". Engineer Vol. 206, August 8, 1958, pp 209-216.
53. Johnson, A. E., et al., "Prediction of Relaxation Stress-Time Curves from Static Tensile Test Data". Metallurgia. Vol. 59, May 1959, pp 215-220.
54. Johnson, A. E., et al., "Pure Torsion Creep Tests on Magnesium Alloy at 20°C and on 0.2 Percent Carbon Steel at 450°C at Low Rates of Strain". Metallurgia. Vol. 58, September 1958, pp 109-117.
55. Jones, M. H., et al., "Creep Damage in a Cr-Mo-V Steel". Transactions of the American Society of Mechanical Engineers. Vol. 70, January 1957, pp 117-125.
56. Kennedy, A. J., "Dependence of Microcreep Properties on the Development of Fatigue in Lead". Journal of the Institute of Metals. Vol. 87, 1958-1959, pp 145-149.
57. Kennedy, A. J., "Problems of Combined Creep and Fatigue Design". Engineer Vol. 204, September 27, 1957, pp 444-447.
58. Kennedy, A. J. and Slade, R. F., "An Automatic Electromechanical Stressing Unit for Creep and Fatigue Testing". Journal of Scientific Instruments. Vol. 33, November 1956, pp 409-410.
59. Klein, B. A., "A Simple Method of Matrix Structural Analysis". Journal of the Aerospace Sciences. Vol. 26, June 1959, pp 351-359.
60. Kornilov, I. I., "A High Temperature Centrifuge for Creep, Rupture and Bend Tests". Journal of Metals. Vol. 10, March 1958, pp 187-189.
61. Larke, L. W. and Whittaker, R. A., "Some Creep Properties of 18-8 Stainless Steels at Room Temperatures, 250°C, 400°C and 500°C". Metal Progress. Vol. 73, January 1958, p. 150.

62. Lin, T. H., "Creep Deflections and Stresses of Beam-Columns". Journal of Applied Mechanics. Vol. 25, March 1958, pp 75-78.
63. Lin, T. H., "Creep Deflections of Viscoelastic Plate Under Uniform Edge Compression". Journal of the Aeronautical Sciences. Vol. 23, September 1956, pp 883-886.
64. Lomnitz, C., "Linear Dissipation in Solids". Journal of Applied Physics. Vol. 28, February 1957, pp 201-205.
65. Lozinskii, M. G. and Autopova, E. I., "Kinetics of the Change in Microstructure of Metals and Alloys During Creep at High Temperatures Under Tension in Vacuum." Metal Progress. Vol. 71, January 1957, p. 203.
66. Ma, B. M., "Creep Analysis of Rotating Solid Disks". Journal of the Franklin Institute. Vol. 267, February 1959, pp 149-165.
67. McKeown, J., "Creep Properties of Three Copper Alloys". Metal Industries. Vol. April 25, 1958, pp 327-329.
68. McKeown, J. and Lushey, R. D. S., "Relative Creep Resistance of Cast Al-Si-Cu Alloys to LM4 and LM21". Metallurgia. Vol. 56, July 1957, pp 27-28.
69. Manjoine, M. J., "Combination Creep Rupture Test Specimen". Metal Progress. Vol. 76, July 1959, p. 152.
70. Manson, S. S., et al., "Procedure for Application of Time-Temperature Parameters to Accelerated Creep Rupture Testing". Metal Progress. Vol. 74, October 1958, p. 208.
71. Manson, S. S., "Thermal Stresses in Design". Machine Design. Vol. July 9, 1959, pp 124-129.
72. Marin, J., "Creep Stresses and Strains in an Axially Loaded Plate with a Hole". Journal of the Franklin Institute. Vol. 268, July 1959, pp 53-60.
73. Marin, J., "Determination of the Creep Deflection of a Rivet in Double Shear". Transactions of the American Society of Mechanical Engineers, Series E, Journal of Applied Mechanics. Vol. 26, June 1959, pp 285-290.
74. Mead, H. W., "Effect of Annealing Treatment on the Structure and Tensile and Creep Properties of a Commercial Titanium Alloy". Journal of the Institute of Metals. Vol. 87, 1958-1959, pp 343-346.
75. Meleka, A. H., "Direct Stress Machine for Combined Fatigue and Creep Testing", Journal of Scientific Instruments. Vol. 36, November 1959, pp 468-471.
76. Mott, N. F., "Creep in Metal Crystals at Very Low Temperatures". Philosophical Magazine. Vol. 8, June 1956, pp 568-572.
77. Muvdi, B. B. and Giemza, C. J., "How to Simplify Tests for Primary Creep Data". S. A. E. Journal. Vol. 66, August 1958, pp 46-48.
78. Patel, S. A., "Buckling of Columns in the Presence of Creep". Aeronautical Quarterly. Vol. 7, Part 2, May 1956, p. 125.

79. Patel, S. A., et al., "Torsion of Cylindrical and Prismatic Bars in the Presence of Steady Creep". Journal of Applied Mechanics. Vol. 25, June 1958, p. 214.
80. Phillips, G. H. "How to Gage Effect of Creep". Electrical World. Vol. 151, March 9, 1959, pp 56-57.
81. Plan, T. H. H., "Variational Theorem for Creep". Journal of the Aeronautical Sciences. Vol. 24, November 1957, pp 846-847.
82. Poritsky, H. and Fend, F. A., "Relief of Thermal Stresses Through Creep". Journal of Applied Mechanics. Vol. 25, December 1958, pp 589-597.
83. Prager, W. W., "Total Creep under Varying Loads". Journal of the Aeronautical Sciences. Vol. 24, February 1957, pp 153-155.
84. Rabotnov, G. N., "Creep Stability of Columns and Plates". Journal of Mechanics and Physics of Solids Vol. 6, January 1957, pp 27-34.
85. Resnik, R. and Seigle, L., "Nucleation of Voids in Metals during Diffusion and Creep". Journal of Metals. Vol. 9, Transactions Section, January 1957, p. 87-94.
86. Rimott, F. P. J., "Creep of Thick Walled Tubes under Internal Pressure considering Large Strains". Journal of Applied Mechanics. Vol. 26, June 1959, pp 271-277.
87. Rudee, M. L., "Effect of Irridiation on Creep". Journal of the American Society of Naval Engineers. Vol. 71, August 1959, pp 453-456.
88. Rush, W. L., "Creep Lengthens Sag by Two Feet". Electrical World. Vol. 151, March 9, 1951, pp 57-58.
89. Schelleng, R. D. and Eash, J. T. "Alloy Ductile Irons Promise Better High Temperature Strength". Materials in Design Engineering. Vol. 48, October 1958, p 97.
90. Schoeck, G., "Influence of Irridiation on Creep". Journal of Applied Physics. Vol. 29, January 1958, p. 112.
91. Shahinian, P., "Effect of Environment on Creep-Rupture Properties of Some Commercial Alloys". Metal Progress. Vol. 70, September 1956, p. 252.
92. Sherby, O. D., "Anelastic Creep of Polymethylmethacralate". Journal of the Mechanics and Physics of Solids. Vol. 6, February 1958, pp 145-161.
93. Shoor, B. F. "The Effect of Nonuniform Heating on Stress Variations in Creep" Soviet Physics Doklady (Russian) Vol. 3, No. 6, pp 1290-1293.
94. Simmons, W. F., "Creep and Design" Battelle Technical Review. Vol. 5, July 1956, pp 10-14.
95. Simmons, W. F., "How to Use Creep Data in Design". Materials and Methods. Vol. 44, November 1956, pp 120-123.

96. Smith, E., "The Tempering of Low Alloy Creep Resistant Steels Containing Chromium, Molybdenum and Vanadium". Iron and Steel Institute Journal, December 1957, pp 314-329.
97. Smith, M. C., et al., "Testing Machine for Short Time Creep and Stress Rupture Testing at 2000° - 2500°C". Review of Scientific Instruments. Vol. 28, July 1957, pp 543-547.
98. Spurr, R. I., "Creep and Static Friction" British Journal of Applied Physics Vol. 6, November 1955, pp 402-403.
99. Stuiwe, H. P., "Creep in Zinc Single Crystals at the Temperature of Liquid Nitrogen". Journal of Applied Physics. Vol. 30, March 1959, pp 450-451.
100. Sully, A. H., "Recent Advances in Knowledge concerning the Process of Creep in Metals". Progress in Metal Physics. Vol. 6, 1956, pp 135-180.
101. Turner, F. H. and Bloomquist, K. E., "Study of the Applicability of Rabotnov's Creep Parameter for Aluminum Alloy". Journal of the Aeronautical Sciences. Vol. 23, December 1956, pp 1121-1122.
102. Underwood, E. E., "Creep of Al-Cu Alloys during Age Hardening". Journal of Metals. Vol. 9, October 1957, pp 1182-1189.
103. Underwood, E. E., "These Curves show How You Can Determine Creep Properties From Short Time Tests". Materials and Methods. Vol. 45, April 1957, pp 127-129.
104. Vankatraman, B., "Creep Behavior for Circular Plates". Journal of the Mechanics and Physics of Solids. Vol. 6, February 1958, pp 163-176.
105. Ver Snyder, F. L. and Guard, R. W., "Directional Grain Structures for High Temperature Strength". Metals Progress. Vol. 76, October 1958, p. 218.
106. Wagner, P., "High Temperature Mechanical Properties of Graphite. I. Creep in Compression". Journal of Applied Physics. Vol. 30, February 1959, pp 148-151.
107. Wahl, A. M., "Further Studies of Stress Distribution in Rotating Discs and Cylinders under Elevated Temperature Creep Conditions". American Society of Mechanical Engineers, New York. Paper 57-A-91 8 pp.
108. Weertman, J., "Compressional Creep on Tin Single Crystals". Journal of Applied Physics. Vol. 28, February 1957, pp 196-197.
109. Wurtman, J., "Creep of Polycrystalline Aluminum as Determined from Strain Rate Tests". Journal of the Mechanics and Physics of Solids. Vol. 4, August 1956, pp 230-234.
110. Wurtman, J. and Breen, J. E., "Creep of Tin Single Crystals". Journal of Applied Physics. Vol. 29, December 1958, pp 1685-1689.
111. Wurtman, J., "Dislocation Model of Low Temperature Creep". Journal of Applied Physics. Vol. 29, December 1958, pp 1685-1689.

112. Wurtman, J., "Steady State Creep Through Dislocation Climb". Journal of Applied Physics. Vol. 28, March 1957, pp 362-364.
113. Wurtman, J., "Theory of Steady State Creep Based on Dislocation Climb". Journal of Applied Physics. Vol. 26, October 1955, pp 1213-1217.
114. Weir, C. D., "The Creep of Thick Tubes under Internal Pressure". Journal of Applied Mechanics. Vol. 24, September 1957, pp 464-466.
115. Wiesinger, F. W., "Creep Data on ASTM Type A-302 Steel". Materials in Design Engineering, Vol. 50, September 1959. p. 172.
116. Zhurkov, S. N., "Relation between Strength and Creep of Metals and Alloys". Soviet Physics - Technical Physics. Vol. 3, No. 8, pp 1586-1592 (Russian).

REPORTS

1. Bloom, M., "Equipment for Measuring the Effect of Creep on the Buckling of Columns". NACA TN-3493, September 1955.
2. Bodine, E. G., et al., "Interaction of Bearing and Tensile Loads on Creep Properties of Joints". NACA TN-3758. October 1956.
3. Deveikis, W. D., "Investigation of the Compressive Strength and Creep of 7075-T6 Aluminum Alloy Plates at Elevated Temperatures". NACA TN-4111, November 1957.
4. Erikson, B., et al., "Experimental Investigation of Cylindrical Circular Plates subjected to Rapid Creep". AFOSR TN 58-51 AD 148093.
5. French, F. W., and Patel, S. A., "Creep Buckling of Cylindrical Shells Subjected to Uniform Axial Compression". Polytechnic Institute of Brooklyn Report No. 489.
6. Heimerl, G. J., "Generalized Master Curves for Creep and Rupture". NACA TN-4112, October 1957.
7. Hoff, N. J., et al., "Creep Bending and Buckling of Thin Cylindrical Shells". NACA RM-57E17, July 23, 1957.
8. Hoff, N. J., "Stress Distribution in the Presence of Creep". AFOSR TN-56-456 AD 97072.
9. Kattus, J. R. and Dotson, C. L., "Tensile, Fracture and Short Time Creep Properties of Aircraft Structural Materials at Very High Temperatures after Rapid Heating". WADC TR 55-391, December 1955.
10. Kemper, J., "Creep Bending and Buckling of Linear Viscoelastic Columns". NACA TN-3136, January 1954.
11. Kemper, J., "Creep Bending and Buckling of Non-linear Viscoelastic Columns". NACA TN-3137, January 1954.
12. Kemper, J. and Hoff, N. J., "Bibliography of Creep for Structural Engineers". WADC TN-56-40, March 1956.

13. Kemper, J. and Patel, S. A., "Creep Buckling of Columns". NACA TN-3138, January 1954.
14. Morfin, L. and Legate, A. C., "Creep Behavior of Structural Joints of Aircraft Materials under Constant Loads and Temperatures". NACA TN-3842 January 1957.
15. Mordfin, L., et al., "Investigations of Creep Behavior of Structural Joints under Cyclic Loads and Temperatures". NASA TN-D-181, October 1959.
16. Pandalai, K. A. V. and Patel, S. A., "A Note on Shear Centers of Thin Walled Closed Sections in the Presence of Creep". Polytechnic Institute of Brooklyn Report No. 487.
17. Patel, S. and Pandalai, K., "Torsion of Cylindrical and Prismatic Bars in the Presence of Primary Creep". AFOSR TN 58-303 AD 154213.
18. Patel, S. A. et al., "Effects of Compressibility on Creep". Polytechnic Institute of Brooklyn Report No. 496.
19. Patel, S. A., et al., "Creep Stress Analysis of Thin Walled Structures". AFOSR TN 59-665.
20. Patel, S. A. and Venkatram, B., "Creep Behavior of Columns". AFOSR TN 59-530 AD 216537.
21. Patel, S. A. and Pandalai, K. A. V., "Creep Analysis of Hollow Spheres Subjected to Uniform Pressure". Polytechnic Institute of Brooklyn Report No. 488.
22. Riparbelli, C., "The Introduction of Creep into Structural Analysis". Institute of the Aerospace Sciences Paper No. 60-9.
23. Rowe, J. P. and Freeman, J. W., "Effect of Overheating on Creep Rupture". NACA TN-4224, March 1958.
24. Sanders, J. L., et al., "A Variational Theorem for Creep with Applications to Plates and Columns". NACA TN-4003, May 1957.
25. Stowell, E. Z., "A Phenomenonological Relation Between Stress, Strain Rate and Temperature for Metals at Elevated Temperatures". NACA TN-4000, May 1957.
26. Venkatraman, B. and Hodge, P. G., "Bending of Rigid Frames in the Presence of Steady Creep". AFOSR TN 56-455 AD 97071.
27. Venkatraman, B., "Solutions of Some Problems in Steady Creep". AFOSR TN 57-388 AD 132463.
28. Yerkovich, L. A., "Investigation of the Compressive, Bearing and Shear Creep Rupture of Aircraft Structural Metals and Joints at Elevated Temperatures". WADC TR 54-270, May 1958.

PREDICTION OF CREEP EFFECTS
IN
AIRCRAFT STRUCTURES

APPENDIX II - MATERIAL DATA

TABLE 41 EFFECT OF VARIOUS TEMPERATURES ON THE MODULUS
OF ELASTICITY OF ALUMINUM ALLOYS

TEMPERATURE °F	APPROXIMATE VALUE OF MODULUS OF ELASTICITY IN TERMS OF 75°F VALUES. (1)	
	75S Alloy	14S, 17S, 24S, 25S, A51S, 52S and 61S Alloys
- 320	112%	112%
- 112	105%	105%
- 18	102%	102%
75	100%	100%
212	95%	98%
300	88%	95%
400	80%	90%
500	68%	80%
600	50%	70%

NOTE: (1) Ref. ANC-5, March 1955.

TABLE 42 AVERAGE COEFFICIENT OF THERMAL EXPANSION FOR SOME
ALUMINUM ALLOYS

ALLOY	AVERAGE COEFFICIENT OF THERMAL EXPANSION IN. PER DEGREE FAHR. (1)		
	TEMPERATURE RANGE		
	68° - 212°F	68° - 392°F	68° - 572°F
14S	0.0000122	0.0000130	0.0000138
17S	0.0000122	0.0000130	0.0000138
25S	0.0000122	0.0000130	0.0000138
A51S	0.0000111	0.0000113	0.0000119
52S	0.0000111	0.0000113	0.0000119
61S	0.0000133	0.0000138	0.0000144
75S	0.0000129	0.0000135	0.0000144

NOTE: (1) Ref. "Alcoa Alloys", 1944.

TABLE 43 AVERAGE COEFFICIENT OF THERMAL EXPANSION FOR VARIOUS
METALS

ALLOY	AVERAGE COEFFICIENT OF THERMAL EXPANSION IN. PER DEGREE FAHR. (1)	
	TEMPERATURE RANGE	
	68° - 212°F.	
Brass	0.0000097 to 0.0000107	
Cast Iron	0.0000059	
Copper	0.0000093	
Lead	0.0000170	
Monel	0.0000078	
Nickel	0.0000072	
Steel	0.0000070	
Zinc	0.0000180	

NOTE: (1) Ref. "Alcoa Alloys" 1944.